2023

MODELLING OF CHLORIDE TRANSPORT IN CONCRETE

Mao, Lixuan

UNIVERSITY OF
PLYMOUTH

MODELLING OF CHLORIDE TRANSPORT IN CONCRETE

by

LIXUAN MAO

A thesis submitted to the University of Plymouth
in partial fulfilment for the degree of

DOCTOR OF PHILOSOPHY

School of Engineering, Computing and Mathematics

August 2023

ACKNOWLEDGEMENT

First and foremost, I wish to express my extremely grateful to my supervisor, Prof. Long-yuan Li for his continuous assistance, outstanding feedback, and patience at every stage of my PhD studies. His immense knowledge and insightful comments are really influential in shaping my academic research method and critiquing my results. Without his encouragement and invaluable support, it would be impossible to complete my thesis. I would also like to appreciate the treasured support and the recommendation of multiple academic workshops from my second supervisor, Dr. Boksun Kim.

Additionally, I would express my deep gratitude to Prof. Qing-feng Liu, Dr. Shan-shan Cheng, Dr. Nan-ting Yu and Dr. Min Yu for their treasured support and insightful suggestions in my academic research and future career. Special thanks go to Dr. Natt Makul for his generous help during my visit Phranakhon Rajabhat University for experiments.

My appreciation also goes out to China Scholarship Council and School of Engineering, University of Plymouth for their financial support all through my PhD studies.

I am grateful to all my friends, Chen Li, Roemer, Zhi Hu, Hong-yun Li, Yang Qin, Jie Ji, and Qi Ye, for their companionship and continuous encouragement when I was really depressed. Finally and most importantly, I want to express my massive thanks to my parents, Chun-feng Wang and Ji-wu Mao, and my sister, Xiu-li Mao for their unwavering support and unconditional love in past years. I could never have reached this point without their love and support.

AUTHOR'S DECLARATION

At no time during the registration for the degree of Doctor of Philosophy has the author been registered for any other University award without prior agreement of the Doctoral College Quality Sub-Committee.

Work submitted for this research degree at the University of Plymouth has not formed part of any other degree either at the University of Plymouth or at another establishment.

This study was financed with the aid of School of Engineering, University of Plymouth and China Scholarship Council for the UK PhD scholarship.

Word count of main body of the thesis: 35540

Signed: Lixuan Mao

Date: 09/08/2023

MODELLING OF CHLORIDE TRANSPORT IN CONCRETE

LIXUAN MAO

ABSTRACT

Chloride-induced corrosion of reinforcing steel has been recognized as the primary factor in degrading the durability of reinforced concrete structures exposed to chloride-rich environments. This research aims to investigate the underlying mechanisms of ionic transport behaviors in both natural and recycled aggregate concrete and to develop accurate and reliable prediction models to estimate the chloride transport processes during diffusion and migration tests. Based on the understanding of ionic diffusion, electromigration, polarization, and physicochemical reactions, several numerical and analytical models for chloride penetration in heterogenous concrete are proposed.

Firstly, Poisson, Laplace, and current conservation models are developed based on Gauss's law and current conservation law to investigate the interaction of different ionic species in concrete. The differences and application scope of the three models are discussed based on the obtained numerical results.

A five-phase numerical model and a two-step analytical model are proposed to characterize the heterogeneous properties of concrete with both natural and recycled aggregates and to investigate the influence of each phase on concrete resistance to chloride ingress.

Polarization-induced potential drop between outside electrodes and concrete surfaces during migration tests and its influences on inner ionic transport are investigated using a multi-species and overpotential model. A sequential non-iterative algorithm (SNIA) is introduced to connect the outside polarization and inner ionic transport.

Physical and chemical reactions between free ions in pore solution and cement hydrates and their influences on chloride penetration are investigated by using a reactive mass transport model and a non-equilibrium binding model.

This thesis has contributed to an improved understanding of the mechanisms of chloride penetration in heterogeneous concrete and provided recommendations for modelling the durability performance of concrete structures in terms of chlorides attack.

KEY WORDS: Chloride, Multi-species coupling, Heterogeneous concrete, Natural and recycled aggregates, Polarization, Overpotential, Physical and chemical reactions.

CONTENTS

LIST OF FIGURES

LIST OF TABLES

ABBREVIATIONS

1-D	one-dimensional
2-D	two-dimensional
3-D	three-dimensional
AC	alternating current
ACMT	accelerated chloride migration test
AFm	calcium aluminate hydrate
AFt	ettringite
C_3A	tricalcium aluminate
CDW	construction and demolition waste
CH	calcium hydroxide
C-S-H	calcium silicate hydrate
DC	direct current
ECR	electrochemical chloride removal
EDL	electrical double layer
EMA	effective medium approximation
FA	fly ash
GGBS	ground granulated blast-furnace slag
HER	hydrogen evolution reaction
ICCP	impressed current cathodic protection
ITZ	interfacial transition zone
MLSA	Multi-layer spherical approximation
NA	natural aggregate
NA+	natural aggregate plus ITZ
NAC	natural aggregate concrete
OER	oxygen evolution reaction

ONA	old natural aggregate in recycled aggregate
ONA+	old natural aggregate plus ITZ
OPC	ordinary Portland concrete
ORR	oxygen reduction reaction
PNP	Poisson-Nernst-Plank
RA	recycled aggregate
RAC	recycled aggregate concrete
RCA	recycled concrete aggregate
RCA+	recycled concrete aggregate plus ITZ
RCM	rapid chloride migration
RCPT	rapid chloride permeability test
SEM	scanning electron microscope
SF	silica fume
SNIA	sequential non-iterative algorithm
Strong-EN	Multi-species transport model driven from Laplace's equation
Weak-EN	Multi-species transport model driven from current conservation law
w/b	water-to-binder ratio
w/c	water-to-cement ratio

NOMENCLATURE

a_0	pore constrictivity parameter of ionic migration
A^f	frequency factor of forward reaction
A_{CSH}	specific area of C-S-H surface
C	concentration
C_0	initial concentration of chloride ions
C_{cl}	concentration of chlorides in the pore solution
C_{CSH}	concentration of C-S-H gel in hardened cement
C_i	concentration of *i-th* ionic species
C_{ij}	concentration of *i-th* species in *j-th* thermodynamic reaction
C_{ls}	concentration of chlorides in the liquid-solid interphase
C_s	boundary concentration of chloride ions
C_x	concentration at chloride penetration depth x
D	diffusion coefficient
D_1	diffusion coefficient of chlorides of phase 1 in two-phase composite
D_2	diffusion coefficient of chlorides of phase 2 in two-phase composite
D_{eff}	effective diffusion coefficient
D_{effo}	effective diffusion coefficient of chlorides in concrete with 100% NA
D_i	diffusion coefficient of *i-th* ionic species
D_k	chloride diffusion coefficient in *k-th* phase
D_{NA}	diffusion coefficient of chlorides in NA
D_{NA+}	effective diffusion coefficient of chlorides in NA plus ITZ
D_{NAC}	effective diffusion coefficient of chlorides in NAC
D_{nitz1}	diffusion coefficient of chlorides in new ITZ in the NA plus ITZ
D_{nitz2}	diffusion coefficient of chlorides in new ITZ in the RCA plus ITZ
D_{nm}	diffusion coefficient of chlorides in new mortar

D_{nssm} non-steady state migration coefficient

D_{oitz} diffusion coefficient of chlorides in old ITZ aggregate

D_{om} diffusion coefficient of chlorides in old mortar

D_{ONA} diffusion coefficient of chlorides in old NA

D_{ONA+} effective diffusion coefficient of chlorides in old NA plus ITZ

D_{RAC} effective diffusion coefficient of chlorides in RAC

D_{RCA} effective diffusion coefficient of chlorides in RCA

D_{RCA+} effective diffusion coefficient of chlorides in RCA plus ITZ

e electron charge

erf error function

$erfc$ complement error function

E electric field

E_a activation energy

f viscous coefficient

F Faraday's constant

h height of the 2-D RAC model

h_{itz} average thickness of ITZ

h_{oitz} average thickness of old ITZ

h_{nitz} average thickness of new ITZ

i current density passing through the electrode-electrolyte interface

i_0 exchange current density

$i_{a,0}$ exchange current density at anode

$i_{c,0}$ exchange current density at cathode

i_L limiting current density

I current density in cement-based materials

I_a current density flow out concrete sample during migration test

I_c	current density flow into concrete sample during migration test
J	flux
J_{OH}	flux of hydroxyl ions
J_i	flux of *i-th* species
k_{itz}	effect of microstructure of ITZ on the chloride diffusivity in ITZ
k_{om}	effect of microstructure of old mortar on the chloride diffusivity in old mortar
k_j^f	forward reaction rate coefficient
k_j^b	backward reaction rate coefficient
k_s	transfer coefficient of ions between liquid phase and liquid-solid interphase
K_{eq}	equilibrium constant of both physical and chemical binding
K_{eqj}	equilibrium constant for *j-th* thermodynamic reactions in concrete
K_{ceq}	equilibrium constant for adsorption reaction between C-S-H and free ionic species
K_{peq}	equilibrium constant of the formation and dissolution of *p-th* hydrate
l	thickness of the 2-D RAC model
L	thickness of the concrete specimen
m	mass of ions
n	total number of the species involved in the pore solution
n_i	stoichiometric coefficient of *i-th* species
n_{ij}	stoichiometric coefficient of *i-th* ionic species in *j-th* thermodynamic reaction
n_{kp}	stoichiometric coefficient of *k-th* ionic species in *p-th* cement hydrate
N_A	Avogadro's number
p_i	absorption proportion coefficient of *i-th* ionic species
R	universal gas constant

R_i mass transfer rate of *i-th* ionic species

r_{ij} reaction rate of *i-th* species in *j-th* thermodynamic reaction

r_j reaction rate of *j-th* thermodynamic reactions in concrete

R_S mass transfer rate between liquid and liquid-solid interphase

R_{NA} average radius of natural aggregate or recycled concrete aggregate

S concentration of bound ions in hardened cement phase

S_{cl} concentration of bound chlorides in the hardened cement paste

T absolute temperature

t time

u advective velocity

U external applied voltage

v migration velocity of ions

V_1 volume fraction of phase 1 in two-phase composite

V_2 volume fraction of phase 2 in two-phase composite

V_{NA} volume fraction of NA in the NA+

V_{NA+} volume fraction of NA+ in concrete

V_{nitz1} volume fraction of new ITZ in the NA+

V_{nitz2} volume fraction of new ITZ in the RCA+

V_{nm} volume fraction of new mortar in concrete

V_{oitz} volume fraction of old ITZ in the RCA

V_{om} volume fraction of old mortar in the RCA

V_{ONA} volume fraction of old NA in the RCA

v_{RCA} volume fraction of RCA in the RCA+

V_{RCA} replacement rate of RCA

V_{RCA+} volume fraction of RCA+ in concrete

V_{TA} total volume fraction of aggregate in concrete

x_d	penetration depth of chloride ions
z	charge number of ions
z_i	charge number of *i-th* ionic species
z_{OH}	charge number of hydroxyl ions
α	constant in binding isotherms
β	constant in binding isotherms
β_{TF}	Tafel slope
β_a	Tafel slope at anode
β_c	Tafel slope at cathode
γ_i	activity coefficient of *i-th* ionic species
γ_{ij}	activity coefficient of *i-th* species in *j-th* thermodynamic reaction
η	overpotential
η_a	overpotential between anode and concrete surface
η_{act}	activation overpotential
η_c	overpotential between cathode and concrete surface
η_{conc}	concentration overpotential
η_{ohmic}	ohmic overpotential
$\eta_{overall}$	overall overpotential
σ	charge density on C-S-H surface
σ_d	charge density in electrical double layer
ψ_d	electric potential in electrical double layer
$\emptyset$	electrostatic potential
Φ_a	electric potential at anode
Φ_c	electric potential at cathode
Φ_{sa}	actual electric potential at the anodic surface of concrete
Φ_{sc}	actual electric potential at the cathodic surface of concrete

Ω	combination resistance between electrode and electrolyte
ζ	zeta potential
ε	permittivity of electrolyte
ε_0	permittivity of a vacuum
ε_r	relative permittivity of water at temperature 298K,
τ	geometric tortuosity of connected pore in concrete
τ_d	tortuosity of ionic diffusion process
τ_m	tortuosity of ionic migration process
ϕ	porosity
Γ_A	adsorption densities of anions on C-S-H surface
Γ_C	adsorption densities of cations on C-S-H surface
Γ_H	adsorption densities of protons on C-S-H surface
Γ_{OH}	adsorption densities of hydroxyl ions on C-S-H surface

CHAPTER 1 INTRODUCTION

1.1. Background

Reinforced concrete structure is the most commonly used form in public infrastructure, industrial and civil construction worldwide. The service environment of concrete structures is complex and changeable, which leads to various durability problems, such as chloride ingress, alkali-aggregate reaction, freeze-thaw cycle, wet and dry cycle, acid sulfate attack, and so on. It can lead to shortening of the service life of concrete structures because of these durability problems.

Early neglect of the durability design of concrete structures results in extraordinarily high repair, refurbishment, and maintenance expenses. For example, in England and Wales, the corrosion cost of bridges was 616.5 million pounds (El-Reedy, 2007). In North American, the repair cost of concrete structures was up to 10 billion dollars (Hansson and Hansson, 1993). The De Sitter's "law of five" presents the significance of the durability design (De Sitter, 1984). It states that one dollar spent in getting structure designed and built correctly is as effective as spending 5 dollars when structures have been constructed but corrosion has yet to start, 25 dollars when corrosion has started at some points, and 125 dollars when corrosion has become widespread. Moreover, the deterioration of concrete structures causes massive consumption of cement, aggregates, and steel bars, which is a big issue on environmental protection and resource allocation, especially in terms of carbon dioxide emissions and depletion of non-renewable natural resources (Meyer, 2009).

Chloride attack is widely recognized as the most common initiating mechanism for reinforcing steel corrosion in concrete (Kitowski and Wheat, 1997). European standard EN 206-1 restricts the maximum chloride contents in construction periods, thereby minimizing corrosion resulting from the presence of chlorides introduced through admixtures, contaminated water, and aggregates (EN206-1, 2013). However, many

countries, such as China, UK, Japan, have a long coastline, which means that numerous reinforced concretes in these countries are inevitably exposed to high-salt environment, and thus have chloride-induced reinforcing steel corrosion problem (Bertolini et al., 2007). The effects of chloride penetration on steel bar's corrosion in concrete can be described as follows:

Firstly, the natural alkaline environment of concrete produces a dense and protective passive film on the surface of steel bar. This passive layer can protect steel bar from corrosion. However, the penetration of chlorides initiates a hydrolysis reaction, resulting in a low-pH micro-environment around steel surface and finally causing the breakdown of passive film. This hydrolysis process can be described as:

$$Fe^{2+}+2H_2O+2Cl^-\rightarrow Fe(OH)_2+2HCl \quad (1.1)$$

After the oxide film is breakdown, rust will appear on the surface of steel bar. In this process, steel bars in passive film broken areas act as anodes and give up electrons as following equation:

$$Fe\text{-}2e^-\rightarrow Fe^{2+} \quad (1.2)$$

The steel passive areas act as cathodes, where oxygen reduction reaction takes place:

$$4H_2O+O_2+2e^-\rightarrow 4OH^- \quad (1.3)$$

Subsequently, ferrous ions Fe^{2+} generated near the iron matrix combine with Cl^- to form $FeCl_2$. The solubility of Ferrous chloride ($FeCl_2$) facilitates the transport of anodic products, specifically Fe2+ ions, over time. Consequently, oxidation-reduction reaction in this region can proceed unhindered and may even be accelerated. At the same time, hydroxyl ions (OH^-) in the pore solution react with Fe^{2+} to form ferrous hydroxide $Fe(OH)_2$, which is subsequently oxidized into rust. As shown in Fig. 1.1, chloride ions

are repeatedly used in this corrosion process without consumption. This indicates that once chloride ions ingress into concrete, they will repeatedly act until steel bars are corroded. It should be noticed that the volume of iron oxides is 2 to 6 times greater than that of iron, which can lead to cracking, spalling or delamination of concrete cover in a short time, thereby providing more paths for chloride ingress (Fig. 1.2). Moreover, chloride has a positive effect on water absorption of concrete, diminishing its electrical resistance and consequently hastening the corrosion process.

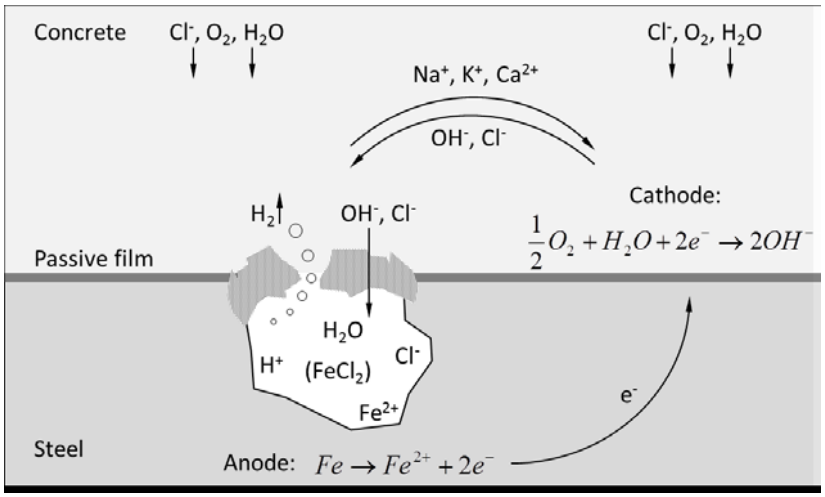

Figure 1.1 Diagrammatic representation of chloride-induced steel corrosion in concrete (Angst, 2011)

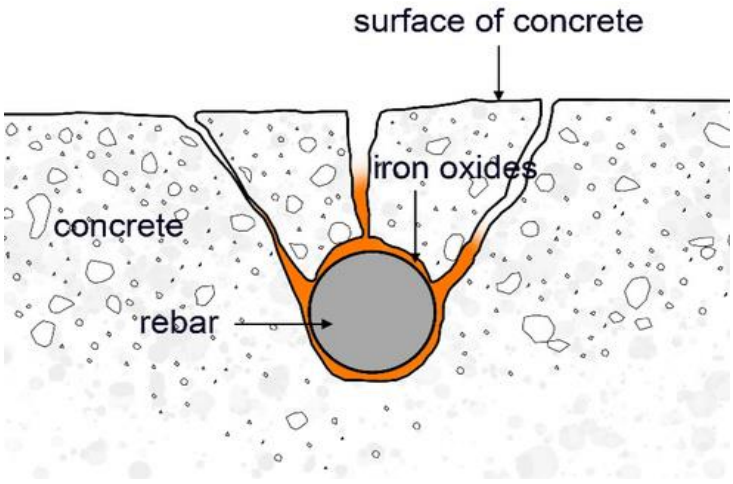

Figure 1.2 Diagrammatic representation of chloride-induced concrete cracking (Koulouris and Apostolopoulos, 2020)

To reduce the economic loss and environmental problem caused by chloride-induced corrosion of reinforcing steel in concrete structures, a large number of experimental, analytical and numerical studies on chloride transport in cementitious materials have been conducted in past four decades.

Since 1980s, numerous laboratory and field tests have been conducted to obtain reliable diffusion coefficients of chlorides in various types of concrete for service life prediction and durability design of concrete structures (AASHTO-T277, 1983; NT BUILD-443, 1995; NT BUILD-492, 1999; ASTM-C1556, 2003; Friedmann et al., 2004; ASTM-C1202, 2012). Additionally, analytical, and numerical models have been developed to understand the underlying mechanisms involved in chloride penetration within heterogenous concrete (Amey et al., 1998; Kassir and Ghosn, 2002; Park et al., 2014; Zheng et al., 2014; Shakouri and Trejo, 2017; Mao et al., 2019; Cheng et al., 2020; Tian et al., 2018; Tran et al., 2018; Cao et al., 2020; Guo et al., 2021b). A reliable and appropriate model can provide key indexes, such as the concentration or ingress depth of chlorides in concrete, for the design and assessment of concrete durability. However, there are still differences between predictions and experimental observations, which may lead to an inaccurate estimation of chloride resistance of concrete.

1.2. Objectives of the research

Considerable research has been carried out to investigate the chloride penetration in cement-based materials using experimental, analytical, and numerical methods. However, there are still a number of questions that remain unanswered about ionic transport behaviors and the modelling of this behavior, including how multi-species coupling influences chloride ingress? How do the heterogeneity and quality of recycled concrete aggregates affect the chloride resistance of concrete? To what extent can the polarization of outside electrodes influence ionic transport during chloride migration test? What reactions are involved in migration process and how do they influence chloride penetration process? The work undertaken in this thesis will therefore have the aim of

providing a better understanding of the mechanism of ionic transport in heterogenous natural and recycled aggregate concrete and developing precise and reliable models to investigate chloride ingress behaviors during chloride diffusion and migration tests. The specific objectives of the research include:

1) To conduct numerical analysis on examining the effects of multi-species coupling on chloride penetration during diffusion and migration tests. And to clarify the differences and application scope of Gauss's method and current conservation law.

2) To develop a multi-phase numerical model and an analytical model to characterize the heterogeneity of natural and recycled aggregate concrete and to investigate the influence of each phase on chloride resistance of concrete.

3) To investigate the variation of polarization-induced overpotential and its influence on ionic transport behaviors within concrete during migration test.

4) To develop a reactive mass transport model and a non-equilibrium binding model to describe the physical and chemical reactions between free ions and cement hydrates and their impacts on chloride penetration in migration test.

1.3. Layout of the thesis

The thesis is organized in eight chapters. Chapter one gives a general introduction to chloride-induced corrosion in concrete and current research on chloride penetration in concrete. In addition, the objectives and outlines of the present research are highlighted.

Chapter two outlines the research background about ionic transport, especially the transport of chlorides, in concrete. Firstly, the meso- and micro-structures of concrete and the components of both liquid and solid phases in concrete are introduced. Mechanisms of each sub-process involved in chloride transport in cement-based materials are also described in detail. Then, a summary of chloride diffusion and migration tests in concrete

is provided. Furthermore, analytical and numerical investigations on the ionic transport and physicochemical reactions in concrete are reviewed. Knowledge gaps of ionic transportation in concrete are also presented at the end of this chapter.

Chapter three presents the development of chloride transport models, which have been extended from a single phase to multiple phases, from a single species to multiple species, and from a single physical field to multiple physical fields. Additionally, the SNIA is proposed to solve the multi-physics coupling problem.

Chapter four presents a numerical analysis of multi-species coupling effects on electric field and ionic distribution in concrete by using Gauss's law and current conservation law. Based on different electrostatic potential descriptions, the time-space distributions of all ionic species in concrete are evaluated and compared. The differences and application scope of Poisson model, Laplace model and current conservation model are also discussed.

In Chapter five, the effective chloride diffusion coefficients of natural aggregate concrete (NAC) and partially replaced recycled aggregate concrete (RAC) are evaluated through a five-phase numerical model and a two-step analytical model. Based on these two models, the variation of effective diffusivities of concrete with the quality of recycled concrete aggregate (RCA), the properties of interfacial transition zone (ITZ), and the shape and volume fraction of aggregates are investigated.

Chapter six investigates the effects of polarization of electrodes on ionic transport under the action of an external electric field based on an overpotential model. Multi-species coupling, and changing electric boundaries caused by the overpotential at electrode-concrete interfaces are involved in this numerical model. Some important factors such as the applied voltage, Tafel parameters, initial condition of pore solution, and replacement rate of RCA are discussed in detail.

Chapter seven reports the effects of physicochemical reactions between free ions in pore

solution and cement hydrates on chloride transport by using a reactive mass transport model and a non-equilibrium binding model. The change in porosity of concrete resulting from the precipitation or dissolution of cement hydrations its influence of chloride transport is investigated through reactive mass transport model. The concentration distributions of ionic species, hardened hydration products after the chloride migration test are discussed. The impacts of AFm content, constrictivity and adhesive rate of old mortar in recycled concrete aggregate (RCA) on chloride ingress and binding in concrete are also examined in this chapter.

Chapter eight summarizes main findings and limitations of present study. Suggestions about future research are also proposed as a continuation of presented work.

CHAPTER 2 LITERATURE REVIEW

2.1. Introduction of concrete

2.1.1. Composition of cement hydration

Four main hydration products of Portland cement are calcium silicate hydrate (C-S-H gel), calcium hydroxide (CH), ettringite (AFt), and calcium aluminate hydrates (AFm) (Garcia-Lodeiro et al., 2015). C-S-H gel is the primary hydration product of belite (C_2S) and alite (C_3S) in cement paste and comprises 50~60% of fully hydrated Portland cement paste by volume (Medina et al., 2019). Chloride ions can be absorbed in the surface layer of C-S-H or trapped in its interlayer spaces, or firmly bound into its lattice. It has been reported that the physical binding of chloride ions is dominantly determined by the concentration or surface reaction sites of C-S-H in concrete (Tang and Nilsson, 1993). This indicates that a higher concentration or greater number of reaction sites of C-S-H results in a higher capacity for chloride binding.

Calcium hydroxide (CH) is another hydration product of C_2S and C_3S, which usually appears as elongated hexagonal plates and is highly crystalline (Kakali et al., 2000). CH accounts for about 15~20% of cement paste by volume and is responsible for maintaining the PH of pore solution in concrete is at a range of 12~13.

Ettringite (AFt) is a crystalline mineral that forms during the early stages of cement hydration, usually within the first day or two. It can be transformed into monosulfatoaluminate or an expansive form when concrete suffers from sulfate attack (Matschei et al., 2007; Baquerizo et al., 2015; Mccarthy and Dyer, 2019).

AFm, a family of calcium silicate hydrates, includes monosulfatoaluminate (SO_4^{2-}-AFm), Hydroxy-AFm (OH^--AFm), Monocarboaluminate (CO_3^{2-}-AFm), and Hemicarboaluminate ($0.5CO_3^{2-}$-AFm). Free chloride ions in pore solution can react with these AFm phases and form Friedel's and kuzel's salts. The mechanism of this chemical

binding process can be described by two ways: ionic-absorption and ionic-exchange. In the former, free ions are absorbed into the interlayer ($[Ca_2Al(OH)_6 \cdot 2O]+$) to balance the charge of AFm system. In the latter, hydroxyl, sulfate, or bicarbonate ions in AFm hydrates can be substituted by free chloride ions in pore solution, which means that chloride binding may incorporate release of other ions from hardened products. Additionally, chemically bound chloride also can be released into pore solution when concrete suffers from carbonization or sulfate attack. Different models have been developed to describe the physical and chemical reactions between aqueous species and cement hydrations, such as isothermal binding models (Shakouri and Trejo, 2017; Shi et al., 2019), non-equilibrium binding models (Spiesz and Brouwers, 2012; Li et al., 2015), and thermodynamic reaction models (Tran et al., 2018; Guo et al., 2021b), etc. The theoretical details of these models will be discussed in following sections.

2.1.2. Aggregate

Aggregate is an important filler material in concrete as it constitutes a significant portion of its volume, typically ranging from 60% to 80%. The mineralogical and physical properties of aggregate (such as size gradation, surface texture, shape, reactivity, density, etc.) have a significant impact on the mechanical properties, workability, and durability of concrete. One important impact of aggregates is their ability to increase the tortuosity of ionic transport path, leading to a slowdown of chloride ingress process (Mao et al., 2019). In addition, the shape or aspect ratio of aggregates also has an impact on chloride diffusivity of concrete. Zheng et al. (2012), Zheng et al. (2014), Xiao et al. (2016) and Zhang et al. (2021) found that effective chloride diffusivity slightly increases with a decrease in aggregate aspect ratio. Irregular crushed aggregates have been reported to exhibit better chloride resistance capacity compared to elliptical aggregates (Jie et al., 2017). Additionally, Liu et al. (2018) found that ionic migration rates increase significantly with an increment in tortuosity caused by a change of aggregate shape, with the impact of aggregate shape becoming more pronounced with an increase in total volume of aggregate.

Aggregate is usually classified into two types in terms of size: fine and coarse aggregates. The size of coarse aggregate is usually in the range of 4.75~63 mm (BS 1097-3, 1998; BS 933-11, 2012). Most commonly adopted coarse aggregate size in practice is 20 mm. Fine aggregate has a particle size less than 4.75 mm. In practice, the size distribution of aggregate plays an important role in the strength, durability and workability of concrete (Siregar et al., 2017; Yang et al., 2022). The probability density curves of aggregate gradation can be expressed as a series of parabolic curves as follows $P=\frac{nd_{max}^{n}d_{min}^{n}}{(d_{max}^{n}-d_{min}^{n})d^{n+1}}$, where P is the probability density of aggregates with a diameter smaller than d by mass, d_{max} and d_{min} are the maximum and minimum diameters of aggregate, respectively, n is the gradation exponential, which is usually in the range of 2.5~3 (Zheng and Zhou, 2007). When the value of n in probability density curves is 2.5, it corresponds to the Fuller gradation, whereas for the equal volume fraction gradation, n is equal to 3. Caré (2003) and Wu et al. (2019) found that concrete with coarser aggregates tends to present lower chloride resistance. However, Zheng and Zhou (2007) and Ying et al. (2013a) reported that the chloride diffusivities of concrete obviously reduce with an increase in aggregate size.

The sources of aggregate are various, and they fall into two main categories, natural and recycled materials. Natural aggregate (NA) usually includes crushed stone, gravel, and sand. Recycled aggregate (RA) is produced from deposited concrete, masonry, rubber, glass, and so on (Kou, 2006). Aggregates derived from deposited concrete are named recycled concrete aggregate (RCA). RCA has been proposed to replace NA in concrete to reduce environmental damage and conserve nonrenewable natural resources since the mid-20th century (Caré, 2003). However, the application of recycled aggregate concrete (RAC) is still not widely adopted in construction. One main reason for this is the adhesive old mortar and old interfacial transition zone in RCA and microcracks generated from crushing process can lead to a variable and uncertain strength and durability of RAC. Duan and Poon (2014) found that increasing old mortar in RCA leads to a significant decrease in chloride resistance of RAC. Moreover, a higher replacement rate of RCA

means a higher attached old mortar content. Experimental studies have found that chloride permeability of RAC significantly increases with the replacement rate of RCA (Bao et al., 2020; Júnior et al., 2019). It has also been reported that parent concrete strength influences the water absorption of old mortar and thus affects the chloride permeability of RAC (Padmini et al., 2009; Andreu and Miren, 2014; Pedro et al., 2014; Kou and Poon, 2015). In order to expand the application of RAC in construction, a thorough and comprehensive evaluation of its chloride resistance is essential.

2.1.3. Interfacial transition zone

ITZ is a tiny and filmy region between aggregate and cement paste. There are two kinds of ITZ in RAC: 1) old ITZ, which is a vulnerable area between original aggregate and adhesive old mortar, 2) new ITZ, which is the region between RCA and new mortar. Scanning electron microscope (SEM) observations showed that the thickness of ITZ is usually only 9~80 μm (Scrivener and Pratt, 1996; Diamond and Huang, 2001; Caré and Hervé, 2004). However, the ITZ plays an essential role in mechanical and durability properties of both NAC and RAC (Poon et al., 2004; Tam et al., 2005a; Tam et al., 2005b). This is because ITZ phase is more porous than hydrated cement paste, and detectable pore area in this phase increases with the distance from aggregate surface. It has been reported that porosity in the innermost 5 μm area of ITZ can increase by up to 30% (Scrivener, 1999; Diamond and Huang, 2001). Hence, ITZ is more vulnerable to chloride ions than cement mortar. The chloride diffusivity in ITZ is mainly dependent on the volume fraction, size distribution, shape of aggregate, water-to-cement (w/c) ratio, and ITZ thickness (Yang and Cho, 2005; Pan et al., 2018). It has also been reported that chloride diffusion coefficient in ITZ is 2~37.8 times larger than that in cement matrix (Bourdette et al., 1995; Yang, 2005; Ying et al., 2013a; Hu et al., 2018; Wang et al., 2018).

To quantitatively assess ITZ effects on chloride penetration, a series of analytical and numerical concrete models have been developed. Caré and Hervé (2004) proposed an n-phase analytical model to calculate the chloride diffusion coefficient by using the volume

fraction and effective diffusivity of continuous cement, dispersed aggregates, and ITZ. Sun et al. (2011) applied this n-phase analytical model to predict the effective chloride diffusion coefficient of NAC with considering the changing porosity in ITZ. Ying et al. (2013a) and Zheng and Zhou (2007, 2008) proposed a series of multi-phase inclusion-based models for RAC that include old aggregate, old ITZ, old mortar, new ITZ and new mortar. In these models, inner layer is usually fully enclosed by outer layer. The volume of ITZ, depending on its thickness, volume fraction and size distribution of aggregates, is crucial for the chloride-resistance of NAC and RAC. Yang and Weng (2013) developed a new model to predict the effective migration coefficient of chloride ions in ITZ by combing the double-inclusion and Mori-Tanaka methods. They found that migration coefficient of chlorides in ITZ decreases with an increase in ITZ thickness.

At the same time, many efforts have been made using numerical simulations. Specifically, Xiao et al. (2012) used a two-dimensional (2-D) five-phase model with only one aggregate to analyze the effects of ITZ and aggregates on chloride diffusion in RAC. After that, they developed a new five-phase model with four pieces of aggregates to investigate the chloride transportation performance in RAC (Ying et al., 2013b). They found that RCA's location has a significant impact on penetration direction and concentration of chloride ions in ITZ. To reduce the computational burden caused by extremely thin ITZ layers, Zheng et al. (2012) treated the aggregate and surrounding ITZ layer as a homogenous particle by using analytical solution and then applied this equivalent aggregate particle into lattice model. Liu et al. (2015a), Du et al. (2014), Tian et al. (2018) and Lin et al. (2021) adopted multi-aggregate three-phase concrete models to obtain effective diffusivity and distribution profiles of chloride ions. They found that both the thickness and diffusivity of ITZ have a significant influence on ionic transport process. The tortuosity effect caused by aggregates decreased with the increase of thickness and diffusivity of ITZ. It should be noticed that, in fact, ITZ is not a uniform shell or a sharp interface surrounding aggregate. For the sake of simplification, a uniform ITZ with a certain thickness regardless of aggregate size was used in abovementioned models. The

three-dimensional (3-D) models with the ITZ phase are also used in simulation of chloride diffusion (Abyaneh et al., 2013; Wu et al., 2020; Yu et al., 2022). It has been reported that the existing ITZ would not lead to an increase in chloride diffusivity when aggregate volume fraction exceeds 30%.

2.1.4. Pore

Concrete is a porous medium. Spaces containing liquid and/or gas distributed within solid phase are known as pores. Some of pores in concrete are interconnected, so a number of paths are provided for harmful agents to travel, such as moisture, chloride, sulfate ions, and so on. The diameter of pores ranges from 10^{-3} to 10^{-9} m (Li, 2022). The diameter of pores in hydration gel is in a range of 10^{-5} to 10^{-6} m. Gel pores are usually filled with liquid. Pores with a single narrow connection to the interconnected space are named capillary pores. The size range of capillary pores, controlled by the w/c ratio, falls between 10^{-6} and 10^{-5} m. Technological pores with diameters ranging from 10^{-4} to 10^{-3} m are generated in processing fresh concrete elements. Generally, the permeability and durability of concrete are determined by the pores with diameter exceeding 5×10^{-5} m (Bensted, 1983). Finer pores are generally associated with lower chloride diffusion coefficients. Specifically, ionic transport in pores that share a similar size range with ions is difficult. Hence, it is suggested that chloride diffusivity should be adjusted with pore size when developing the chloride transport model (Roy, 1988; Li et al., 2015).

Liquid present in pores is not pure water but rather a concentrated solution that is rich in ions, such as sodium, potassium, and hydroxyl ions. The concentration of calcium ions in concrete pore solution is relatively low and usually ignored in modelling. The concentration of hydroxyl ions in pore solution generally ranges from 200 to 1000 mol/m^3 and increases with the content of alkalis dissolved in pore solution (Thomas et al., 2017; Mccarthy and Dyer, 2019). Harmful agents, such as chloride, sulfate, and carbonate ions, may appear when concrete suffers from different durability deteriorations. The composition of pore solution is also determined by chemical properties of binders,

mixture proportions, and hydration degree of cement. Therefore, different types of concrete may have different initial ionic concentrations in pore solution system, which may influence ionic transport, especially when an external electric field is applied (Xia and Li, 2013; Spragg et al., 2016; Mao et al., 2022). Moreover, the transport of each individual ionic species can influence the performance of all other ionic species. Existing analytical and numerical studies reported that the interactions between different ions are crucial for chloride transport in concrete (Samson and Marchand, 2007b; Johannesson et al., 2009). The details of multi-species interactions in mass transport will be discussed in following sections.

In conclusion, concrete can be characterized as a complex and heterogeneous material consisting of various phases, such as cement, aggregates, pores, and interfacial transition zones. Each phase can affect the durability of concrete, particularly with respect to its resistance to chloride ions. Specifically, penetrated chloride ions can be absorbed into or released from solid cement matrix. Aggregates play a crucial role in retarding the ingress of chlorides into concrete due to their low permeability. Interfacial transition zones, characterized by their higher porosity, are more vulnerable to chloride penetration. Connected pores in cement matrix and ITZ can create pathways for moisture and harmful ions, which can ultimately lead to the deterioration of embedded metals in concrete. Abovementioned observations suggest that the distinct contribution of each phase to ionic transport should be taken into consideration in numerical simulations.

2.2. Theoretical Background

Chloride transportation in concrete is essentially a mass transfer process of charged particles in the pore solution of porous medium. In the chloride-rich environments, such as marine, de-icing area, chloride penetration in concrete can be influenced by multiple driving forces, including but not limited to concentration gradients between pore solution and exposed environments, electrostatic potential gradients generated by the interaction between different ionic species and/or supplied by external electric power, bulk flow of

pore solution, physical and chemical reactions, and polarization at electrodes. In order to develop appropriate models for concrete serviced in different environments, the underlying mechanisms of each driving force and the interaction between them are clarified in this section.

2.2.1. Ionic diffusion

Ionic diffusion is a physical process that describes the movement of ions from an area of higher concentration to an area of lower concentration. When pore solution in concrete is saturated and there are no reactions between ionic species and hydration products, chloride penetration is driven purely by the concentration gradient between environment and concrete. This diffusion process can be described by Fick's Laws as follows (Liu, 2014),

Fick's first Law $$J = -D\nabla C \tag{2.1}$$

Fick's second Law $$\frac{\partial C}{\partial t} = -\nabla J = D\nabla^2 C \tag{2.2}$$

where J, D, and C represent the flux, diffusion coefficient, and concentration of free ions in pore solution, respectively, and t is time. Fick' s first law (Equation (2.1)) describes the relationship between the flux and concentration of ions, whereas Fick's second law (Equation (2.2)) represents the mass conservation of ions. Note that both the flux and concentration vary with time unless the system becomes steady-state, in which case the flux becomes a constant and the concentration becomes time-independent. For a homogenous medium, the distribution of chlorides in a non-steady-state diffusion process can be obtained analytically by solving Equation (2.2) and expressed as follows,

$$C(x,t) = C_0 + (C_s - C_0) - \left(1 - erf\left(\frac{x}{2\sqrt{D*t}}\right)\right) \tag{2.3}$$

where C_0 the initial concentration of chlorides in concrete pore solution, C_s is the concentration of chlorides in the environment where the concrete is exposed, and *erf* is error function, which is defined as:

$$erf(z) = \frac{2}{\sqrt{\pi}} \int_0^{\pi} e^{-z^2} dz \tag{2.4}$$

Equations (2.2)-(2.4) have been used to predict the service life of concrete structures. However, it should be noted that interactions between different ionic species and physicochemical reactions can also influence the penetration process of chloride ions in concrete. As a result, the service life prediction based on Fick's Law may not be very accurate and needs to be improved. Therefore, it is necessary to consider the mechanisms of other factors involved in ionic transport, which will be discussed in following sections.

2.2.2. Ionic convection

Ionic convection is the ionic movement from one region to another due to the bulk flow of pore solution in concrete. The convection term of ionic transport can be expressed as:

$$J = -C \cdot u \tag{2.5}$$

where u is the bulk velocity of ionic solution. When the pore solution in concrete is fully saturated, it does not move in concrete and thus the bulk velocity of ionic solution can be ignored. In the present study, all concrete specimens are assumed to be fully saturated and thus the contribution of convection to ionic transport is not considered.

2.2.3. Electromigration of ions

An external electric field is commonly employed in chloride migration tests to obtain chloride migration coefficient in a short time, in electrochemical rehabilitation to repair

concrete suffers from chloride attack or carbonization, or in accelerated corrosion tests to simulate corrosion process of steel bars. The directional transport of ionic species in pore solution under the action of an external electric field is called electromigration. This phenomenon occurs due to the migration of charged ions towards oppositely charged electrodes.

Under the action of external electric field, each ionic species in pore solution is subject to both electrical and viscous forces. According to Newton's second law, the migration velocity of ions can be described as:

$$m\frac{dv}{dt} = zeE - fv \tag{2.6}$$

$$v = \frac{z\,e\,E}{f}\left(1 - exp\left(-\frac{f\,t}{m}\right)\right) \tag{2.7}$$

where *m, v,* and *z* represent the mass, migration velocity, charge number of ions, respectively; *f* is viscous coefficient (N*s/m), *t* is migration time (s), *e* is electron charge 1.6×10^{-19} C, and *E* is electric field intensity. Due to the relatively small mass of ions compared to their viscous force, the ionic migration velocity tends to stabilize in a short time, so that,

$$v = \frac{zeE}{f} \tag{2.8}$$

Thus, migration flux can be expressed as:

$$J = -C \cdot v = -\frac{zCFE}{fN_A} \tag{2.9}$$

where *F* is Faraday's constant (96487 C/mol) and N_A is Avogadro's number. According to Stockes-Einstein equation, substituting $f = RT/D$ into Equation (2.9), it yields,

$$J=-\frac{DzFC}{RT}\nabla\emptyset \tag{2.10}$$

where $\emptyset$ is electrostatic potential (V). Therefore, when an external electric field is employed, ionic flux in saturated concrete can be expressed by using Nernst-Plank equation (Yang and Su, 2002):

$$J_i=-D_i\nabla C_i-D_iC_i\frac{z_iF}{RT}\nabla\emptyset \qquad i=1,2,...n \tag{2.11}$$

where the subscript i represents the species and n is the total number of species *i-th* considered in the solution.

Pore solution of cement-based material is a multi-species system, including sodium, potassium, hydroxyl, calcium, chloride, sulfate ions, and so on. The distribution of each ionic species can influence electrostatic potential in concrete, which in turn influences the transportation of other ionic species (Johannesson, 2010a; Liu, 2014). The ion-ion interactions between different ionic species in pore solution is named multi-species coupling in the present thesis. Three different methods can be used to determine local electrostatic potential in concrete. One is Gauss's Law method, in which the relationship between electrostatic potential and net charge can be determined by Poisson's equation as follows (Johannesson, 2010b),

$$\nabla^2\emptyset=-\frac{F}{\varepsilon_0\varepsilon_r}\sum_{i=1}^{n}z_iC_i \qquad i=1,2,...n \tag{2.12}$$

where D_i, C_i, and z_i is the diffusion coefficient, concentration, and charge number of *i-th* ionic species in pore solution, respectively. ε_0=8.854×10^{-12} C/(V·m) is permittivity of a vacuum, ε_r=78.3 is relative permittivity of water at temperature 298K. Mathematically, the order-of-magnitude of $\frac{F}{\varepsilon_0\varepsilon_r}$ in Equation (2.12) is up to 10^{14}, which means that an extremely insignificant net charge ($\sum_{i=1}^{n}z_iC_i\approx 0$) is needed to generate a strong Laplacian

potential. However, it should be noticed that this insignificant net charge $\sum_{i=1}^{n} z_i C_i \approx 0$ is quite different from the electroneutral condition $\sum_{i=1}^{n} z_i C_i = 0$, although numerically they seem to be similar. When electroneutrality condition ($\sum_{i=1}^{n} z_i C_i = 0$) is adopted in Gauss's law, the governing equation of electric potential can be simplified as:

$$\nabla^2 \emptyset = 0 \tag{2.13}$$

This indicates that in one-dimensional (1-D) chloride migration problem, the term electric field·$\nabla\emptyset$ remains constant. The value of this term can be determined purely by the externally applied voltage ($\Delta\emptyset$) and the distance between two electrodes.

The second method is current conservation law method, in which the relationship between the current density and ionic fluxes of different ionic species can be described as follows (Li and Page, 2000),

$$I = F \sum_{i=1}^{n} z_i J_i \qquad i=1,2,\ldots n \tag{2.14}$$

Assuming that there are no chemical reactions between ionic species in the pore solution, the mass conservation for each ionic species is expressed as:

$$\frac{\partial C_i}{\partial t} = -\nabla J_i \tag{2.15}$$

The mass conservation Equation (2.15) can be extended as,

$$\frac{\partial}{\partial t}(F \sum_{i=1}^{n} z_i C_i) = -\nabla \cdot (F \sum_{i=1}^{n} z_i J_i) \qquad i=1,2,\ldots n \tag{2.16}$$

With the assumption of electroneutral condition ($\sum_{i=1}^{n} z_i C_i = 0$), Equation (2.16) can be simplified as,

$$\nabla\cdot(F\sum_{i=1}^{n} z_i J_i) = 0 \qquad i=1,2,\ldots n \tag{2.17}$$

Substituting Equation (2.14) into (2.17) leads to,

$$\nabla\cdot I = 0 \tag{2.18}$$

Equation (2.18) implies that the current density flowing into any point within concrete is equivalent to the current density flowing out of that point. Substituting Equations (2.11) and (2.14) into (2.18) leads to,

$$\nabla\emptyset = -\frac{RT}{F}\left(\frac{I/F + \sum z_i D_i \nabla C_i}{F\sum z_i^2 D_i C_i}\right) \qquad i=1,2,\ldots n \tag{2.19}$$

$$\nabla\cdot\left(F\sum_{i=1}^{n}(-z_i D_i \nabla C_i - \frac{z_i^2 D_i C_i F}{RT}\nabla\emptyset)\right) = 0 \qquad i=1,2,\ldots n \tag{2.20}$$

Equations (2.19) and (2.20) can be used to describe the interactions between multiple ionic species within concrete when subjected to externally applied current or voltage, respectively.

2.2.4. Adsorption and desorption of ions

2.2.4.1 Equilibrium binding of ions

At a state of equilibrium, the relationship between free and bound chlorides at a certain temperature can be described by three binding isotherms: Linear, Langmuir, and Freundlich isotherms. These isotherms describe the relationship between free and bound chlorides.

Linear binding isotherm

Linear binding isotherm was proposed by Tuutti (1982). This isotherm and its binding

capacity in mass transport can be expressed as follows:

$$S=\alpha C \tag{2.21}$$

$$R_S=-\alpha\frac{\partial C}{\partial t} \tag{2.22}$$

where α is a constant determined by experiments, R_S is the change rate of bound chlorides in concrete. The linear absorption has been found in long-term field-exposed concrete and has been used in early modelling (Sergi et al., 1992; Saetta et al., 1993). However, it has been reported that the linear binding model is oversimplified and does not fit well with experimental results (Liu et al., 2012). As shown in Fig. 2.1, chloride binding capacity in linear isotherm is overestimated at high free chloride concentrations and underestimated at low free chloride concentrations (Martın-Pérez et al., 2000; Hassan, 2001).

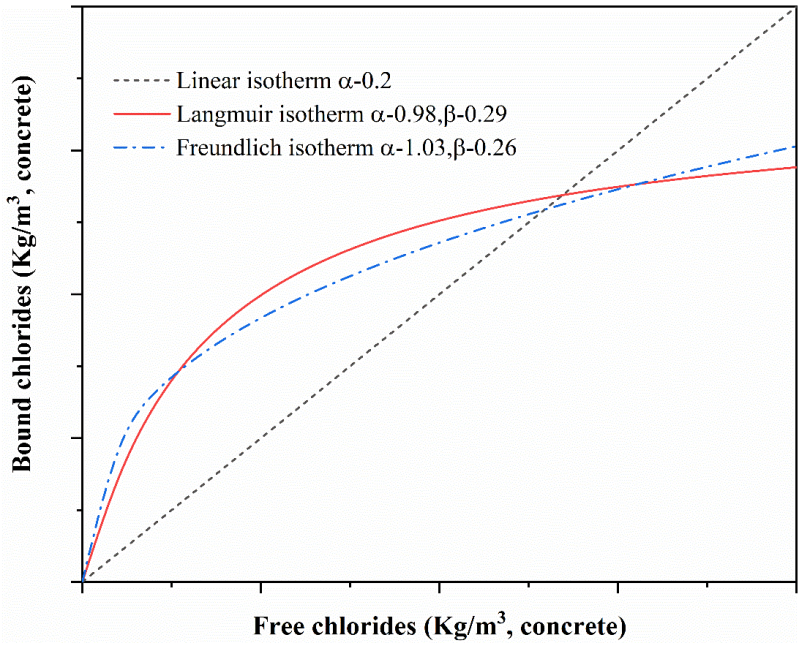

Figure 2.1 Plots of Linear, Langmuir and Freundlich isotherms (Hassan, 2001)

Langmuir binding isotherm

Langmuir isotherm is assumed to be monolayer adsorption, which suggests there is an

upper limit of bound chloride in cement matrix. Hence, as shown in Fig. 2.1, its binding capacity tends to zero at high free-chloride concentrations. Mathematically, it can be expressed as,

$$S=\alpha C/(1+\beta C) \tag{2.23}$$

$$R_S=-\frac{\alpha}{(1+\beta C)^2}\frac{\partial C}{\partial t} \tag{2.24}$$

where α and β are constants, which are influenced by the mixture proportion of binder and water-to-binder (w/b) ratio. For example, Sergi et al. (1992) reported that α and β of ordinary Portland concrete (OPC) is 1.67 and 4.08 when w/b ratio is 0.5 (the units of free and bound chlorides are expressed as mol/L and mmol/g, respectively). When w/b ratio is 0.48, Yuan et al. (2009) found that the calibrated α and β are 9.46 and 0.37, 17.79 and 1.26 for concrete with 100% cement and 20% fly ash plus 80% cement, respectively (the units of free and bound chlorides are expressed as mol/L and mg/g, respectively). Note that the values of these two parameters should be recomputed based on the units employed in modelling. Tang and Nilsson (1993) reported that Langmuir isotherm is restricted to lower free chloride concentrations in pore solution, specifically those below 0.5 mol/L.

Freundlich isotherm

The third one is Freundlich binding isotherm, which is another nonlinear binding isotherm, assuming that adsorption capacity of cement decreases as ionic concentration in liquid phase increases. It can be expressed as (Tang and Nilsson, 1993),

$$S=\alpha C^{\beta} \tag{2.25}$$

$$R_S=-\alpha\beta C^{\beta-1}\frac{\partial C}{\partial t} \tag{2.26}$$

where α and β are empirical constants calculated by using regression analysis of experimental results. Their values also vary with w/b ratio and types of binder used in concrete. For Freundlich isotherm, the suitable range of free chloride concentration changes from 0.01 to 1 mol/L. This range encompasses the concentration levels encountered in most field or experimental work. Hence, it can be widely used in the prediction models of chloride penetration in concrete.

2.2.4.2 Non-Equilibrium binding

Physical or chemical reactions between free ions and cement matrix in concrete are not instantaneous processes. Existing literature reported that it usually takes 7~14 days to achieve equilibrium between free chloride ions in pore solution and bound chloride in hardened cement (Tang and Nilsson, 1993). Hence, equilibrium binding isotherms are applicable for modelling long-term diffusion processes in concrete. However, for short-term migration tests (less than two days), the above-mentioned isotherms are no longer applicable. To describe this non-equilibrium binding in migration process, a three-phase binding system has been suggested, which involves pore solution, hardened cement paste, and interphase between them (Spiesz et al., 2012). The mass transfer process from pore solution to cement matrix is divided into two steps. Take chloride adsorption as an example, free chloride ions are first driven into liquid-solid interphase by concentration gradient, and then partly bound onto hardened cement surface. This process repeats many times until there is no concentration difference between the pore solution phase and interphase. The resistance of interphase to mass transfer is responsible for non-equilibrium binding in concrete, and it is defined as a transfer coefficient, k_s. Therefore, mass transfer rate between pore solution and liquid-solid interphase can be expressed as,

$$R_S = -k_s(C - C_{ls}) \tag{2.27}$$

where C_{ls} is chloride concentration in liquid-solid interphase. Assuming that chloride adsorption and desorption take place immediately between the interphase and the solid

cement matrix, C_{ls} can be calculated by the binding isotherms as follows,

$$S=\alpha C_{ls};\ S=\frac{\alpha C_{ls}}{1+\beta C_{ls}}\ ;S=\alpha C_{ls}^{\beta} \tag{2.28}$$

Substituting Equation (2.28) into (2.27), it yields,

$$R_S=-k_s\ (C-S/\alpha);\ \ R_S=-k_s(C-S/(\alpha-\beta S));\tag{2.29}$$

$$R_S=-k_s\ (C-(S/\alpha)^{1/\beta})$$

Therefore, this non-equilibrium binding mechanism can be defined as follows: while the free chloride concentration in interphase is less than that in pore solution, chloride ions continue to transfer into interphase, and bound-chloride concentration in cement increases accordingly. When free-chlorides concentration in interphase is greater than that in pore solution, they are transferred from interphase to liquid phase. In order to maintain charge balance, bound chloride will be released from cement paste into interphase (Spiesz et al., 2012; Spiesz and Brouwers, 2012; Spiesz and Brouwers, 2013; Li et al., 2015).

2.2.4.3 Thermodynamic reactions

Abovementioned binding isotherms are widely adopted in numerical modelling of ionic absorption in chloride penetration process. Nevertheless, there are two limitations of these pre-designed isotherms. One is the binding capacity of chlorides, referring to parameters in binding isotherms, which varies significantly with the pH value, types and content of binder, w/b ratio, and so on. Therefore, the determination of binding parameters of isotherms for different concrete types must depend on specific experimental data. Another is that the formation of chloroaluminate salt (Friedel's and Kuzel's salt) and reduction of cementitious components can lead to a change in pore structures (mainly the porosity of concrete). However, existing isothermal binding models usually ignore the change in pore

structure caused by chemical binding of chlorides. Therefore, it is essential to elucidate the mechanisms of real physicochemical reactions in order to gain a more profound comprehension of chloride ingress process.

The penetration of chloride ions will break the equilibrium between free ions in pore solution and cementitious hydrations in solid phase and lead to new precipitation/dissolution of hydration products and physical adsorption/ desorption on C-S-H surfaces, for instance, the formation of chloroaluminate salt (Friedel's and Kuzel's salt) and a corresponding reduction of AFm phases. The thermodynamic reactions involved in chloride transport are given in Table 2.1.

Table 2.1 Thermodynamic reactions involved in this study and their forward reaction rate coefficients k_f (mol/m^2/s) and equilibrium constants.

Phase	Thermodynamic reactions	k_f (Baur et al., 2004)	Log (Keq) (Hosokawa et al., 2011b)
AFt	$C_3A\cdot3CaSO_4\cdot32H_2O \leftrightarrow 6Ca^{2+}+2Al(OH)_4^-+3SO_4^{2-}+4OH^-$	7.08×10^{-13}	-45.09
AFm (S)	$C_3ACaSO_4\cdot12H_2O \leftrightarrow 4Ca^{2+}+2Al(OH)_4+SO_4^{2-}+4OH^-$	6.76×10^{-12}	-29.4
Friedel's Salt	$C_3ACaCl_2\cdot10H_2O \leftrightarrow 4Ca^{2+}+2Al(OH)_4^-+2Cl^-+2OH^-$	instantaneous	-27.1
C-S-H	$\equiv SiOH+OH^- \leftrightarrow \equiv SiO^-+H_2O$	instantaneous	-12.7
	$\equiv SiOH+Ca^{2+} \leftrightarrow \equiv SiOCa^+ + H^+$	instantaneous	-9.4
	$\equiv SiOH+Ca^{2+}+SO_4^{2-} \leftrightarrow \equiv SiOCaSO_4^- + H^+$	instantaneous	-8.5
	$\equiv SiOH+Cl^- \leftrightarrow \equiv SiOHCl^-$	instantaneous	-0.35
	$\equiv SiOH+Na^+ \leftrightarrow \equiv SiOHNa^+$	instantaneous	-13.6
	$\equiv SiOH+K^+ \leftrightarrow \equiv SiOHK^+$	instantaneous	-13.6

Thermodynamic equilibrium of reactions in concrete refers to the state at which the rates of forward and reverse reactions are equal, resulting in no net change in the concentration of the reactants and products. The thermodynamic equilibrium constants of precipitation/dissolution of cement hydrates or aqueous complexation can be described by the law of mass action as follows (Gao et al., 2022),

$$K_{peq} = \prod_{k} (\gamma_k C_k)^{n_{kp}} \; p = 1, \ldots L \tag{2.30}$$

where K_{peq} is the equilibrium constant of the formation/ dissolution of *p-th* hydrate phase in concrete at a given temperature, γ_k, and C_k represent the activity coefficient and concentration of *k-th* ionic species, respectively. n_{kp} is stoichiometric coefficient of *k-th* ionic species in *p-th* cement hydrate in concrete. In the case of concrete chemistry, equilibrium constants can help predict the stability and formation of various hydration products and physically bound species, as well as the potential for phase changes. Specifically, when the value of right-hand term of Equation (2.30) is greater than the equilibrium constant, the formation of hydration products or physically bound chloride is favored. Conversely, the dissolution of hydration products or the release of bound chlorides from C-S-H gel is favored.

There are several semi-empirical equations that can be employed to calculate the activity coefficient of ionic species, such as Debye-Huckel equation (DH) (Debye and Hückel, 1923), Davies equation (Davies, 1962), modified Davies equation (MD) (Samson et al., 1999a), extended Debye-Huckel (EDH) equation (Samson et al., 1999a), and WATEQ Debye-Huckel (WDH) equation (Truesdell and Jones, 1974). The expressions and valid range of them are given in Table 2.2.

Table 2.2 The semi-empirical equations of activity coefficient of ions in pore solution

Abbr.	Equation	Valid range
DH (Debye and Hückel, 1923)	$log\gamma_k = -Az_k^2\sqrt{\mu}$	$\mu < 10^{-2.3} M$
EDH (Samson et al., 1999a)	$log\gamma_k = -\frac{Az_k^2\sqrt{\mu}}{1+Ba_k\sqrt{\mu}}$	$\mu < 0.1M$
Davies (Davies, 1962)	$log\gamma_k = -Az_k^2(\frac{\sqrt{\mu}}{1+\sqrt{\mu}} - 0.3\mu)$	$\mu \leq 0.5M$
WDH (Truesdell and Jones, 1974)	$log\gamma_k = -\frac{Az_k^2\sqrt{\mu}}{1+Ba_k\sqrt{\mu}} + b_k\mu$	$\mu \leq 1M$
MD (Samson et al., 1999a)	$log\gamma_k = -\frac{Az_k^2\sqrt{\mu}}{1+Ba_k\sqrt{\mu}} + \frac{(b_k\mu+0.2)Az_k^2\mu}{\sqrt{1000}}$	$\mu \leq 1.5M$

where, z_k is valence of *k-th* ionic species, a_k, and b_k are the ion-specific parameters and can be calculated using the mean-salt activity coefficient data. μ is the ionic strength, which can be expressed as follows,

$$\mu = \frac{1}{2}\sum_k z_k^2 C_k \tag{2.31}$$

Ionic species in pore solution include both free ionic species (Cl^-, K^+, Na^+, Ca^{2+}, OH^-) and aqueous complexes ($Al(OH)_4^-$). A and B are the constants determined by temperature and dielectric constant as follows,

$$A = \frac{\sqrt{2}F^2 e}{8\pi(\varepsilon_r\varepsilon_0 RT)^{3/2}} \tag{2.32}$$

$$B = \sqrt{\frac{2F^2}{\varepsilon_r\varepsilon_0 RT}} \tag{2.33}$$

For the pore solution at room temperature (298K) with $\varepsilon_r\varepsilon_0$ =6.95×10^{-10} C^2/(J·m), A=0.5085 (M$^{-1/2}$) and B=3.281 (M$^{-1/2}$/nm). Take chloride ions as an example, the activity coefficient γ_k gradually decreases with the increase of ionic strength.

Most physical reactions take place on the surfaces of C-S-H gel. The silanol (≡SiOH) and silandiol (≡Si(OH)$_2$) sites on C-S-H surfaces can absorb protons, anions and cations via van der Walls and electrostatic forces. Note that the surface reactions between pore solution and silandiol sites are rarely involved in existing reactive models and reportedly can be neglected (Guo et al., 2018; Tran et al., 2018). Thus, only the silanol aroused ionic absorption is considered in this study. More importantly, these physical reactions result in an electric charge on the surface of C-S-H. Subsequently, an electrical double layer (EDL) forms at the interface between pore solution and C-S-H gel. The influence of EDL on ionic transport was highlighted in some research (Friedmann et al., 2008b). To describe the mass-action, mole-balance and charge-potential at surface, surface complexation model was proposed based on EDL theory (Elakneswaran et al., 2010; Tran et al., 2018). Gouy-Chapman theory is applied to describe ionic distribution with the assumption that activities of these surface species given in Table 2.1 (such as ≡SiOHCl$^-$, ≡SiOHNa$^+$, ≡SiO$^-$) are mathematically equal to their concentration (Elakneswaran et al., 2010). Therefore, charge density can be calculated as follows,

$$\sigma = F\left\{\Gamma_H - \Gamma_{OH} + \sum z_C\Gamma_C + \sum z_A\Gamma_A\right\} \tag{2.34}$$

$$= \frac{F}{A_{CSH}C_{CSH}}\left\{\left[\equiv SiOH_2^+\right] - \left[\equiv SiO^-\right] + \left[\equiv SiOHC^+\right] - \left[\equiv SiOHA^-\right]\right\}$$

where Γ_H, Γ_{OH}, Γ_C, and Γ_A are the adsorption densities of protons, hydroxyl ions, cations, and anions, respectively. z_C and z_A are the valences of the adsorbing cations and anions. A_{CSH} is the specific area of C-S-H surface (500 m^2/g), C_{CSH} is the content of C-S-H gel in hydrate phase (g/m^3). Terms in brackets represent concentrations of surface species (mol/m^3). Charge balance in double layer can be expressed as follows,

$$\sigma+\sigma_d=0 \tag{2.35}$$

The relationship between surface potential and charge density in diffuse layer can be expressed by Gouy-Chapman theory as follows (Elakneswaran et al., 2010),

$$\sigma_d=-(8\varepsilon_r\varepsilon_0 RT\mu)^{1/2}sinh(\psi_d F/2RT) \tag{2.36}$$

Substituting Equations (3.46) and (3.44) into (3.45), it yields,

$$\frac{F}{AS}\left[\left(\equiv SiOH_2^+\right)-(\equiv SiO^-)+\left(\equiv SiOHC^+\right)-(\equiv SiOHA^-)\right] \tag{2.37}$$

$$=(8\varepsilon_r\varepsilon_0 RT\mu)^{1/2}sinh(\psi_d F/2RT)$$

At an equilibrium state, the reactions between free ions and surfaces sites can be determined by using law of mass action as follows (Hosokawa et al., 2011b),

$$K_{ceq}=\frac{[\equiv SiOHX]}{[\equiv SiOH]\gamma_X[X]}exp\left(\frac{-F\psi_d}{RT}\right) \quad X=K^+,Ca^{2+},Na^+,Cl^- \ldots \tag{2.38}$$

where K_{ceq} is the equilibrium constant for adsorption/desorption reactions between C-S-H and *X-th* ionic species, and γ_X is the activity coefficient of *X-th* ionic species. The equilibrium constants for sorption reactions of main species in pore solution are given in Table 2.1. For sodium and potassium ions, equilibrium constants are related to Ca/Si ratio in C-S-H, whereas those for chloride and calcium ions are not (Tran et al., 2018; Guo et al., 2022). Ca/Si ratio is assumed to be unchanged in this study. Thus, the initial equilibrium constants for all physiochemical reactions are constants as shown in Table 2.1. The number of reaction sites on C-S-H surface is determined by the specific surface area exposed to pore solution and concentration of C-S-H. In the present thesis, the specific surface area of C-S-H is 500 m^2/g (Pointeau et al., 2006).

For elementary (single-step) reactions, the reaction rates are assumed to be proportional to the decline in reactant concentrations and the increase in product concentrations. Mathematically, it can be described as follows,

$$r_j = k_j^f \prod_{i \epsilon react} (\gamma_i C_i)^{n_{ij}} - k_j^b \prod_{i \epsilon prod} (\gamma_i C_i)^{n_{ij}} \tag{2.39}$$

where j is the *j-th* thermodynamic reaction in concrete, k_j^f and k_j^b are forward and backward reaction rate coefficients, respectively, γ_i and C_i are the activity coefficient and concentration of *i-th* species, respectively, and n_{ij} is stoichiometric coefficient of *i-th* species in *j-th* thermodynamic reaction.

Forward or backward reaction rate coefficients are temperature-related and can be calculated by Arrhenius equation as follows (Samson and Marchand (2007)),

$$k_j^f = A^f exp(\frac{-E_a}{RT}) \tag{2.40}$$

$$k_j^b = k_j^f / K_{eq} \tag{2.41}$$

where A^f is the frequency factor of forward reaction, E_a is activation energy, which is the minimum amount of energy required for a reaction to take place, and K_{eq} is the reaction equilibrium constant for physical or chemical reactions. The forward reaction coefficients at room temperature are given in Table 2.1.

Each ionic species is involved in more than one reaction. Therefore, the mass transfer rate of a specific species in concrete can be calculated as follows,

$$R_i = \sum_j n_{ij} r_{ij} \quad j=1,\ldots,n \tag{2.42}$$

where R_i is the mass transfer rate of *i-th* species between liquid and solid phase, n_{ij} and r_{ij} are the stoichiometric coefficient and reaction rate of *i-th* species in *j-th* reaction, respectively.

Pore evolution refers to the changes in pore size, shape, and distribution and overall porosity within concrete over time. It can affect the mechanical, transport, and durability properties of concrete. Every type of cement hydrate in concrete has its own individual volume density as listed in Table 2.3, which indicates that thermodynamic reactions can change the volume of all cement hydrates and eventually change the porosity of concrete. Based on the phase equilibrium calculated by thermodynamic reaction term, the time-dependent porosity can be calculated by,

$$\rho_t = \rho_0 - \sum \frac{m_p}{\theta_p}(C_p^t - C_p^0) \tag{2.43}$$

where m_p and θ_p are the molar mass and density of *p-th* hydrate phase, respectively. ρ_t and ρ_0, C_p^t and C_p^0 represent the porosities of concrete and the concentrations of *p-th* hydrate phase at time *t* and 0, respectively. Table 2.3 gives the molar mass and density of hydration products involved in this study.

Table 2.3 The average molar mass and density of each solid phase (Balonis and Glasser, 2009).

Phase (formula)	Molar mass (g/mol)	Density (g/cm^3)
AFt ($C_3A{\cdot}3CaSO_4{\cdot}26H_2O$)	1255.1	2.331
AFm ($C_3A{\cdot}CaSO_4{\cdot}12H_2O$)	622.5	2.015
Friedel's salt ($C_3A{\cdot}CaCl_2{\cdot}10H_2O$)	561.3	2.064
C-S-H ($5CaO{\cdot}3SiO_2{\cdot}6.3H_2O$)	574.2	2.331
CH ($Ca(OH)_2$)	74.1	2.111

A positive correlation exists between porosity and ionic diffusion coefficient. As porosity increases, the ionic diffusivity tends to increase, indicating that ions can more easily penetrate or move in or out from concrete matrix. This is because a higher porosity results in a more permeable material with a greater number of interconnected voids, providing easier pathways for ionic transport. Samson and Marchand (2007) proposed a refined Kozeny-Carman model to describe the relationship between effective diffusion coefficient and variation of porosity, which is expressed as,

$$D_i = D_i^0 \left(\frac{\rho_t}{\rho_0}\right)^3 \left(\frac{1-\rho_0}{1-\rho_t}\right)^2 \tag{2.44}$$

where D_i, D_i^0 is the initial diffusion coefficient of *i-th* ionic species at time t and 0, respectively.

2.2.5. Polarization

2.2.5.1 Overpotential

Polarization is the change in potential of an electrode from its equilibrium state due to the passage of current in a galvanic or electrolytic cell. This change is caused by reactions taking place at electrode surfaces, which can modify the distribution of charge and consequently alter electrode potential. Polarization can be observed in both cathode and anode, leading to either a more negative or positive potential, respectively. Therefore, in an electrochemistry system of concrete, such as rapid chloride migration test (RCM), accelerated chloride migration test (ACMT), impressed current cathodic protection (ICCP), and electrochemical chloride removal (ECR), polarization can lead to a potential drop between electrode and concrete surface. In other words, an extra potential (overpotential) required for the electrochemical reactions can reduce the actual voltage applied on concrete and affect the efficiency and performance of RCM, ACMT, ICCP or ECR.

For example, NT BUILD-492 (1999) suggested a fixed overpotential with a value of 2 V to reflect the negative effect of polarization on non-steady-state migration process for the calculation of chloride migration coefficient as follows,

$$D_{nssm} = \frac{0.0239TL}{(U\text{-}2)t} * \left[x_d\text{-}0.0238 \sqrt{\frac{TLx_d}{U\text{-}2}} \right] \tag{2.45}$$

where D_{nssm} (x10^{-12} m^2/s) is non-steady-state migration coefficient, U is pre-designed voltage of external direct current (DC) power, L (mm) is the thickness of concrete specimen, t (hour) is migration test duration, and x_d (mm) is penetration depth of chloride ions. "*U-2*" (voltage) represents actual output voltage on concrete surfaces. Therefore, the voltage of "-2" was applied to compensate for the overpotential effect. However, other studies reported that overpotential value varies with applied time, voltage and electrode materials. Mcgrath and Hooton (1996) proposed a new conduction setup to examine overpotential at electrode-concrete interfaces in migration tests by applying two reference electrodes. They found that overpotential increases from 1.91 to 2.36 V as external voltage is raised from 6 to 30 V. Spiesz and Brouwers (2012) investigated the variation of overpotential with different materials for electrodes when a 30 V voltage is applied. It was found that the magnitude of the overpotential change with current was in the range of 1.8~2.2 V for stainless steel electrodes and 1.5~1.8 V for MMO-TiO2 electrodes. The external voltage and conditions of electrolyte applied in existing migration tests are not fixed. For example, the external voltage suggested in NT BUILD 492 (1999) is in the range of 6~60 V. The concentration of NaCl solution in cathodic cell and electrode material in different experiments are different (Chen et al., 2021; Spiesz and Brouwers, 2012; Jiang et al., 2013). However, there is limited experimental data about overpotential in migration tests. So, it is still not certain whether a 2-V overpotential is applicable for all cases with different electrode materials, external voltages, and various types of concrete. Moreover, the effects of polarization on inside chloride penetration during migration tests have not been investigated in either experimental or numerical studies.

The application of an external electric field in an ICCP system also results in a change in potential at electrodes. This potential shift refers to the change in overpotential caused by polarization process. A 100-mV potential shift at cathode is necessary to ensure the effectiveness of cathodic protection as given in BS 7361-1 (1991). Oleiwi et al. (2018) found that overpotential shift at cathode varies with chloride-contaminated conditions, applied currents through concrete, and time. Hassanein et al. (2002) and Muehlenkamp et al. (2005) developed two 2-D numerical models to investigate potential shift in ICCP system by introducing a time-varying electrical boundary at cathode. They discovered that the value of overpotential shift is significantly influenced by the cathodic Tafel slope, external voltage, and pore saturation of concrete.

Overpotential at electrode-electrolyte can be classified into three categories: activation, ohmic and concentration overpotential. An activation overpotential is an extra potential above equilibrium potential expected to overcome the activation barriers of electrochemical reactions. It can be calculated by the Tafel equation as follows,

$$\eta_{act} = \beta_{TF} \log \frac{i}{i_0} \tag{2.46}$$

where η_{act} is activation overpotential, β_{TF}, i_0, and i represent the Tafel slope, exchange current density, and current density passing through electrodes. Tafel parameters are determined by experiments. There are many factors that can influence the value of these parameters, such as the types of electrochemical reactions, concentrations of electrolyte, materials of electrodes, temperature, and so on. The Tafel parameters for the oxygen reduction reaction (ORR) and hydrogen evolution reaction (HER) taking place at cathode and oxygen evolution reaction (OER) taking place at anode are summarized in Table 2.4.

Table 2.4 Tafel parameters for different electrochemical reactions involved in migration tests (Xia et al., 2019; Wang et al., 2020).

Tafel parameters	Notation	ORR	HER	OER
Tafel Slope (mV/decade)	β_{TF}	100~490	30~208	24~199
Exchange current density ($\times 10^{-7}$A/m^2)	i_0	62.5~2000	1400~10000	6~1000

Concentration overpotential is aroused by the concentration difference between electrolyte and electrode surface. It occurs when an electrochemical reaction is quick enough to lead to an accumulation of products or depletion of reagents near electrode surfaces. The value of concentration overpotential is described as:

$$\eta_{conc} = \frac{RT}{nF} ln(1 - \frac{i}{i_L}) \tag{2.47}$$

where n represents the number of transferred electrons in electrochemical reactions, and i_L is the limiting current density.

Ohmic overpotential can be calculated by using Ohm's law as follows,

$$\eta_{ohmic} = I\Omega \tag{2.48}$$

where I is current and Ω is the combination resistance between electrode and electrolyte.

2.2.5.2 Electrochemical reactions

In electrochemical system of concrete, cathodic reactions taking place at cathode surfaces can be expressed as:

$$2H_2O + O_2 + 4e^- = 4OH^- \quad (2.49)$$

$$4H_2O + 4e^- = 4OH^- + 2H_2 \quad (2.50)$$

Whereas oxygen evolution reactions at anode can be described as:

$$4OH^- = 2H_2O + O_2 + 4e^- \quad (2.51)$$

$$2H_2O - 4e^- = 4H^+ + O_2 \quad (2.52)$$

Based on charge conservation, current density flow through cathode is carried by flux of generated hydroxyl ions. Current density flow through anode is contributed by fluxes of hydrogen and hydroxyl ions. So that the flux boundary conditions at anode and cathode are (Li and Page, 2000):

$$\frac{I_c}{F} = z_{OH} J_{OH} \quad (2.53)$$

$$\frac{I_a}{F} = z_{OH} J_{OH} + z_H J_H \quad (2.54)$$

$$J_i|_{x=0,\ x=L} = 0, \qquad i \neq OH^-, H^+ \quad (2.55)$$

This means that the fluxes of hydroxyl and hydrogen ions at electrodes are determined by an externally applied electric field, while the fluxes of other ionic species can be assumed to be zero. In electrochemical rehabilitation process, current density at electrode, I_c or I_a, is equal to externally applied current density. Hydroxyl ions generation reactions (2.49) and (2.50) at inside steel bar can lead to a high alkaline environment in concrete to protect the passive film at steel surface (Liu and Shi, 2012; Mao et al., 2019).

For rapid chloride penetration systems, such as RCM and ACMT tests, both anodes and

cathodes are placed out of concrete rather than inside of concrete. Due to the volume of two electrolyte reservoirs located outside of concrete is much larger than that of pore solution in concrete, the influence of the generation and/or consumption of hydroxyl and hydrogen ions is usually ignored in existing numerical modelling (Xia and Li, 2013; Liu et al., 2015a; Yu et al., 2019).

2.2.6. Coupling of multi-physical fields

The penetration process of chloride ions in concrete is always a combination of basic physical and chemical processes introduced in Section 2.2.1 to 2.2.5, such as diffusion, convection, electromigration, reactions, and so on. Different service environments for concrete structures involve different combinations of these basic processes. Based on the mechanisms of diffusion, convection, reactions and migration, the flux of *i-th* species taking place in a transport medium under the action of multi-physical field can be written as:

$$J_i = -D_i \nabla C_i - D_i C_i \frac{z_i F}{RT} \nabla \emptyset + C_i u \tag{2.56}$$

With consideration of physical and chemical reactions between free ions and hardened cement matrix, the mass conservation of ions in concrete can be expressed as,

$$\frac{\partial C_i}{\partial t} + \nabla \cdot J_i = R_i \tag{2.57}$$

where R_i is the mass transfer rate of *i-th* ionic species in concrete, which can be calculated by Equations (2.22), (2.24), (2.26), (2.29), and (2.42). Substituting Equation (2.56) into (2.57), it yields,

$$\frac{\partial C_i}{\partial t} = \nabla\left[\underbrace{D_i \nabla C_i}_{①} + \underbrace{D_i C_i \frac{z_i F}{RT} \nabla \emptyset}_{②} + \underbrace{C_i u}_{③}\right] + \underbrace{R_i}_{④} \tag{2.58}$$

where terms ①, ②, ③, and ④ represent the diffusion, migration, convection, and reactions processes involved in chloride ingress in concrete. The selection of specific terms in governing Equation (2.58) is determined by the conditions of service environment. Coupled with the governing equations of electric field (Equations (2.12), (2.13), (2.19), and (2.20)) and reaction items (Equations (2.22), (2.24), (2.26), (2.29), and (2.42)), the time and space distribution of each ionic species and/or solid hydrate within concrete can be evaluated. This thesis focuses on the study of saturated concrete. Therefore, convection term will not be included in models presented in Chapter 3.

In conclusion, this section provides a summary and discussion of the mechanisms of each sub-process involved in chloride transport in concrete. These include diffusion, convection, electromigration, physicochemical adsorption, desorption, and polarization at electrodes. Based on the above-described individual mechanisms and basic equations, a coupling theoretical model is presented and expected to describe chloride transport in concrete structures serviced in varying and complex environments.

2.3. Experimental methods of chloride transport in concrete

2.3.1. Chloride diffusion test

2.3.1.1 Bulk diffusion test

Bulk diffusion test was originally developed in AEC laboratory to measure non-steady-state chloride diffusion coefficient based on Fick's Second Law, which was adopted in standard NT BUILD-443 (1995). To avoid convection and adsorption processes, concrete specimens in this test are initially cured for 28 days at 20℃ and subsequently immersed in limewater until they reach a fully saturated state. This means that only ionic diffusion

is involved in this test. As shown in Fig. 2.2, only one surface of a concrete sample is exposed to 2800 mol/m^3 NaCl solution, while all other surfaces are sealed. The typical exposure period for normal concrete is 35 days, but for high strength concrete, this period should be extended to more than 90 days. Once exposed period is complete, concrete specimens are sliced into sections with a thickness of 0.5~1 mm, and these slices will be ground off to obtain chloride concentration.

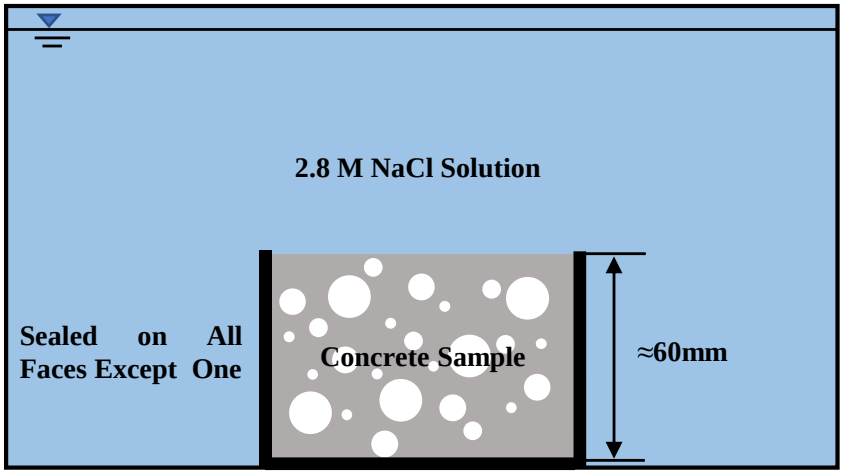

Figure 2.2 Schematic of bulk diffusion test

2.3.1.2 Salt ponding test

Ponding test has been standardized as AASHTO-T259 (1980) to evaluate the apparent diffusion coefficient of chloride ions. A concrete sample in ponding test is required to be moist-cured for 14 days, and then placed in a room with 50% relative humidity for 28 days. As shown in Fig. 2.3, the surrounding four faces of a sample are sealed, while top surface is covered by 3% (520 mol/m^3) NaCl solution and bottom surface is exposed to environment with 50% relative humidity. After 90-day testing, the mean chloride concentration is measured for each 12.7mm-thick slice to plot chloride profiles. This thickness is much larger than that in Bulk diffusion test and may lead to an inaccurate diffusion coefficient. It should be noted that both diffusion and capillary suction are involved in ponding test, and the latter may influence the diffusion coefficient obtained from the test.

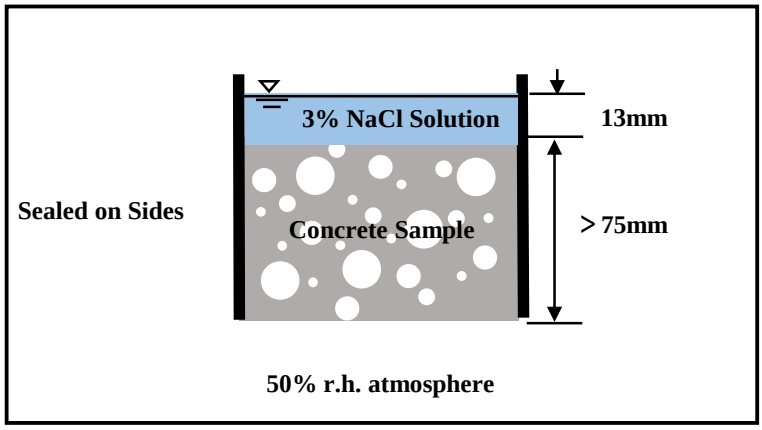

Figure 2.3 Schematic of salt ponding test

2.3.1.3 Short-term immersion test

Bulk diffusion and ponding tests take several months to get a sufficient chloride profile for estimating the chloride resistance of concrete. In order to reduce test duration, Park et al. (2014) designed a new immersion test that involves minimizing the size of concrete samples. As shown in Fig. 2.4, the setup of the test resembles that of ponding test. In contrast to long-term tests, where chloride concentration in source solution is approximately constant, chloride concentration in this short-term test gradually decreases due to the limited size of solution container. After testing, the variation of chloride concentration in container rather than that in samples is measured to calculate chloride diffusion coefficient.

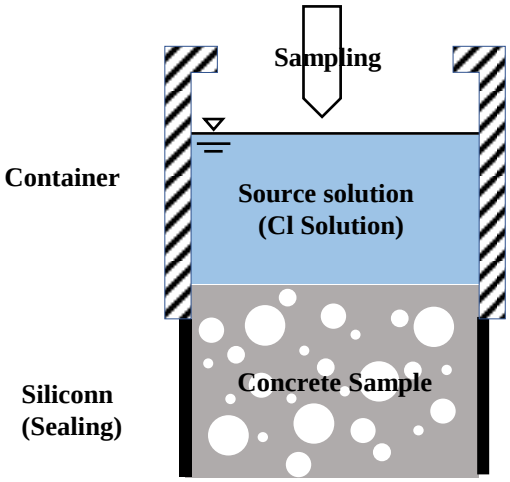

Figure 2.4 Schematic of short-term immersion test

2.3.2. Chloride migration test

Diffusion tests usually take a long time to obtain information on chloride penetration. The application of an external electrical field can help speed up the movement of chloride ions. Many migration tests, including coulomb test, steady-state migration test and non-steady-state migration test, have been proposed to assess chloride diffusivity in concrete in a reasonable time (Whiting, 1981; ASTM-C1202, 2012; Truc et al., 2000; NT BUILD-492, 1999).

2.3.2.1 Coulomb test

Coulomb test and rapid chloride permeability test (RCPT) were originally developed by Whiting (1981) and later standardized by American Association of State Highway and Transportation Officials (AASHTO) and American Society of Testing and Materials (ASTM) as AASHTO-T277 (1983) and ASTM-C1202 (2012), respectively. As shown in Fig. 2.5, a saturated sample is placed between two chambers filled with 520 mol/m^3 NaCl solution and 300 mol/m^3 NaOH solution, respectively. A 60 V DC power was applied to auxiliary electrodes placed on concrete surfaces during Coulomb test. The total charge passed through concrete sample after a 6-hour test is used to calculate the chloride permeability of concrete. Several empirical equations were established to reflect the relationship between passing charge and diffusion coefficient in concrete (Berke and Hicks, 1992; Wee et al., 2000; Kou, 2006; Huang and Yang, 2018; Huang and Yang, 2020).

In the past two decades, this method has been criticized by many researchers for two reasons. One is the temperature rise during Coulomb test caused by high external current, which would increase the electrical conductivity of concrete and result in decomposing of some hydration products (Shi et al., 2019). The other is the contribution of other ionic species in pore solution has a remarkable effect on total charge passed through concrete. Mcdonald (1994), Shane et al. (1999), and Shi (2004) confirmed that the inclusion of supplementary cementing materials or corrosion inhibitors in concrete can change the

ionic strength in pore solution and eventually affect the electrical conductivity of concrete. Mcdonald (1994) found that the increase in chloride penetration depth is much lower than the increase in coulomb value. To mitigate the impact of temperature increase during the coulomb test, it is recommended to assess chloride diffusivity based on the charge passed in initial 30 minutes and the initial current or conductivity (Feldman et al., 1999). RCPT has been developed to reduce the impact caused by all other ions in pore solution. This method uniformizes the conductivity of pore solution for different concrete specimens by saturating concrete samples with a high concentration (4000 mol/m^3) of NaCl solution.

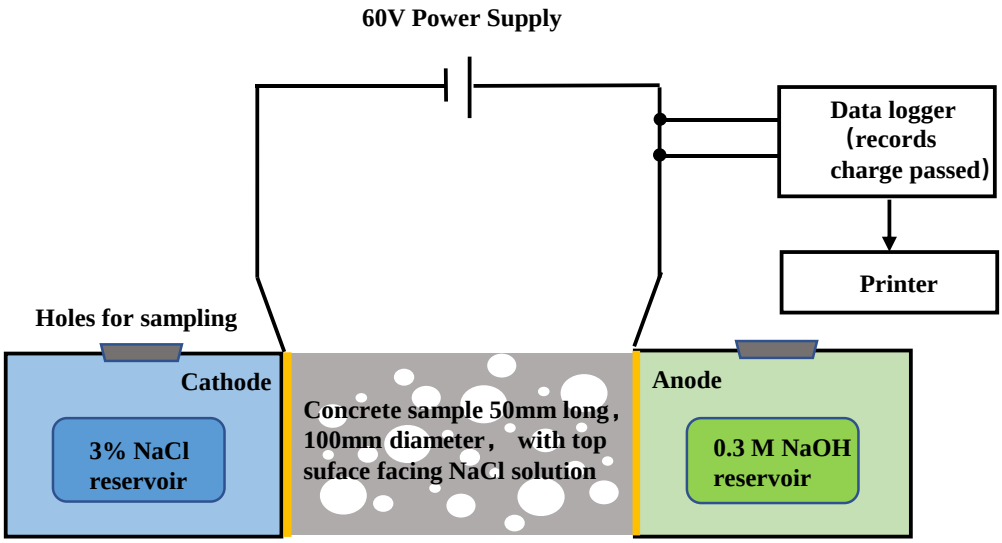

Figure 2.5 Schematic of rapid chloride permeability test (AASHTO-T277, 1983)

2.3.2.2 Steady-state migration test

To avoid the drawbacks of RCPT test, NT BUILD-335 (1997) provided a new method to determine chloride diffusion coefficient. As shown in Fig. 2.6, a constant voltage is applied to the concrete specimens, so that chloride ions can migrate from negative compartment with 5% NaCl (1000 mol/m^3) solution to positive compartment with 300 mol/m^3 NaOH solution. To reduce the influence of other factors in pore solution, concrete cylinder is immersed in saturated $Ca(OH)_2$ solution until mass stability is achieved prior to testing.

The applied voltage is at least 12 V. And it cannot be too high to keep temperature below 40°C during steady-state migration test. To maintain the chloride concentration approximately constant in the negative compartment, NaCl should be added through top hole during the test. Chloride migration coefficient can be calculated using the Nernst-Plank equation when the change in chloride concentration in downstream cell remains approximately a constant.

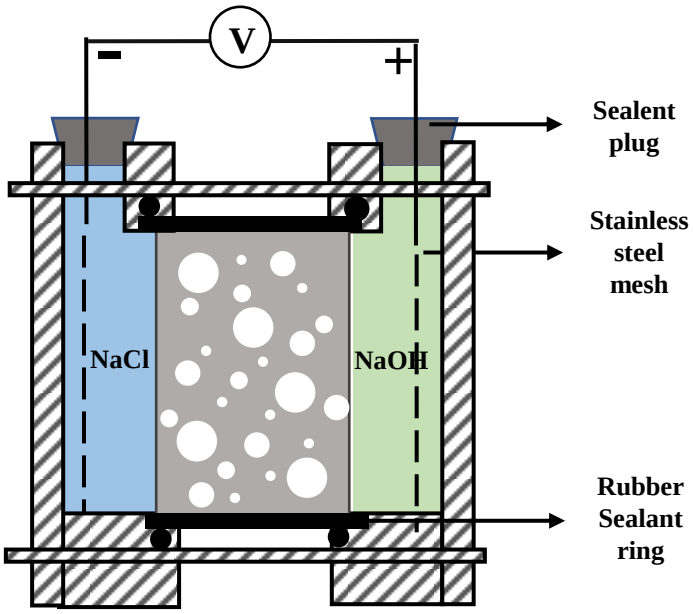

Figure 2.6 Schematic of steady-state migration test (NT BUILD-335, 1997)

It is worth noting that, in NT BUILD-335 (1997), electrical potential used for chloride diffusivity calculation is the value between two electrodes instead of that between two surfaces of specimen. This means that the polarization of electrodes is ignored. Mcgrath and Hooton (1996) modified the setup of NT BUILD-335 to measure the actual electrical potential across concrete specimens. As shown in Fig. 2.7, two reference electrodes are applied between specimen surfaces and wire mesh electrodes. Additionally, the quick migration process may lead to an accumulation or consumption of chloride ions in NTbuild 355 system. Therefore, an agitating facility was introduced to eliminate concentration gradients in both negative and positive cells (Delagrave et al., 1997). It also takes a long time to reach a steady-state condition in downstream cell of NT BUILD-335

(1997) test. Therefore, Truc et al. (2000) developed a novel method to calculate the chloride migration coefficient by using the flux of chloride ions at the upstream surface. This method assumed that the inward flux of chloride ions at negative surface of specimen is equal to the outward flux at positive surface under steady-state condition. They found that the flux in upstream cell can reach a constant state in two or three days. It was suggested that this upstream method could also be employed to determine chloride migration coefficient of concrete that has already suffered from chloride attack.

In addition, a larger electrolyte cell was used to mitigate temperature rise aroused by Joule effect in this steady-state migration test by Yang et al. (2002). However, the effect of electrochemical reactions at anode is difficult to quantify. For instance, the generation of chlorine gas in the downstream cell would result in an uncertain chloride migration coefficient.

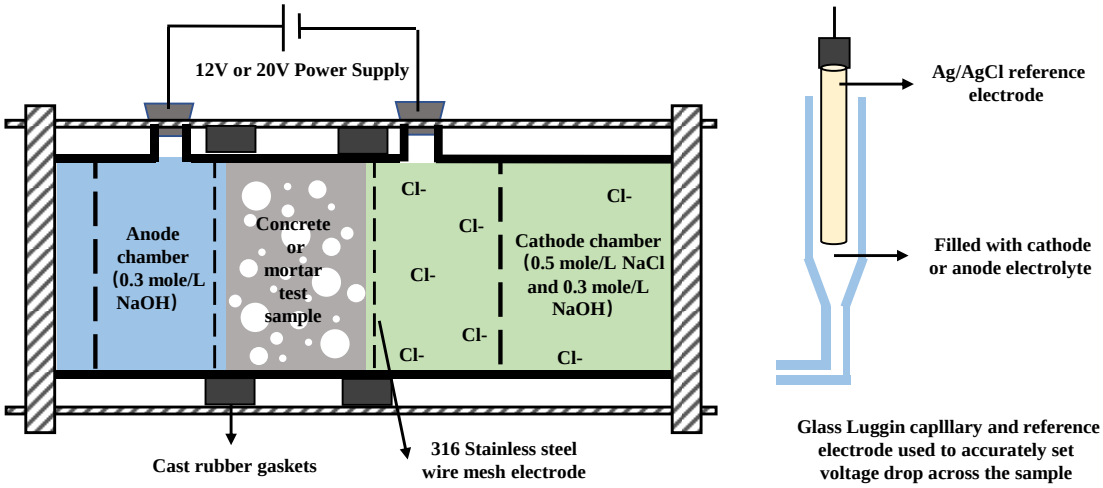

Figure 2.7 Schematic of steady-state migration test setup modified by Mcgrath and Hooton (1996)

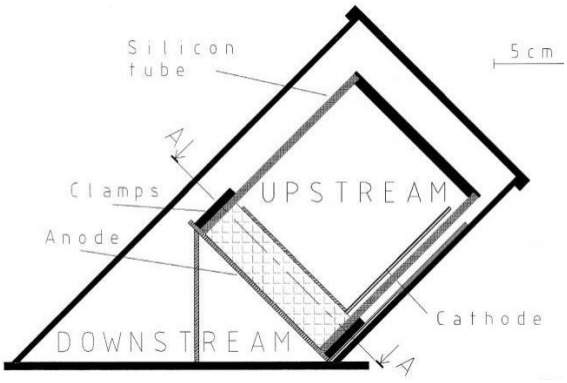

Figure 2.8 Schematic of upstream test setup (Truc et al., 2000)

2.3.2.3 Non-steady-state migration test

To shorten the test duration, a non-steady-state migration test, named rapid chloride migration test (RCM), was proposed to calculate migration coefficient by measuring chloride penetration depth (Tang and Nilsson, 1992). Lately, this method has been standardized as NT BUILD-492 (1999). As shown in Fig. 2.9, a concrete specimen with 100 mm diameter and 50 mm thickness is placed in a rubber sleeve, and then it is tilted into the cathodic cell filled with 10% (2000 mol/m^3) NaCl solution.

The external applied voltage and test duration are determined by the magnitude of initial current obtained from a pre-test with a 30 V initial voltage. The application of varied voltages and durations aims to minimize significant temperature rising and achieve a suitable chloride penetration depth. After testing, the penetration depth is determined by using a colorimetric method. For OPC specimens, colorimetric method suggests that the chloride concentration at boundary, where a notable color change is observed, is 70 mol/m^3. This value may exhibit variation depending on the specific types of binders used in concrete (Liu et al., 2017; Zhao et al., 2021; Meck and Sirivivatnanon, 2003). Due to its short testing duration, simple measurement and calculation procedure, RCM test has been widely used for evaluating chloride resistance in various concrete types.

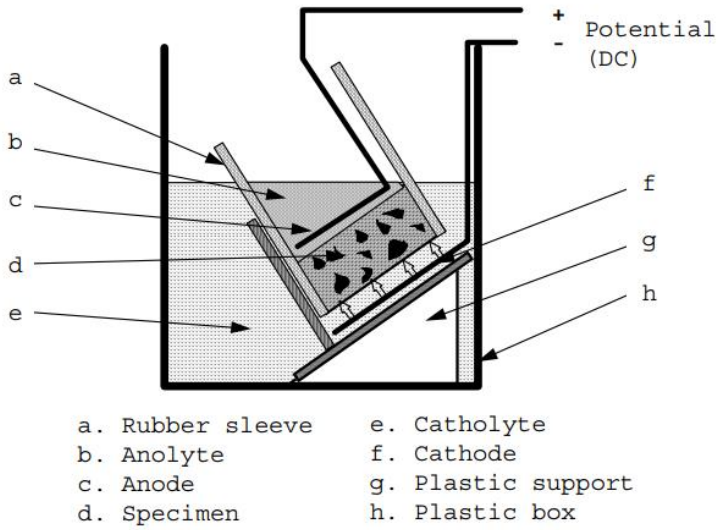

Figure 2.9 Schematic of RCM test (NT BUILD-492, 1999)

2.3.2.4 Resistivity Techniques

Electrical resistivity, the reciprocal of conductivity, is a measure of the resistance of a material to the flow of electric current. The diffusivity of ions in a solution is directly proportional to the product of solution conductivity and ionic mobility, as elucidated by Nernst-Einstein equation (Snyder and Marchand, 2001; Streicher and Alexander, 1995;). Therefore, the conductivity of pore solution can provide a useful estimate of chloride diffusivity in concrete. The relationship between pore solution conductivity and chloride diffusivity is described in articles (Backe et al., 2001; Sengul and Gjørv, 2008; Polder and Peelen, 2002; Sengul, 2014; Yoo et al., 2017). The conductivity of concrete can be determined by a direct or alternating current electric circuit. The applied voltage in resistivity tests is less than or equal to 10 V to avoid heating during testing. In this method, concrete specimen is first dried and then vacuum saturated. It assumes that saturating solution is identical before and after vacuum saturation process, which means that the conductivity of pore solution is equal to that of saturating solution. Nevertheless, there is a possibility that other ionic species may undergo precipitation during drying process. Once the saturation process takes place, these previously precipitated ions may dissolve and return to pore solution, thereby affecting its conductivity (Xia and Li, 2013).

Therefore, a high-conductivity saturating solution is suggested in resistivity tests to minimize the impact of other ionic species. Due to the short test duration and simple operation, this technique is a sound method to obtain the chloride diffusivity of concrete. However, it should be noted that this method does not consider the chloride binding and the microcracks generated in drying process.

In conclusion, effective chloride diffusivity is a key index for both durability design and service life prediction of concrete in chloride-rich environments. Both chloride diffusion and migration tests offer valuable insights into the chloride penetration mechanism and the effective evaluation of chloride diffusivity. Diffusion tests are relatively simple and easy to perform, making them accessible to many laboratories and technicians. However, diffusion tests take several months to obtain an appropriate result, which limits their applicability to different concrete types, especially high-strength concrete. The setup of chloride migration tests is more complex and requires specialized equipment. However, migration tests offer faster results and are applicable to a wider range of concrete mixtures and exposure conditions. Nowadays, rapid chloride migration and accelerated chloride migration tests are widely used in laboratories. The application of an external electric field in these migration tests may result in polarization and enhance the ion-ion interactions between different ionic species. Therefore, further investigations should be conducted to find out the underlying impacts of the external electric field in migration test.

2.4. Analytical methods of chloride transport in concrete

2.4.1. Empirical models of chloride transport

2.4.1.1 Macro-scale model

The error function solution of Fick's second law has been used to predict the diffusion coefficient in chloride diffusion tests, which is based on the assumption that concentration gradient is the only factor influencing chloride transport in concrete. However, it should

be noticed that the surface concentration of chlorides undergoes changes over time during the long-term natural diffusion process. Amey et al. (1998) summarized a linear function to describe the buildup of chloride concentration at concrete surfaces in different service environments. Weyers (1998) found that chloride concentration at the surface of bridge decks increases with time and reaches a constant after 5-year exposure. Upon analyzing the results obtained from Weyers's study, an exponential function that relates surface chloride concentration to time has been summarized by Kassir and Ghosn (2002). Similarly, Pang and Li (2016) proposed an exponential model that describes a non-linear increase in surface-chloride concentration over a period of 20-year exposure. Shakouri and Trejo (2017) improved the time-variant model by considering the variation of surface-chloride concentration with both time and chloride concentration in exposure environments. Park et al. (2014) proposed an analytical solution for a short-time immersion test where the surface chloride concentration changes with time.

Additionally, the permeability of concrete structures continually changes during their service life due to the ongoing hydration process of cement-based materials. Therefore, an empirical equation has been developed to describe the time-dependent behavior of chloride diffusion coefficient as follows,

$$D_t = D_{ref} \left(t_{ref} / t \right)^m \tag{2.60}$$

where D_t *and* D_{ref} is the diffusion coefficients at any time t and at reference time t_{ref}, respectively, m is a constant dependent on binder types. This equation has been widely used in analytical models of chloride transport based on Fick's second law (Stanish and Thomas, 2003; Tang, 2008; Yang et al., 2018).

Nernst-Plank equation has been widely adopted to describe chloride migration process under the action of an externally applied electric field. Tang and Nilsson (1992) proposed a semi-infinite analytical model of non-steady-state migration by assuming that the interactions between chloride and other ionic species and cement matrix can be ignored.

The analytical solution can be expressed as follows,

$$C_x = \frac{C_s}{2}\left[e^{\frac{zFEx}{RTL}} erfc\left(\frac{x+(\frac{zFE}{RTL})D_{nssm}t}{2\sqrt{D_{nssm}t}}\right) + erfc\left(\frac{x-(\frac{zFE}{RTL})D_{nssm}t}{2\sqrt{D_{nssm}t}}\right)\right] \quad (2.61)$$

where C_s *and* C_x is the chloride concentrations at concrete surface and at penetration depth x, respectively, *erfc* is the complement error function. *F, R, E and* D_{nssm} *represent* Faraday's constant, gas constant, electric field, and non-steady-state migration coefficient, respectively. Chloride profile calculated by this model has a sharp front, which is not consistent with what was observed in RCM tests. Stanish et al. (2004) introduced two material parameters to eliminate sharp fronts in prediction results. This analytical solution can be expressed as,

$$C_x = C_s\left[1-f(\frac{xRT}{zFEDt}, \alpha_1, \alpha_2)\right] + C_{ini} \quad (2.62)$$

where D, C_{ini}, α_1 and α_2 represent the diffusion coefficient, the initial concentration in pore solution, the variation and average modification parameter of penetrability, respectively. Jiang et al. (2013) suggested a semi-empirical model to obtain the time and space distribution of chlorides in migration test, in which chloride migration coefficient varies with source concentration and penetration depth. It can be written as follows,

$$D_{nssm} = \frac{RT}{zFE}\frac{a_1 x + a_2 x^2}{t} \quad (2.63)$$

where a_1 *and* a_2 are fitting parameters for source concentration employed in migration tests.

Moreover, w/c ratio and supplementary cementing materials in concrete also have a significant influence on chloride diffusivity. For the replacement rate of fly ash below 50%

and that of slag below 70%, the diffusion coefficient can be described as follows (Violetta, 2002),

$$D=1\times10^{(-12.06+2.4*w/c*m)} \tag{2.64}$$

$$m=0.2+0.4*(\%FA/50+\%GGBS/70) \tag{2.65}$$

For the replacement rate of silica fume below 15%, it can be expressed as follows,

$$D_{SF}=D_{OPC}\times e^{-0.165*\%SF} \tag{2.66}$$

where *FA, GGBS,* and *SF* represent fly ash, ground granulated blast-furnace slag and silica fume, respectively, D_{OPC} and D_{SF} are chloride diffusion coefficients of ordinary Portland concrete and concrete with silica fume, respectively.

2.3.1.2 Micro-scale model

In the micro-scale view of ionic transport, the effective diffusivity of porous materials is determined by pore structure, including porosity, tortuosity and constrictivity. According to Archie equation and Bruggeman asymmetric medium theory, the conductivity of cement-based materials can be confirmed as follows (Backe et al., 2001; Sengul and Gjørv, 2008; Liu et al., 2013),

$$\sigma=\sigma_p\phi^n \tag{2.67}$$

where σ and σ_p represent the conductivity of porous material and pore solution, respectively, ϕ is porosity, and n is determined by the constrictivity and tortuosity of pore structure and is usually in the range of 1~2. Based on the Nernst-Einstein equation and Archie equation, the correlation between the diffusion coefficient and conductivity in terms of cement-based materials can be expressed as $D/D_p= \sigma/\sigma_p$ (Yoo et al., 2017).

Therefore, the relationship between chloride diffusion coefficient and porosity is given as follows,

$$D=D_p\phi^n \tag{2.68}$$

where D_p is the chloride diffusivity in pore solution. To specifically describe the effects of tortuosity and constrictivity, the relationship is rewritten as follows (Sun et al., 2011),

$$D=D_p\frac{\delta}{\tau^2} \tag{2.69}$$

where τ and δ represent tortuosity and constrictivity of pore structure, respectively. Moreover, it has been reported that the streamline of unsteady transport process in medium with multiple pore sizes, such as ionic migration in concrete, does not follow the centerline of connected pore paths, which leads to a more tortuous migration path (Gommes et al., 2009; Holzer et al., 2013). Therefore, the relationship between tortuosities of diffusion and migration processes can be described as follows (Yang et al., 2017),

$$\tau_m=a_0\tau_d \tag{2.70}$$

where a_0 represents the pore constrictivity parameter of ionic migration, which is highly influenced by the size ratio between the smallest and largest pores and is in the range of 1.5~3 for various cementitious materials used in concrete (Yang et al., 2017).

Damrongwiriyanupap et al. (2011) suggested that the relationship between pore structure and chloride diffusion coefficient in each phase in RAC can be calculated as follows,

$$D=\frac{2(1-(V_p+V_p^c))}{S^2}(V_p+V_p^c)^{4.2} \tag{2.71}$$

where V_p is the porosity of each phase, V_p^c is critical porosity (the porosity at which pore space is first connected) of each phase, and S is surface area of pore.

Garboczi and Bentz (1996) suggested a non-linear dependency of ionic diffusivity on the distance approaching the aggregate surface. It can be described as follows,

$$D_x=D_p(0.001+0.07\phi(x)^2+1.8\cdot H(\phi(x)-0.18)\cdot(\phi(x)-0.18)^2) \tag{2.72}$$

where $\phi(x)$ is the porosity at a distance x approaching to aggregate surface, H is Heaviside function, and 0.18 is a critical connection porosity of capillary pore. This changing porosity in ITZ has been observed in an image analysis conducted by Diamond and Huang (2001).

Zheng et al. (2014) proposed a power-law equation to calculate the chloride diffusivity in cement and ITZ subjected to external mechanical loading, which can be expressed as,

$$D=D_p\frac{2\phi^{2.75}D_p}{\phi^{1.75}(1-3\phi)+14.4(1-\phi)^{2.75}} \tag{2.73}$$

2.4.2. Effective medium models of chloride transport

The effective medium theory is a theoretical framework used to describe the behavior of composite materials and their physical properties. This theory assumes that the composite material can be treated as a homogeneous medium with effective properties that are different from those of its constituent materials. The effective properties are determined by the geometrical and physical properties of the composite, such as the volume fraction, shape, and size of the constituent particles or pores. The heterogeneous concrete can be treated as a composite consisting of cement matrix, aggregate, and ITZ. With the knowing chloride diffusivity and volume fraction of each individual phase, a series of effective medium models have been proposed to calculate the effective chloride diffusivity of

heterogenous concrete by using different homogenized methods.

Hobbs (1999) proposed two two-phase composite concrete models, in which aggregates and cement paste were assumed to be parallel. With the assumption that the decrement of chloride concentration and mass transport content of chlorides are the same in both aggregate and cement paste, the upper and lower bounds of effective diffusivity D_{eff} are estimated by following equations,

$$D_{eff}^{min} = \frac{1}{V_a/D_a + (1-V_a)/D_m} \tag{2.74}$$

$$D_{eff}^{max} = V_a D_a + (1-V_a)/D_m \tag{2.75}$$

where D_a, D_m and V_a are the diffusion coefficients of aggregate and mortar, and the volume fraction of aggregate, respectively.

Xi and Bažant (1999) applied Maxwell's model to estimate effective diffusivity, in which aggregates were conceptualized as inclusions embedded within a homogeneous cement medium. By using the provided volume fraction and diffusivity for each phase, the effective chloride diffusion coefficient can be calculated as follows,

$$D_{eff} = D_p \frac{2D_p(1-V_a)+D_a(1+V_a)}{D_p(2+V_a)+D_a(1-V_a)} \tag{2.76}$$

A n-layer sphere model was originally developed to obtain the effective elastic and thermal behavior of multiply coated composites (Hervé and Zaoui, 1995). Caré and Hervé (2004) treated concrete as a three-phase composite consisting of aggregate, ITZ and cement paste and first used n-layer sphere approximation method to predict the effective chloride diffusivity of concrete. Under the assumptions that aggregates are uniformly coated by ITZ and that aggregates themselves are impermeable, the effective chloride diffusivity of concrete can be calculated as follows (Lu and Torquato, 1992),

$$D_{eff}=D_p\frac{6D_p(1-V_a)(V_a+V_I)+2V_I(D_I-D_P)(1+2V_a+2V_I)}{3D_p(2+V_a)(V_a+V_I)+2V_I(D_I-D_P)(1-V_a-V_I)} \tag{2.77}$$

where D_I is diffusion coefficient of ITZ, and V_I is volume fraction of ITZ. Zheng and Zhou (2007) used this three-phase sphere model to investigate the effects of the thickness of ITZ, maximum diameter, and grading curve of aggregate. Subsequently, Zheng and Zhou (2008) proposed a three-phase lattice model to examine the effects of aggregate shape, in which the effective diffusivity of equivalent aggregate, D_{ea}, is estimated as follows,

$$D_{ea}=D_I-D_I\frac{(1+\mu)^2V_a(2V_a+V_I)}{2\left((1+\mu)V_a+V_I\right)\left((1+\mu)V_a+\mu V_I\right)} \tag{2.78}$$

where μ is the ratio between the long and short axes of elliptical aggregate.

Sun et al. (2011) proposed a three-phase sphere model to predict the effective chloride diffusion coefficient of concrete, in which the non-linear distribution of porosity in ITZ was included. Ying et al. (2013a) proposed a five-phase analytical model of partially replaced aggregate concrete, which includes old aggregate, old ITZ, old residual mortar, new ITZ, and new mortar.

Yang and Weng (2013) developed a new analytical model to predict effective migration coefficient in two stages. In the first stage, the diffusivity of equivalent aggregate (aggregate plus ITZ) is determined by a double-layer sphere model. In the second stage, the overall migration coefficient, M_c, is calculated by using Mori-Tanaka theory, which is expressed as follows,

$$M_c=\left\{\frac{1}{M_m}+\frac{V_f\left(M_e-M_m\right)}{M_m\left(1-V_f\right)\left(M_e-M_m\right)S-V_f\left(M_e-M_m\right)+M_m}\right\}^{-1} \tag{2.79}$$

where M_m *and* M_e is migration coefficients of cement paste and equivalent aggregate, V_f is total volume fraction of aggregate and ITZ in concrete, and S is Eshelby tensor for inclusion solely existing in an infinite homogeneous medium.

Zheng and Zhou (2013) used Bruggeman's model to predict the chloride diffusivities of two-phase material composed of cement paste and equivalent aggregate. It can be described as follows,

$$V_{ea}\frac{D_{ea}-D_{eff}}{D_{ea}+2D_{eff}}+V_{cp}\frac{D_{cp}-D_{eff}}{D_{cp}+2D_{eff}}=0 \tag{2.80}$$

where V_{ea} *and* D_{ea} is volume fraction and diffusivity of equivalent aggregate, V_{cp} *and* D_{cp} is volume fraction and diffusivity of cement paste.

In conclusion, there are a large number of analytical ionic transport models proposed in the literature to predict effective chloride diffusivity. Empirical models have been developed by analyzing and summarizing the relationship between chloride diffusivity and time, surface-chloride concentration, and concrete pore structure. Effective medium models have been employed to characterize the impact of each individual phase (aggregates, cement paste, and ITZ) on the chloride diffusivity of multi-phase concrete. It should be noticed that most existing models have focused on concrete containing either 100% NA or 100% RA, and very few models are developed for concrete that includes both natural and recycled aggregates.

2.5. Numerical methods of chloride transport in concrete

2.5.1. Modelling of single-species transport

Assuming that there are no ion-ion interactions in pore solution and no reaction between free ions and hardened cement paste, a series of single-species models have been developed to simulate chloride diffusion process in composite concrete by using Fick's

second law. Tang (2008) proposed a ClinConc model to predict the distribution of free and total chloride in concrete containing silica fume and pozzolanic ash. In this 1-D model, the effects of temperature and binder types on chloride binding are investigated. Zeng (2007) presented a 2-D heterogeneous model consisting of circular aggregate and cement paste to investigate the influence of chloride binding and time-reducing effects on chloride diffusion coefficient in cement matrix. Li et al. (2012) developed a 2-D concrete model to investigate the effects of the volume fraction and shapes of aggregate on chloride diffusion in concrete. Based on numerical results, they suggested an upper and lower bound for effective diffusivity of heterogeneous concrete. Abyaneh et al. (2013) proposed a 3-D concrete model composed of three phases with distinct diffusivities to examine the effects of the orientation and axial ratio of elliptical aggregate on chloride diffusion coefficient.

At the same time, a series of five-phase models were established to evaluate the effective chloride diffusivity of RAC, in which original aggregate, old and new ITZs and mortars are included. Xiao et al. (2012) conducted a simulation that included only one piece of aggregate to estimate the effects of the aggregate shape, thickness of ITZ, adhesive rate of old mortar, and volume fraction of RCA. Then the influences of replacement rate and distribution of RA are investigated in a four-piece aggregate model presented by Ying et al. (2013b). Subsequently, a multi-aggregate five-phase model has been proposed to access general chloride diffusivity of RCA, in which aggregates are randomly distributed and generated following Fuller gradation (Hu et al., 2018).

Assuming that chloride transport is completely independent of the transportation of all other ionic species in pore solution, various models of chloride migration have been conducted based on Nernst-Plank equation. In these models, electrical fields are assumed to be constants and determined by applied voltages and the size of concrete specimens. Spiesz et al. (2012) and Spiesz and Brouwers (2012) proposed a homogenous model to obtain chloride concentration profiles in RCM test when different external voltages are applied. They suggested that non-equilibrium chloride binding can offer a more accurate

simulation of an electrically forced migration process. Li (2014) and Li et al. (2015) simulated chloride penetration process in migration tests with considering the pore size distribution in concrete. They found that the distribution of pore size and ion-exchange rate between large and small pores have significant influences on the wave front of chloride profiles in RCM tests. Du et al. (2020) developed a single-species transport model of accelerated corrosion test for concrete with cracks. They found that the width of cracks in concrete has a greater impact on electrically accelerated corrosion than natural corrosion.

2.5.2. Modelling of multi-species transport

Electric potential distribution in concrete can be influenced by each ionic species in pore solution, such as potassium, sodium, chloride, hydroxyl ions, and so on (Johannesson, 2010a; Liu, 2014). In turn, electrostatic potential would influence ionic transport process as given in Equation (2.11). However, the interactions between electric field and ionic species distribution in concrete are not included in abovementioned single-species modelling. Therefore, a series of multi-species transport models have been proposed. Numerical simulation of multi-species transport process can be characterized into two groups: current conservation law and Gauss's law methods.

2.5.2.1 Solving electrical field by using current conservation law

As given in Section 2.2.3, the relationship between ionic distribution and electrical field in concrete can be described by Equations (2.19) and (2.20), which are derived from current conservation law. This method can be used for cases with either a current density or a voltage boundary.

When there is no external electric field applied on concrete, current conservation method is called the zero current method, which is adopted to investigate the ionic diffusion in pore solution of concrete. Marchand (2001) investigated the influence of electrolytes with varying concentrations and ionic species by Fick's second Law and zero current method.

They found that the apparent diffusion coefficient calculated by current conservation law (Equation (2.19)) is time-dependent rather than the constant one adopted in Fick's Law. Khitab et al. (2005) calculated the chloride ingress profiles for both diffusion and immersion tests by using Nernst-Plank equation and zero current method. The numerically obtained penetration depths of chlorides are very close to the measurements in experiments. Johannesson (2010a) also simulated the multi-species diffusion in saturated porous material by using zero current method. Xia et al. (2019) used the zero current method to simulate multi-species transport and subsequent corrosion of steel bars induced by chloride ions.

Current conservation law also has been adopted to predict the efficiency of electrochemical rehabilitation techniques, where an external current density is applied to remove chlorides out of concrete or increase internal alkalinity of concrete. Li and Page (1998, 2000) and Wang et al. (2001) proposed several multi-species models to investigate the effects of activity coefficient, external current density, treatment time, chloride binding, and tortuosity on chloride removal. They found that the total amount of removed chlorides increased with the increase in current density and treatment time. Kubo et al. (2007) employed current conservation method to predict the efficiency of corrosion inhibitors injection and pH around steel when concrete is subjected to an external current density. They found that corrosion inhibitors distribution and pH obtained from their numerical model fitted well with the experimental results. Liu and Shi (2012) and Mao et al. (2019) proposed a series of three-phase models to simulate electrochemical chloride removal and/or electrochemical lithium migration process in concrete. Numerical results exhibited that existing aggregates show two opposite effects on ionic transport. On the one hand, aggregates increase the tortuosity of ionic transport path, on the other hand, they reduce current density flowing through concrete specimen. More recently, Cheng et al. (2020) presented a new multi-species transport model that incorporates stirrup and porosity changes during ECR process. Their study revealed that chlorides removal has an obvious influence on concrete porosity. Additionally, the efficiency of chloride removal

is enhanced by stirrup.

Moreover, a series of numerical models have been developed to describe multi-species transport under the action of externally applied voltage by using current conservation method as given in Equation (2.20). Narsilio et al. (2007) explored the influence of chloride concentration in cathodic chambers and applied voltages on chloride diffusion coefficients, considering the interactions between different ionic species. Their findings revealed that an increase in upstream concentration will lead to a rise in the non-linearity of electrical potential. Friedmann et al. (2008a) investigated the variation of current density in migration test with considering chloride binding and concrete porosity. Marriaga and Claisse (2009) adopted this method to simulate membrane potential caused by different mobility of ionic species in concrete during ASTM test. Guo et al. (2021b) proposed a current conservation model to simulate the electrochemical corrosion control of concrete exposed to NaCl solution, in which electrochemical reactions at electrodes are involved.

2.5.2.2 Solving electrical field by using Poisson's equation

Poisson's equation is a partial differential equation that describes the relationship between electrostatic potential and charge distribution in a region of space, as given in Equation (2.11).

Samson et al. (1999b) originally employed Poisson-Nernst-Plank equation (PNP) to simulate multi-species diffusion in cement-based materials. Johannesson et al. (2007) proposed a 1-D model to investigate the multi-species diffusion and corresponding chemical reactions during the process. Numerical results showed that internal electrical field is very small but not equal to zero, which is aroused by multi-species coupling. Subsequently, Johannesson (2010a) simulated multi-species diffusion in saturated porous material by using zero current method and PNP method, respectively. The results showed that two approaches give the same distribution profiles for each species, although the

electroneutral condition is included in zero current method.

PNP equation has been used to investigate the mechanism of multi-species transport in non-steady-state migration tests. The effect of temperature on chloride penetration in migration test was investigated using a homogenous multi-species migration model proposed by Samson and Marchand (2007a). They found that an average constant temperature in simulation can lead to an overestimated or underestimated chloride diffusion coefficient due to different temperatures in service environments. At the same time, the effects of temperature on porosity, tortuosity, saturation of pore solution, and chemical reactions are also included in their model. Xia and Li (2013) investigated the effects of externally applied voltage and initial ionic concentration in pore solution on the distribution of ionic species and electrical field in migration test. Liu et al. (2012, 2015a, 2018) developed a series of multi-species and multi-phase models to investigate the influence of the presence of aggregates, ITZ, cracks in concrete and geometric shape of aggregates on chloride penetration during migration test. Recently, Yang et al. (2017) proposed a modified PNP model to predict the accelerated ionic transport with considering the effect of pore constrictivity on migration path. Numerical results demonstrated that this refined PNP model can effectively modify the chloride migration profiles in the RCM test, bringing them closer to the experimental results. Yu et al. (2019) considered the coupling of multi-species transport and moisture transport to generate an accurate simulation of chloride penetration in unsaturated concrete experiencing seasonal variations.

As mentioned above, both Poisson's equation and current conservation law were used to describe the relationship between the distribution of multiple ionic species and electric potential in concrete. It should be noticed that Xia et al. (2013) and Liu et al. (2015a) have highlighted that the assumption of electroneutrality inherent in the current conservation law represents a mathematical approximation that may result in numerical inaccuracies. Nevertheless, despite the aforementioned limitations, the current conservation law has been consistently used in simulating multi-species transport in concrete during migration

tests and electrochemical rehabilitation (Mao et al., 2019; Guo et al., 2021b; Chen et al., 2021). The differences and application scope of Gauss's law (Poisson's equation) and current conservation law in simulating multi-species transport have not been addressed.

2.5.3. Modelling of reactive multi-species transport

Chloride in concrete exists in two different forms: free chloride ions in pore solution and bound chloride that is physically or chemically adsorbed in cement hydrates. Although bound chloride does not contribute to steel corrosion in concrete, it can still have an impact on the service life of concrete structures by slowing down ionic transport and reducing the amount of free chloride ions near steel bars. To describe the influence of chloride binding on ionic transport, several binding isotherms were proposed to calculate the concentration of bound chloride as given in Section 2.2.4. In the abovementioned single-species and multi-species models, the effects of chloride binding on ionic transport are described as a time-dependent diffusion coefficient calculated by binding isotherms (Sergi et al., 1992; Glass and Buenfeld, 2000; Baroghel-Bouny et al., 2011; Spiesz et al., 2012; Jiang et al., 2013; Liu et al., 2015a; Shakouri and Trejo, 2017; Shi et al., 2019; Mao et al., 2019). Nevertheless, there are two limitations of these pre-designed binding isotherms. Firstly, binding parameters in each isotherm vary significantly depending on various factors, such as pH value, the type and content of binder, w/b ratio, etc. Therefore, the determination of these parameters for different concretes must depend on specific experimental data. Secondly, isothermal binding models usually ignore pore evolution caused by the formation of chloroaluminate salt (Friedel's and Kuzel's salt) and/or the change of other cement hydrates. To resolve the abovementioned problems, a series of reactive mass transport models have been developed to simulate chloride binding in different types of concrete.

Physical adsorption of chloride, potassium, calcium, and sodium ions on C-S-H gel has been calculated by a surface complexation model, in which these physical binding reactions are influenced by double electrical layer on C-S-H surface (Elakneswaran et al.,

2010). The predicted distribution profiles of total chlorides showed good agreement with experimental profiles after a 91-day exposure to sea water.

Hosokawa et al. (2011b) divided chloride penetration into two parts: mass transport and thermodynamic equilibrium. Multi-species mass transport is solved by using Poisson-Nernst-Plank equation. Thermodynamic equilibrium part is calculated by using PHREEQC programme, in which the precipitation/dissolution of cement hydrates and interactions between C-S-H and ions are separately solved. Then a sequential operator splitting method was used to assemble mass transport and chemical/physical equilibrium processes to obtain the time-varying distribution of both solid-phase composition and ionic species in pore solution. Subsequently, Jensen (2014) considered the coupling of chemical equilibrium between cement hydrates and free ions and ionic transport to simulate chloride transport and the variation of solid phase when concrete is exposed to NaCl solution.

Tian et al. (2018) and Tran et al. (2018) considered both thermodynamic equilibrium of cement hydrates and surface complexation on C-S-H gel to predict the chloride binding capacity of concrete with different binder types, and various water/binder ratios, and different cation types in exposed environments. Physical binding onto C-S-H surface and chemical binding to AFm are presented in their study. They found that the total amount of bound chloride decreases in the following order: $CaCl_2$, $MgCl_2$, NaCl, and KCl solution.

Guo et al. (2018) adopted thermodynamic equilibrium to estimate the effects of chloride concentration in exposed solution, saturation degree of pore solution, and temperature on physical and chemical chloride binding capacity for cement-based materials. In their modelling, the variation of porosity caused by chemical reactions is considered. They found that the formation of Friedel's salt needs a higher chloride concentration than that of C-S-H-Cl. After that, Guo et al. (2021b) proposed 2-D homogenous models that coupled thermodynamic reactions, pore evolution and multi-species transport to predict chloride penetration in ordinary Portland cement concrete and coral aggregate concrete.

More recently, this thermodynamic model has been used to investigate the chloride binding affected by carbonization (Guo et al., 2022), sulfate-attack attack (Cao et al., 2020), and hydrate cement leaching in nitrate solution (Arnold et al., 2017).

In conclusion, numerical simulation has been adopted as an efficient and effective way to investigate the mechanism of ionic transport in cement-based materials. Over the years, the development of numerical models has undergone significant advancements, which can be summarized in the following stages: 1) from ideal diffusion process to electrically accelerated migration process, 2) from single-species transport to multi-species transport, 3) from homogenous concrete models to multi-phase heterogenous concrete models. However, there are still differences in the results between the existing numerical models and experimental observations.

2.6. Knowledge gaps

This chapter presents a literature review on experimental, analytical, and numerical studies on chloride transport in concrete. The basic mechanisms of ionic transport, heterogeneity of concrete, multi-species coupling in pore solution, and physical and chemical reactions between free ions and cement hydrates are also described. Some conclusions as well as research gaps drawn from the literature are summarized as follows:

1) Pore solution of concrete is a multi-species system, and each ionic species has a distinct mobility, which can result in a non-linear distribution of electrostatic potential in concrete. Current conservation law and Gauss' law methods have been proposed to investigate the influence of multi-species coupling on chloride penetration. However, the differences between these two methods and their application scope are not clarified. Therefore, the study of multi-species transport is conducted based on these two methods, as presented in Chapter 4.

2) The heterogeneous properties of both NAC and RAC have been widely recognized. Each phase in composite concrete has its own individual chloride

diffusivity and can influence the general chloride resistance of concrete. However, there is still a lack of literature on effective chloride diffusion coefficient of concrete including both NA and RA. Therefore, the study of chloride transport in partially replaced RAC will be investigated by using a 2-D finite element method model and an infinite analytical model, as presented in Chapter 5.

3) In chloride migration tests, electrical potential difference across concrete specimen is different from that applied on electrodes due to polarization at outside electrodes. However, the influence of polarization on chloride transport is still not discussed in existing simulations. Therefore, a 2-D numerical model will be developed to combine the inside ionic transport and outside polarization during migration tests, which is presented in Chapter 6.

4) Simulation of chloride binding is widely based on empirically designed binding isotherms. There is no single binding isotherm that can cover all binding modes observed in general concrete. Furthermore, the pore evolution resulting from chloride binding has not been accounted for in existing binding isotherms. An insight into thermodynamic reactions between ions in pore solution and cement hydrates is required to understand the influence of chloride binding in migration tests. Therefore, a reactive mass transport model will be proposed to describe the actual reactions involved in chloride penetration in concrete, which is presented in Chapter 7.

CHAPTER 3 METHODOLOGY

This chapter presents the development of analytical and numerical models employed in this study to suit different research objectives. To validate the reliability and accuracy of each model proposed, a series of benchmark models are established based on experimental or numerical studies conducted by other researchers. The details of geometric configuration, diffusion properties, boundary conditions, and solution procedure used in each model are addressed. Two commercial software packages are employed in the present study: 1) COMSOL Multiphysics, engaged for numerical simulation considering multiple physical fields. 2) MATLAB, employed for analytical simulation as well as pre- and post-processing of numerical simulations.

3.1. Multi-species and single-phase model of chloride transport

In this section, three numerical models are developed to understand the multi-species coupling effects on chloride transport during diffusion and migration tests and to elucidate the distinctions between the models based on Gauss's law and the models based on current conservation law. As shown in Fig. 3.1, during chloride penetration tests, a concrete specimen is placed between two reservoirs filled with 520 mol/m^3 NaCl and 300 mol/m^3 NaOH solutions, respectively. When an external voltage of 24 V is applied, the apparatus is set up for the migration test, whereas when there is no external voltage (0 V) is enforced, the apparatus is regarded as the one for chloride diffusion test.

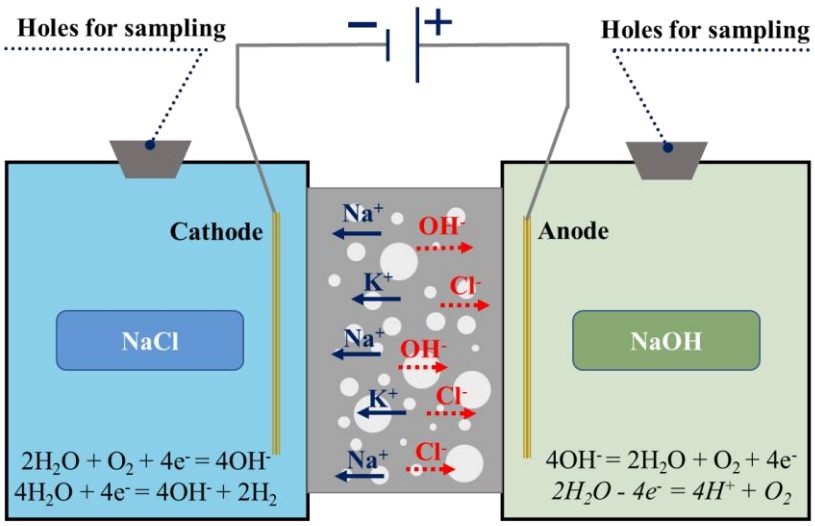

Figure 3.1 Schematic representation of the chloride migration test (representing for diffusion test when external voltage is 0 V)

3.1.1. Governing equations

Assuming that the concrete specimen is saturated and there are no physical and chemical reactions between free ions and cement hydrates, only ionic diffusion and electromigration of ions are involved in chloride penetration process. Therefore, terms ① and ② in Equation (2.58) are selected to describe the multi-species mass transport in concrete as follows,

$$\frac{\partial C_i}{\partial t} = D_i \nabla^2 C_i + D_i \frac{z_i F}{RT} \nabla (C_i \nabla \emptyset) \qquad i=1,2,...n \tag{3.1}$$

As given in Section 2.2.3, electrostatic potential gradient, $\nabla\emptyset$, can be calculated by Equations (2.12), (2.13) or (2.20). Herein, the multi-species transport model based on Poisson's equation (Equation (2.12)) is named as Poisson model. Equations (2.13) and (2.20) are derived with the assumption of electroneutrality. Hence, models based on Equations (2.13) and (2.20) are named as Strong-EN model and Weak-EN model in this thesis, respectively.

3.1.2. Geometry and meshing

In this section, concrete is assumed to be a homogenous material. Therefore, a 1-D single-phase geometric model can be used to conduct multi-species transport analysis. Sample length L is 50 mm. A small uniform element size of 0.05 mm is used in all three models.

3.1.3. Diffusion properties and boundary conditions

Four ionic species, potassium, sodium, chloride, and hydroxyl are considered in this section. Other ionic species, such as calcium and sulfate ions, are ignored due to their low concentrations in the pore solution, which was demonstrated in the experimental tests carried out by Bertolini (1995). The electrodes in chloride migration test are placed on the surfaces of a concrete specimen as shown in Fig. 3.1. The influence of electrochemical reactions at electrodes is considered negligible, as explained in Section 2.2.5.2. This means that ionic concentrations in reservoirs on both sides of concrete remain constant, as listed in Table 3.1. The diffusion coefficient, initial and boundary conditions of each ionic species, and external voltage in three models are given in Table 3.1.

Table 3.1 Initial and boundary conditions, charge number and diffusion coefficients of four ionic species in mortar specimen.

Field variables	Potassium (mol/m^3)	Sodium (mol/m^3)	Chloride (mol/m^3)	Hydroxide (mol/m^3)	External voltage(V)
Initial conditions	200	100	0	300	0
Boundary conditions x=0cm	0	520	520	0	0
Boundary conditions x=5cm	0	300	0	300	0/24
Charge number	1	1	-1	-1	N
Diffusion coefficient $\times 10^{-11}$ m^2/s	1.960	1.334	2.032	5.260	N

3.1.4. Solution procedure

Mass transport derived by Equation (3.1) and electric field derived by Equations (2.12), (2.13), or (2.20) can be synchronously solved by the Transport of Diluted Species module and PDE module in COMSOL Multiphysics. With the initial and boundary conditions listed in Table 3.1, the distributions of all ionic species and electric potential can be obtained.

3.2. Multi-phase and single-species model of chloride transport

In this section, a five-phase numerical model and a two-step analytical model are proposed to predict the effective chloride diffusion coefficients of heterogenous concrete containing various contents of both NA and RCA. Only a single species, chlorides, is involved in the simulation of diffusion tests. Based on these two heterogenous models of concrete, the effects of each individual phase, such as the volume and chloride diffusivity of old ITZ, attached old mortar, new ITZ, and new mortar, can be assessed.

3.2.1. Multi-phase numerical models of heterogenous concrete

3.2.1.1 Governing equations

Assuming that pore solution in concrete is saturated and there is no reaction between chlorides and cement, single-species transport during diffusion test can be described by Fick's second Law as given in Section 2.2.1. When it is extended to a 2-D heterogeneous concrete, Fick's Law (Equation (2.2)) can be expressed as follows,

$$\frac{\partial C(t, x, y)}{\partial t} = D_k \nabla^2 C(t, x, y) \qquad k=1, 2, 3, 4, 5 \tag{3.2}$$

where $C(t,x,y)$ is chloride concentration at time t (s) and position (x, y) (mol/m^3), D_k is chloride diffusion coefficient in *k-th* phase, and $k = 1, 2, 3, 4,5$ stands for old aggregate,

old ITZ, attached old mortar, new ITZ, and new mortar, respectively. With the initial and boundary conditions, the distribution of chlorides in a multi-phase concrete can be determined by solving Equation (3.2) numerically.

3.2.1.2 Geometry and meshing

Figs. 3.2 and 3.3 show a series of 50 × 50 mm multi-phase concrete models with different replacement rates of RCA, different volume fractions of old mortar, and different shapes of aggregate. New and old natural aggregates (white region) in all models are assumed to be impermeable. The total volume fraction of aggregates in this section is assumed to be 0.5. In NAC and RAC models, NA and/or RCA are generated and located randomly in cement matrix using a MATLAB programme (as shown in Appendix A). The size distribution of both NA and RCA follows the Fuller gradation, with their radii ranging from 2 mm to 15 mm.

As shown in Fig. 3.4, old ITZ, old mortar, and new ITZ are assumed to be uniform shells that surround impermeable old aggregate layer by layer. Blue and red shells in Fig. 3.4 represent new and old ITZs, respectively. Existing research has concluded that the thickness of new and old ITZs usually varies from 20 to 80 μm (Diamond and Huang, 2001; Caré and Hervé, 2004; Xiao et al., 2013). To better understand the effect of each phase on chloride penetration, a parametric analysis is conducted with various property settings. Table 3.2 shows the parameter setting of the replacement rate of RCA (V_{RCA}), old ITZ thickness (h_{oitz}), new ITZ thickness (h_{nitz}), total volume fraction of aggregates e (V_{TA}), and volume fraction of old mortar in RCA (V_{om}) in standard case and parametric analysis cases.

Fig. 3.5 shows the finite element mesh of a five-phase RAC model. Due to the extremely thin interfacial transition zone and the significant difference in chloride diffusivity between individual phases, the finite element size near interfaces between two phases must be extremely small to get a convergent numerical solution. Triangular meshing is

adopted with a minimum mesh element size of 1.5×10^{-5} m, requiring a total of 537607 free triangle elements in the domain.

Table 3.2 Volume parameters and chloride diffusivities of each phase in standard and parametric analysis cases.

	Standard case	Parametric cases
Volume fraction of total aggregate V_{TA}	0.5	0, 0.1, 0.3, 0.5
RCA replacement rate V_{RCA}	0.5	0, 0.2, 0.5, 1
Volume fraction of old mortar in RCA V_{om}	0.3	0.1, 0.3, 0.5
Old or new ITZ thickness h_{oitz}, h_{nitz} (μm)	40	40, 80, 120
Chloride diffusivity in new mortar $\times10^{-11}$ m^2/s	2.03	2.03
Diffusivity ratio between ITZ and mortar k_{itz}	5	2~20
Diffusivity ratio between old and new mortars k_{om}	1.5	0.2, 1.5, 3

To validate the accuracy of the present multi-phase numerical model, a benchmark model was developed in accordance with experimental research conducted by Kou and Poon (2012). Mix design used in the experiment was 410 kg/m^3 of binder (75%OPC+25%FA), 611 kg/m^3 of sand, and 1017-1048 kg/m^3 of natural and recycled coarse aggregates. Accordingly, the total volume fraction of coarse aggregates is about 0.4. Four replacement rates of RA (combined stone, RCA, and masonry aggregate), 0, 0.2, 0.5, and 1, were employed in experiments and adopted in benchmark model. The volume fraction of old mortar in RA is 0.13, which is estimated based on the density of NA and RA given in Kou and Poon (2012). The thicknesses of old and new ITZs adopted in benchmark model are the same as those used in standard case.

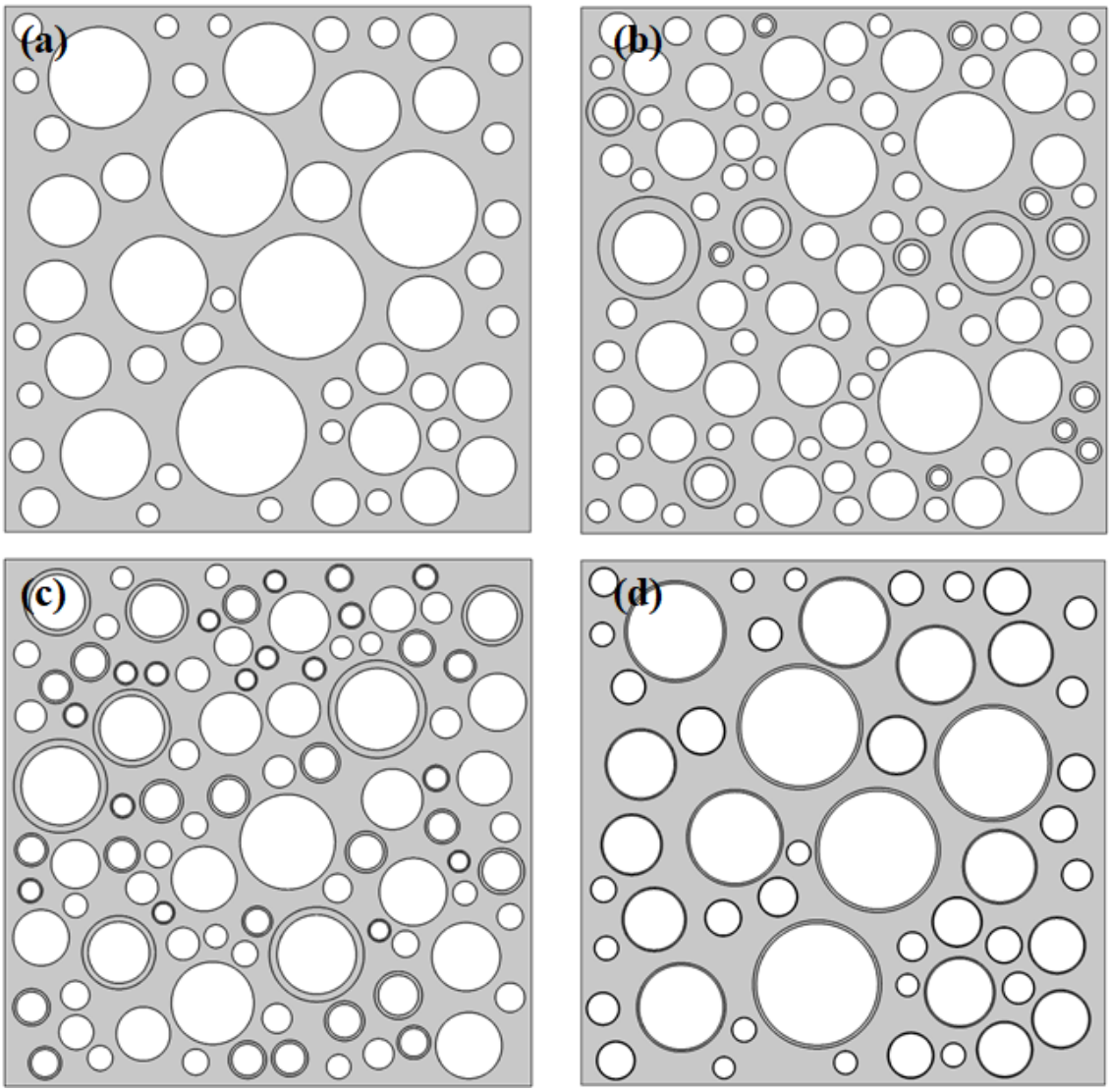

Figure 3.2 Multi-phase concrete models with circular aggregates (a) $V_{RCA} = 0$, $V_{om} = 0$, (b) $V_{RCA} = 0.2$, $V_{om} = 0.5$, (c) $V_{RCA} = 0.5$, $V_{om} = 0.3$, (d) $V_{RCA} = 1$, $V_{om} = 0.1$

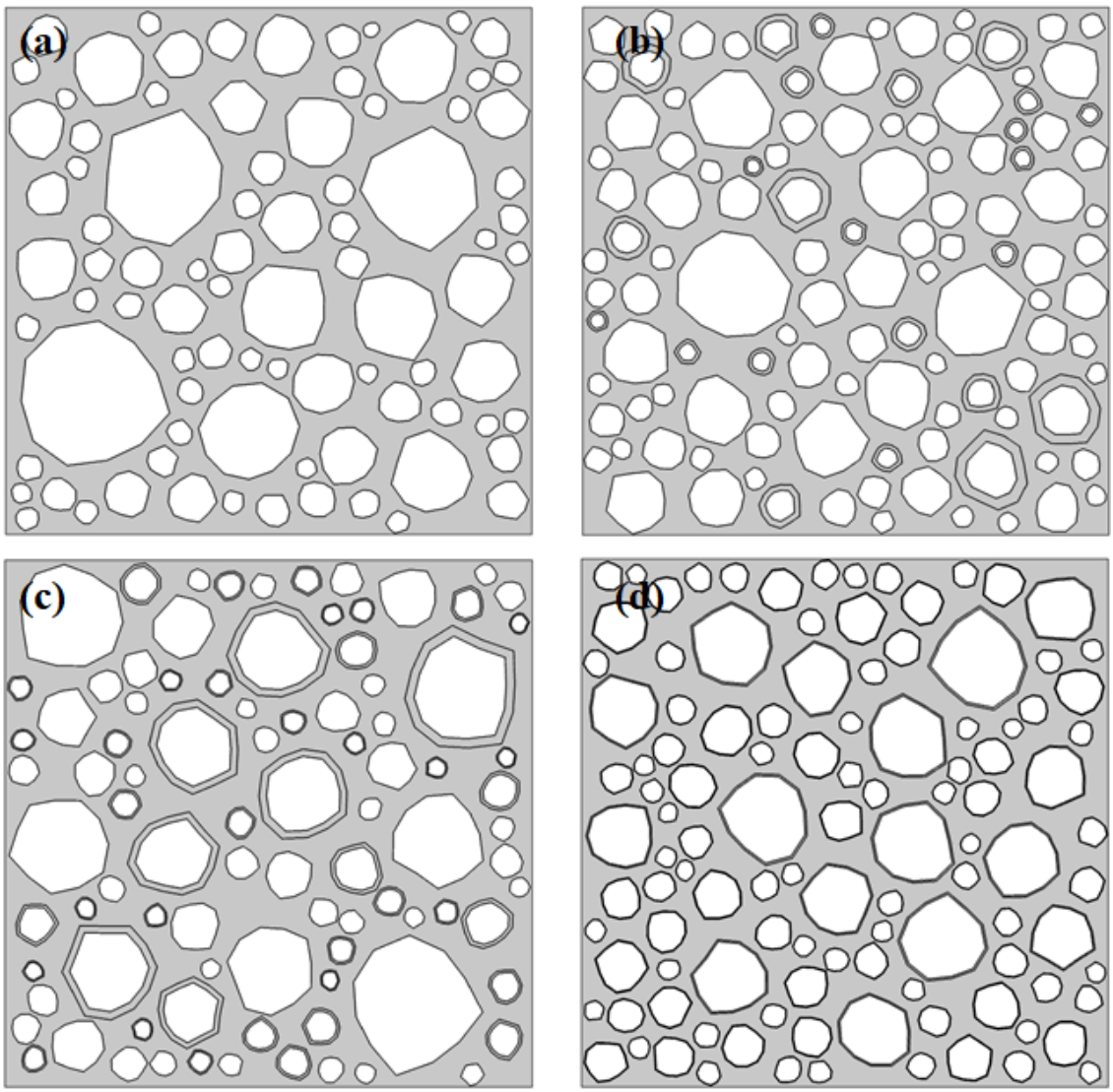

Figure 3.3 Multi-phase concrete models with unregular aggregates (a) $V_{RCA} = 0$, $V_{om} = 0$, (b) $V_{RCA} = 0.2$, $V_{om} = 0.5$, (c) $V_{RCA} = 0.5$, $V_{om} = 0.3$, (d) $V_{RCA} = 1$, $V_{om} = 0.1$

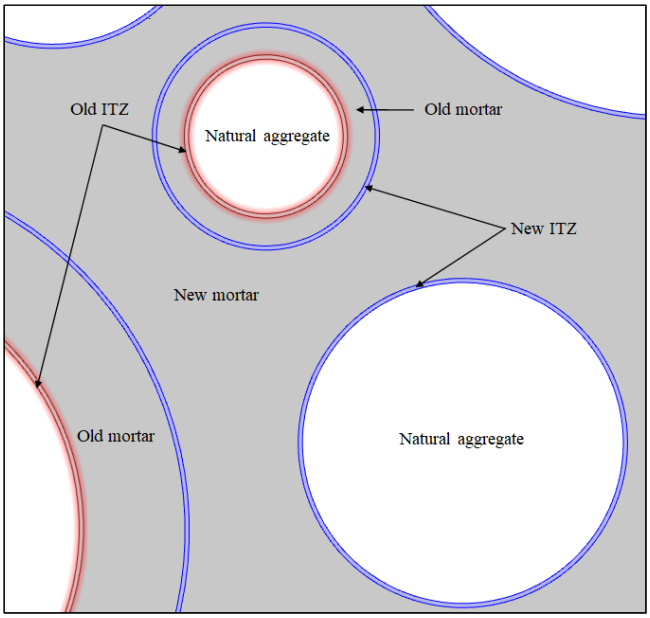

Figure 3.4 Zoomed-in schematic of RAC (V_{RCA} = 0.5, V_{om} = 0.5, h_{nitz} = h_{oitz} = 40 μm)

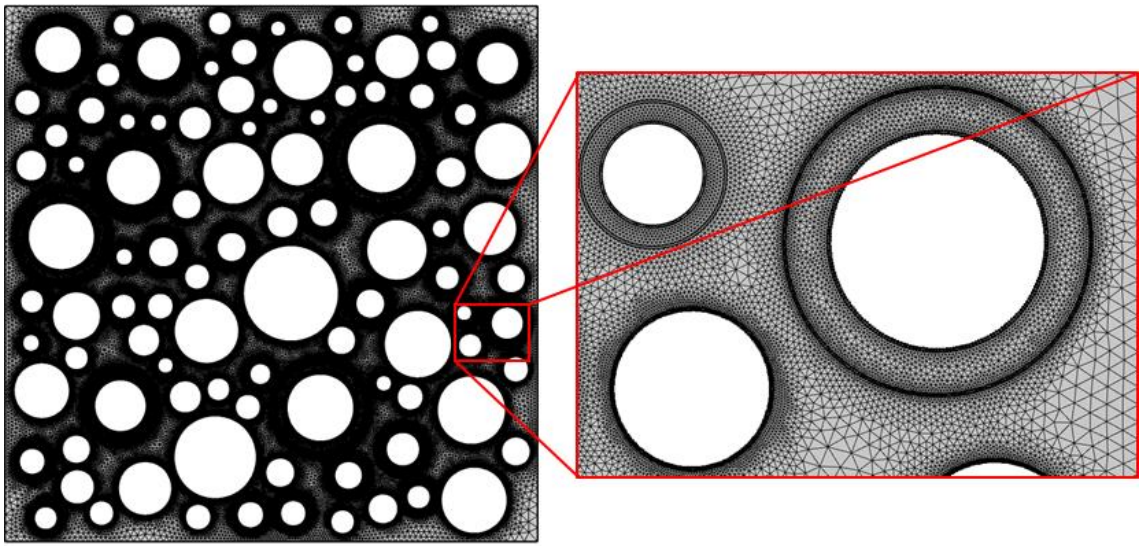

Figure 3.5 Meshing of RAC model (V_{RCA} = 0.5, V_{om} = 0.5, h_{nitz} =h_{oitz} = 40 μm)

3.2.1.3 Diffusion properties and boundary conditions

In these multi-phase models, chloride ions have distinct diffusion coefficients in each individual phase. Previous studies concluded that the ratio of chloride diffusivity between ITZ and mortar (k_{itz} = D_{nm} / D_{nitz} = D_{om} / D_{oitz}) varies in the range of 1.3~18.5 times (Xiao et al., 2012; Hu et al., 2018). The chloride diffusivity ratio between old and new mortars

($k_{om} = D_{om} / D_{nm}$) commonly ranges from 0.24 to 5 times (Kou and Poon, 2006; Kou and Poon, 2012; Xiao et al., 2012; Yu and Lin, 2020). To investigate the influence of chloride diffusivity in old ITZ, new ITZ, and old mortar, various chloride diffusion coefficients of each phase are considered in simulation and given in Table 3.2.

In benchmark model, the chloride diffusion coefficients of new mortar and ITZ are the same as those in standard case. The diffusivity ratio between old and new mortars is determined by their w/b ratios. Two w/b ratios of new mortar, 0.45 and 0.55, are adopted in benchmark experiment. Correspondingly, the calibrated diffusivity ratio between old and new mortars is 1.8, and 0.6 for w/b=0.45 and w/b=0.55, respectively. The initial and boundary conditions of chlorides are the same as the values in diffusion test listed in Table 3.1.

3.2.1.4 Solution procedure

Transport of Diluted Species module in COMSOL Multiphysics is selected to solve single-species transport in saturated concrete (Equation (3.2)). When chloride diffusion reached steady state, the average flux of chloride at the boundary exposed to NaOH solution, as shown in Fig. 3.1, can be expressed as,

$$J_{x=l}=\frac{\int_0^h J(t=\infty,\, l,\, y)\, d\, y}{h} \tag{3.3}$$

where l and h are the length and height of 2-D concrete models. In the macro-scale view, the 50 mm×50 mm concrete specimen can be treated as a representative homogeneous element. Therefore, the average steady-state flux of chloride at the right boundary of meso-concrete can also be described as,

$$J_{x=l}=-D_{eff}\frac{\partial C}{\partial x}=D_{eff}\frac{C_s}{l} \tag{3.4}$$

where D_{eff} is the effective chloride diffusion coefficient of NAC or RAC, C_s is the chloride concentration at the boundary exposed to NaCl solution as shown in Fig. 3.1. Substituting Equation (3.3) into (3.4), the effective chloride diffusion coefficient can be solved as follows,

$$D_{eff} = -\frac{l}{C_s h}\int_0^h J(t=\infty, l, y)\, dy \tag{3.5}$$

3.2.2. Two-step analytical models of heterogenous concrete

To get a convergent solution, element sizes in previous five-phase numerical models are extremely fine (Fig. 3.5), which will lead to a high computational burden. In this section, a simple analytical model is developed to reduce computational burden. In this analytical model, RAC is considered as a three-phase composite consisting of NA plus ITZ (NA+), RCA plus ITZ (RCA+), and new mortar as shown in Fig. 3.6. The effective chloride diffusion coefficient in RAC can be calculated in two steps. Firstly, NA+ and RCA+ are assumed to be two-layer and four-layer particles, respectively, as shown in Fig. 3.6. The effective diffusivities of NA+ and RCA+ can be calculated using a multi-layer spherical approximation (MLSA). Secondly, the effective diffusivity of this three-phase RAC is obtained using an effective medium approximation (EMA).

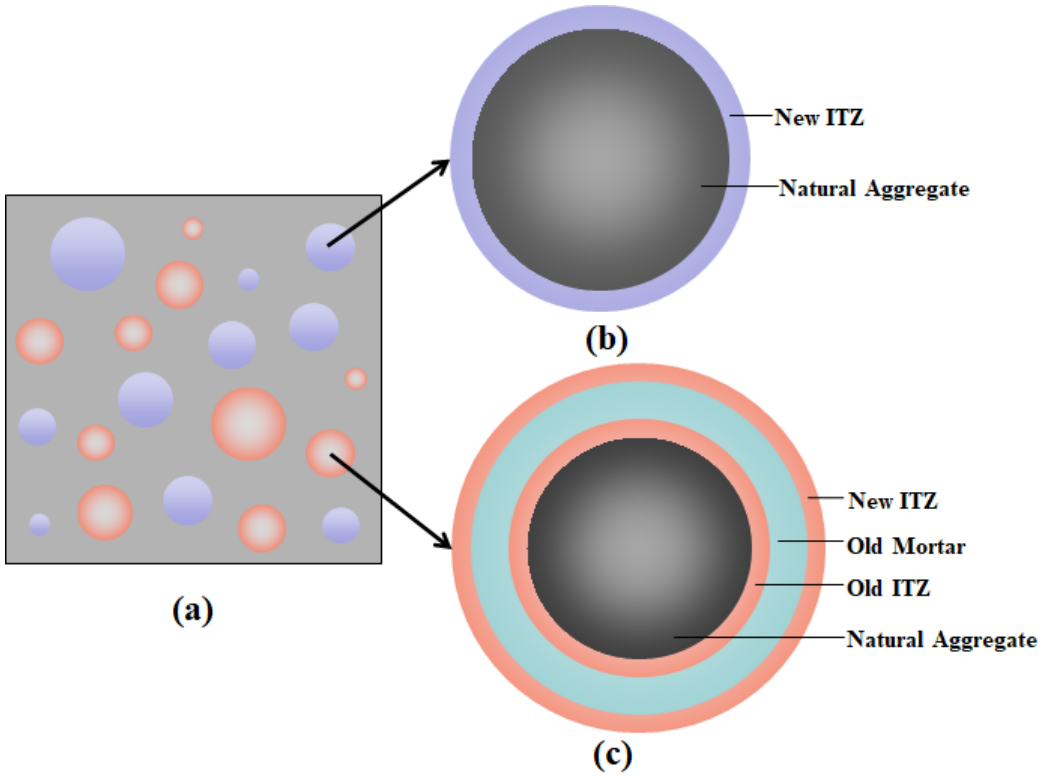

Figure 3.6 The schematic representation of (a) concrete with both NA and RCA, (b) natural aggregate plus ITZ, (c) recycled concrete aggregate plus ITZ

3.2.2.1 Multi-layer spherical approximation

As shown in Fig. 3.6 (b), NA+ phase is composed of natural aggregate and enclosed new ITZ. Based on two-layer spherical approach (Caré and Hervé, 2004), the effective chloride diffusion coefficient of NA+ can be described as:

$$D_{NA+}=\frac{(3-2V_{nitz1})D_{NA}+2V_{nitz1}D_{nitz}}{V_{nitz1}D_{NA}+(3-V_{nitz1})D_{nitz}}D_{nitz} \tag{3.6}$$

where D_{NA} and D_{nitz} are the chloride diffusivity in NA and new ITZ, respectively. V_{nitz1} and V_{NA} represent the volume fractions of ITZ and NA in NA+ phase, respectively, and thus $V_{nitz1} + V_{NA} \equiv 1$. Generally, NA can be considered as impermeable and thus $D_{NA} = 0$ is adopted in this section. Equation 3.6 can be rewritten as,

$$D_{NA+}=\frac{2}{(3-V_{nitz1})}V_{nitz1}D_{nitz} \tag{3.7}$$

Since the order of magnitude of ITZ thickness is significantly less than that of the aggregate radius, the following approximations can be made,

$$V_{nitz1}=\frac{(R_{NA}+h_{nitz})^3-R_{NA}^3}{(R_{NA}+h_{nitz})^3}\approx\frac{3h_{nitz}}{R_{NA}} \tag{3.8}$$

$$D_{NA+}\approx\frac{2}{3}V_{nitz1}D_{nitz} \tag{3.9}$$

where R_{NA} and h_{nitz} are the average values of NA's radius and new ITZ's thickness, respectively.

Similarly, the effective chloride diffusivity of RCA+ can be calculated as follows,

$$D_{RCA+}=\frac{3D_{RCA}+2V_{nitz2}D_{nitz}}{V_{nitz2}D_{RCA}+3D_{nitz}}D_{nitz} \tag{3.10}$$

where V_{nitz2} and v_{RCA} represent the volume fractions of new ITZ and RCA in RCA+ phase, respectively, and $V_{nitz2} + v_{RCA} \equiv 1$, D_{RCA} is the effective chloride diffusion coefficient of permeable RCA.

It should be noted that the configuration of NA, old ITZ, and old mortar in RCA may vary significantly from one to another. As an approximation, RCA can be modelled as a three-layer sphere, as shown in Fig. 3.7. The effective diffusivity of this three-layer RCA can be calculated by the recursion of two-layer spherical model. Firstly, similar to the NA+ phase, the effective diffusion coefficient of the impermeable old NA plus old ITZ (ONA+) phase can be expressed as,

$$D_{ONA+}=\frac{2V_{oitz}}{(3V_{ONA}+2V_{oitz})}D_{oitz} \tag{3.11}$$

where V_{oitz} and V_{ONA} represent the volume fractions of old ITZ and old NA in RCA, respectively, D_{oitz} is the chloride diffusion coefficient in old ITZ.

RCA can be treated as an auxiliary two-layer model, including ONA+ and old mortar. Hence, the effective diffusivity of RCA can be described as,

$$D_{RCA}=\frac{(3-2V_{om})D_{ONA+}+2V_{om}D_{om}}{V_{om}D_{ONA+}+(3-V_{om})D_{om}}D_{om} \tag{3.12}$$

where D_{om} is the chloride diffusion coefficient of old mortar and V_{om} is the volume fraction of old mortar in RCA, and $V_{om} + V_{ONA} + V_{oitz} \equiv 1$. Substituting Equation (3.11) into (3.12), it yields,

$$D_{RCA}=\frac{2(3-2V_{om})V_{oitz}D_{oitz}+2(3V_{ONA}+2V_{oitz})V_{om}D_{om}}{2V_{om}V_{oitz}D_{oitz}+(3V_{ONA}+2V_{oitz})(3-V_{om})D_{om}}D_{om} \tag{3.13}$$

Thus, the effective chloride diffusivity of RCA+ phase can be obtained by solving Equations (3.10) and (3.13). The chloride diffusion coefficients and volume parameters of each phase in standard case are given in Table 3.3.

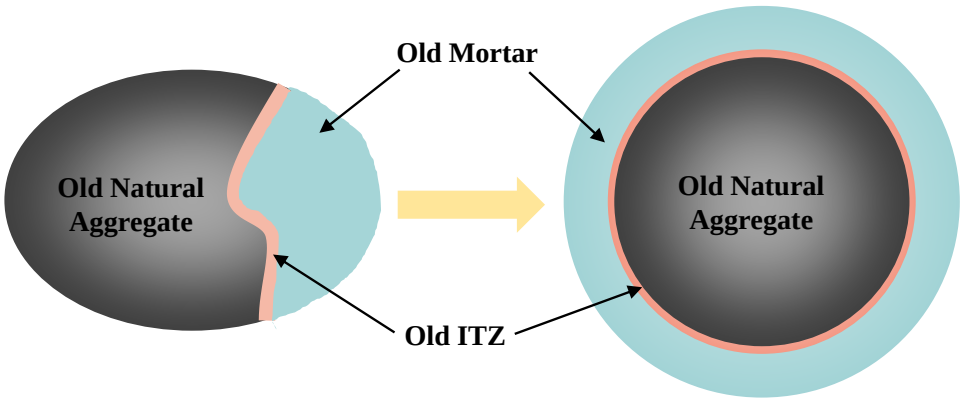

Figure 3.7 Three-layer spherical RCA model

Table 3.3 The chloride diffusion coefficients and volume parameters of each phase in standard case.

Composite	Component	Volume fraction in each composite	Diffusion coefficient ($\times 10^{-11}$ m^2/s)
RAC	New mortar	0.5	2.03
	NA+	$0.5\times(1-V_{RCA})$	Equation (3.9)
	RCA+	$0.5\times V_{RCA}$	Equation (3.10)
NA+	New ITZ (NA)	0.03	$k_{itz}\times 6.0$ (k_{itz} = 5)
	NA	1-0.03	0
RCA+	New ITZ (NA)	0.03	$k_{itz}\times 6.0$ (k_{itz} = 5)
	RCA	1-0.03	Equation (3.13)
RCA	Old mortar	0.28	$k_{om}\times 6.0$ (k_{om} = 1.5)
	Old ITZ	0.02	$k_{itz}\times k_{om}\times 6.0$ (k_{om} = 1.5, k_{itz} = 5)
	Old NA	0.70	0

3.2.2.2 Effective medium approximation

After multi-layer spherical approximation, NA+ and RCA+ particles can be considered as two isotropic phases with individual diffusion coefficients. The RAC can be treated as a three-phase composite made up of mortar matrix, randomly distributed NA+ and RCA+ particles. Due to their individual diffusion properties and independent distribution, both NA+ and RCA+ contribute independently to the effective diffusivity of RAC. To reflect the independent effects of NA+ and RCA+, an effective medium approximation (EMA) is adopted here. EMA was developed by Bruggeman and Landauer to describe the macroscopic properties of a two-phase material by averaging the arbitrary values of the randomly oriented inclusions (Bruggeman, 1935; Landauer, 1952). There are many versions of EMA, such as the Maxwell-Eucken model (Eucken, 1940), the Maxwell-

Garnett model (Garnett, 1904), and so on. These models can provide acceptable predictions under different conditions. Mathematically, when it comes to chloride diffusion, EMA can be described as,

$$\frac{D_{eff}-D_1}{2D_{eff}+D_1}V_1+\frac{D_{eff}-D_2}{2D_{eff}+D_2}V_2=0 \tag{3.14}$$

where D_{eff} represents the effective diffusivity of a two-phase mixture, D_1, D_2, V_1 and V_2 are the diffusion coefficients and volume fractions of components 1 and 2, respectively. Equation (3.14) can be rewritten as follows,

$$\frac{V_1}{\frac{1}{3}D_1+\frac{2}{3}D_{eff}}+\frac{V_2}{\frac{1}{3}D_2+\frac{2}{3}D_{eff}}=\frac{1}{D_{eff}} \tag{3.15}$$

Equation (3.15) indicates that phase 1 with volume fraction V_1 and phase 2 with volume fraction V_2 can be considered as connected in series, provided that the diffusion coefficients in two phases are taken as (D_1/3 and $2D_{eff}$/3) and (D_2/3 and $2D_{eff}$/3), respectively. This means that the relationship between the effective diffusivity and volume of individual phases and overall composite in EMA model is similar to the relationship between the total and partial voltage and current in a series-parallel circuit, as shown in Fig. 3.8. Therefore, for a three-phase RAC, Equation (3.15) can be easily extended as follows,

$$\frac{V_{nm}}{\frac{1}{3}D_{nm}+\frac{2}{3}D_{RAC}}+\frac{V_{NA+}}{\frac{1}{3}D_{NA+}+\frac{2}{3}D_{RAC}}+\frac{V_{RCA+}}{\frac{1}{3}D_{RCA+}+\frac{2}{3}D_{RAC}}=\frac{1}{D_{RAC}} \tag{3.16}$$

where V_{nm}, V_{NA+}, V_{RCA+} are respectively the volume fractions of new mortar, NA plus ITZ, and RCA plus ITZ in concrete ($V_M + V_{NA+} + V_{RCA+} \equiv 1$), and D_{RAC} is the effective chloride diffusion coefficient of RAC. Note that one of the conditions for applying EMA is that the volume fraction of zero diffusion coefficient phase must be less than 2/3. In three-

phase concrete, neither NA+ phase nor RCA+ phase has a volume fraction greater than 2/3. Moreover, since both NA+ and RCA+ phases involve the ITZ, the diffusion coefficients in the NA+ and RCA+ phases would not be zero.

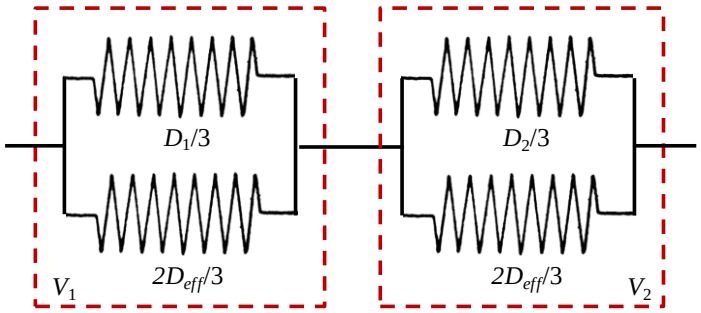

Figure 3.8 The schematic representation of effective medium approximation

The effective diffusivity of concrete is influenced by several important factors, as described in Equations (3.9), (3.10), and (3.13), including the volume fractions of ITZ, new mortar, and adhesive old mortar, the RCA replacement rate, and the diffusivity ratio between each phase. Therefore, Equation (3.16) can be converted as:

$$D_{eff}=D_{eff}(V_{nm}, V_{nitz}, V_{oitz}, V_{RCA}, V_{om}, k_{itz}, k_{om}, D_{nm}) \quad (3.17)$$

where V_{RCA} is the replacement rate of RCA in terms of volume fraction. With given parameters in Equation (3.17), the effective diffusivity of RAC can be calculated using a MATLAB programme (as shown in APPENDIX B). It is obvious that $D_{RAC} = D_{NAC}$ when V_{om} or V_{RCA} is zero, where D_{NAC} is the effective chloride diffusion coefficient of NAC. As given in Table 3.3, k_{om} is adopted to describe the influence of the w/b ratio of parent concrete and the crushing process on the chloride diffusivity of old mortar. k_{itz} is used to describe the influence of w/b ratio of concrete on the chloride diffusivity of new and old mortars.

3.3. Overpotential model of chloride transport

In this section, an overpotential model is developed considering multi-species transport in a multi-phase concrete to find out the variation of overpotential at electrode-concrete interfaces and how it influences internal ionic transport in a heterogenous concrete during chloride migration tests.

3.3.1. Governing equations

As mentioned in Section 3.1, without consideration of chloride binding, ionic mass transport in saturated concrete during a migration test can be expressed as Equation (3.1). In Section 3.3, the relationship between the distributions of electric field and multiple ionic species in concrete is calculated using the current conservation law method.

3.3.2. Geometry and meshing

Figs. 3.9 and 3.10 show the geometric configuration of three-phase NAC and five-phase RAC models employed in this section. The size of all concrete models is 50 mm × 50 mm. NA and RCA are randomly generated and located by the MATLAB code given in APPENDIX A. The diameters of aggregates are in the range of 2~15 mm, and the total volume fraction of them is 0.5.

Previous experiments indicated that the effective chloride diffusivity of concrete significantly increases with an increase in RCA replacement rate (Kou and Poon, 2012; Júnior et al., 2019; Bao et al., 2020). Based on Equation (2.14), the current density flowing through concrete may be influenced by the replacement rate of RCA, leading to variations in overpotential at electrode-concrete interfaces. To investigate the influence of using RCA on the overpotential, two replacement rates of 0.5 and 1 are employed. The volume fraction of old adhesive mortar in RCA is taken as 0.3, and the thickness of old and new ITZs is 40 μm. Fig. 3.9 shows the meshing of present multi-phase overpotential model. It is worth noting that free triangle elements used in overpotential model should

be finer compared to those used in Section 3.2 (Fig. 3.5) due to the involvement of multi-species coupling.

Two benchmark models are developed to validate the reliability of overpotential model. The volume fraction of aggregates and size of specimens in benchmark models are adjusted to be consistent with two chloride migration experiments conducted by Castellote et al. (1999) and Jiang et al. (2013), as given in Table 3.6. Figs. 3.11 and 3.12 plot the geometric configuration of two benchmark models.

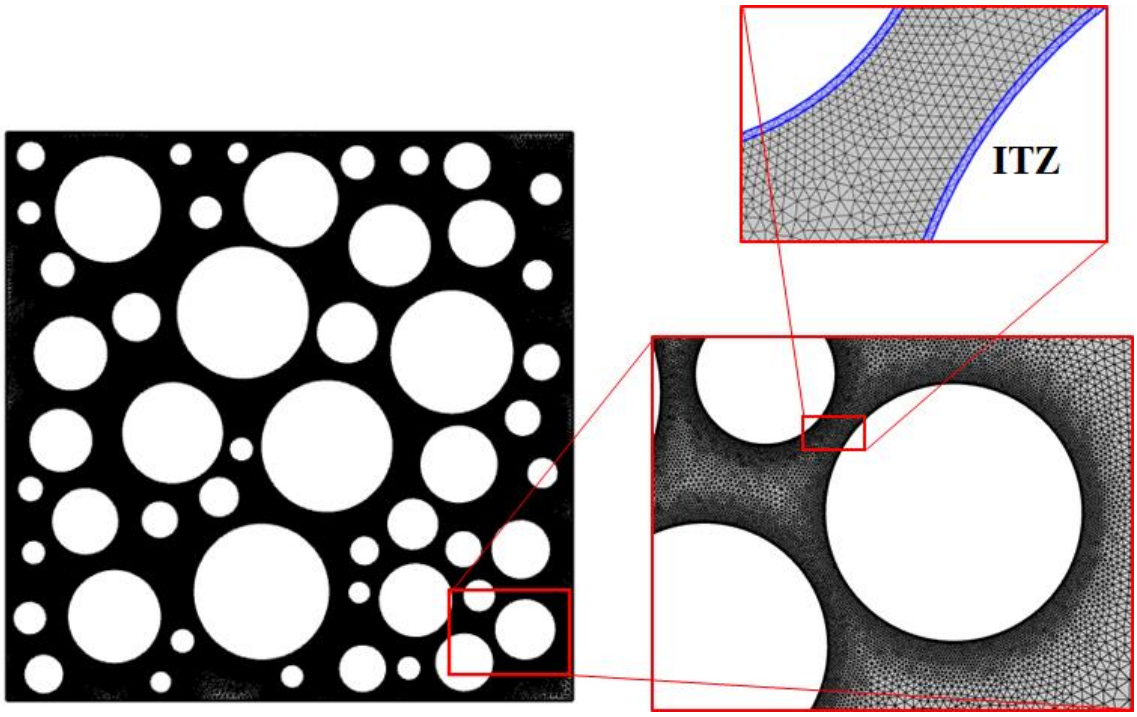

Figure 3.9 The geometric model and meshing of natural aggregate concrete

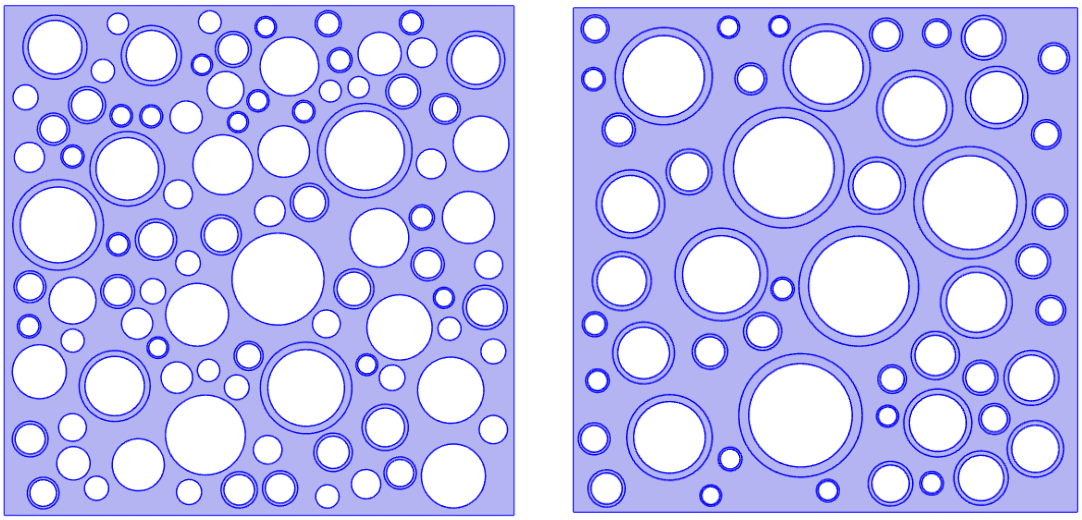

(a) V_{RCA}-0.5 (b) V_{RCA}-1

Figure 3.10 The geometric models of RAC with different replacement rates of RCA

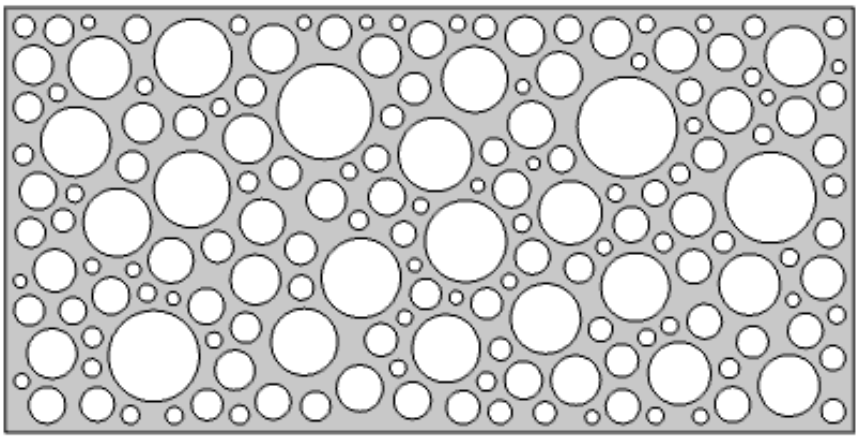

Figure 3.11 The geometric configuration of benchmark model for experiment conducted by Castellote et al. (1999)

Figure 3.12 The geometric configuration of benchmark model for experiment conducted by Jiang et al. (2013)

3.3.3. Diffusion properties and boundary conditions

3.3.3.1 Diffusion properties of ionic species

Four ionic species, namely potassium, sodium, chloride, and hydroxyl ions, are involved in Section 3.3. The diffusion coefficients of those ionic species in new mortar are the same as those mentioned in Section 3.1 (Table 3.1). According to Equations (2.11) and (2.14), the current density flowing through concrete can be influenced by ionic concentrations in pore solution and externally applied voltage, which may lead to a variation in overpotential. Therefore, a parametric analysis of initial ionic concentrations and external voltage is conducted, and the values of them in parametric study cases are given in Tables 3.4 and 3.5.

In benchmark models, initial ionic concentrations, external DC voltage, anolyte and catholyte solutions, and duration of test (as shown in Table 3.6) are taken or estimated from experiments conducted by Castellote et al. (1999) and Jiang et al. (2013). Note that calcium and sulfate ions are also ignored in benchmark model due to their low concentrations in pore solution. To maintain electroneutrality in pore solution, the initial concentrations of other species are slightly adjusted.

Table 3.4 In parameters used in Standard and Parametric study cases.

Parameter	Notation	Standard case	Parametric cases	Reference
Aggregate volume fraction	V_a	0.5	0.5	
Initial concentration (mol/m^3)	K^+	200	50 and 400	(Liu et al., 2012)
	Na^+	100	25 and 200	
	Cl^-	0	0	
	OH^-	300	75 and 600	
Tafel parameters	β_c	180 (Mv/decade)	100 and 280 (Mv/decade)	(Xia et al., 2019; Wang et al., 2020)
	$i_{c,0}$	10 ($\times 10^{-6} A/m^2$)	6 and 100 ($\times 10^{-6} A/m^2$)	
	β_a	120 (Mv/decade)	60 and 200 (Mv/decade)	
	$i_{a,0}$	10 ($\times 10^{-7} A/m^2$)	6 and 50 ($\times 10^{-7} A/m^2$)	
Voltage applied	$\Delta\Phi$	24 V	8 and 16 V	
Limiting current density	i_L	100 (A/m^2)	100 (A/m^2)	(Haverkort and Rajaei, 2020)

Table 3.5 Initial ionic concentrations in pore solution in parametric study (mol/m3)

	Potassium	Sodium	Chloride	Hydroxide
Case 1	50	25	0	75
Case 2	200	100	0	300
Case 3	400	200	0	600

Table 3.6 Input parameters in benchmarked models.

Parameters	Notation	Jiang's expt. (Jiang et al., 2013)	Castellote's expt. (Castellote et al., 1999)
Size of specimen (mm×mm)	-	50×100	75×150
Initial ionic concentration (mol/m^3)	K^+	600	700
	Na^+	202	200
	Cl^-	0	0
	OH^-	802	900
External DC power	$\Delta\Phi$	30V	12V
Aggregate volume fraction	V_a	0	0.75
Anolyte (mol/m^3)	$NaOH$	300	300
Catholyte (mol/m^3)	$NaCl$	500	500
RCM test time	-	28 Days	36 Hours

3.3.3.2 Electric and ionic boundaries

During chloride migration tests, polarization leads to a more positive potential at anode and a more negative potential at cathode. Therefore, the actual electric potential employed on cathodic (Φ_{sc}) and anodic (Φ_{sa}) concrete surfaces can be expressed as follows,

$$\Phi_{sc}=\Phi_c+\eta_c \tag{3.3}$$

$$\Phi_{sa}=\Phi_a-\eta_a \tag{3.4}$$

where Φ_a, η_a, Φ_c, and η_c represent electric potential, and overall overpotential at anode and cathode, respectively. Due to the low resistance of line segment for electrode, ohmic overpotential is neglected in present modelling. Therefore, as discussed in Section 2.2.5, the overall overpotential at electrodes in migration tests can be calculated as follows,

$$\eta_a=\beta_a \, log\frac{I_a}{i_{a,0}}+\frac{RT}{nF} \, ln(1-\frac{I_a}{i_L}) \tag{3.5}$$

$$\eta_c=\beta_c \, log\frac{I_c}{i_{c,0}}+\frac{RT}{nF} \, ln(1-\frac{I_c}{i_L}) \tag{3.6}$$

where I_a and I_c represent the current density at anode and cathode, respectively. The current flowing through electrodes is assumed to be equal to that flowing through concrete surfaces, based on Equation (2.14), which can be described as follows (Li and Page, 1998; Li and Page, 2000),

$$I_c=F\sum_{i=1}^{n} z_i J_i \Big|_{x=0} \tag{3.7}$$

$$I_a=F\sum_{i=1}^{n} z_i J_i \Big|_{x=L} \tag{3.8}$$

The ionic fluxes flowing through concrete surfaces are time-varying, which implies that the electric boundaries calculated by Equations (3.3) and (3.4) also vary with time. According to Equations (3.5) and (3.6), overpotential is also influenced by Tafel parameters, which are dependent on the electrode material, electrolyte, and electrochemical reactions. Based on the range of Tafel parameters given in Section 2.2.5, five sets of Tafel parameters are selected for parametric analysis, as listed in Table 3.7.

Table 3.7 Input Tafel parameters in parametric analysis

	β_a (Mv/decade)	$i_{a,0}$ (10^{-7}A/m^2)	β_c (Mv/decade)	$i_{c,0}$ (10^{-6}A/m^2)
Highest case	200	6	280	6
High case	200	50	280	100
Base case	120	10	180	10
Low case	60	6	100	6
Lowest case	60	50	100	100

3.3.4. Solution procedure

Mass transportation within concrete and polarization at electrodes have been considered in the present overpotential model. The former is used to describe the internal multi-species transport using Transport of Diluted Species module and PDE module in COMSOL Multiphysics. The latter is employed to reflect the time-varying overpotentials in migration tests using Boundary Probe in COMSOL Multiphysics. As shown in Fig. 3.13, a sequential non-iterative algorithm (SNIA) is employed to combine the mass transport and polarizing processes. The electric potential boundaries are updated at each time increment step in SNIA. So that an accurate and unique solution for chloride penetration in concrete can be achieved. The solution procedure at each time step can be concluded as follows:

1. Initializing the boundary and initial conditions of all variables.

2. Calculating the uncorrected ionic concentrations without considering polarization and the corresponding overpotential.

3. Updating electric potential boundaries according to Equations (3.3) and (3.4) and recomputing ionic concentrations.

4. Updating corrected ionic concentrations in the next time step and repeating steps 2 to 4 until the total time of simulation is reached.

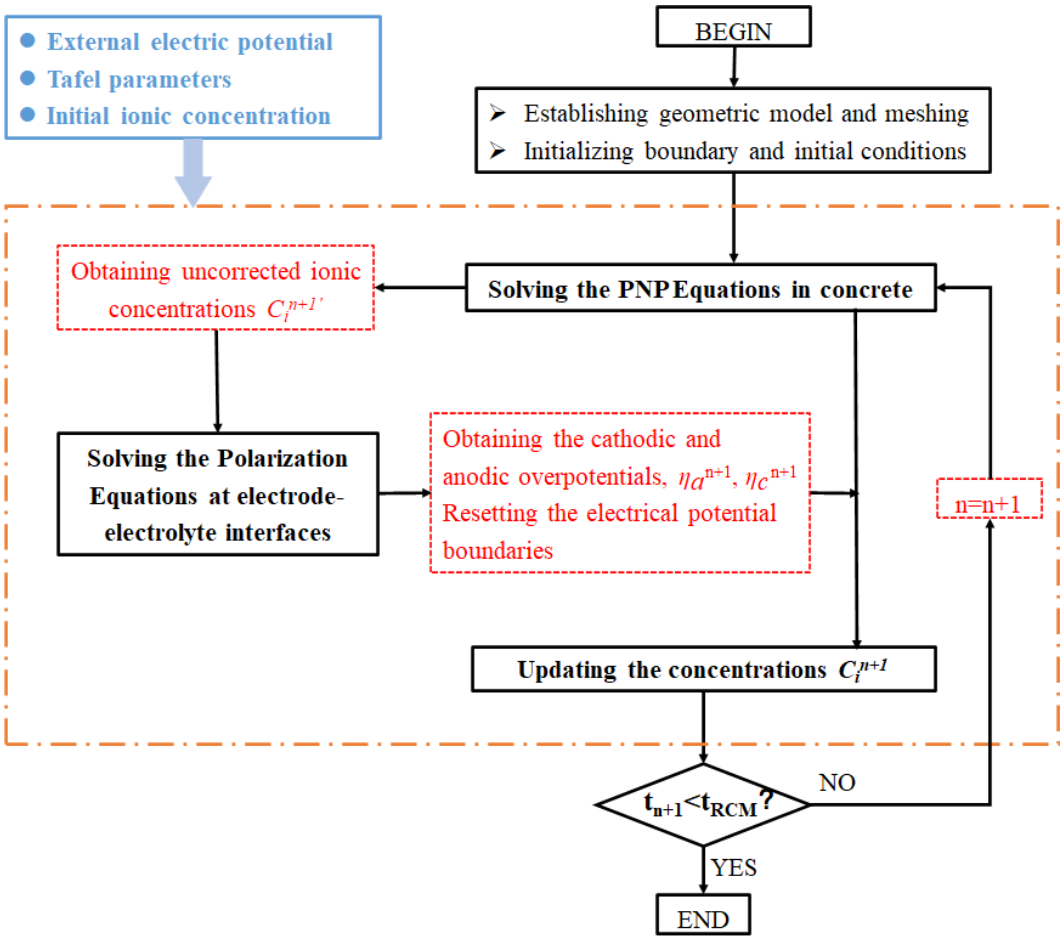

Figure 3.13 Solution procedure employed in the overpotential model

3.4. Reactive mass transport model of chloride transport

In this section, a reactive mass transport model and a non-equilibrium binding model are proposed to investigate the physicochemical reactions between free ions and cement hydrates and their influences on free- and bound-chloride distribution are examined. In reactive mass transport model, the formation/dissolution of cement hydrates and reactions on C-S-H surfaces are involved in chloride penetration by introducing thermodynamic

equilibrium. In non-equilibrium binding model, chloride binding is described by a pre-designed Langmuir isotherm.

In Sections 3.1 and 3.3, Ca^{2+}, SO_4^{2-}, and $Al(OH)_4^-$ are disregarded due to their low concentrations. However, it is important to include these three ionic species in the present reactive mass transport model to account for the thermodynamic reactions associated with chloride penetration, as discussed in Section 2.2.4.3 (Table 2.1). Therefore, this section involves the simulation of seven ionic species (Na^+, K^+, Ca^{2+}, Cl^-, OH^-, SO_4^{2-}, and $Al(OH)_4^-$) in pore solution and five hydrate phases (AFt, AFm (S), Friedel's salt, and C-S-H) in cement matrix.

3.4.1. Governing equations

With the consideration of physical and chemical reactions between free ions and cement hydration products, as discussed in Section 2.2.6, mass transport equation in saturated concrete during a migration test can be written as follows,

$$\frac{\partial C_i}{\partial t} = D_i \nabla^2 C_i + D_i \frac{z_i F}{RT} \nabla(C_i \nabla \emptyset) + R_i \tag{3.9}$$

Under the action of external electrical field, ionic transport does not always follow the centerline of connected pore path. This implies that the tortuosity effect to ionic migration is greater than that to ionic diffusion, as discussed in Section 2.4.1 (Equation (2.70)). To investigate the influence of pore size distribution on ionic transport during migration tests, the pore constrictivity parameter of ionic migration is introduced in reactive and non-equilibrium binding models. Hence, the ionic mass transport can be rewritten as,

$$\frac{\partial C_i}{\partial t} = D_i \nabla^2 C_i + \frac{D_i}{a_0^2} \frac{z_i F}{RT} \nabla(C_i \nabla \emptyset) + R_i \tag{3.10}$$

where a_0 is pore constrictivity parameter, which varies with the binder types used in

concrete. Three pore constrictivity parameters, 1.5, 2, and 3, are used in parametric analysis to investigate the influence of the binder types on ionic transport.

In reactive mass transport model, reaction term R_i can be calculated by Equations (2.39) and (2.42). The ionic diffusion coefficient of each ionic species D_i varies with the variation in porosity, as discussed in Section 2.2.4 (Equation (2.44)).

The concentration of cathodic electrolyte used in non-equilibrium binding model is 520 mol/m^3 NaCl solution. As suggested in Section 2.2.4.1, Langmuir binding isotherm is appropriate to describe the relationship between free and bound ions. The binding capacity of sodium, potassium, calcium, sulfate, and hydroxyl ions is assumed to be proportional to that of chloride. Based on Equation (2.29), reaction term R_i in non-equilibrium binding model can be expressed as:

$$R_i = p_i\, k_s \left(C_{cl} - \frac{S_{cl}}{\alpha - \beta S_{cl}} \right) \tag{3.11}$$

where $C_{cl,}$ and S_{cl} represent free and bound chloride concentrations, respectively. To keep charge balance in liquid-solid interphase, the binding proportion coefficient p_i of Cl^-, Na^+, K^+, Ca^{2+}, OH^-, SO_4^{2-}, and $Al(OH)_4^-$ can be simplified as 1, 1/8, 1/8, 1/8, -1/8, -1/8, and -1/8, respectively (Liu et al., 2014).

In non-equilibrium binding model, the governing equation of electric field can be described by Poisson's equation (Equation (2.12)). Note that the surface species absorbed by C-S-H also influence the distribution of electric potential in concrete. Therefore, in reactive mass transport model, Poisson's equation has been rewritten as follows,

$$\nabla^2 \emptyset = -\frac{F}{\varepsilon_0 \varepsilon_r} \sum_{i=1}^{n} (z_i C_i + z_c C_c) \tag{3.12}$$

where z_c and C_c are the valence number and concentrations of surface species.

3.4.2. Geometry and meshing

Fig. 3.14 shows the geometric models of three-phase NAC and five-phase RAC used in this section. The gradation, volume fraction, shape, and size distribution of aggregates and the dimension of concrete model are identical to those in the standard case outlined in Section 3.3. The old mortar in RCA not only provides an additional transport path for chlorides but also has the ability to absorb free ions. To examine the effect of old mortar on chloride penetration in concrete, three volume fractions of old mortar (represented by blue shells), 0.3, 0.4, and 0.5, are used, as shown in Fig. 3.14. The replacement rates of RCA in all RAC models are 0.5. To validate the reliability of the present reactive multi-species mass transport model, a homogeneous benchmark model with a size of 50 mm × 100 mm is developed based on the experiment conducted by Jiang et al. (2013).

The significant scale difference between ITZ and other phases and the coupling of thermodynamic reactions and multi-species transport will lead to a huge computational burden to obtain a convergent solution for reactive mass transport in concrete. Therefore, a thicker thickness of old and new ITZs, 100 μm, is used in this section to reduce the numerical scheme (as shown in Fig. 3.14).

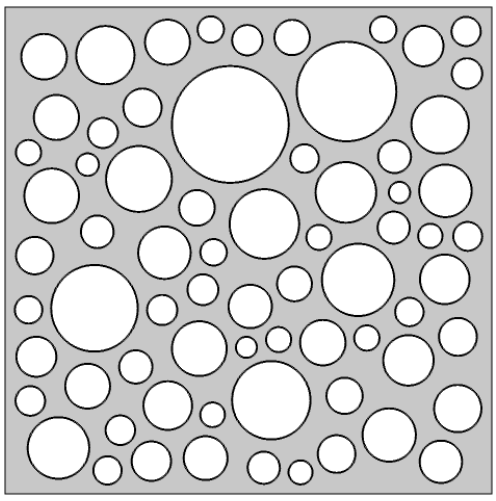

(a) NAC

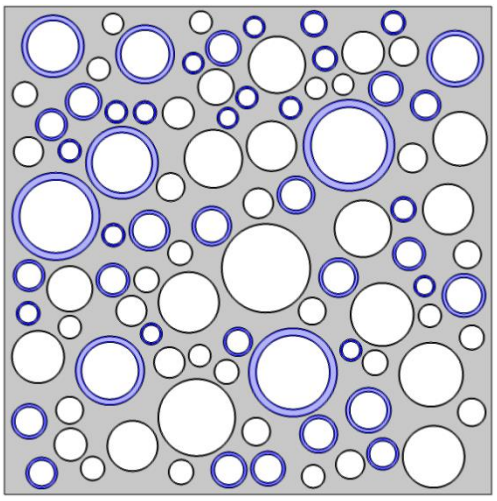

(b) RAC (V_{om}=0.3)

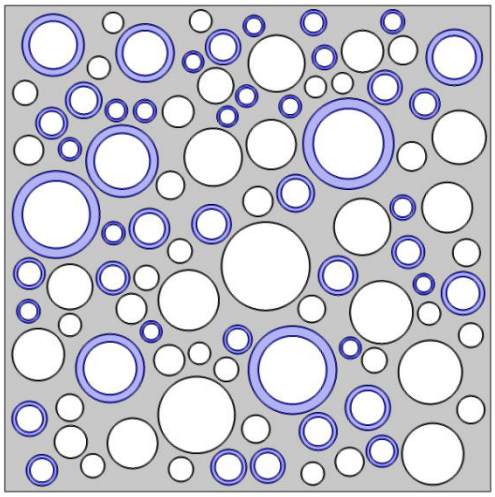

© RAC (V_{om}=0.4)

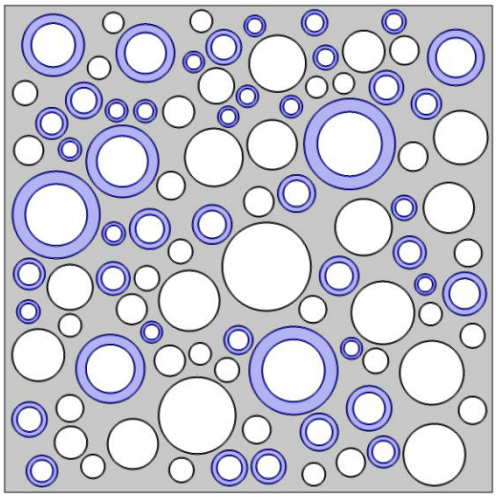

(d) RAC (V_{om}=0.5)

Figure 3.14 The geometric models of NAC and RAC with different volume fractions of old mortar (V_{om}) (The blue rings represent old adhesive mortar located between new and old ITZs)

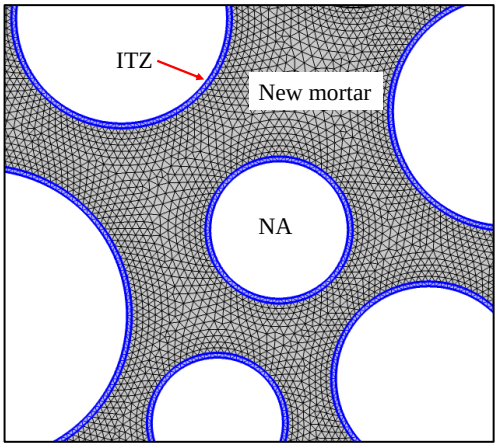

(a) NAC

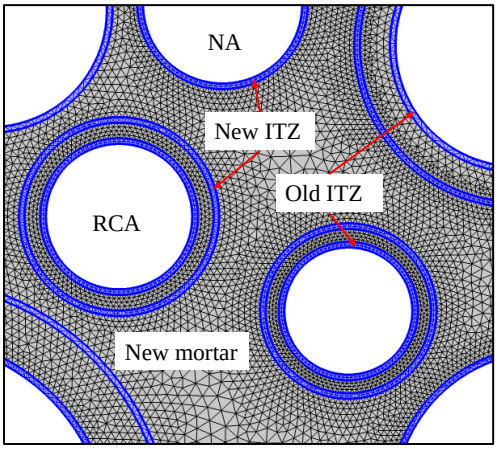

(b) RAC (V_{om}=0.4)

Figure 3.15 The zoom-in meshing of NAC and RAC

3.4.3. Diffusion properties and boundary conditions

3.3.3.1 Diffusion properties of ionic species

The diffusion coefficients and initial concentrations of all ionic species in new mortar, new ITZ, old mortar, and old ITZ are given in Table 3.8. Initial concentrations of cement hydration and binding constants are taken from Guo et al. (2021a) and Yuan et al. (2013)

and recomputed for the concentration unit (mol/m^3) used in this thesis. The concentration of cement hydrate varies with the types of concrete, which can influence the reactions between free ions and cement hydrates, specifically the reaction between chlorides and AFm. To investigate the influence of the concrete types on chloride binding, three AFm concentrations are used in parametric analysis, as given in Table 3.8.

Table 3.9 shows the input parameters used in benchmark model, derived from the experimental research conducted by Jiang et al. (2013). Considering the inclusion of supplementary cementitious materials (FA, SF, and GGBS) in this experiment, a higher pore constrictivity (a_0 = 3) is employed in benchmark model, following the recommendation by Yang et al. (2017). Initial concentrations of cement hydrates are assumed to be identical to those used in standard case as indicated in Table 3.8.

Table 3.8 The input parameters in the present reactive mass transport and non-equilibrium binding models for chloride migration tests

Parameter	Notation	Standard case	Parametric cases	Reference
Duration (hour)	t	24	24	
Voltage applied (V)	$\Delta\Phi$	24	24	
Initial porosity (%)	ϕ	13.6	13.6	(Guo et al., 2021a)
Adsorption/desorption rate (1/s)	k_s	5.0×10^{-4}	5.0×10^{-4}	(Li et al., 2015)
Binding constants	α	1.40	1.40	(Yuan et al., 2013)
	β	0.0008 (m^3/mol)	0.0008 (m^3/mol)	
Aggregate volume fraction	V_a	0.5	0.5	
Constrictivity factor	a_0	2	1.5, 2, 2.5	(Yang et al., 2017)
Diffusion coefficient in new mortar ($\times10^{-11}$ m^2/s)	$Ca2^+$	0.79	0.79	(Samson and Marchand, 2007a; Hosokawa et al., 2011a)
	SO_4^{2-}	1.07	1.07	
	$Al(OH)_4^-$	5.04	5.04	
	OH^-	5.26	5.26	
	$Ca2^+$	0.79	0.79	
	SO_4^{2-}	1.07	1.07	
	$Al(OH)_4^-$	5.04	5.04	
Diffusivity ratio between ITZ and mortar	k_{itz}	2	2	(Hu et al. 2018)
Diffusivity ratio between old and new mortar	k_{om}	1.5	1.5	(Hu et al. 2018)
Initial concentration (mol/m^3)	K^+	400	400	(Guo et al., 2021a)
	Na^+	100	100	
	Cl^-	0	0	
	OH^-	500	500	
	$Ca2^+$	3	3	
	SO_4^{2-}	2	2	
	$Al(OH)_4^-$	2	2	
	CH	2660	2660	
	AFm	150	100, 150, 250	
	AFt	160	160	
	CSH reaction sites	2132	2132	
	Fridel's salt	0	0	

Table 3.9 Input parameters in benchmarked models.

Parameters	Notation	Jiang's expt. (Jiang et al., 2013)
Size of specimen (mm×mm)	-	50×100
Water/cement ratio	w/c	0.5
Adsorption/desorption rate	k_s	5.0×10^{-4} (1/s)
Constrictivity factor	a_0	3
Binding constants	α	1.686
	β	0.0099
Initial ionic concentration (mol/m^3)	K^+	602
	Na^+	200
	Cl^-	0
	OH^-	800
	$Ca2^+$	1
	SO_4^{2-}	1
	$Al(OH)_4^-$	2
Electric potential at anode	Φ_a	30 V
Electric potential at cathode	Φ_c	0 V
Aggregate volume fraction	V_a	0
Anolyte (mol/m^3)	$NaOH$	300
Catholyte (mol/m^3)	$NaCl$	500
RCM test time	-	36 hours

3.4.3.2 Electric and ionic boundaries

The ionic concentrations and electric potential at boundaries in standard and parametric study cases are the same as those employed in Section 3.1, as listed in Table 3.1. In benchmark model, the ionic concentrations and electric potential at boundaries are given in Table 3.9.

3.4.4. Solution procedure

For the non-equilibrium binding model, mass transport (Equations (3.9) and (3.11)) and electric potential distribution (Equation (2.12)) can be synchronously solved by the Transport of Diluted Species module and PDE module in COMSOL Multiphysics. For the reactive mass transport model, physicochemical reactions between hardened cement and free ions, multi-species transport in pore solution, and porosity change are interacting

and inter-influencing. To resolve this multi-field coupling problem, SNIA is adopted for reactive mass transport in concrete. Generally, the solution procedure can be divided into the following steps:

1. Initializing input parameters, including initial and boundary conditions of hydrate phases and free ions, diffusion coefficients of all ionic species in new mortar, new ITZ, old mortar, old ITZ, electrical boundary, and pore constrictivity parameter.
2. The distribution of all hydrates and free ions at each time step is determined by simultaneously solving thermodynamic equilibrium and multi-species transport using the Transport of Diluted Species, PDE, and Reaction modules in COMSOL Multiphysics.
3. The calculated concentrations of cement hydrates in step 2 are used to update the porosity of concrete based on their molar mass and density. The updated porosity is subsequently used to recompute the concentrations of all ionic species and hydrates.
4. Updating corrected ionic concentrations in the next time step and iterating through steps 2 to 4 until the total simulation time is reached.

3.5. Summary

This chapter provides a theoretical framework and methodology for modelling the chloride penetration in saturated NAC and RAC during chloride diffusion and migration tests. The first section presents three multi-species models simulating the chloride diffusion or migration test. The second section details the construction of 2-D multi-phase diffusion models to analyze the effective chloride diffusion coefficient in heterogeneous concrete, incorporating the impact of various parameters of NA and RCA. The third section investigates the effect of polarization at electrodes on ionic transport in concrete during migration tests. The fourth section presents the reactive mass transport model, considering multi-species transport, thermodynamic reactions, and pore evolution during the course of ionic transport.

CHAPTER 4 INFLUENCE OF MULTI-SPECIES COUPLING ON CHLORIDE PENETRATION IN CONCRETE

4.1. Introduction

The purpose of this chapter is to characterize the influence of multi-species coupling on chloride penetration in concrete during the chloride diffusion and migration tests. The numerical scheme of this chapter is covered in Section 3.1 and in relation to objective 1, outlined in Section 1.2. Based on Poisson, Strong-EN, and Weak-EN models, the time-space distributions of four ionic species (K^+, Na^+, Cl^-, and OH^-) and the electric potential gradient in concrete during chloride diffusion and migration tests can be evaluated and compared. The differences and application scopes of these three models are discussed and concluded in this chapter.

4.2. Numerical results of chloride diffusion test

Figs. 4.1-4.2 present the distributions of electric potential and potential gradient in concrete calculated by Poisson, Strong-EN, and Weak-EN models. When Poisson's equation or current conservation law is employed as the governing equation, the electrostatic potential and potential gradient in Poisson and Weak-EN models do not remain at zero, even when no external voltage is applied during diffusion tests. The presence of a small internal electric field in Poisson and Weak-EN models can be attributed to the different mobilities of various ionic species in pore solution, as described by Equations (2.12) and (2.20). Laplace's equation (Equation (2.13)) used in Strong-EN model releases the interactions between different ions. Hence, it is evident that the electric potential and potential gradient in Strong-EN model are observed to be zero.

Figs. 4.3-4.6 show the distributions of chloride, hydroxyl, potassium, and sodium ions after a 14-day diffusion test. The chloride profiles obtained from Poisson model and Weak-EN model are almost the same, which is consistent with the findings from Johannesson (2010a). Chloride penetration depths obtained from Poisson and Weak-EN

models are slightly deeper compared to those from Strong-EN models. Due to the multi-species coupling, the ionic distribution profiles in Poisson model and Weak-EN model for other species are correspondingly altered. This means that the internal electric field arising from multi-species coupling has the potential to accelerate ionic transport in concrete. It is important to note that the difference in chloride ingress depth due to multi-species coupling in diffusion tests is minimal, measuring less than 0.5 mm. This indicates that the dominant driving force is still the concentration gradient, and the effect of multi-species coupling is relatively minor and can be disregarded in diffusion test simulations. Strong-EN model demonstrates its accuracy and simplicity in simulating the diffusion process in saturated concrete.

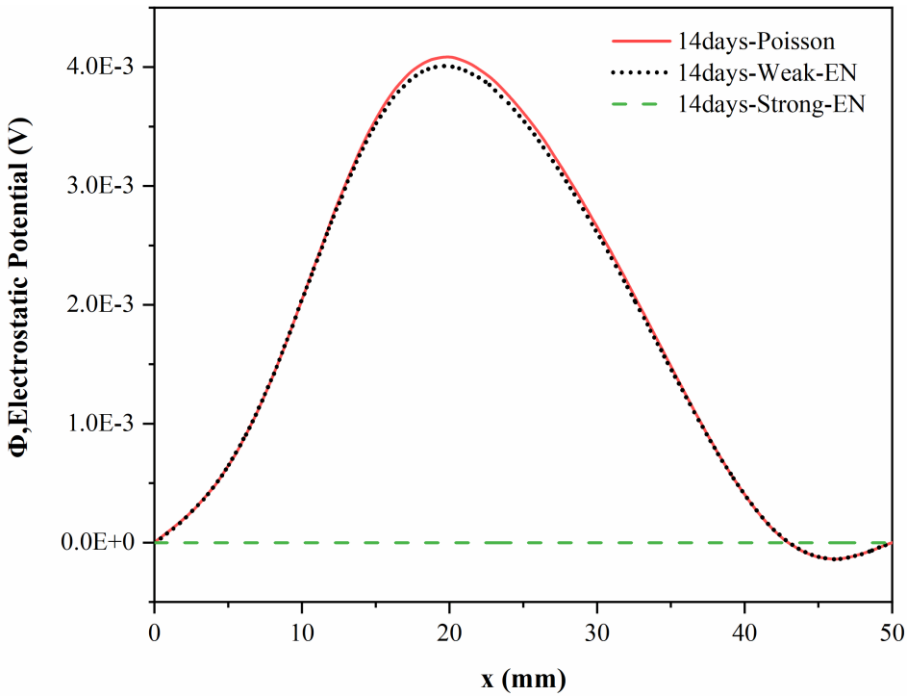

Figure 4.1 Comparison of electrostatic potential distribution profiles calculated by Poisson, Weak-EN, and Strong-EN models after 14-day diffusion

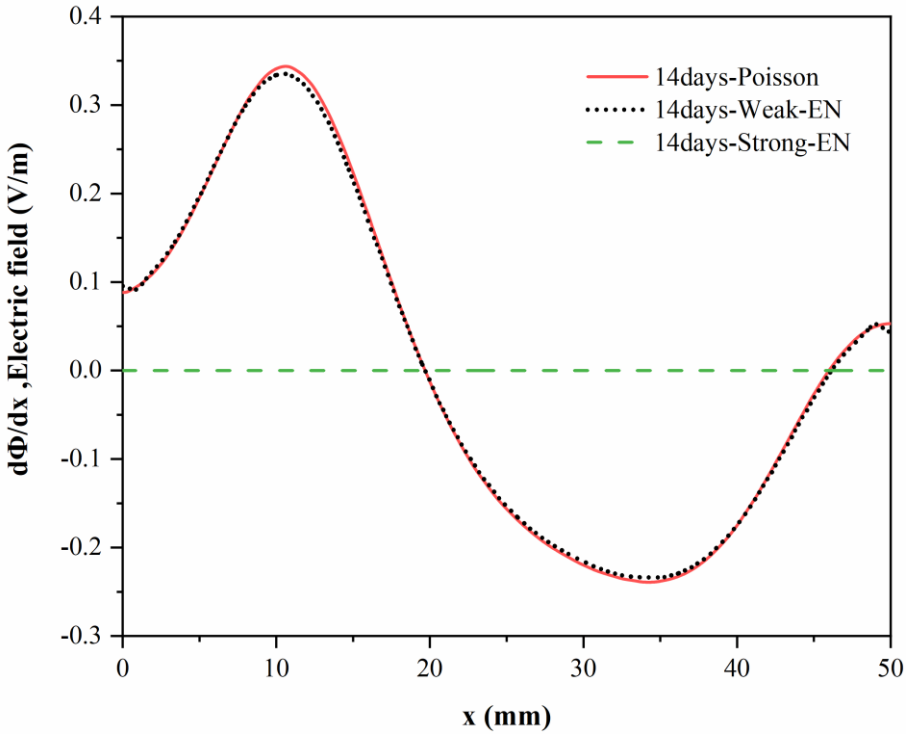

Figure 4.2 Comparison of electrostatic potential gradient distribution profiles calculated by Poisson, Weak-EN, and Strong-EN models after 14-day diffusion

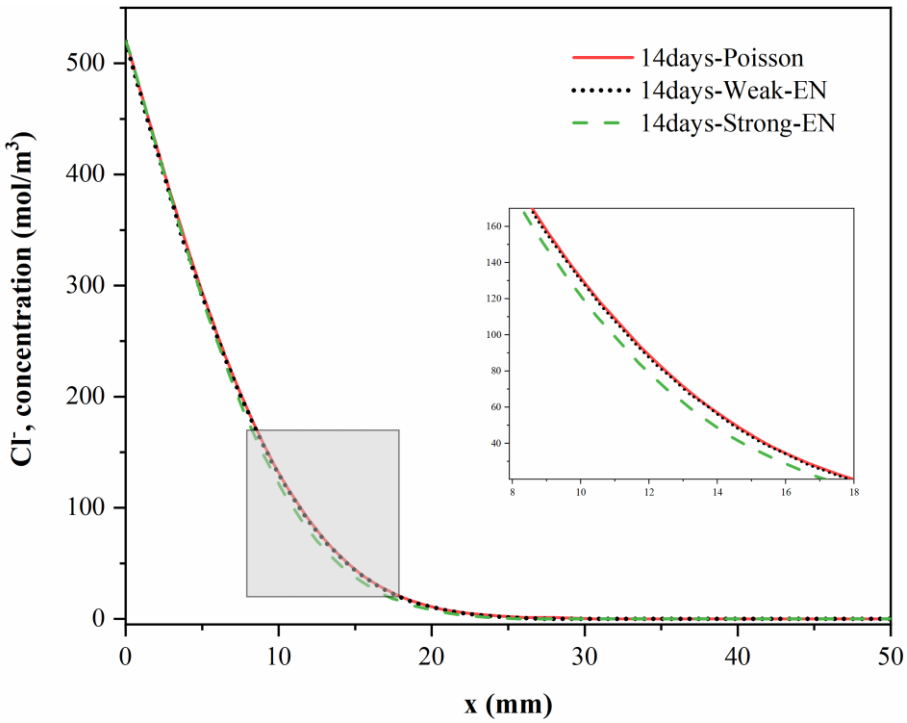

Figure 4.3 14-day diffusion profiles of chlorides calculated by Poisson, Weak-EN, and Strong-EN models

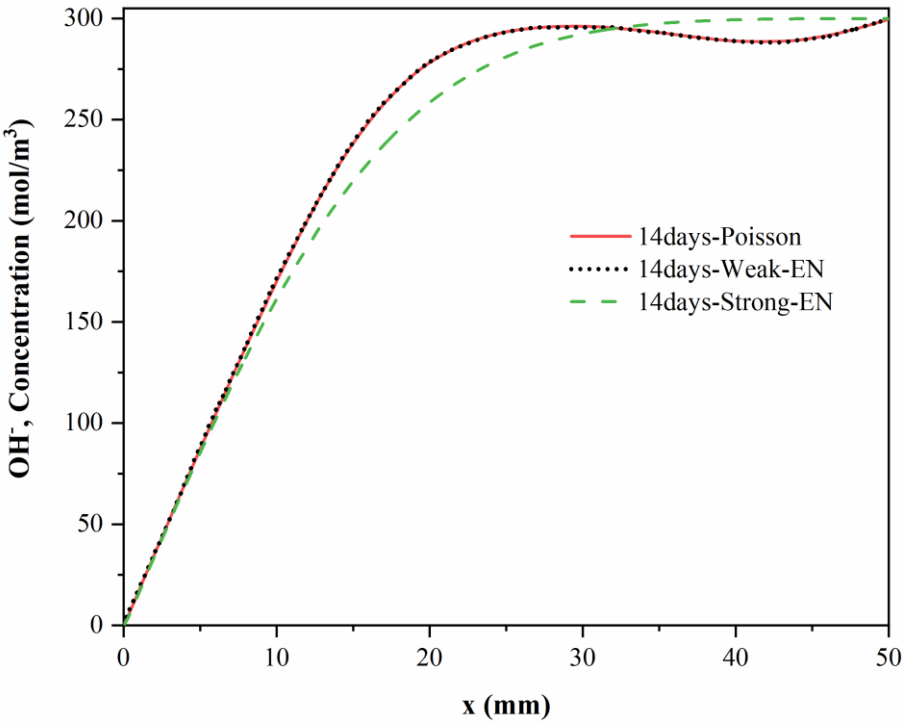

Figure 4.4 14-day diffusion profiles of hydroxyl ions calculated by Poisson, Weak-EN, and Strong-EN models

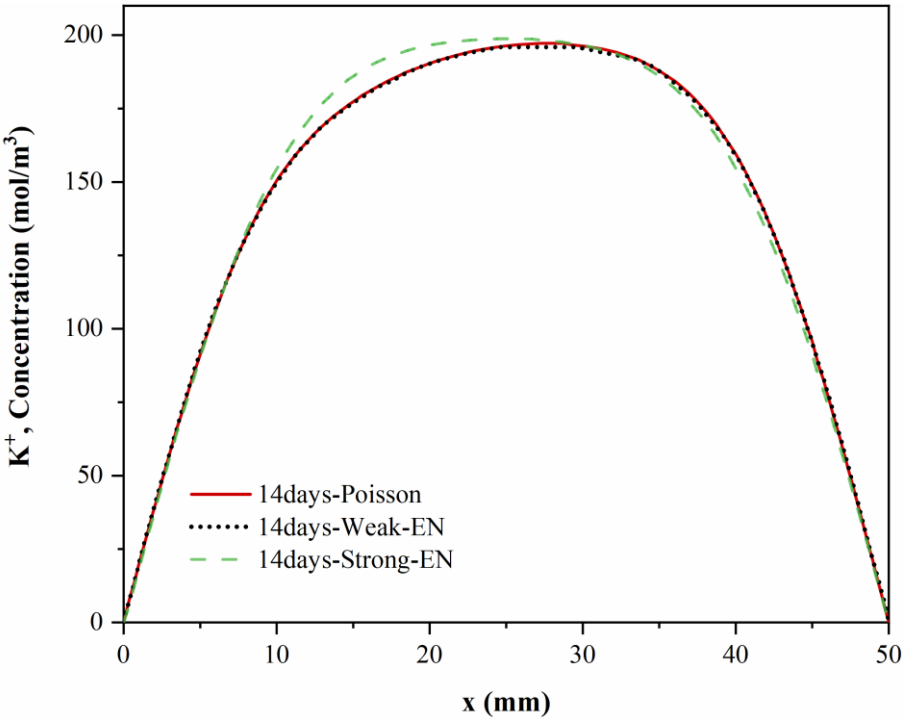

Figure 4.5 14-day diffusion profiles of potassium ions calculated by Poisson, Weak-EN, and Strong-EN models

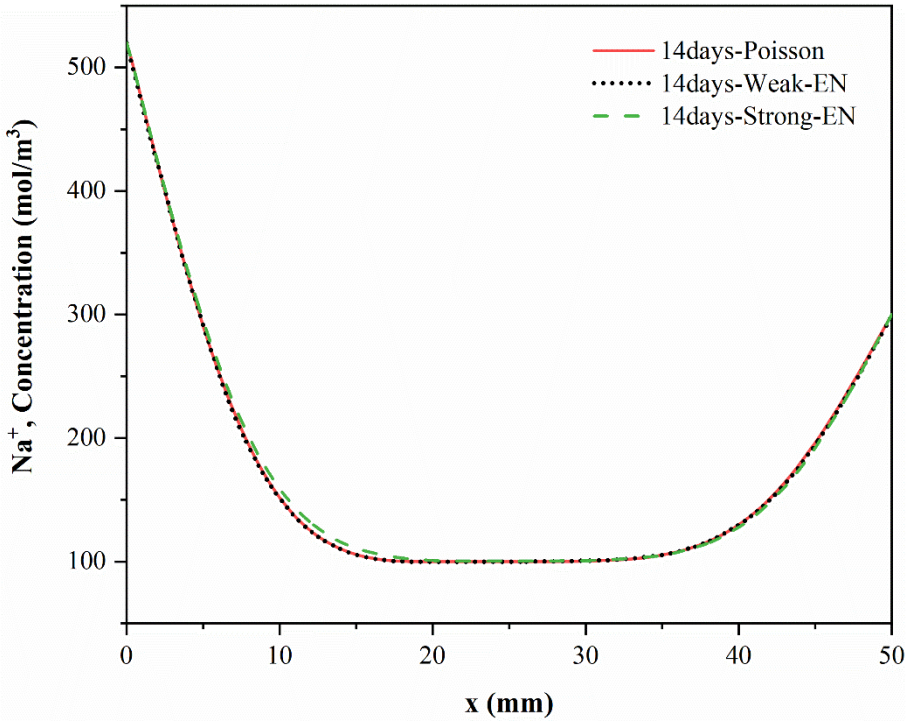

Figure 4.6 14-day diffusion profiles of sodium ions calculated by Poisson, Weak-EN, and Strong-EN models

4.3. Numerical results of chloride migration test

Figs. 4.7-4.8 show the distribution profiles of electric potential and potential gradient concrete after an 8-hour chloride migration test. According to Laplace's equation (Equation (2.13)), the electric potential gradient in Strong-EN model is constant and only determined by the externally applied voltage and length of concrete, that is $\nabla\emptyset = \Delta\emptyset/L = 480$ V/m. This constant electric potential gradient indicates that the interactions between different ionic species are released in Strong-EN model. However, the electrostatic potential gradients obtained from Poisson and Weak-EN models exhibit pronounced non-linearity and remarkable similarity. The observation in Fig. 4.8 highlights the presence of sudden jumps in the potential gradients in Poisson and Weak-EN models, which vary both in position and time. The time- and space-varying electric potential gradient in Poisson and Weak-EN models indicates that the migration velocity of each ionic species varies with position and time. This is in contrast to the Strong-EN model, where the electric potential gradient remains constant.

Figs. 4.9-4.12 show that the ionic transport behaviors in Strong-EN model differ significantly from those in Poisson and Weak-EN models under the action of different electric potential fields. Generally, negatively charged chloride and hydroxyl ions migrate towards the anode, while positively charged potassium and sodium ions move toward the cathode. In Strong-EN model, the migration wave fronts of four species exhibit noticeable differences and are proportional to their diffusion coefficients. For example, the diffusion coefficient and wave speed of hydroxyl ions are nearly three times greater than those of chloride ions. This observation further emphasizes that ionic transport occurs independently from one to another in Strong-EN model.

In contrast, in Poisson and Weak-EN models, the wave fronts of similarly charged ionic species are aligned at the same depth. For example, despite the significant difference in diffusion coefficients between chloride and hydroxyl ions, their wave fronts are located at the same position (approximately 25 mm from cathodic surface), as shown in Figs. 4.9 and 4.10. This phenomenon implies that multi-species coupling can accelerate chloride ingress and slow down the removal of hydroxyl ions. Similarly, Figs. 4.11 and 4.12 show the correspondingly altered transport behaviors of positively charged potassium and sodium ions in Poisson and Weak-EN models. It is worth noting that, in contrast to findings from the simulation of diffusion test (Section 4.2), the difference in ionic distributions between linear and non-linear electric potential models for migration tests is significant. This implies that an externally applied field can significantly enhance the influence of multi-species coupling on ionic transport. These findings highlight the significance of ion-ion interactions between different ionic species in simulating chloride migration and indicate that such interactions cannot be ignored in the following study.

Fig. 4.13 shows the distributions of all variables obtained from Poisson and Weak-EN models at three different times. It can be observed from Fig. 4.13 (a) that the nonlinearity of electric potential becomes less noticeable over time. This phenomenon indicates that the difference in migration speeds of different ionic species gradually decreases as chloride ions permeate concrete. There are minor discrepancies in ionic distributions

between Poisson model and Weak-EN model at the cathodic boundary. These differences do not affect the calculation of chloride migration coefficients as given in Equation (2.45).

Despite the inclusion of electroneutral assumption $\sum(z_i{*}C_i) \approx 0$ in Weak-EN model, the distributions of all ionic species and electric potential obtained from it are almost the same as those obtained from Poisson model. This demonstrates that both Poisson model and Weak-EN model proposed in Section 3.1 can be used to simulate multi-species transport in migration tests. However, it is important to note that each model has a specific scope of application. Firstly, as discussed in Section 2.2.3, Weak-EN model is suitable for tests involving current or voltage boundaries, whereas Poisson model is limited to solving problems with voltage boundaries. Secondly, due to the order-of-magnitude of $\frac{F}{\varepsilon_0\varepsilon_r}$ in Poisson's equation reaching up to 10^{14}, the net charge $\sum(z_i{*}C_i)$ in concrete should be a very small number to ensure that $\nabla^2\emptyset$ remains a finite value. Consequently, the solution of Poisson model involves the multiplication of a very large number and an extremely small number. This indicates that Poisson model requires higher precision, finer elements, and longer computation times compared to Weak-EN model. Therefore, numerically, Weak-EN model is a preferable option for achieving a balance between simulation accuracy and the computational burden involved in modelling multi-species coupling. Lastly, it should be noticed that the derivation of Equations (2.19) or (2.20) used in Weak-EN model neglected the effects of other important phenomena, such as physical and/or chemical reactions between ions and cement hydrates. The additional reaction terms cannot be included in the constitutive assumption of current conservation law (Equation (2.14)). In contrast, Poisson's equation establishes a direct relationship between the distribution of ions and electric field. Therefore, Poisson model is applicable for modelling ionic transport while considering factors such as chloride binding and/or other reactions involved in chloride penetration.

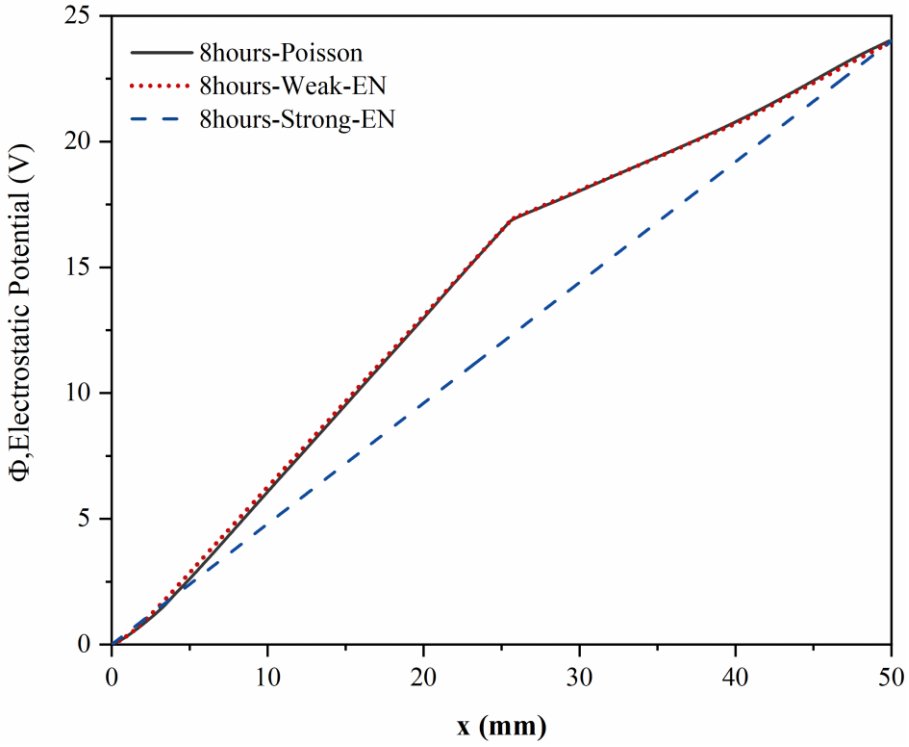

Figure 4.7 Comparison of electrostatic potential distribution profiles calculated by Poisson, Weak-EN, and Strong-EN models after 8-hour migration test

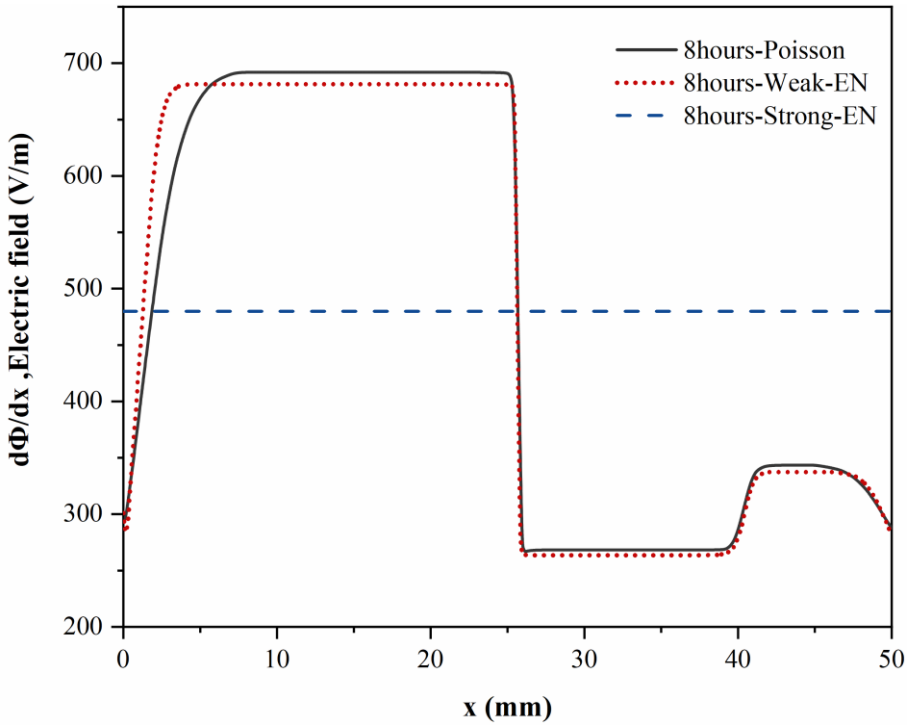

Figure 4.8 Comparison of electrostatic potential gradient distribution profiles calculated by Poisson, Weak-EN, and Strong-EN models after 8-hour migration test

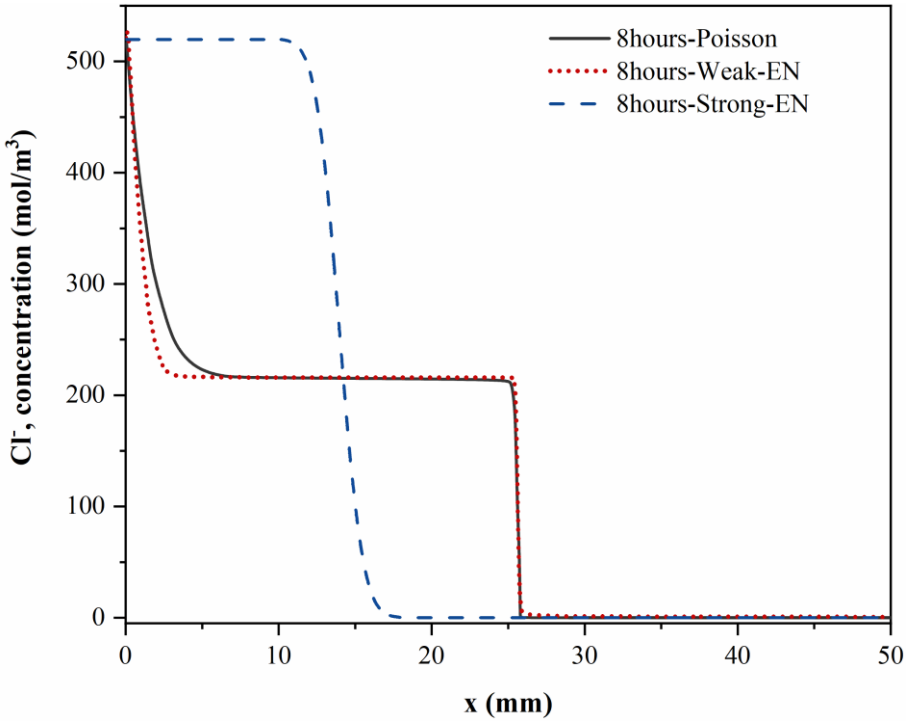

Figure 4.9 Distribution profiles of chlorides calculated by Poisson, Weak-EN, and Strong-EN models after 8-hour migration test

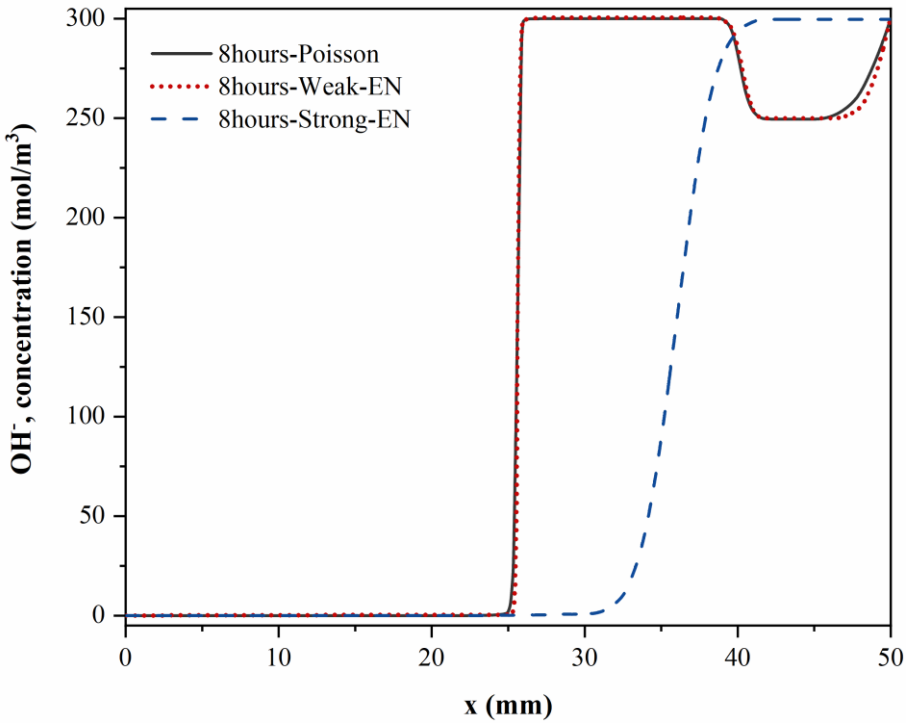

Figure 4.10 Distribution profiles of hydroxyl ions calculated by Poisson, Weak-EN, and Strong-EN models after 8-hour migration test

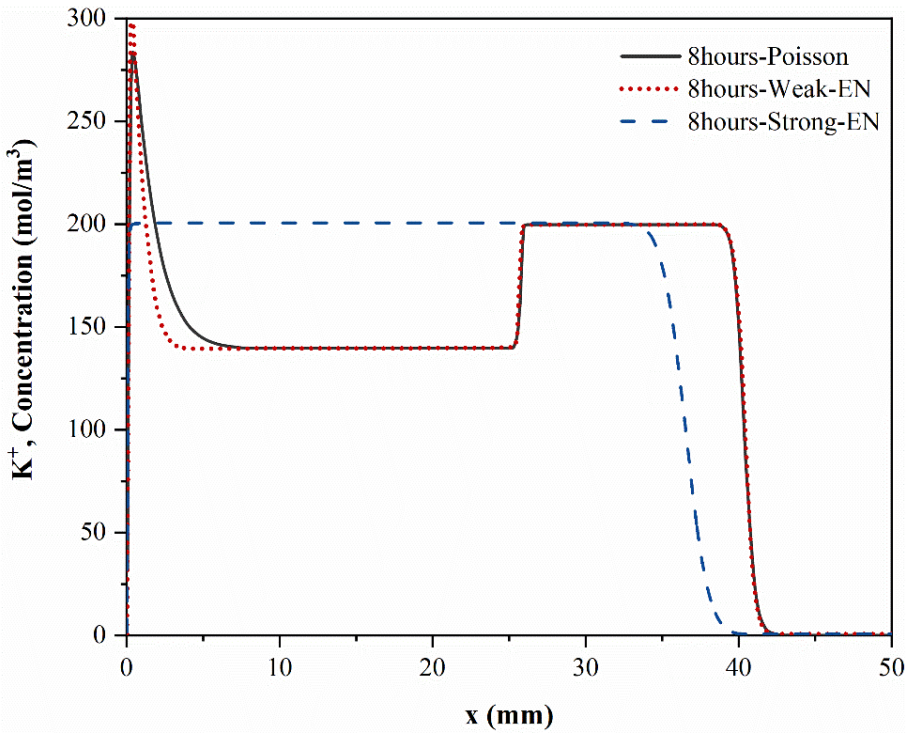

Figure 4.11 Distribution profiles of potassium ions calculated by Poisson, Weak-EN, and Strong-EN models after 8-hour migration test

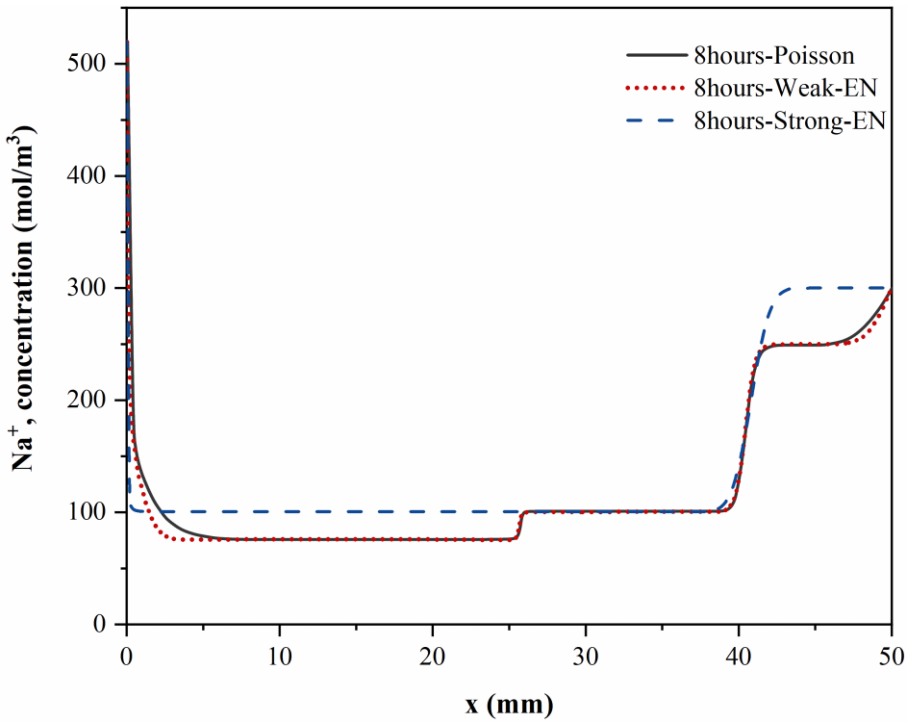

Figure 4.12 Distribution profiles of sodium ions calculated by Poisson, Weak-EN, and Strong-EN models after 8-hour migration test

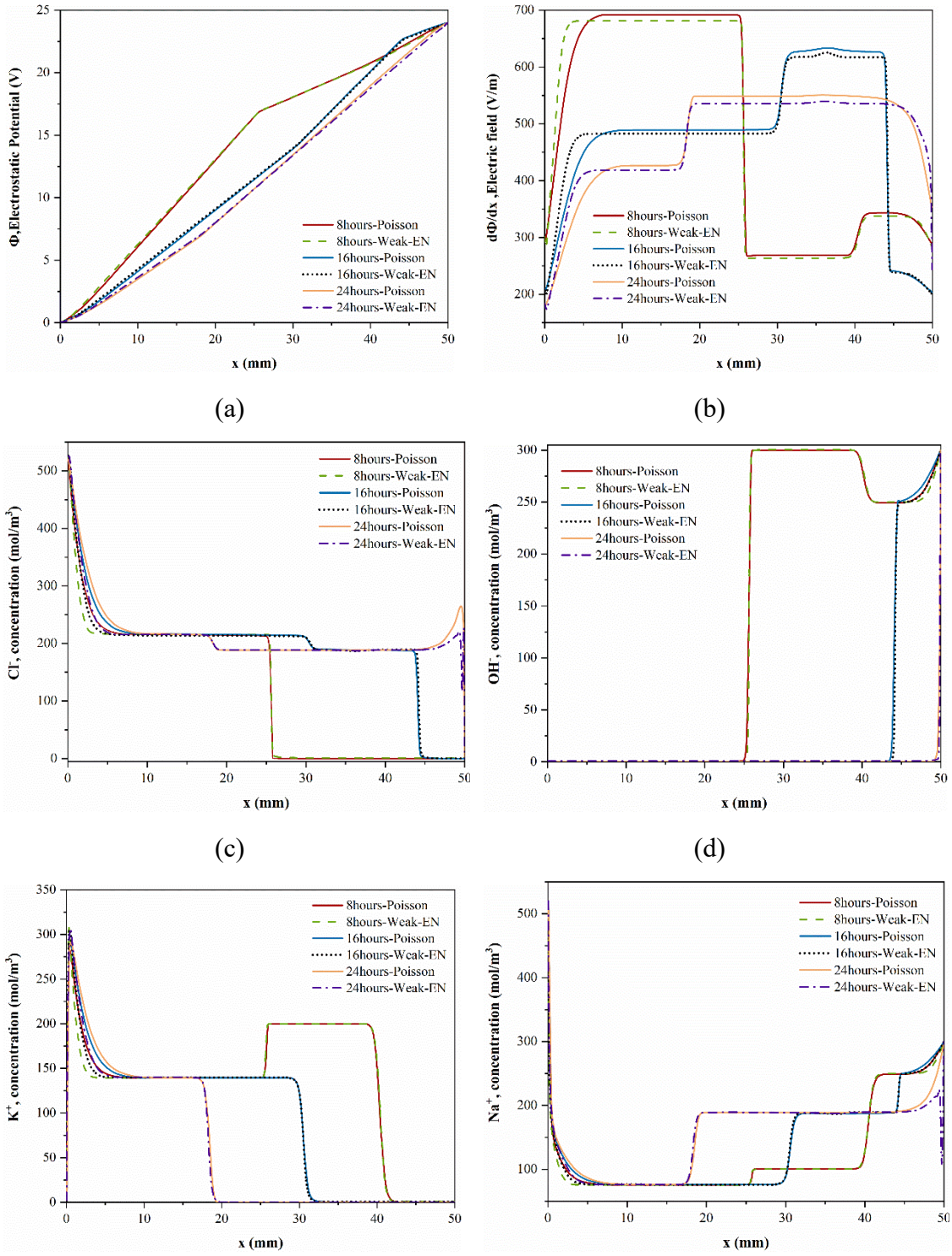

Figure 4.13 Distribution profiles at three different times for (a) electrostatic potential, (b) electrostatic potential gradient, (c) chloride ions, (d) hydroxyl ions, (e) potassium ions, (f) sodium ions

4.4. Summary

In this chapter, three multi-species models based on Poisson's equation, Laplace's equation, and current conservation law are used to investigate the influence of ion-ion interactions on chloride transport during diffusion and migration tests. By comparing the distributions of individual ionic species and electric potential obtained from each model, the following conclusions can be drawn:

1) The influence of multi-species coupling on chloride diffusion (when there is no external electric field involved) is quite limited and can be ignored.

2) Laplace's equation used in Strong-EN model releases the multi-species coupling. Therefore, when conducting simulations focused solely on the diffusion process, Strong-EN model is a suitable choice due to its accuracy and simplicity.

3) During the simulation of chloride migration tests, multi-species coupling significantly increases the nonlinearity of electric field and accelerates chloride ingress, making it imperative to consider multi-species coupling in simulations.

4) The similarity of ionic distribution profiles obtained from Poisson and Weak-EN models implies that both Poisson's equation and the current conservation law can adequately capture the influence of ion-ion interactions between different ionic species.

5) Poisson model is suitable for simulating migration tests that involve the application of voltage, while Weak-EN model is appropriate for migration tests with either external current or voltage.

6) The solution of Poisson model requires high precision in finite element calculation and a longer computation time. Weak-EN model offers a better balance between computation burden and accuracy when modelling multi-species transport in

migration tests.

7) Poisson model establishes a direct relationship between the distribution of ions and the electric field in concrete. In comparison to Weak-EN model, it is more adaptable for simulating cases involving chemical and/or physical reactions.

CHAPTER 5 INFLUENCE OF HETEROGENEITY OF CONCRETE ON CHLORIDE PENETRATION

5.1. Introduction

As has been mentioned in Chapter 4, ion-ion interactions between different ionic species can be ignored when there is no external electric field involved. This means that chloride transport in diffusion tests can be assumed to be independent of the transportation of other ionic species. Hence, only chloride is considered in the five-phase numerical model and two-step analytical model used in this chapter.

This chapter focuses on chloride transport properties in heterogenous NAC and RAC during chloride diffusion tests, considering the presence of different phases, including the old ITZ, old mortar, new ITZ, and new mortar. The numerical scheme of this chapter is covered in Section 3.2 and in relation to objective 2, outlined in Section 1.2. The variation of effective chloride diffusivity of RAC is investigated with respect to different volume fractions and quality of old mortar and old ITZ, replacement rate of RCA, properties of new ITZ, and total volume fractions of aggregates. The accuracy of both analytical and numerical models is validated against existing experimental and numerical studies published in literature.

5.2. Results and Discussion

5.2.1. Numerical results

The distribution of aggregates in five-phase concrete models exhibits variability and uncertainty because all aggregates are randomly generated and positioned, as described in Section 3.2.1. Fig. 5.1 shows several geometric models with the same aggregate parameters (V_{TA}=0.3, V_{om}=0.3, V_{RCA}=0.5, d_{min}=2mm, d_{max}=15mm, Fuller gradation). Yu and Wu (2019) reported that the mechanical and durability properties of NAC or RAC may vary due to the random distribution of aggregates. And they found that the

mechanical properties of concrete gradually tend to be stable as the number of samples increases. If the number of numerical samples is too small, effective chloride diffusivity cannot be accurately assessed. A large number of numerical samples will lead to time-consuming computation. Hence, it is crucial to determine an appropriate number of numerical samples before investigating the influences of each phase in concrete.

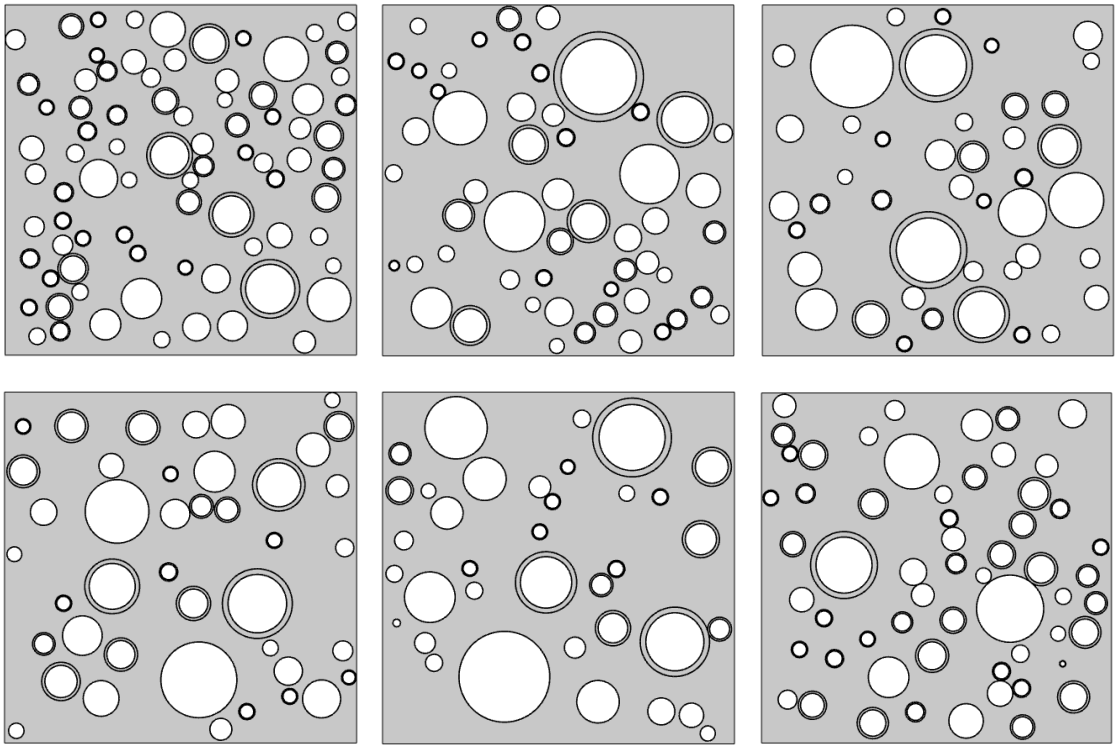

Figure 5.1 Geometric models with randomly generated and located aggregates (V_{TA}=0.3, V_{om}=0.3, V_{RCA}=0.5, d_{min}=2mm, d_{max}=15mm, Fuller gradation)

For comparison, the chloride diffusivity of RAC is normalized as a ratio between the effective diffusivity of RAC and that of new mortar (D_{eff}/D_{nm}). Figs. 5.2 and 5.3 demonstrate the variations of the average and standard deviations of normalized diffusivity with the number of numerical samples. Four RCA replacement rates, 0, 0.2, 0.5, and 1, are involved, and other parameters are the same as those in a standard case as listed in Table 3.2. When the number of numerical samples reaches 15, both the average values and standard deviations of chloride diffusivity of RAC remain almost unchanged, indicating that 20 random trials for each specific RAC model are adequate for the following investigation.

Moreover, aggregate shape varies and is irregular in realistic situations. However, in most existing numerical models, aggregates are assumed to be perfect circles. To investigate the influence of aggregate shape, NA and/or RCA are assumed to be circles and irregular polygons, respectively. Other aggregate parameters are the same as those used in Fig. 5.1. Chloride diffusivities in each phase are identical to the values listed in Table 3.2 under the standard case. To avoid the influence of the random distribution of aggregates, 20 numerical samples are generated for each concrete model with different aggregate shapes. Fig. 5.4 plots the average normalized chloride diffusivities of concrete with different RCA replacement rates and different aggregate shapes. Aggregate shape has an insignificant impact on chloride diffusion in both NAC and RAC, with a maximum difference of only 2.3% between circular and irregular aggregate cases. This indicates that the shape effects on chloride transport can be neglected. Thus, the circular aggregates can be used in subsequent investigations.

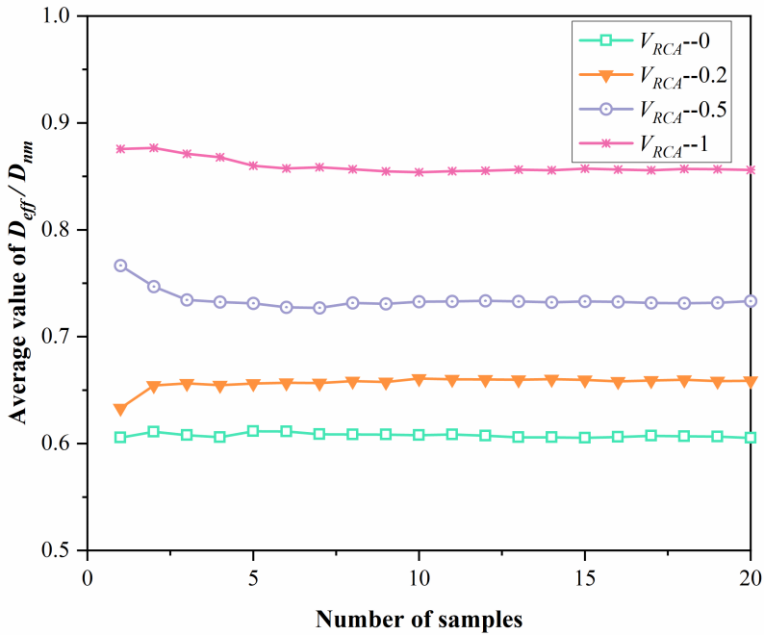

Figure 5.2 Average D_{eff}/D_{nm} in NAC and RAC

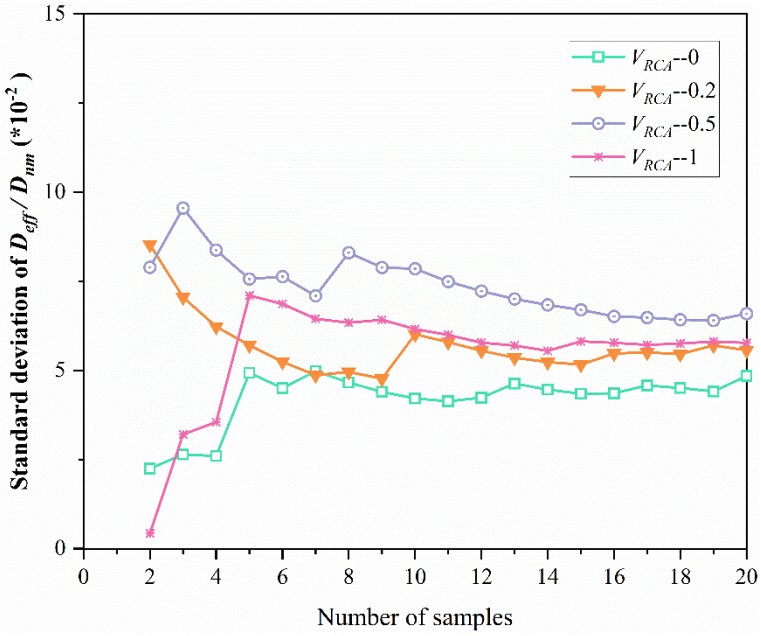

Figure 5.3 Standard deviation of D_{eff}/D_{nm} in NAC and RAC

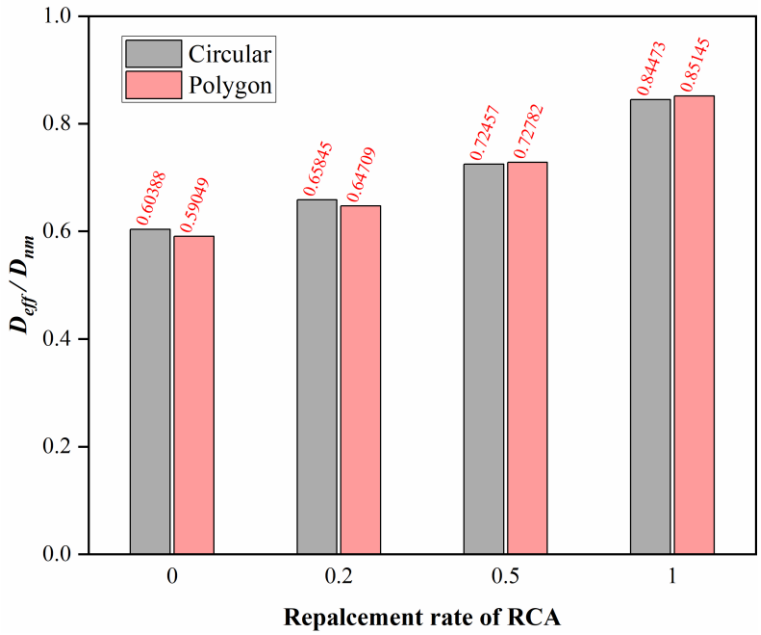

Figure 5.4 Normalized chloride diffusivity in NAC and RAC with various aggregate shapes

The most notable difference between RCA and NA is the presence of old mortar in RCA that cannot be completely removed. An investigation of the content and chloride resistance of old mortar in RCA is conducted in this section with four RCA replacement

rates. Other input parameters are identical to those used in standard case (Table 3.2). Fig. 5.5 presents the variation of the normalized diffusion coefficient in RAC with different volume fractions of old mortar in RCA. As expected, the old mortar content in RCA has a significant impact on the chloride resistance of RAC. Specifically, when there is a greater amount of mortar adhering to old natural aggregates, the chloride resistance of RAC is reduced. The negative effect of old mortar becomes more pronounced as the replacement rate of RCA increases. Specifically, when V_{om} increases from 0.1 to 0.5, the effective diffusivity increases by 0%, 3.7%, 11.5%, and 31.3% for a given V_{RCA} of 0, 0.2, 0.5, and 1, respectively. This can be explained by the fact that, when V_{om} in RCA is constant, the total amount of old mortar in concrete increases as V_{RCA} increases.

Fig. 5.6 illustrates the variation of normalized chloride diffusivity of RAC with different chloride diffusivities of old mortar. The results demonstrate that when V_{om} is 0, RAC is essentially equivalent to NAC, and effective chloride diffusivity is unaffected by the chloride permeability of old mortar. In cases where V_{om} is non-zero, the chloride resistance of RAC increases with decreasing diffusivity in old mortar. This tendency is particularly noticeable in RAC with a higher content of old mortar. Even when RCA is obtained from high-quality parent concrete (low chloride diffusivity, k_{om} = 0.2), the chloride resistance of RAC is still lower than that of NAC. That highlights the importance of prioritizing chloride prevention in concrete structures utilizing RCA.

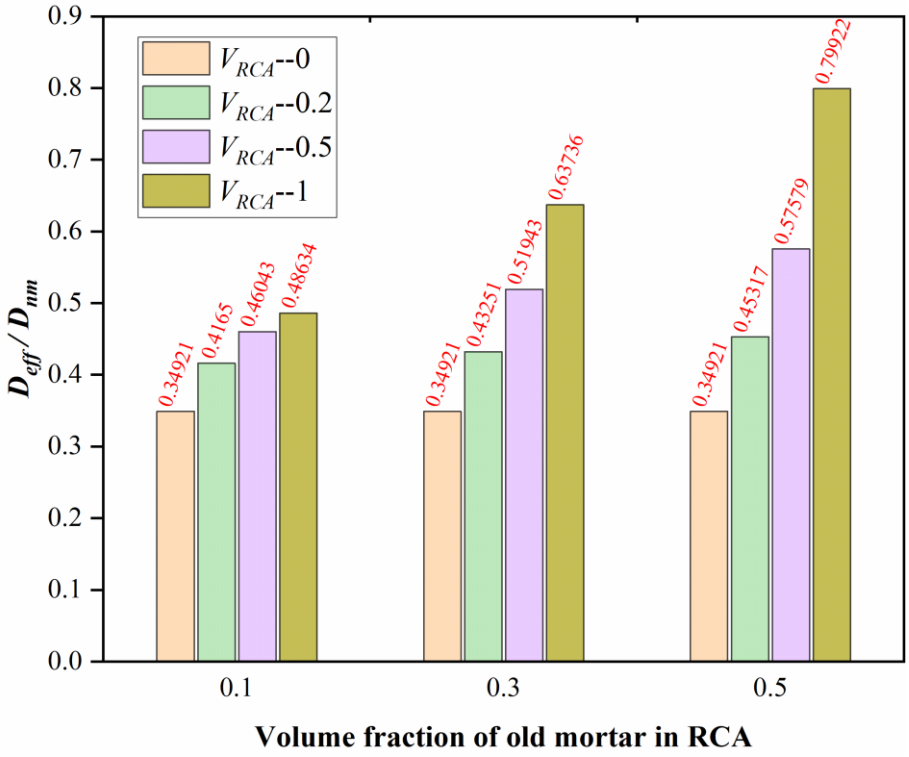

Figure 5.5 Normalized chloride diffusivity in NAC and RAC with various volume fractions of old mortar in RCA

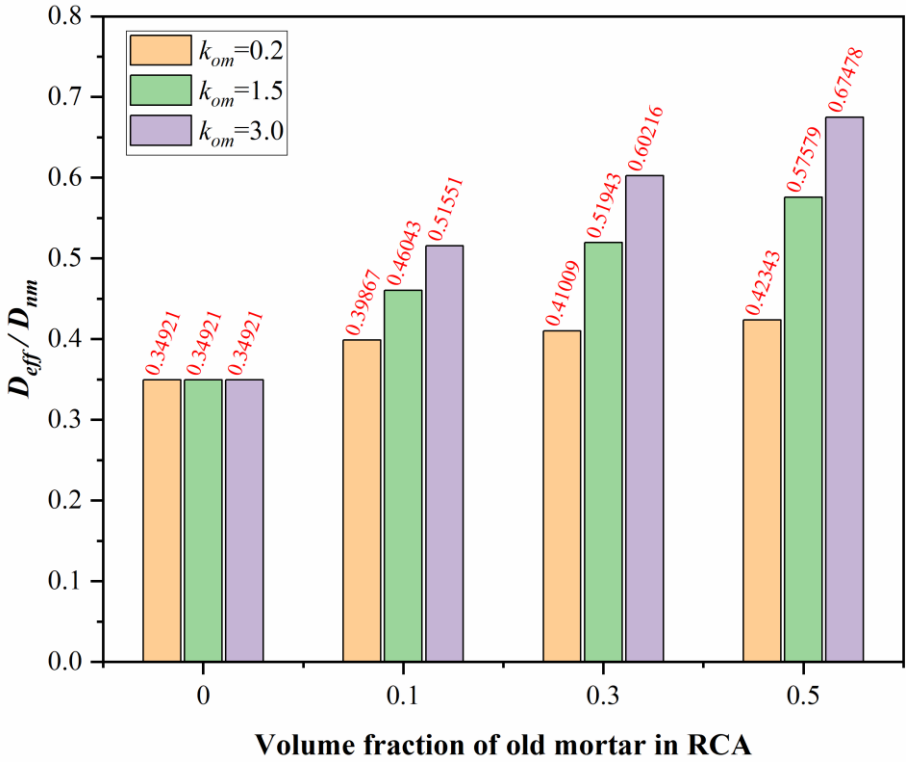

Figure 5.6 Normalized chloride diffusivity in NAC and RAC with various diffusivities of old mortar

As shown in Fig. 3.4, the assumption of a uniform coating of old ITZ on aggregate surface may underestimate or overestimate the volume fraction of old ITZ. To examine the effects of volume fraction of old ITZ, three different thicknesses of old ITZ (40 μm, 80 μm, 120 μm) are employed in analysis. Other input parameters remain the same as those employed in Table 3.2 (standard case). Fig. 5.7 shows the variation of effective chloride diffusion coefficients for RAC with varying old ITZ thicknesses. With an increase in the replacement rate of RCA from 0.2 to 1, the increasing amplitude of effective diffusivity changes from 6.8% to 19.2% to 42.4% when the thickness of old ITZ ranges from 40 to 80 μm. This indicates that the presence of old ITZ, even though it is relatively small in scale, can still affect the durability of concrete in terms of chloride resistance.

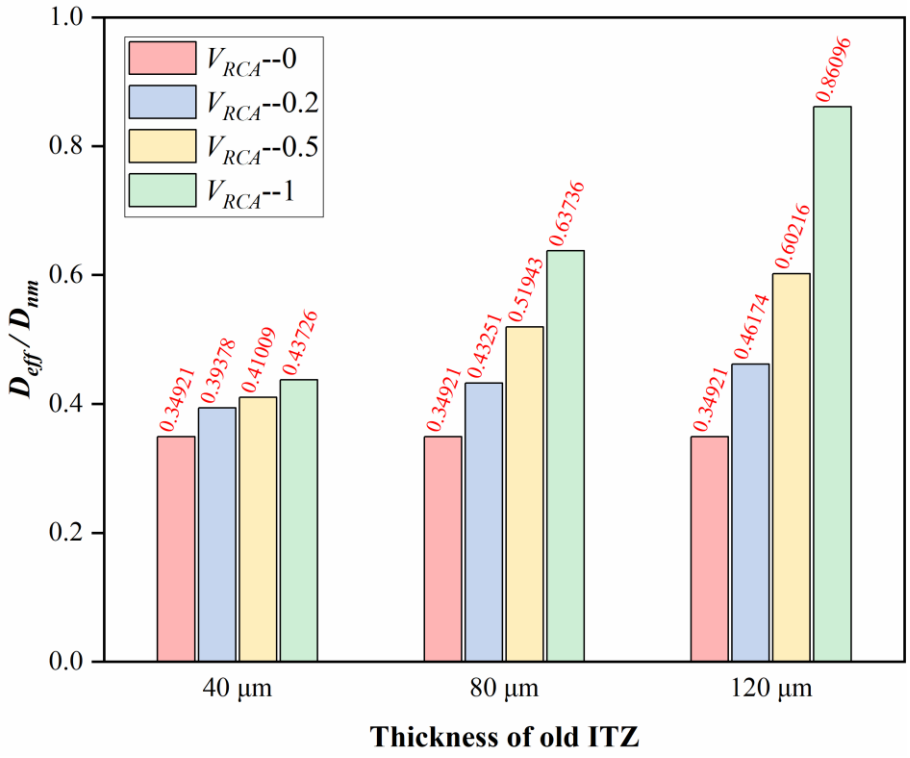

Figure 5.7 Normalized chloride diffusivity in NAC and RAC with various thicknesses of old ITZ

As a bond connecting two phases with different properties, ITZ is inherently more porous (Scrivener, 1999; Diamond and Huang, 2001). In practice, the diffusion properties of old and new ITZs vary from batch to batch. Existing studies have summarized that the

diffusivity ratio between ITZ and mortar (k_{itz}) is in the range of 1.3~18.5 (Hu et al., 2018). Five diffusivity ratios (k_{itz}), 1, 5, 10, 15, and 20, are selected to demonstrate the impact of ITZ diffusion properties. The RCA replacement rate ranges from 0 to 1 while maintaining a fixed old mortar content of V_{om}=0.3. Figs. 5.8 and 5.9 show the variation of normalized chloride diffusivity of concrete with various diffusivities of new and old ITZs. It is clear that the chloride resistance of RAC consistently decreases with increasing chloride diffusivities in both new and old ITZs. The relationship between the diffusivity in new ITZ and the chloride resistance of concrete is not influenced by the replacement rate of RCA. For example, when k_{itz} of new ITZ increases from 1 to 20, the effective diffusivity of concrete increases by 19.6%, 26.4%, 24.8%, and 18.2% for a given V_{RCA} of 0, 0.2, 0.5, and 1, respectively. However, the influence of diffusivity in old ITZ obviously increases with RCA replacement rate. Specifically, when k_{itz} of old ITZ increases from 1 to 20, the effective diffusivity of concrete increases by 0%, 2.8%, 8.7%, and 16.8% for a given V_{RCA} of 0, 0.2, 0.5, and 1, respectively. This is probably because a higher RCA replacement rate can result in a greater total volume fraction of old ITZ, thereby significantly increasing the influence of old ITZ. While the RCA replacement rate does not show a clear correlation with the total volume fraction of new ITZ in the present five-phase model.

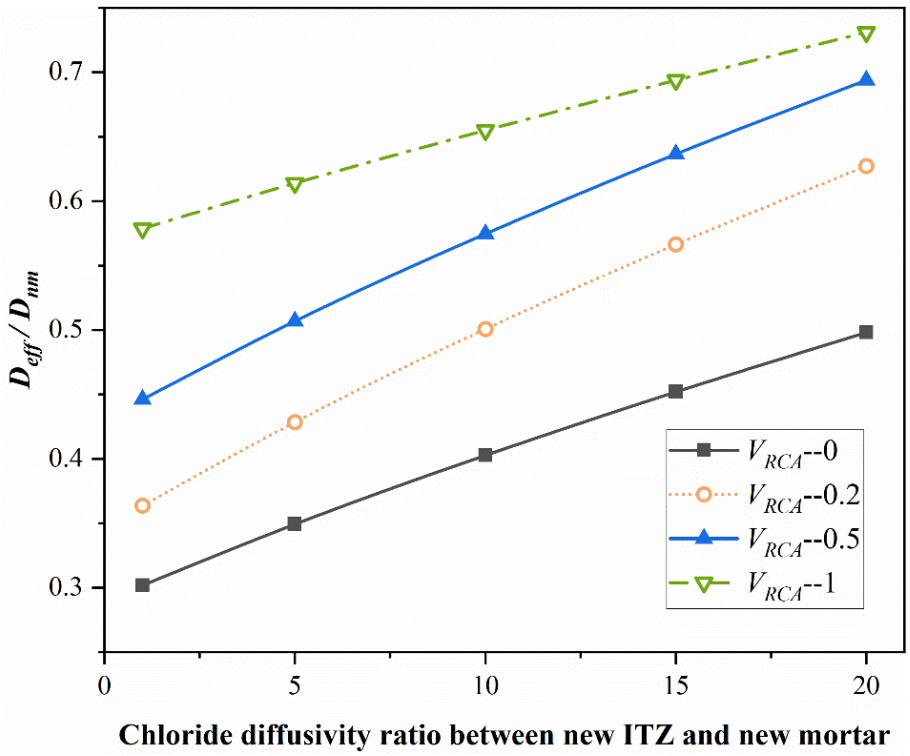

Figure 5.8 Normalized chloride diffusivity in NAC and RAC with various diffusivities of new ITZ

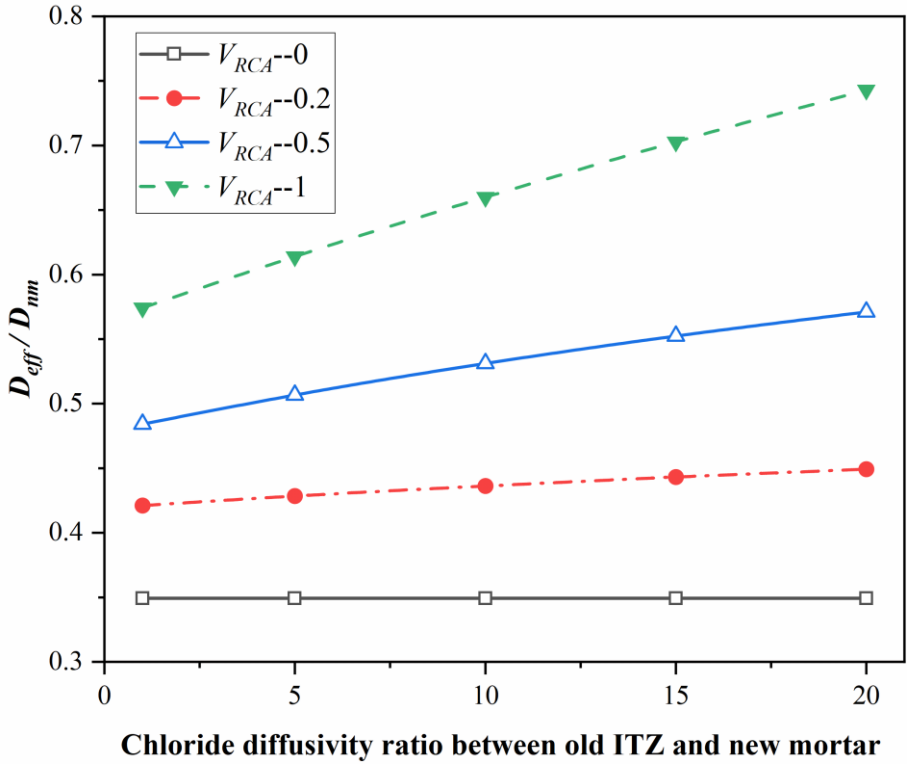

Figure 5.9 Normalized chloride diffusivity in NAC and RAC with various diffusivities of old ITZ

Fig. 5.10 shows the effects of the total volume fraction of aggregate on the normalized chloride diffusivity of concrete with four different RCA replacement rates. As expected, the chloride diffusivity of RAC decreases with an increased volume fraction of all aggregates, while it increases with an increase in RCA replacement rate. It can be found that the effective diffusivity of concrete is consistently lower than that of new mortar due to the presence of impenetrable parts in both NA and RCA, which differs from the findings from Ying et al. (2013a) and Hu et al. (2018). The possible reason is that the volume fractions and chloride diffusion coefficients of old mortar within RCA used in their models are higher than those used in present five-phase models.

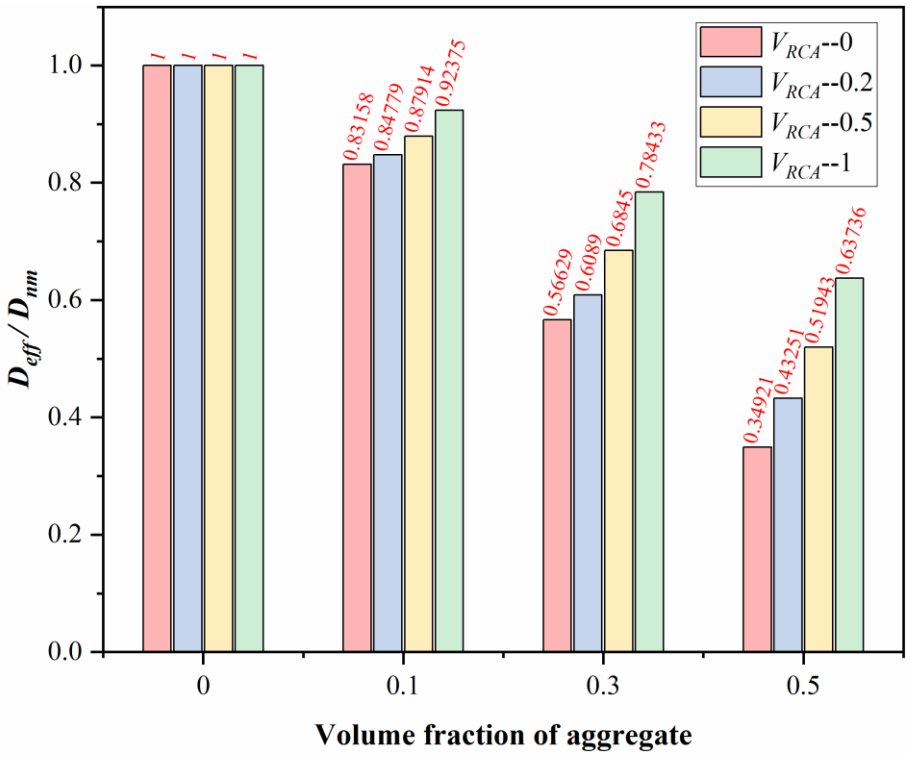

Figure 5.10 Normalized chloride diffusivity in NAC and RAC with various total volume fractions of aggregate

5.2.2. Validation of five-phase numerical model

To validate the accuracy of the present multi-phase model, a benchmark model has been developed in Section 3.2. All input parameters are directly taken or estimated from

experimental data from Kou and Poon (2012), as given in Section 3.2.1. For comparison, the chloride resistance capacity of RAC is normalized as the ratio between the effective diffusivity of RAC and NAC (D_{eff}/D_{effo}). D_{eff} and D_{effo} represent the effective chloride diffusion coefficient of RAC and NAC, respectively.

Fig. 5.11 shows that the predicted results agree well with the experimental results. This confirms the accuracy and appropriateness of the present multi-phase numerical model for calculating the effective chloride diffusivity of both NAC and RAC. Additionally, the normalized chloride diffusivity decreases with increasing w/b in new mortar. It should be noted that the normalized value represents the chloride diffusivity ratio between RAC and NAC, rather than the absolute chloride diffusion coefficient of concrete. Therefore, this decreasing trend does not imply that RAC with lower w/b in new mortar exhibits higher chloride resistance. Instead, it suggests that the use of RCA has a more significant influence on the chloride resistance of concrete with a lower w/b ratio.

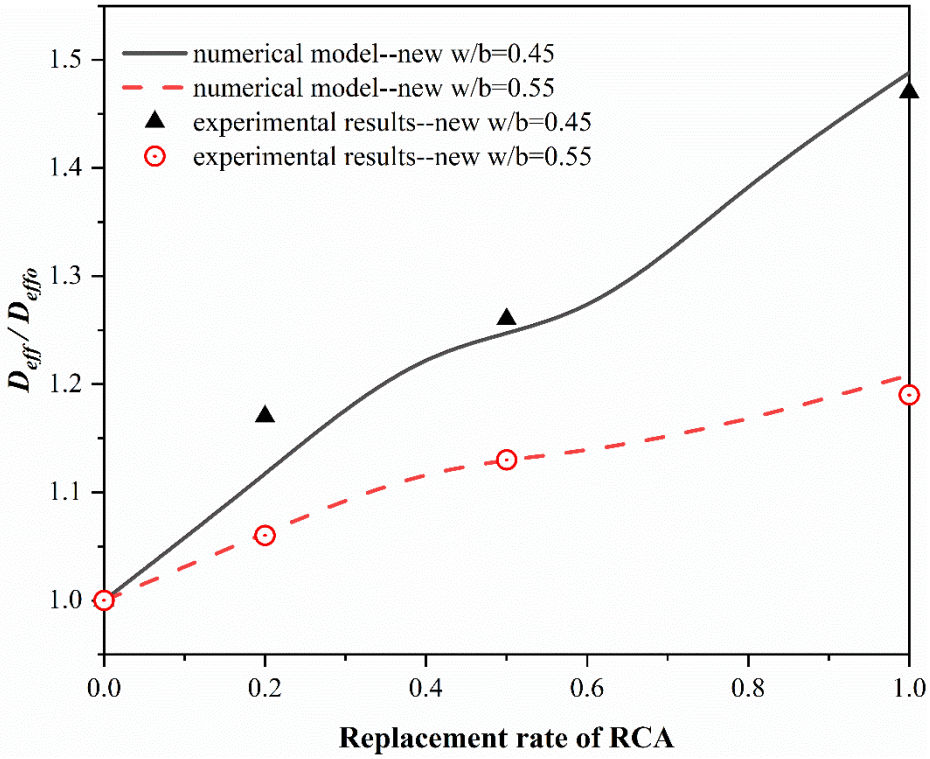

Figure 5.11 Comparison of relative chloride diffusion coefficient of predicted results from present five-phase model and measured results from experiments conducted by Kou (2012)

5.2.3. Analytical results

Numerical results from Section 5.2.1 (Fig. 5.4) have shown that the shape of aggregate has a negligible effect on the effective chloride diffusivity of concrete. Thus, the assumption of spherical aggregates in EMA and MLSA used in two-step analytical model is appropriate.

The effect of RCA on the diffusivity of RAC is mainly due to its permeable feature caused by the adhering old mortar and ITZ in the RCA. Thus, it would be of interest to see how the effective diffusion coefficient of RCA varies with the volume fraction of old mortar in the RCA. The effects of the volume fraction and diffusivity of old mortar on the effective chloride diffusion coefficient for RCA are depicted in Fig. 5.12. The chloride resistance of RCA increases with both the content and diffusivity of old mortar. Moreover, it seems that the effect of the chloride diffusivity of old mortar is more remarkable than the effect of its volume fraction. Specifically, when the volume fraction varies from 0.1 to 0.8, the effective diffusivity of RCA increases by 13% for a given k_{om} of 0.2. Whereas the increase becomes more significant, exceeding 200%, when k_{om} is set to 3.0. When the normalized diffusivity of RCA exceeds one, it becomes the most vulnerable part of RAC to chloride attack. Hence, RCA with high-content and low-chloride-resistance mortar should be avoided in construction. Compared with old mortar, the volume fraction of ITZ in RCA is very limited. However, Fig. 5.13 shows the significant impact of old ITZ on the durability of RCA in terms of chloride penetration. For example, when the volume fraction of old ITZ in RCA increases from 0.01 to 0.04, the effective diffusivity of RCA increases by 5.2%, 7.9%, and 14.1% for a given k_{itz} of 5, 10, and 20, respectively.

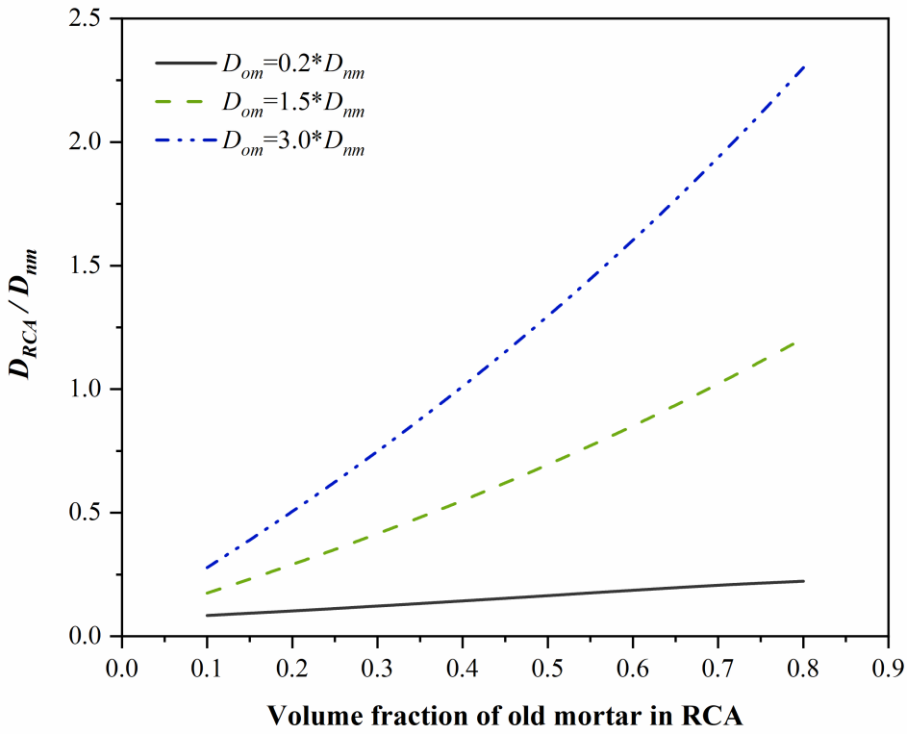

Figure 5.12 Variation of effective chloride diffusivity for RCA with different volume fractions of old mortar

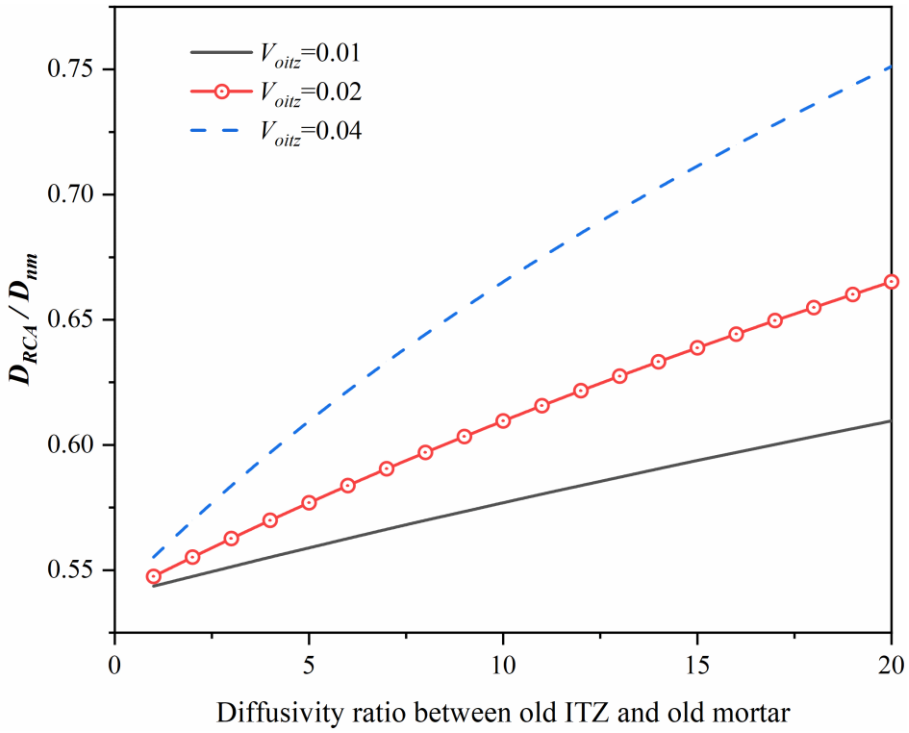

Figure 5.13 Variation of effective chloride diffusivity for RCA with different diffusivities of old ITZ

Fig. 5.14 shows the variation of the effective chloride diffusivity of concrete with different total volume fractions of aggregate. As expected, the chloride resistance of concrete increases with an increasing volume fraction of aggregates, regardless of the RCA replacement rate. This can be explained by the fact that the total amount of impermeable parts in both RAC and NAC increases with an increasing volume of aggregate in concrete. Additionally, the increasing rate varies significantly depending on RCA replacement rates used. The chloride diffusivity of concrete with a higher replacement rate of RCA decreases at a much slower rate than that of concrete with a lower replacement rate of RCA. Specifically, in the case of $V_{TA} = 0.5$, the normalized effective diffusivity of concrete with $V_{RCA} = 0.2$ is almost 1.6 times that of the fully replaced RAC ($V_{RCA} = 1$).

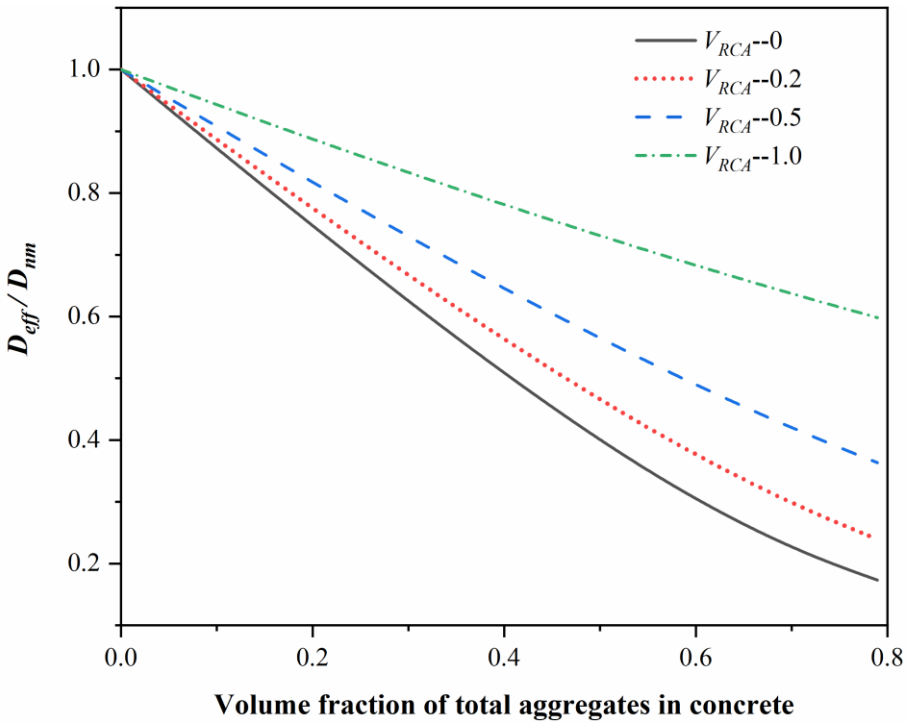

Figure 5.14 Effect of total volume fraction of aggregate on normalized chloride diffusivity for RAC

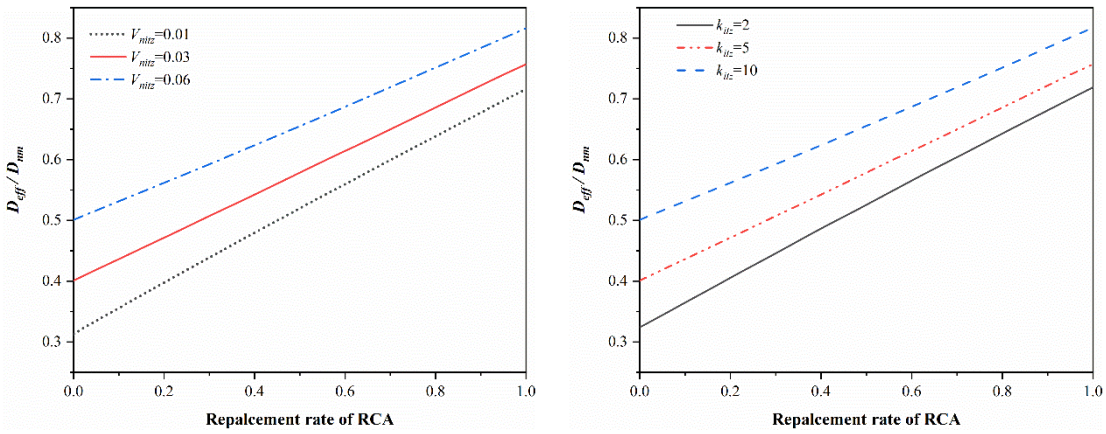

(a) (b)

Figure 5.15 Effect of the new ITZ on normalized chloride diffusion coefficient for concrete. (a) Volume fraction of new ITZ and (b) diffusivity in new ITZ

Fig. 5.15 shows the impact of volume fraction and diffusivity of new ITZ on the chloride resistance of concrete. The normalized chloride diffusion coefficient in concrete exhibits a linear increase with the replacement rate of RCA. The increasing rate slightly declines with increasing volume fraction and chloride diffusivity of new ITZ. Moreover, it seems like the effect of volume fraction and diffusivity of new ITZ on chloride diffusion appears to be nearly equivalent. For instance, in the case of $V_{RCA} = 0.5$, when D_{nitz} is doubled while keeping V_{nitz} fixed, the effective chloride diffusivity of RAC increases by approximately 13.2%. Similarly, when V_{nitz} is doubled while keeping D_{nitz} fixed, the increase in chloride diffusivity is about 13.8%.

5.2.4. Validation of two-step analytical model

To validate the accuracy of the present two-step model, the effective chloride diffusivities obtained from the two-step analytical model and those from the numerical model proposed by Yu and Lin (2020) are compared. The effect of w/c ratio in old mortar is investigated. Input parameters in benchmark model are directly taken or estimated from a multi-phase numerical model conducted by Yu and Lin (2020). The total volume

fraction of coarse aggregate in concrete and the volume fraction of old mortar in RCA are 0.22 and 0.35, respectively. The calibrated chloride diffusivities and volume fractions of each phase used in benchmark model are D_{om}=2.25k_{om}×10^{-12} m/s^2, k_{itz}=1.5, D_{nm}=6.0 ×10^{-12} m/s^2, V_{oitz}=V_{nitz1}=V_{nitz2}=0.01, where k_{om} is a constant with k_{om} =1.0 and 3.25 for w/b=0.45 and 0.65, respectively, for the two types of RCA used. For comparison, the chloride resistance capacity is normalized as the ratio between the effective diffusivity of RAC and NAC. Fig. 5.16 shows the impacts of w/c in old mortar on the chloride resistance of concrete with different RCA replacement rates. It can be seen from the figure that the chloride resistance of concrete can be improved by enhancing the quality of RCA, such as by using RCA with a lower w/c ratio (Vázquez et al., 2014; Ozbakkaloglu et al., 2018). It is evident that analytically predicted chloride diffusivities coincide well with those from Yu's simulation. This high level of agreement indicates that the two-step analytical model is reliable and accurate in predicting the effective chloride diffusivity of concrete containing both NA and RCA.

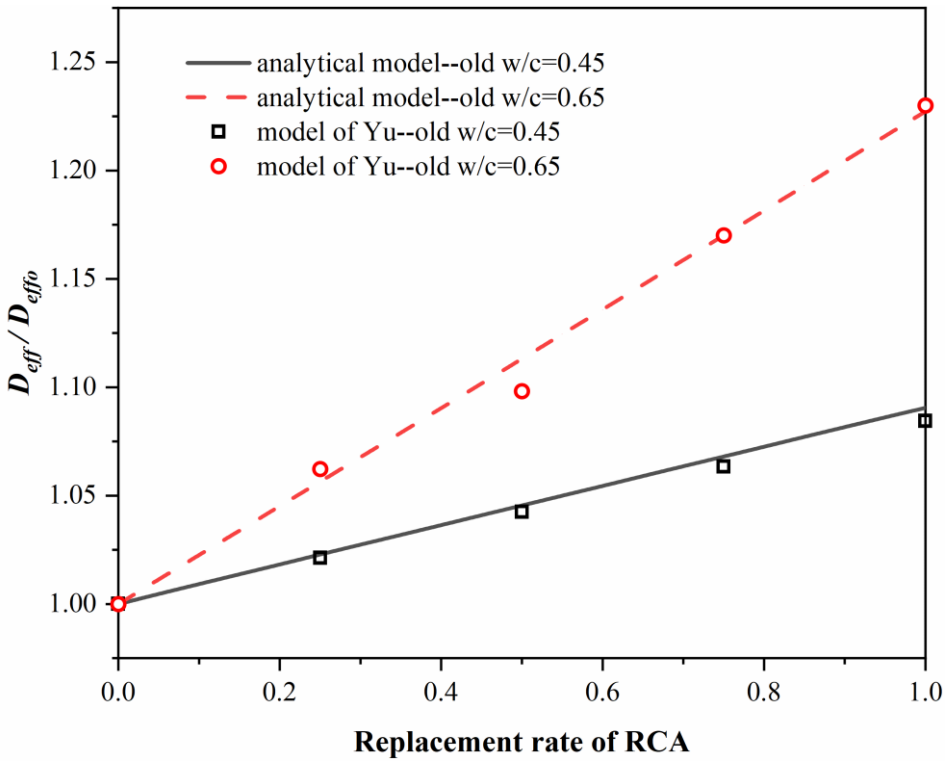

Figure 5.16 Comparison of effective chloride diffusivities from present two-step analytical model and numerical model proposed by Yu and Lin (2020) (D_{effo} represents the effective chloride diffusion coefficient of NAC)

5.3. Summary

Based on the five-phase numerical model and two-step analytical model proposed in Section 3.2, the influence of each phase, such as old aggregate, old ITZ, old mortar, new ITZ, and new mortar, on the chloride resistance of concrete has been evaluated. Numerical and analytical results lead to the following conclusions:

1) Aggregate shape shows insignificant influence on the effective chloride diffusion coefficient in RAC or NAC. Circular aggregates can be employed in the multi-phase numerical simulations.

2) Replacing NA with RCA in concrete can increase the effective chloride diffusion coefficient in concrete because RCA is generally not impermeable. The magnitude of the increase in effective diffusivity of concrete is dependent on the quality of RCA, including the volume fraction and chloride diffusivity of old mortar and ITZ.

3) Despite the volume fraction of ITZ is relatively small, its influence on the effective chloride diffusivity of concrete is significant and cannot be ignored. An increased volume fraction and chloride diffusivity of ITZ can result in lower chloride resistance in concrete.

4) The effective diffusion coefficient shows a decline as the total volume fraction of aggregates increases, regardless of the RCA replacement rate. Moreover, concrete with a higher RCA replacement rate exhibits a smaller decrease in effective diffusivity compared to concrete with a lower RCA replacement rate.

5) Comparison between predicted effective diffusivities and those obtained from experimental tests or numerical simulations demonstrates that the present five-phase numerical model and two-step analytical are reliable and appropriate for simulating chloride diffusion in concrete containing both NA and RCA.

CHAPTER 6 INFLUENCE OF POLARIZATION AT ELECTRODES ON CHLORIDE TRANSPORT IN MIGRATION TEST

6.1. Introduction

As mentioned in Chapter 5, the shape of aggregates has a negligible influence on chloride transport in concrete. Results from Chapter 4 emphasize the importance of considering multi-species coupling when simulating migration tests. Hence, the overpotential model used in this chapter incorporates multi-species coupling and circular aggregates.

This chapter focuses on chloride transport properties in heterogenous NAC and RAC during chloride migration tests, considering the influence of polarization at electrodes. The numerical scheme of this chapter is covered in Section 3.3 and in relation to objective 3, outlined in Section 1.2. The distribution of chloride, hydroxyl, sodium, and potassium ions within concrete, as well as the time-varying overpotential at electrode-concrete interfaces, are quantitatively predicted using SNIA. The simulation results are verified with experimental data published in the literature. In addition, the effects of externally applied voltage, Tafel parameters, initial ionic concentration in pore solution, and RCA on the overpotential and chloride penetration are analyzed in a quantitative manner.

6.2. Validation of overpotential model

To validate the reliability of the present overpotential model and estimate the influence of polarization on chloride ingress in migration tests, two benchmark models are proposed in Section 3.3. All input parameters are directly taken or estimated from experiments conducted by Castellote et al. (1999) and Jiang et al. (2013), as given in Table 3.6. The non-steady-state migration coefficient is calculated based on a specific chloride ingress depth (Equation (2.45)). In this chapter, a threshold concentration of 70 mol/m^3 is used as the criterion to determine chloride penetration depth in both numerical and experimental studies, following the recommendation in NT BUILD-492 (1999).

Fig. 6.1 plots a comparison between the numerical and experimental results of effective chloride penetration depth. It is evident that results from overpotential models are in good agreement with those from experiments. This means that the present overpotential model is rational to simulate the chloride transport in concrete under the action of an external electrical field. The fluctuations and small deviation observed in the simulation of Castellote's experiments may be attributed to the random distribution of aggregates, as shown in Fig. 3.11. Moreover, the obvious discrepancy between the experimental and non-overpotential numerical results indicates that chloride diffusivity would be overestimated if the overpotential between electrode and concrete surface is ignored. Hence, the simulation of chloride transport within concrete must include the external polarizing process.

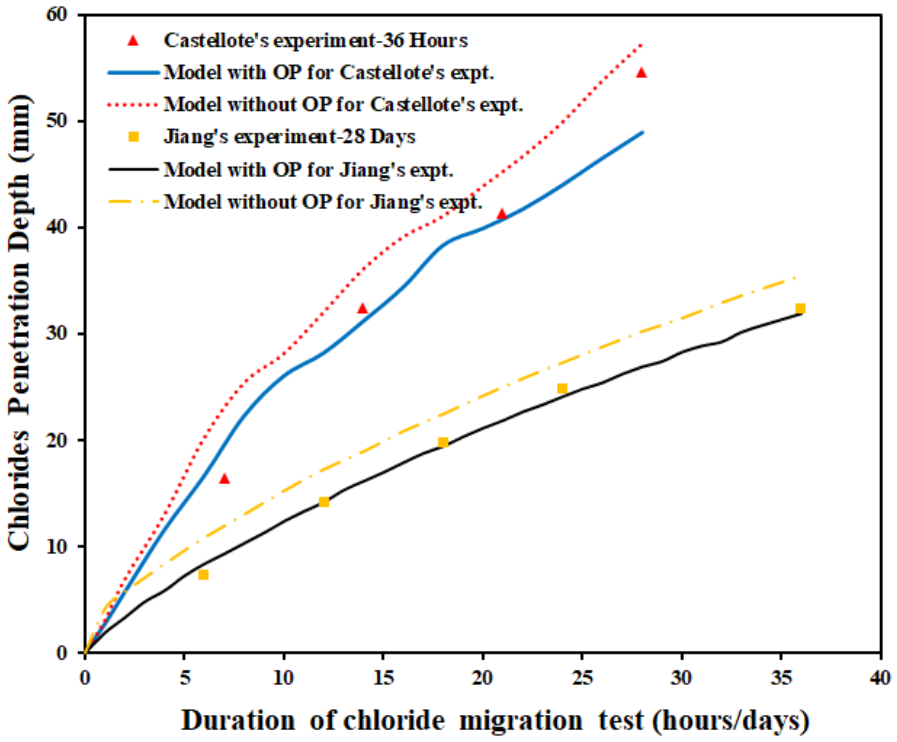

Figure 6.1 Comparison of chloride penetration depths between experimental and numerical research

6.3. Results and discussion

6.3.1. Applied voltage

In this section, three external voltages (8, 16, 24 V) are employed in simulation to investigate the variation in overpotential and ionic concentration distribution during migration test. Other input parameters are the same as those in standard case, listed in Table 3.4.

Fig. 6.2 shows that the overall overpotential slightly increases with the increase in externally applied voltage, ranging from 2.07 to 2.24 V. This finding is consistent with the findings from Megrath and Hooton (1996), where the overpotential ranged from 1.91 to 2.36 V when the externally applied potential increased from 6 to 30 V. According to Equations (3.5)-(3.8), the increase in overpotential can be attributed to the increase in current density, as shown in Fig. 6.3. It is observed that both the difference in overpotential between 8 V-, 16 V- and 24 V-models and the value of overpotential show a decreasing trend with time. This is because the discrepancies in current density between 8 V-, 16 V- and 24 V-models decrease quickly during the first 12 hours (see Fig. 6.3).

The external overpotential in turn affects the concentration distribution of chlorides within concrete. Taking the 24 V-model as an example, the overall overpotential gradually decreases over time from 2.26 to 2.14 V. Correspondingly, based on Equations (3.3) and (3.4), the actual electric potential difference throughout concrete decreases approximately 8.9~9.4% compared to that applied on two electrodes. This means that the driving force for ionic transport, offered by external electric field, is reduced by the outside polarizing process. Therefore, the chloride penetration depths in overpotential models are significantly smaller than those in non-overpotential models, as shown in Fig. 6.4. The red line in Fig. 6.4 represents the effective chloride penetration depth, determined by a threshold concentration of 70 mol/m^3.

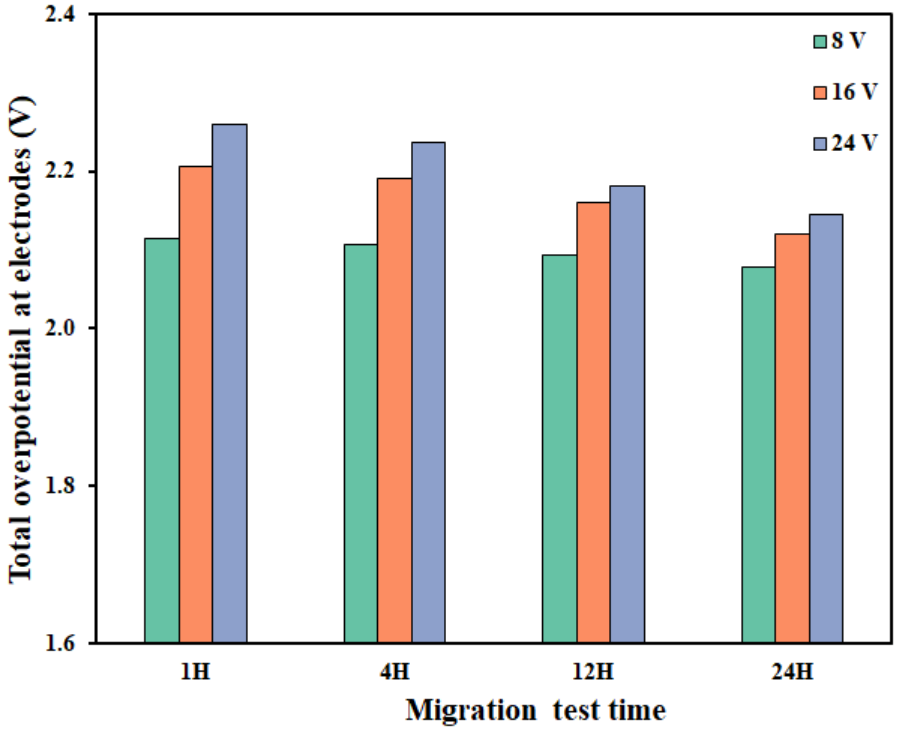

Figure 6.2 Variation of overall overpotential at electrode-concrete interfaces for models with different external voltages

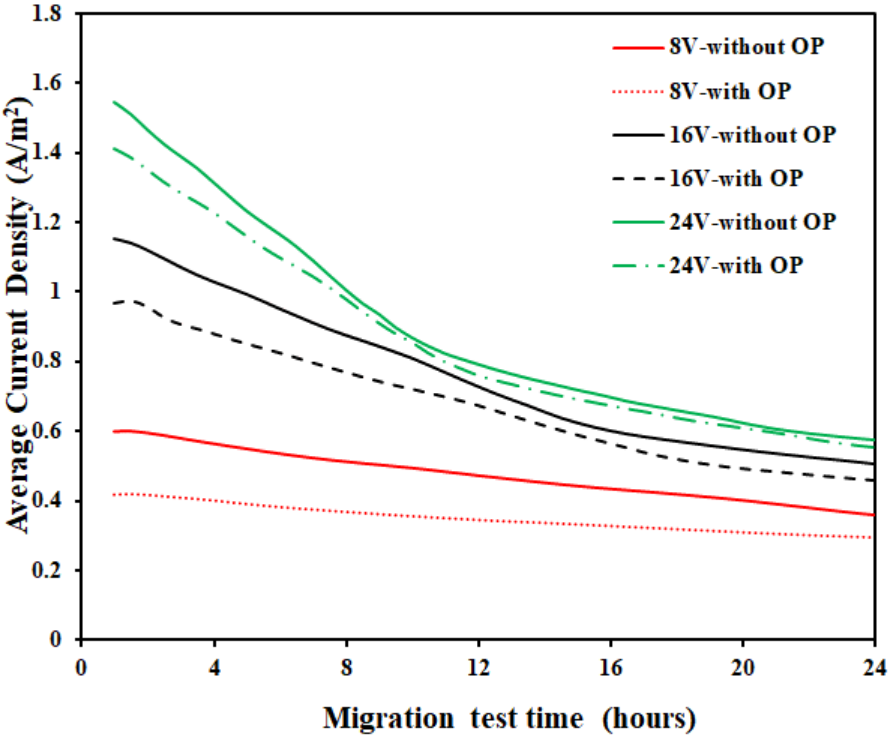

Figure 6.3 Average current density flowing into/out from concrete during RCM test for models with different external voltages

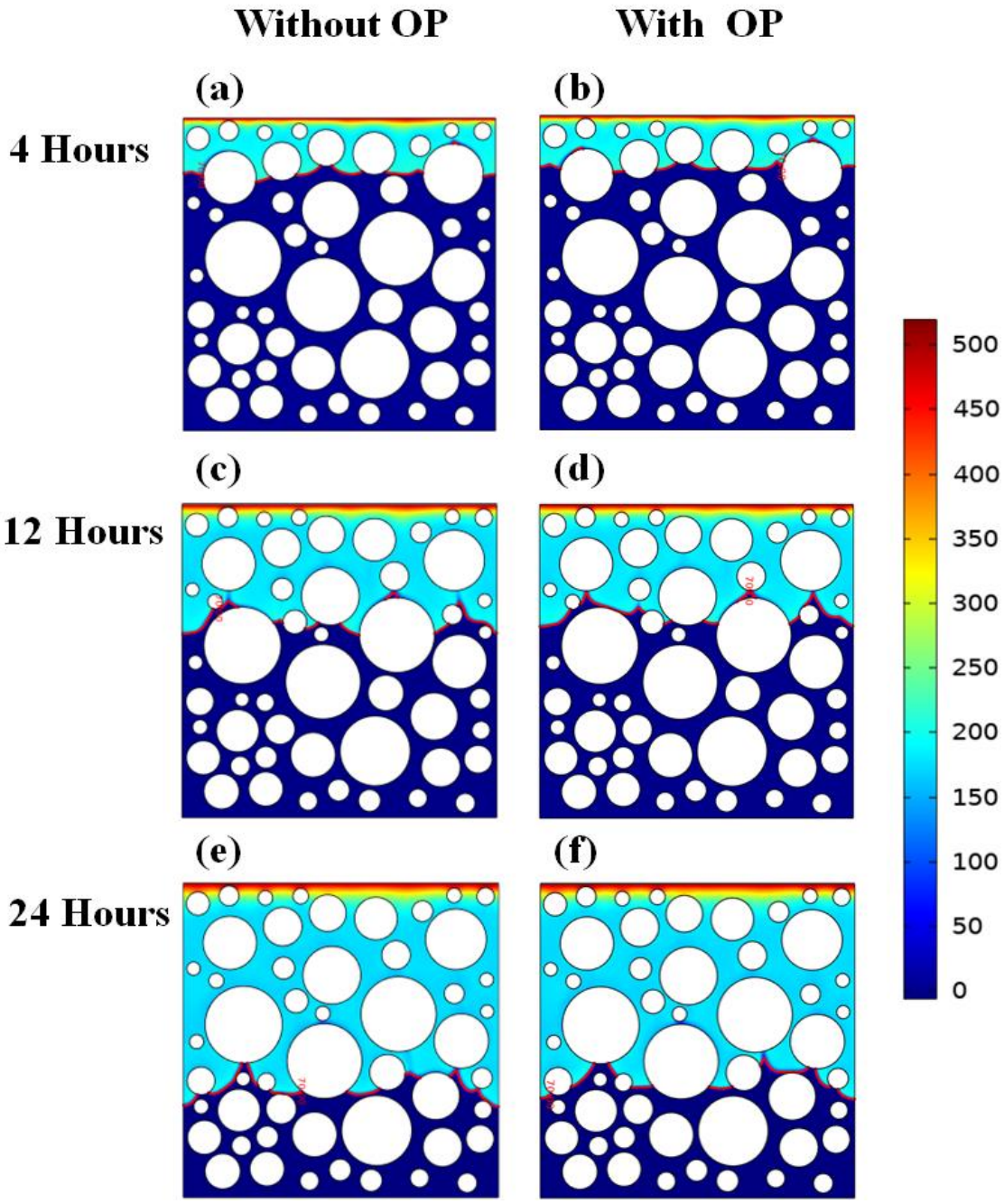

Figure 6.4 Concentration distributions of chlorides in 24V-models with and without overpotential

To provide a more intuitive description of the influence of overpotential, Figs. 6.5 and 6.6 present the concentration profiles of all ionic species at different times and applied voltages. The profiles are obtained by averaging ionic concentrations at each depth in concrete. Fig. 6.5 shows that the difference in chloride penetration depth between models with and without considering overpotential becomes more pronounced over time, even

though total overpotentials decrease during this process. It can be observed from Fig. 6.6 that with an increase in external voltage, the depth of chloride ingress into concrete also increases. This is because the movement speed of each ionic species in concrete is higher under a stronger electric field. However, the effect of overpotential on chloride penetration tends to increase as external voltage decreases. Specifically, the polarization-induced reduction in chloride penetration depth is approximately 1.5 times greater at 8 V applied voltage compared to 16 V applied voltage and 2.4 times greater at 8 V compared to 24 V. This discrepancy arises because the overpotential causes a proportional reduction of the electric driving force by approximately 25% in the 8 V-case, whereas in the 24 V-case, this reduction is around 7%. This indicates that the decrease in chloride ingress is determined not only by the magnitude of overpotential but also by its proportion to external voltage.

The transportation of potassium, sodium, and hydroxyl ions is also affected by external polarization. Figs. 6.4 and 6.5 show that the influence of overpotential on positively charged potassium ions is more significant compared to its impact on sodium ions. This can be attributed to two potential reasons. Firstly, potassium ions have larger diffusion coefficients than sodium ions. Secondly, the NaOH solution employed in an anodic electrolyte could provide a sufficient supply of sodium ions moving through concrete specimens.

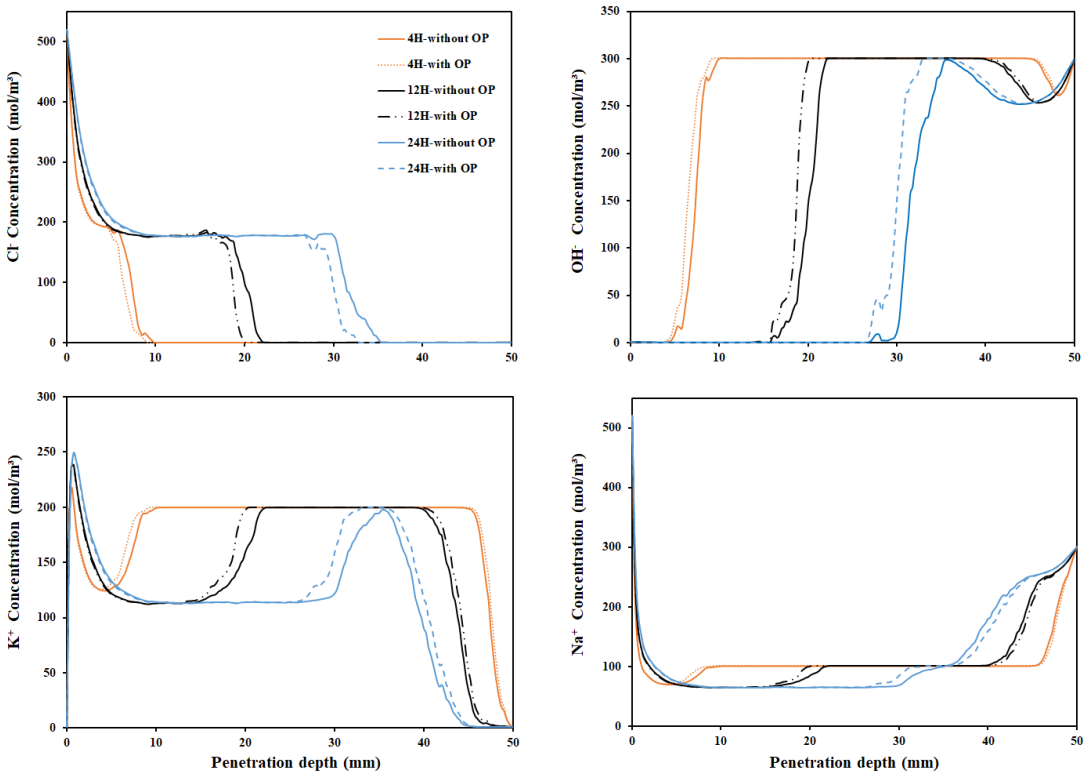

Figure 6.5 Concentration profiles of Cl^-, OH^-, K^+, Na^+ ions in 24V-models with and without overpotential at three different times

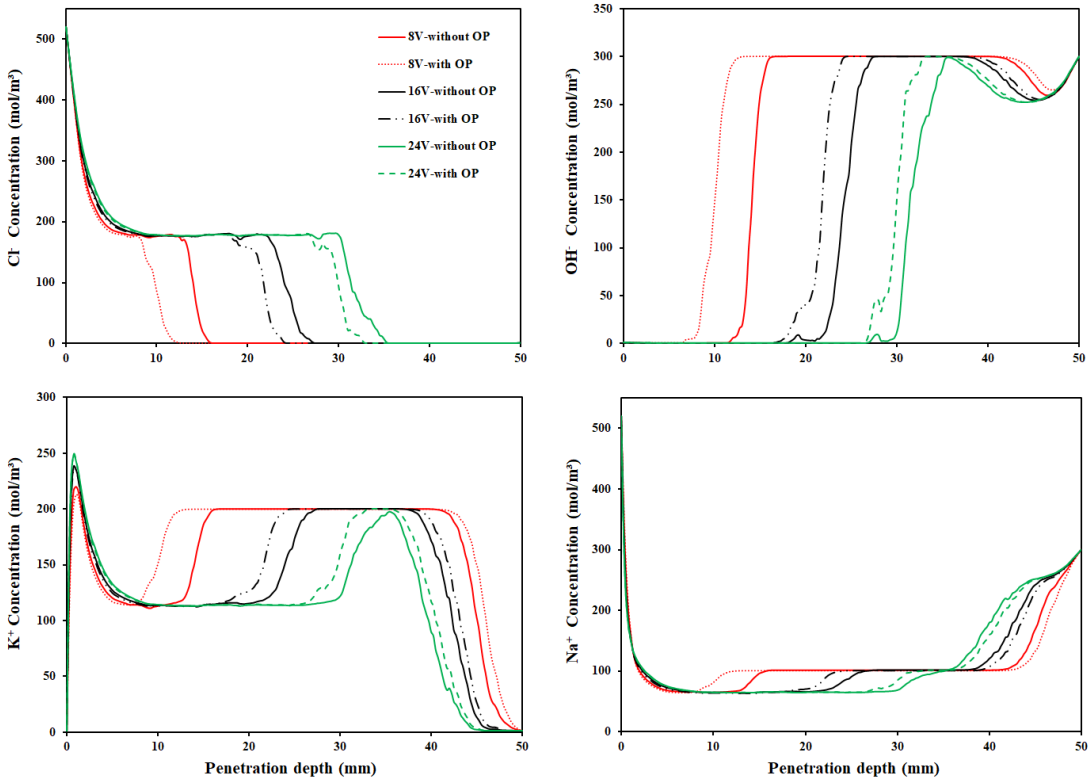

Figure 6.6 Concentration profiles of Cl^-, OH^-, K^+, Na^+ ions in the models with and without overpotential when three different voltages employed

6.3.2. Tafel parameters

In this section, the effects of Tafel slope and exchange current density, which describe the electrode and electrolyte conditions, are investigated through five cases: Highest case, High case, Base case, Low case, and Lowest case. The Tafel parameters used for each case are given in Table 3.7. External voltage and initial ionic concentrations are the same as those listed in Table 3.4.

Fig. 6.7 presents the overall overpotentials in cases with different Tafel slopes and exchange current densities after 1-hour, 12-hour, and 24-hour migration tests. As expected, the overall overpotential is inversely proportional to exchange current density and is proportional to Tafel slope. Moreover, the influence of Tafel slope on overpotential value is significantly greater than that of exchange current density. Specifically, the value of overpotential in Highest or High case is three times higher than that in Lowest or Low case. In Highest and High cases, the overall overpotential holds in the range of 3.09~3.71 V, which is significantly higher than values measured or adopted in Megrath and Hooton's (1996) or NT BUILD-492 (1999). Therefore, selecting appropriate Tafel parameters is crucial for conducting numerical studies on migration tests.

For comparison, Fig. 6.8 summarizes the concentration profiles in overpotential models with different Tafel parameters and the non-overpotential model. A lower overall overpotential caused by polarization leads to a higher electric potential difference throughout concrete in migration tests, resulting in an increased chloride penetration depth. It can be observed that there is no significant difference in ionic concentration between Lowest case and Low case, or between Highest case and High case. Conversely, there is a noticeable difference between Low case and Base case, as well as between High case and Base case. This implies that the impact of Tafel slope on ionic transport is more pronounced compared to that of exchange current density. Additionally, a high Tafel slope can magnify the effect of exchange current density on both the overpotential value and chloride penetration depth.

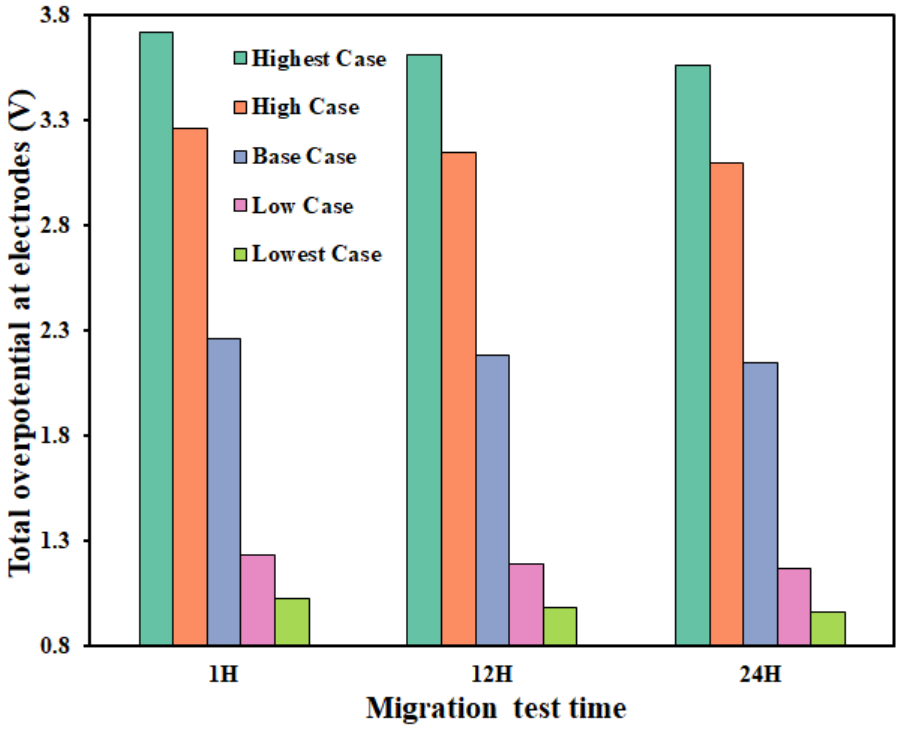

Figure 6.7 Variation of overall overpotential at electrode-concrete interfaces for models with different Tafel parameters

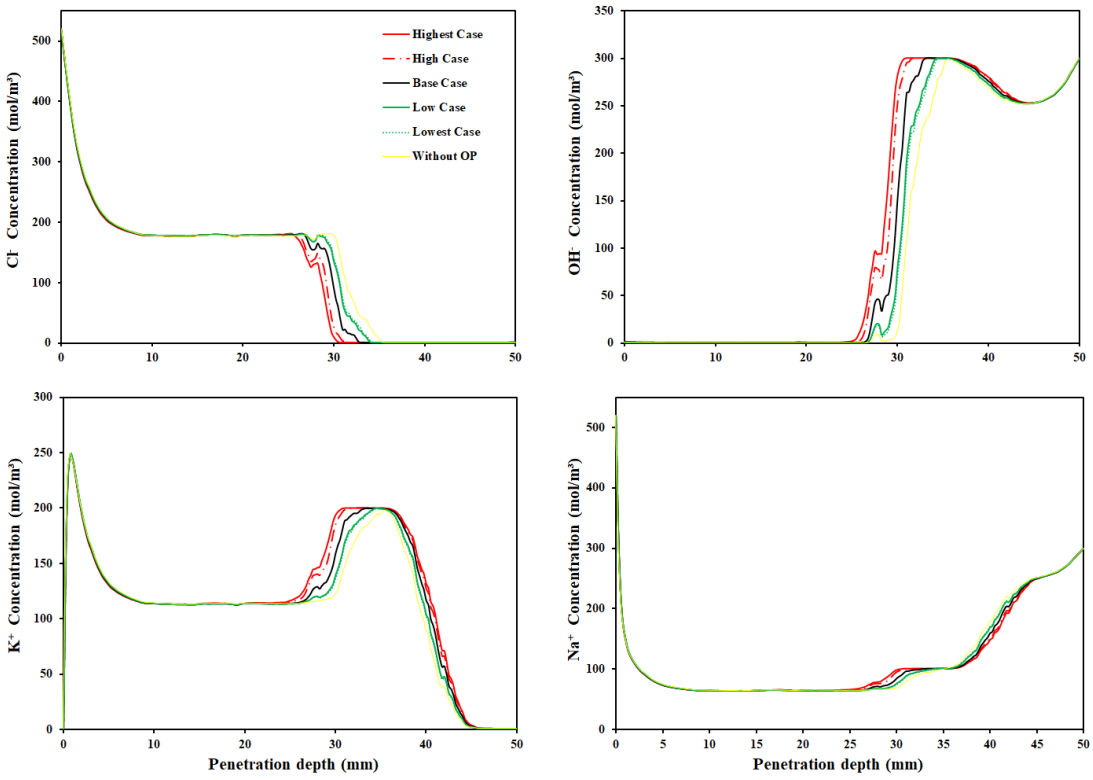

Figure 6.8 Concentration profiles of Cl^-, OH^-, K^+, Na^+ ions in models with different Tafel parameters after 24-hour migration test

6.3.3. Initial concentration

This section investigates the effect of initial ionic concentrations of all ionic species, which are influenced by the choice of binders and mix design in concrete. Three cases, Case1, Case2, and Case3, are presented in Table 3.5 to represent different initial ionic concentration scenarios. External voltage and Tafel parameters used in each case are provided in Table 3.4.

Fig. 6.9 clearly demonstrates that overall overpotential increases with the increase in initial concentration in pore solution. This can be explained by the fact that a higher ionic concentration results in a greater current density flowing through the concrete boundaries, as illustrated in Fig. 6.10. Consequently, this affects the magnitude of overpotential. Furthermore, it is evident from Fig. 6.10 that the differences in current densities among the three cases remain relatively constant over time. Correspondingly, the differences in overpotential between each case remain nearly constant over time, with values ranging from 0.1 to 0.2 V. Fig. 6.11 exhibits the distribution profiles of all ionic species in concrete with varying initial ionic concentrations. It demonstrates that initial ionic concentrations have a considerable impact on the total amount of chlorides that penetrate into concrete. Higher initial concentrations result in a greater total amount of chloride ions penetrating concrete. However, the variation in chloride penetration depth is relatively small in three cases. Additionally, it is evident that the influence of overpotential on chloride penetration depth becomes more obvious when the initial ionic concentrations are higher.

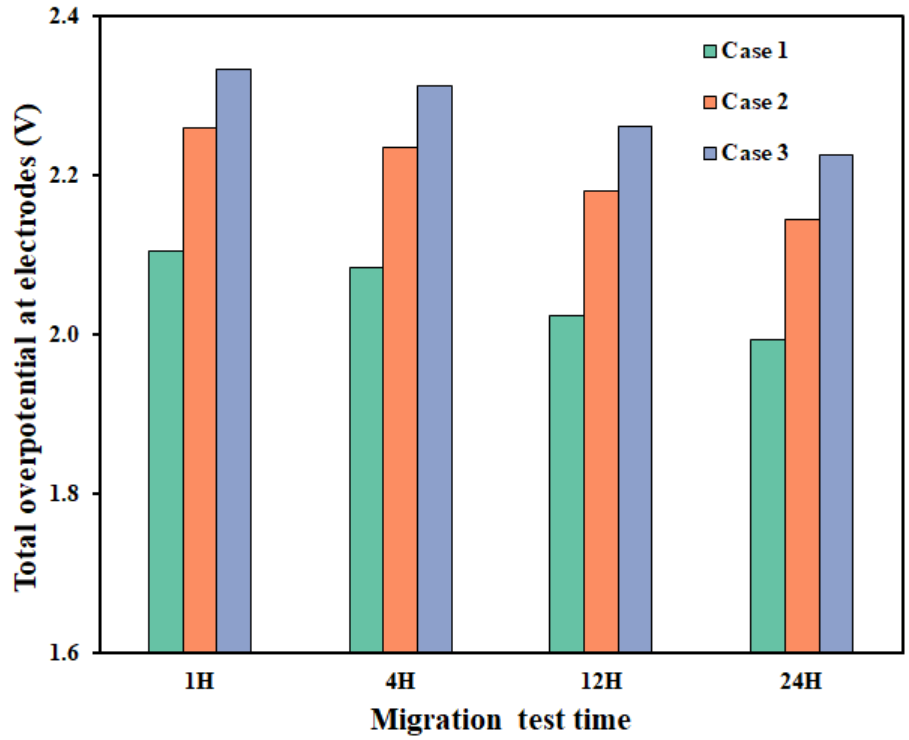

Figure 6.9 Variation of overall overpotential at electrode-concrete interfaces for models with different ionic initial concentrations

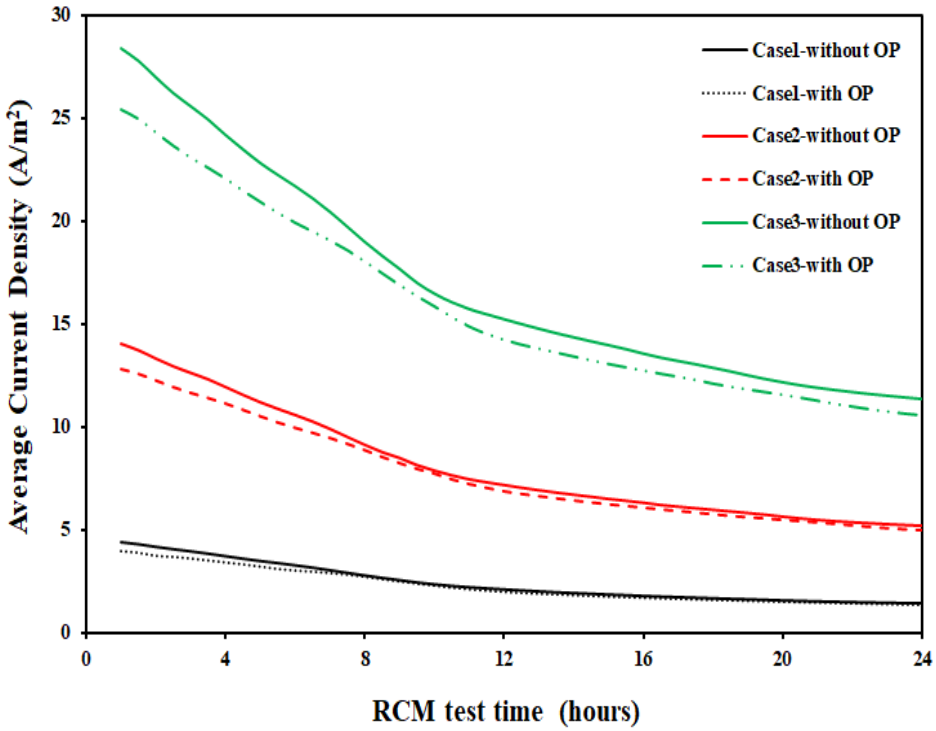

Figure 6.10 Average current density flowing into/out from concrete during RCM test for models with different ionic initial concentrations

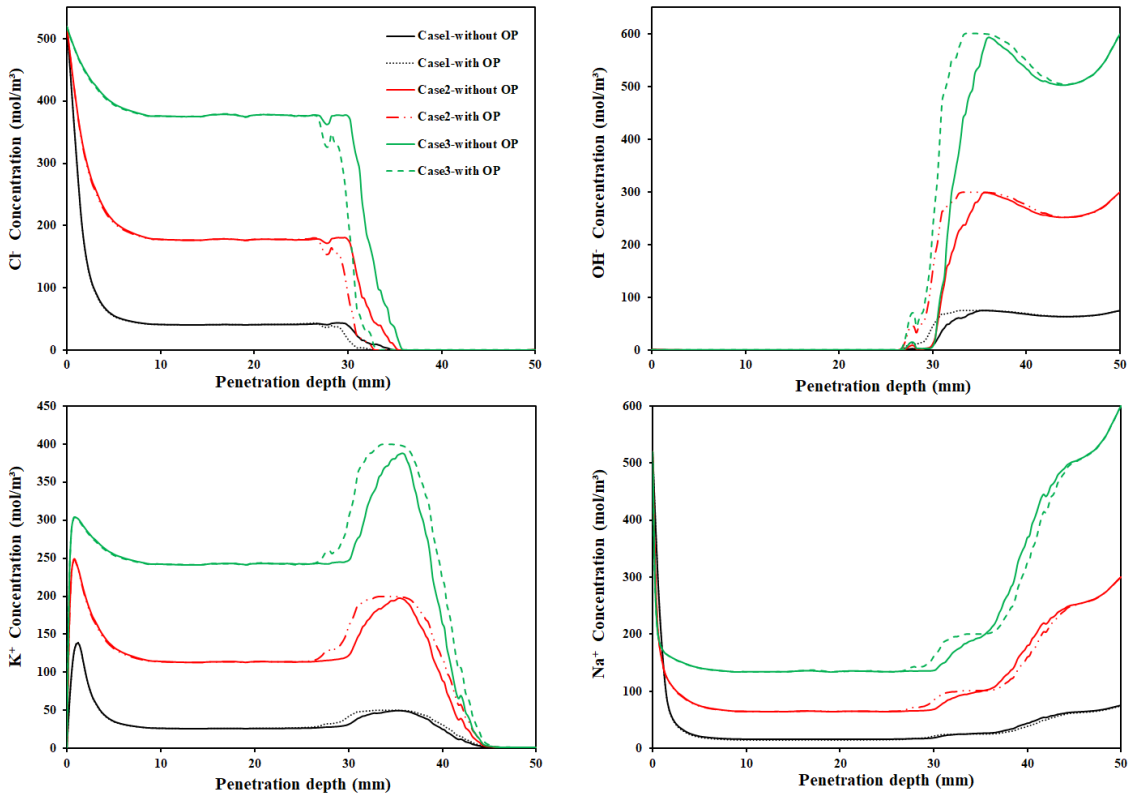

Figure 6.11 Concentration profiles of Cl^-, OH^-, K^+, Na^+ ions in models with different ionic initial concentrations after 24-hour migration test

6.3.4. Recycled concrete aggregate

As presented in Figs. 5.5 and 5.7, the effective chloride diffusivity of concrete increases significantly with an increase in RCA replacement rate. Hence, based on Equation (2.14), the current flow through concrete would vary with RCA replacement rate, ultimately affecting the value of overpotential at electrode-concrete interfaces. This section examines the influence of incorporating RCA in concrete on overpotential and ionic distributions. Three replacement rates (0, 0.5, and 1) are employed.

Fig. 6.12 summarizes the variation of overall overpotential with different RCA

replacement rates. It shows a positive correlation between the volume fraction of RCA used in concrete and the magnitude of overpotential. The influence of using RCA in concrete on overpotential is limited. It suggests that the same overpotential can be used to simulate ionic transport in both NAC and RAC specimens. Fig. 6.13 indicates that the presence of RCA has an obvious impact on chloride ingress. An increase in the volume fraction of RCA results in a greater depth of chloride penetration. Specifically, the chloride penetration depth increases by 37% when all natural aggregates are replaced by recycled aggregates. Simultaneously, the distributions of potassium, sodium, and hydroxyl ions undergo corresponding changes. The overpotential has a limited effect on the migration of sodium ions, which is identical with the results from Fig. 6.5. The explanation for this phenomenon is provided in Section 6.3.1.

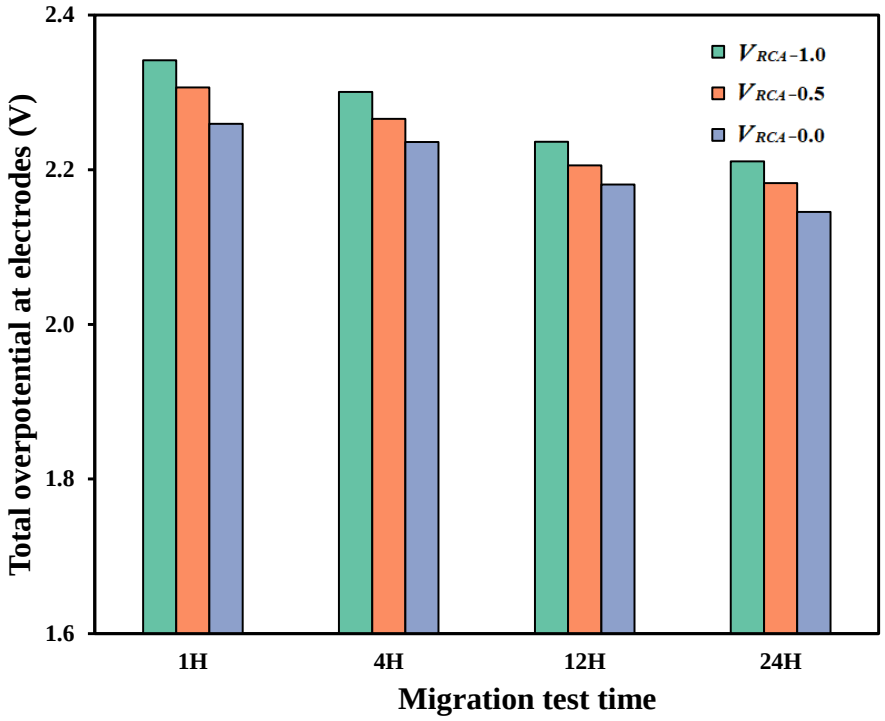

Figure 6.12 Variation of overall overpotential at electrode-concrete interfaces for models with different replacement rate of RCA

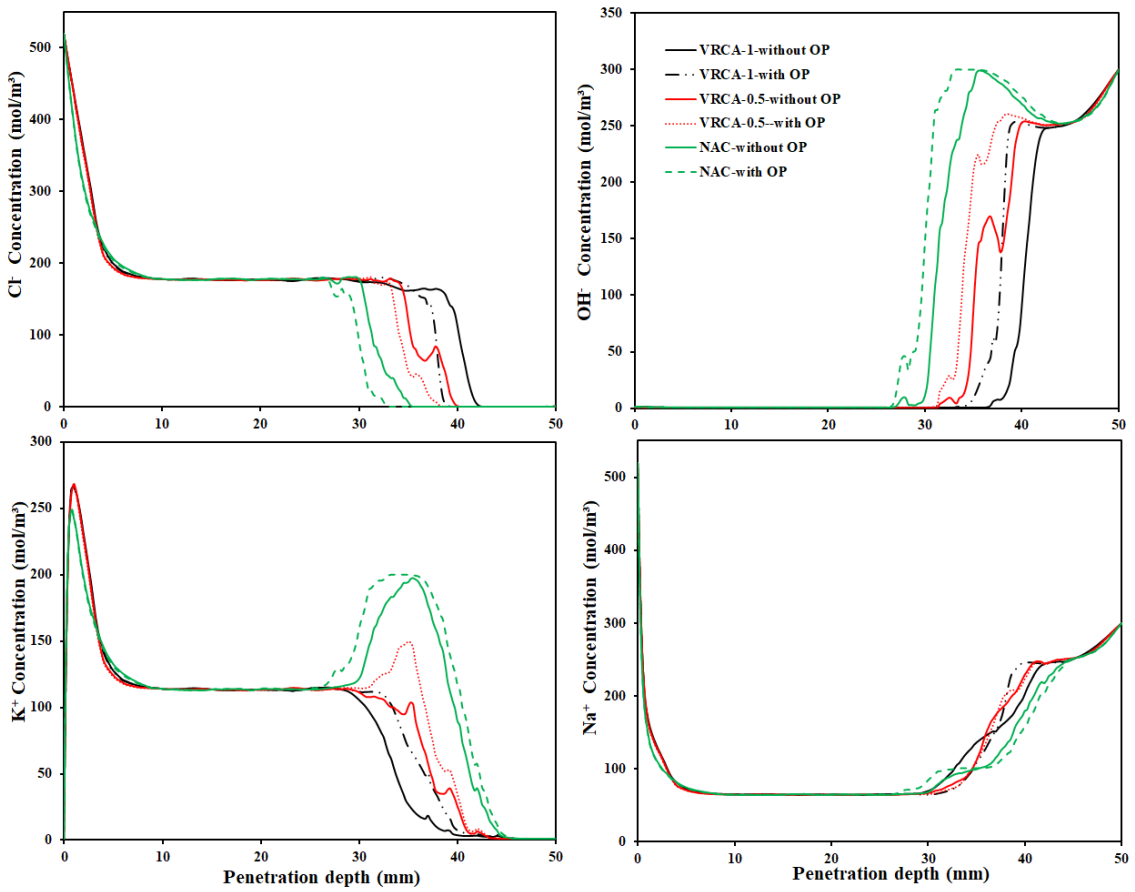

Figure 6.13 Concentration profiles of Cl^-, OH^-, K^+, Na^+ ions in models with different replacement rate of RCA after 24-hour migration test

6.4. Summary

Based on the overpotential model proposed in Section 3.3, the variation of overpotential and its effects on the time and space distributions of all ionic species in concrete during chloride migration tests are presented. This chapter also performed a parametric analysis on the external voltage, initial ionic concentration, Tafel parameters, and replacement rate of RCA. Based on the numerical results obtained, the following conclusions can be drawn:

1) Taking into account the polarization at electrodes, the potential difference across a concrete specimen is reduced by 7~25% compared to externally applied voltage in various cases, resulting in a decrease in chloride penetration depth.

2) Overall overpotential gradually decreases over time as the current density decreases

during the migration test. However, the influence of overpotential on the ionic distribution of all ionic species becomes more evident with time.

3) The influence of polarization on ionic transport depends on both the value of overpotential and its magnitude relative to externally applied voltage. Overpotential effect on chloride penetration is less pronounced at higher externally applied voltages.

4) Overall overpotential significantly increases with the increase in Tafel slope, whereas it slightly drops with the increasing exchange current density.

5) Initial ionic concentration in pore solution has a limited effect on both overpotential and chloride penetration depth. However, there is a noticeable increment in the total amount of penetrated chloride ions with an increase in initial ionic concentration.

6) The application of RCA significantly reduces the chloride resistance of concrete, but its effect on overpotential is limited.

CHAPTER 7 INFLUENCE OF CHLORIDE BINDING ON IONIC TRANSPORT IN MIGRATION TEST

7.1. Introduction

In Chapter 7, a numerical analysis has been conducted on the chemical and physical reactions between free ions in pore solution and cement hydrates, specifically focusing on the chloride binding reactions and their influence on ionic transport in migration tests. The numerical scheme of this chapter is covered in Section 3.4 and in relation to objective 4, outlined in Section 1.2. In reactive mass transport model, the formation and/or dissolution of cement hydrates related to chloride ingress, along with the corresponding variation in porosity, as well as the physical reactions on C-S-H surface are included. In non-equilibrium binding model, the adsorption and desorption of all ionic species are considered using a Langmuir binding isotherm. As suggested in Chapter 4, multi-species coupling is considered in these two migration models. The application of thermodynamic reaction equilibrium and non-equilibrium binding in simulating chloride migration tests is calibrated with existing experimental research. The comparison results indicate that the reactive mass transport model is more accurate and reliable for predicting chloride transport within concrete during migration tests.

7.2. Validation of reactive mass transport model

To compare the differences between reactive mass transport model and non-equilibrium binding model and to determine which one provides a more accurate simulation of chloride profiles during migration tests, the normalized distribution profiles of chlorides (C_{Cl}/C_{Cl0}) from these two numerical models are compared with those obtained from an experiment conducted by Jiang et al. (2013).

Fig. 7.1 compares the normalized distribution of chlorides at three different times from experiments, non-equilibrium binding modelling, and no binding modelling. It exhibits that when binding effect is ignored in simulation, chloride ions ingress into a deeper layer

of concrete, resulting in an overestimation of chloride migration coefficient. Chloride penetration depth obtained from non-equilibrium model fits well with that from Jiang's experiment. However, it is evident that the chloride concentration profiles obtained from non-equilibrium binding model present a sharp migration front, which is significantly different in shape compared to the experimental profiles. In the numerical models of migration tests conducted by Xia and Li (2013), Šavija et al. (2014), Liu et al. (2015a), and Liu et al. (2015b), the chloride profiles also exhibit an obvious migration front. The difference between the chloride profiles obtained from numerical simulations and experimental measurements indicates that non-equilibrium binding model cannot accurately capture the transport behavior of chlorides during migration tests. One possible explanation for this difference is that the pre-designed binding isotherm used in non-equilibrium binding model is unsatisfactory in describing the real reaction kinetics in concrete during the chloride ingress process (Tang, 1996).

Fig. 7.2 presents a comparison of the normalized distribution of chlorides at three different times obtained from experiments and reactive mass transport modelling. Chloride profiles from reactive model present a gradual shape that agrees well with that from experiment. This indicates that the thermodynamic equilibrium (dissolution and formation of solid cement hydrates and surface reactions on C-S-H) used in reactive model is rational and appropriate for simulating chloride migration tests. Therefore, reactive mass transport model, rather than non-equilibrium binding model, is employed in subsequent parametric analyses. Fig. 7.3 exhibits that the porosity of concrete slightly increases as chloride ions ingress into it, which is consistent with the findings from Qiao et al. (2018). One possible explanation for the limited change in porosity could be the relatively short duration of migration tests in the present simulations, which may not have allowed sufficient time for reactions between free ions and cement hydrates (Lothenbach, 2010). In turn, the variation of porosity slightly speeds up the ionic transport in concrete, as shown in Fig. 7.2. The difference between results obtained from reactive models with and without considering pore evolution is negligible due to the limited variation of porosity.

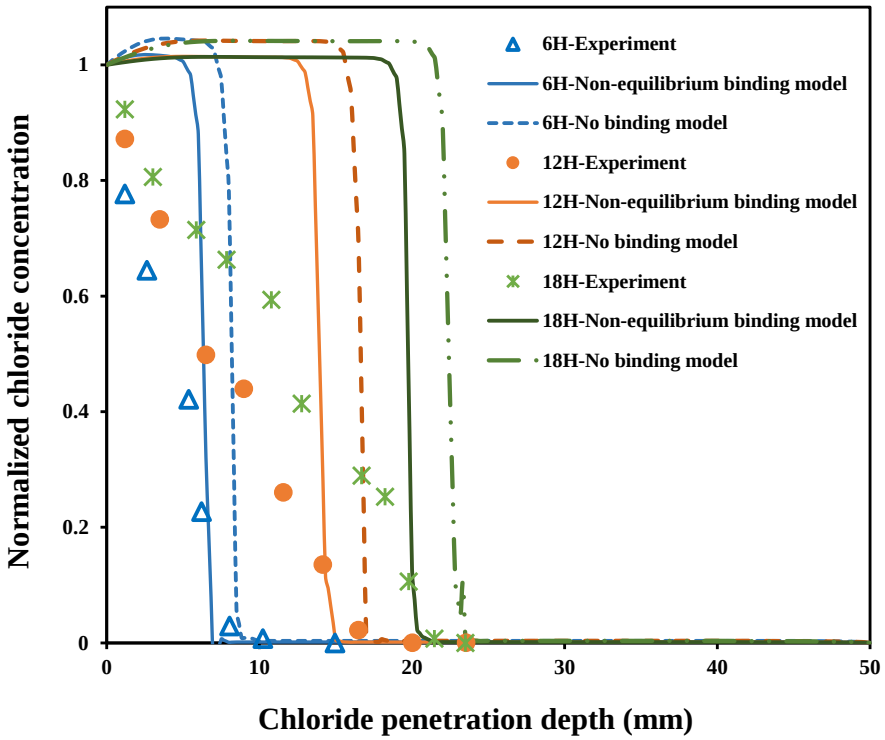

Figure 7.1 Comparison of distribution profiles of chloride ions obtained from experiment, non-equilibrium binding and no binding models

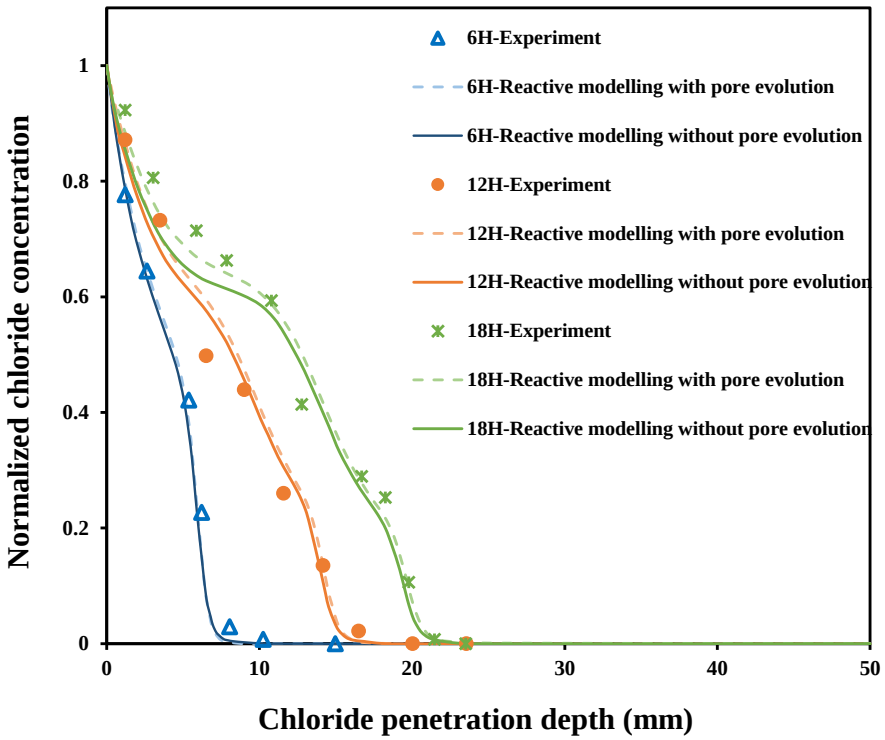

Figure 7.2 Comparison of distribution profiles of chloride ions obtained from experiment and reactive mass transport model

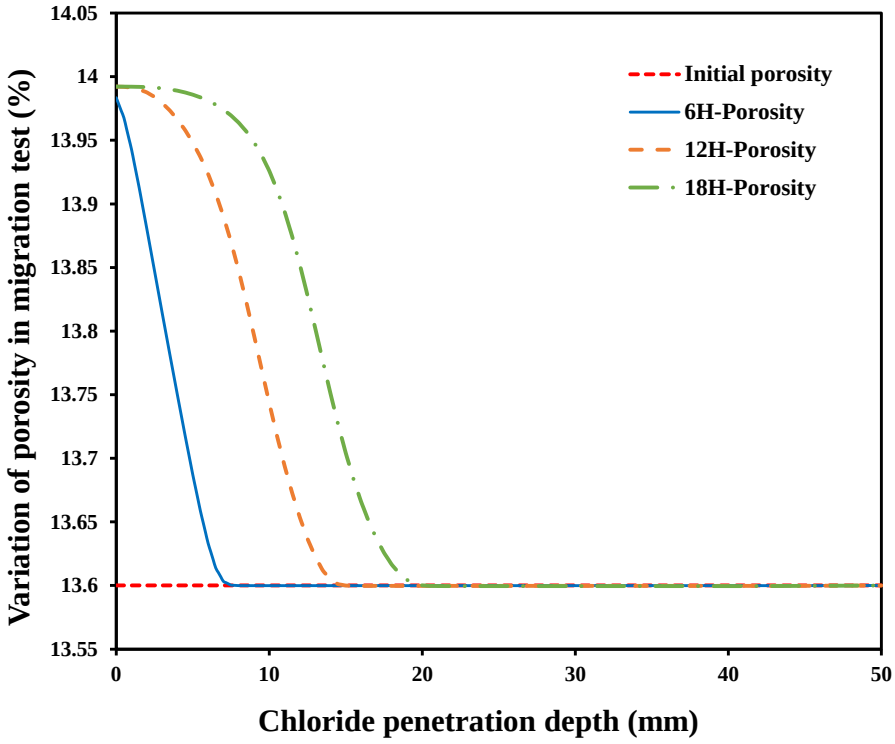

Figure 7.3 Variation in porosity during the chloride migration test

7.3. Results and discussion

7.3.1. Distributions of ionic species and hydration products

Fig. 7.4 presents the distributions of free chloride ions in pore solution, related cement hydrates, and porosity after a 24-hour migration test. Under the action of an external electric field, negatively charged chloride ions migrate towards the anode. The ingress of chlorides can break the equilibrium between free ions and cement hydrates, resulting in the precipitation or dissolution of hydration products and new thermodynamic reactions between chloride ions and C-S-H as listed in Table 2.1 (Lothenbach, 2010; Hosokawa et al., 2011; Tran et al., 2018). These reactions eventually lead to a decrease in the content of AFm phase and C-S-H reaction sites, while simultaneously promoting the formation of Friedel's salt and $\equiv SiOCl^-$, as shown in Figs. 7.4 (c) and (d). As given in Table 3.8, the concentration of C-S-H reaction sites is significantly greater than that of AFm phase. Nevertheless, the concentration of chemically bound chloride is much higher than that of

physically bound chloride, which agrees with the findings of simulations conducted by Hosokawa et al. (2011b) and Yu et al. (2019). This explains the fact that C-S-H has a lower chloride-binding ability compared to AFm (Florea and Brouwers, 2012). Figs. 7.4 (d) and (f) indicate a similar increasing trend in both porosity and Friedel's salt as chlorides ingress into concrete. This can be attributed to the lower average molar density of Friedel's salt compared to that of AFm phase, as listed in Table 2.3.

Figs. 7.5-7.7 summarize the distributions of OH^-, SO_4^{2-}, and $Al(OH)_4^-$ ions and the corresponding cement hydrates. Under the action of an electrical field, all negatively charged ions move towards the anode. Despite having different diffusion coefficients, their migration fronts are nearly identical due to the multi-species coupling. It should be pointed out that the initial concentration of sulfate ions is only 2 mol/m^3. However, Fig. 7.6 (a) reveals that sulfate ions gradually accumulate within concrete, reaching over 35 mol/m^3 after a 24-hour migration test. This accumulation is attributed to the chemical reaction between AFm and chlorides, which releases sulfate ions into pore solution. The released sulfate ions can then react with AFm and C-S-H to form AFt and $\equiv SiOCaSO_4^-$, as shown in Figs. 7.6 (b) and (c). According to the reaction equations listed in Table 2.1, the dissolution of AFm phase can also release $Al(OH)_4^-$ ions from solid phase to pore solution. However, the distribution of $Al(OH)_4^-$ will not accumulate in concrete as shown in Fig. 7.7. This is because once $Al(OH)_4^-$ ions dissolve into pore solution, they instantaneously react with chloride and calcium ions and form Friedel's salt (Baur et al., 2004), as given in Table 2.1.

From Figs. 7.8-7.10, it is observed that positively charged ionic species migrate towards the cathode during migration test. Sodium ions exhibit a different behavior compared to other cations, likely due to the NaOH solution in an anodic cell supplies sufficient sodium ions for the migration process. The variation in distribution profiles for physically bound cations follows a similar trend to that of free cations. Additionally, the concentrations of physically bound hydroxyl, potassium, sodium, and calcium are significantly lower compared to physically bound chloride. This can be attributed to the infinitesimal

equilibrium constants of reactions between these ionic species and C-S-H, as provided in Table 2.1.

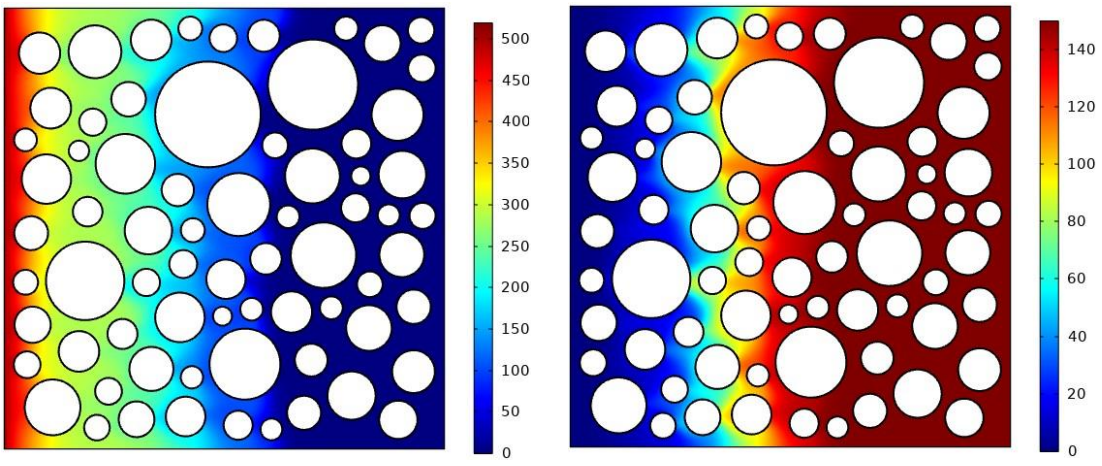

(a) Chloride ions (b) AFm phase

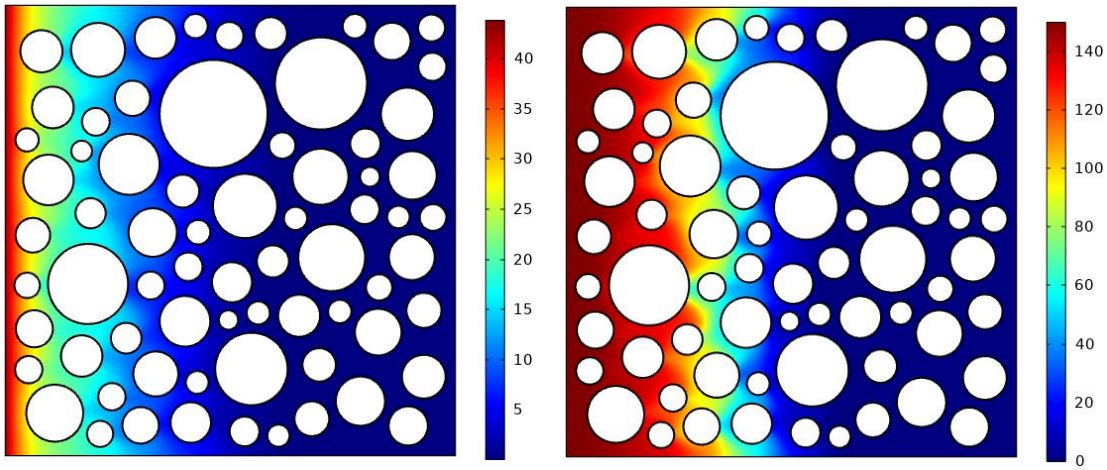

(c) Physically bound chloride (d) Friedel's salt

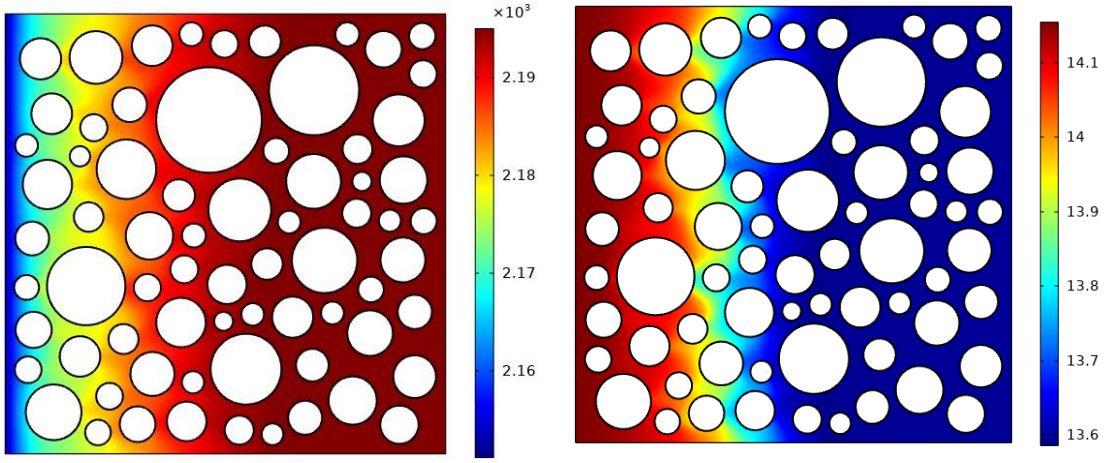

(e) Reaction sites on C-S-H surfaces (f) Porosity (%)

Figure 7.4 Distribution of chloride ions, related hydrate phases, and porosity in concrete after 24-hour migration test (mol/m^3)

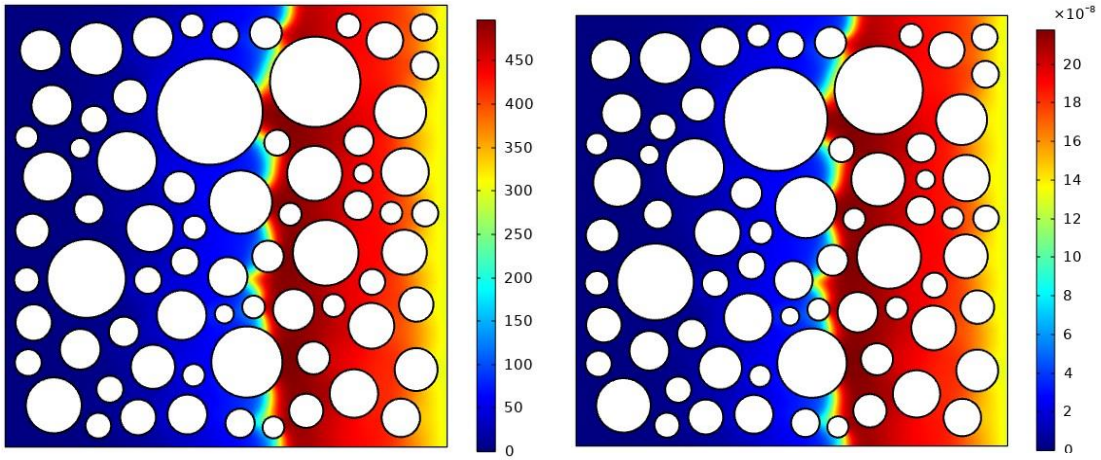

(a) Free hydroxyl ions (b) Physically bound hydroxyl

Figure 7.5 Distribution of free and bound hydroxyl in concrete after 24-hour migration test (mol/m^3)

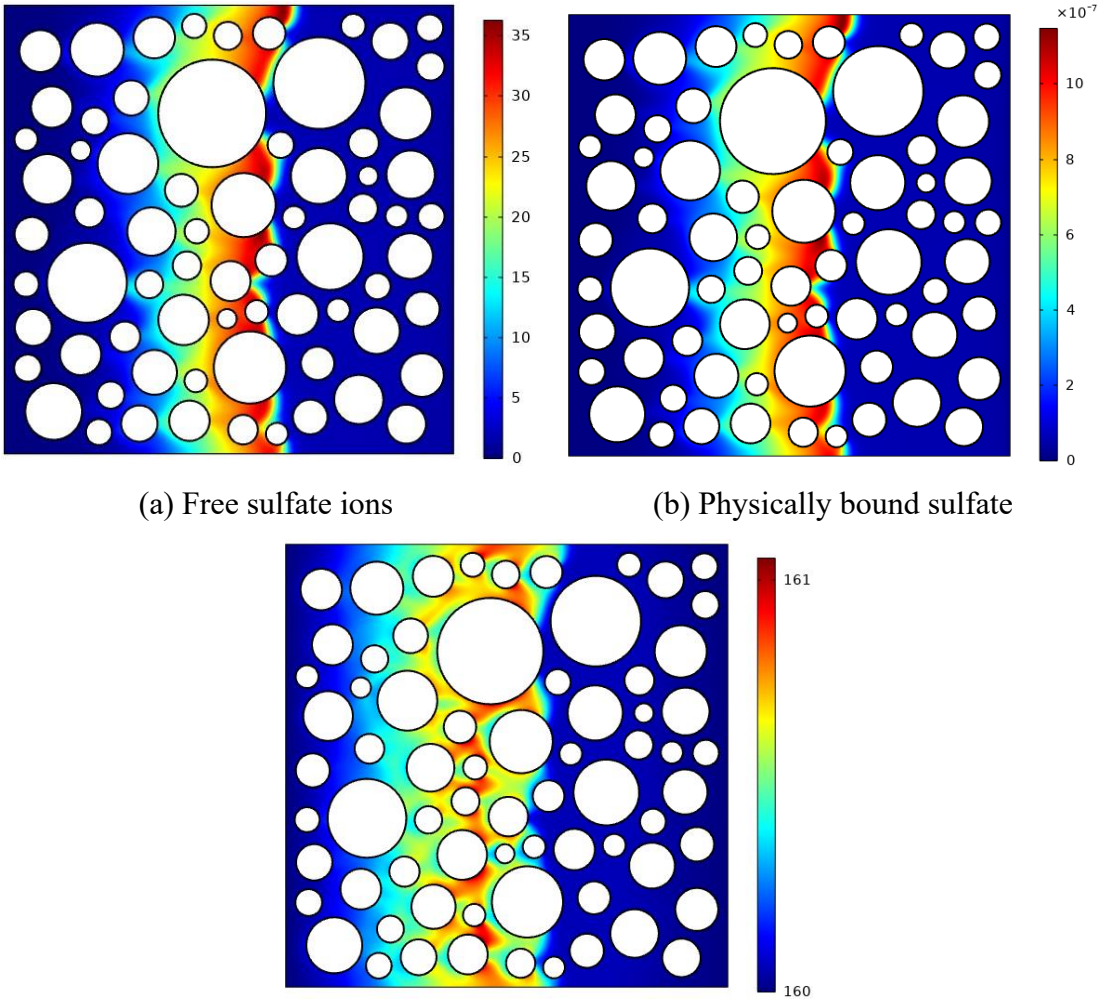

(a) Free sulfate ions (b) Physically bound sulfate

(c) AFt

Figure 7.6 Distribution of free sulfate ions and related solid phase in concrete after 24-hour migration test (mol/m^3)

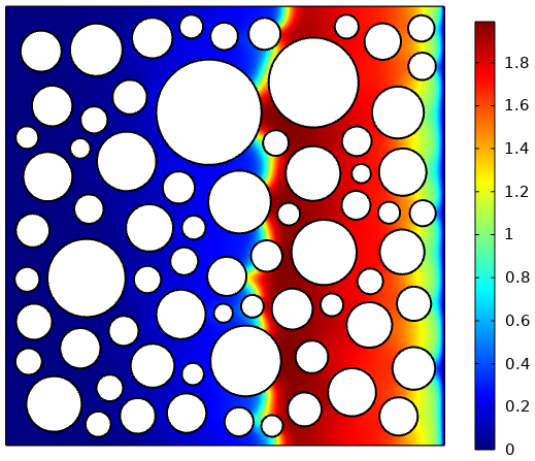

Figure 7.7 Distribution of $Al(OH)_4^-$ ions in concrete after 24-hour migration test (mol/m^3)

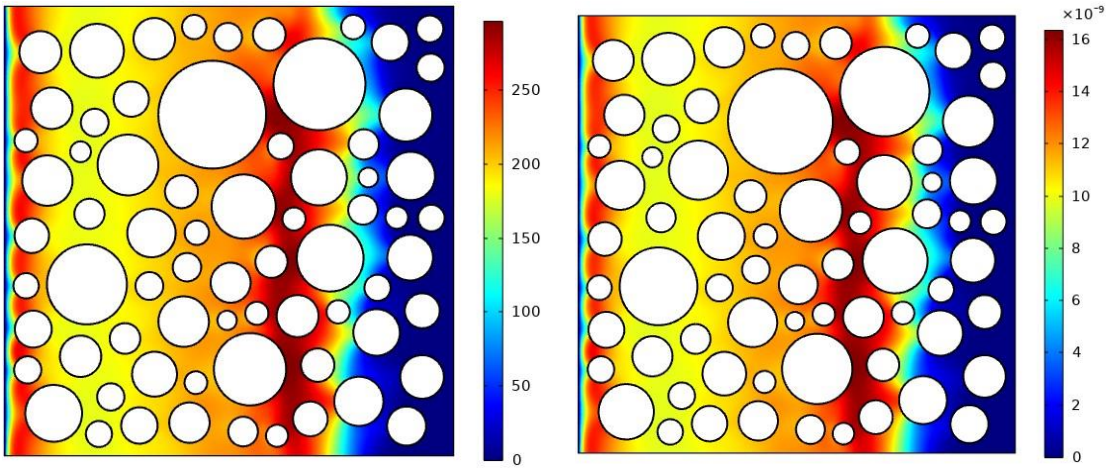

(a) Free potassium ions (b) Physically bound potassium

Figure 7.8 Distribution of free and bound potassium after 24-hour migration test (mol/m^3)

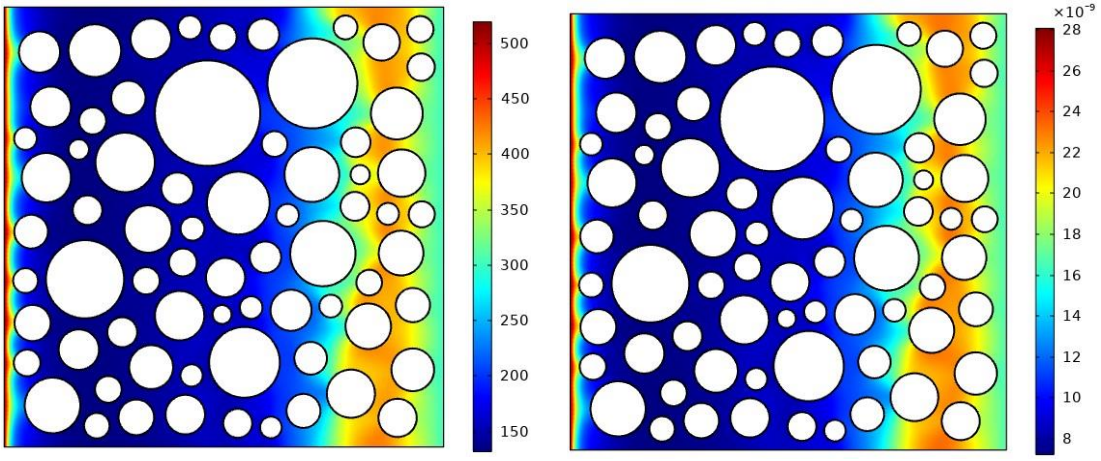

(a) Free sodium ions (b) Physically bound sodium

Figure 7.9 Distribution of free and bound sodium in concrete after 24-hour migration test (mol/m^3)

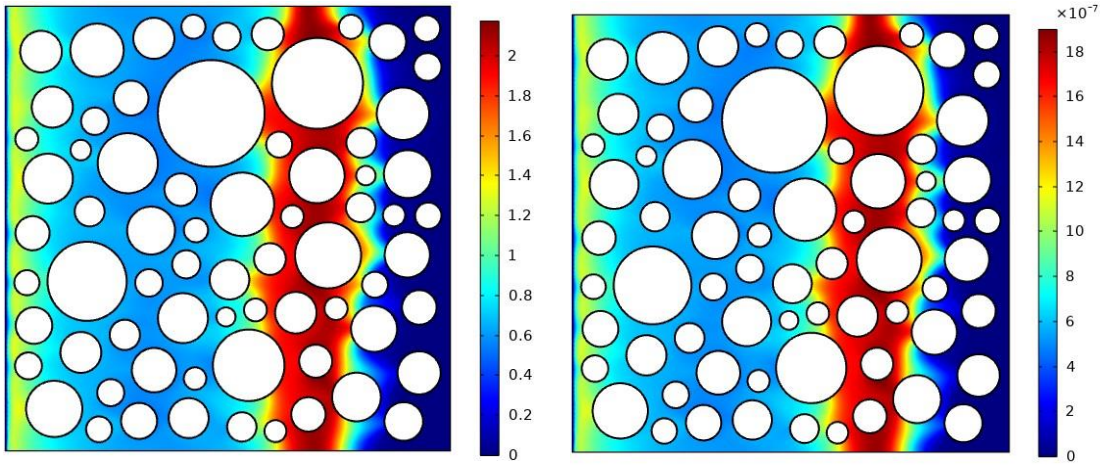

(a) Free calcium ions (b) Physically bound calcium

Figure 7.10 Distribution of free and bound calcium in concrete after 24-hour migration test (mol/m^3)

7.3.2. AFm content

In this section, three different initial concentrations of AFm phase are considered: 100 mol/m^3 in Case 1, 150 mol/m^3 in Case 2, and 250 mol/m^3 in Case 3. The corresponding variations in chloride transport behavior are then examined.

Fig. 7.11 shows the distribution profiles of free chloride ions in concrete with different initial concentrations of AFm. It can be seen that chloride penetration depths in these three different cases are almost the same. This suggests that the initial concentration of AFm phase has a limited influence on the rate of ionic movement during migration tests. However, it is notable that the concentration of chloride ions decreases with an increase in AFm content. This can be explained by the fact that a higher presence of AFm in concrete results in more chloride ions being bound to solid phase. Furthermore, Fig. 7.11 reveals an interesting observation: unlike the findings from Chapters 4 and 6 (Figs. 4.9 and 6.5), chloride profiles from reactive mass transport model exhibit a gradual migration front, aligning with the profiles observed in experimental studies conducted by Yang and Chiang (2013) and Jiang et al. (2013). This may be attributed to several factors: 1) Time-space dependent chloride binding rate calculated by thermodynamic equilibrium (Equations (2.37) and (2.40)), which allows for a more realistic representation of chloride

profiles. 2) Effect of other ionic species, such as released sulfate ions from AFm phase, as shown in Fig. 7.6. 3) Considering the pore constrictivity in ionic transport, which can slow down the velocity of ionic migration in concrete (Yang et al., 2017). Moreover, the presence of impermeable natural aggregates may contribute to some minor fluctuations in chloride profiles, as it can result in local variations in ionic transport properties.

Fig. 7.12 illustrates the gradual decrease in AFm content in concrete as it transforms into Friedel's salt due to the ingress of chloride ions. Fig. 7.13 provides insights into the relationship between Friedel's salt, AFm phase, and chloride ions. Interestingly, it is observed that an increase in AFm content does not always lead to a higher formation of Friedel's salt. This is because the formation of Friedel's salt depends on the concentrations of both free chloride ions in pore solution and AFm phase in hardened cement. When the concentration of chloride ions is sufficiently high, AFm content becomes a dominant factor in the formation of Friedel's salt. Otherwise, if the concentration of chloride ions is relatively low, chemical binding is primarily determined by their concentration instead.

Similarly, the physical adsorption of chloride ions is also influenced by the concentrations of both C-S-H reaction sites and free chloride ions. The distribution of free chloride ions changes with varying AFm content in concrete. Therefore, the concentration of physically bound chloride decreases with increasing AFm content, even though the concentrations of C-S-H reaction sites are the same in all three cases, as shown in Fig. 7.14. The variation of porosity in concrete exhibits a similar increasing trend as the formation of Friedel's salt, as shown in Fig. 7.15. An increase in Friedel's salt leads to higher porosity in concrete, and vice versa. This variation in porosity can be attributed to the difference in average molar volume between Friedel's salt and AFm phase, as given in Table 2.3.

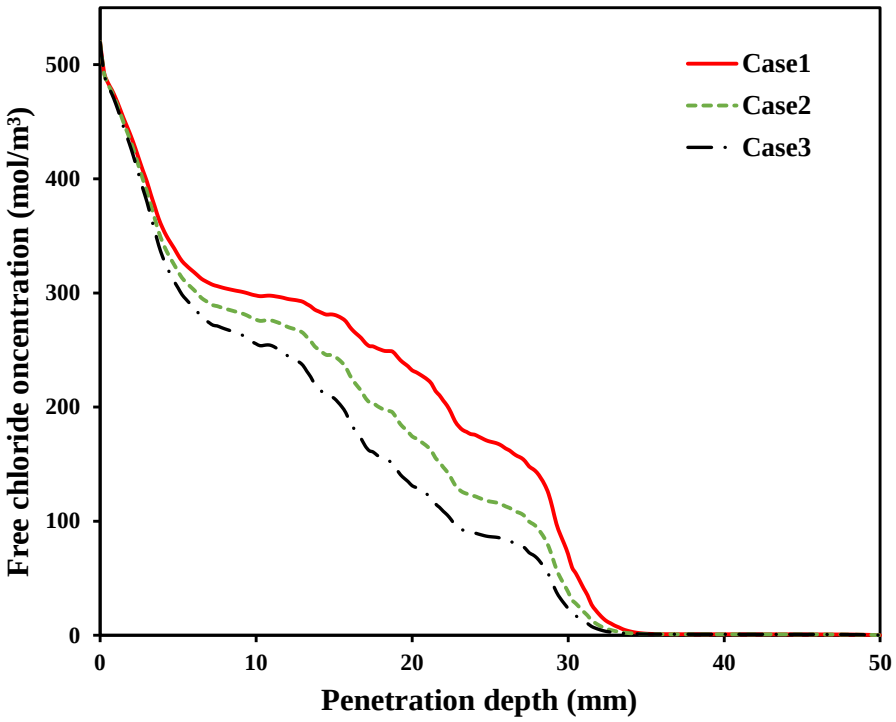

Figure 7.11 Concentration profiles of free chloride ions in models with three different initial AFm contents after 24-hour migration test

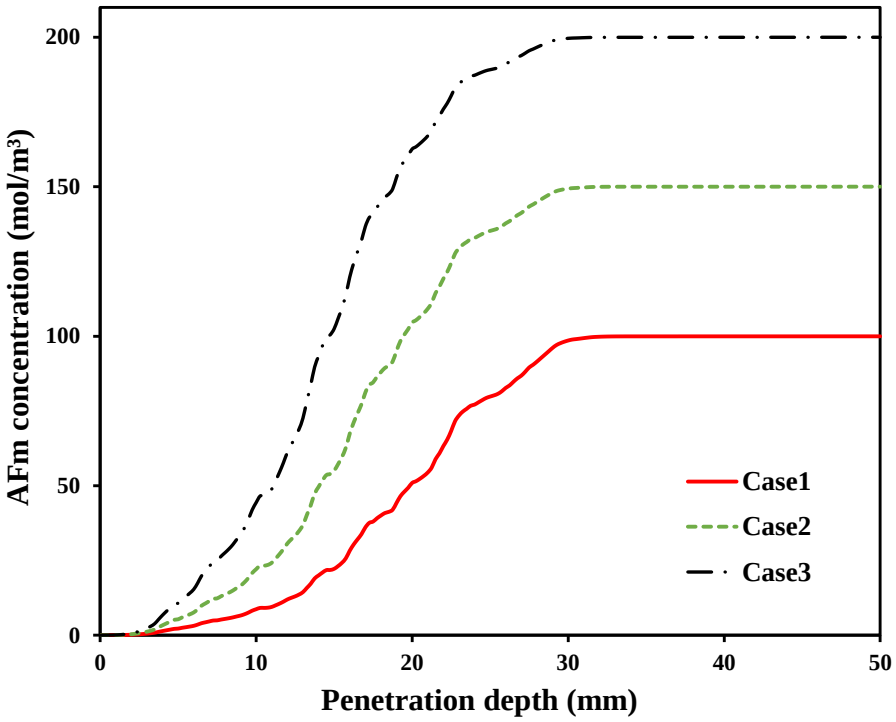

Figure 7.12 Distributions of AFm phase in models with three different initial AFm contents after 24-hour migration test

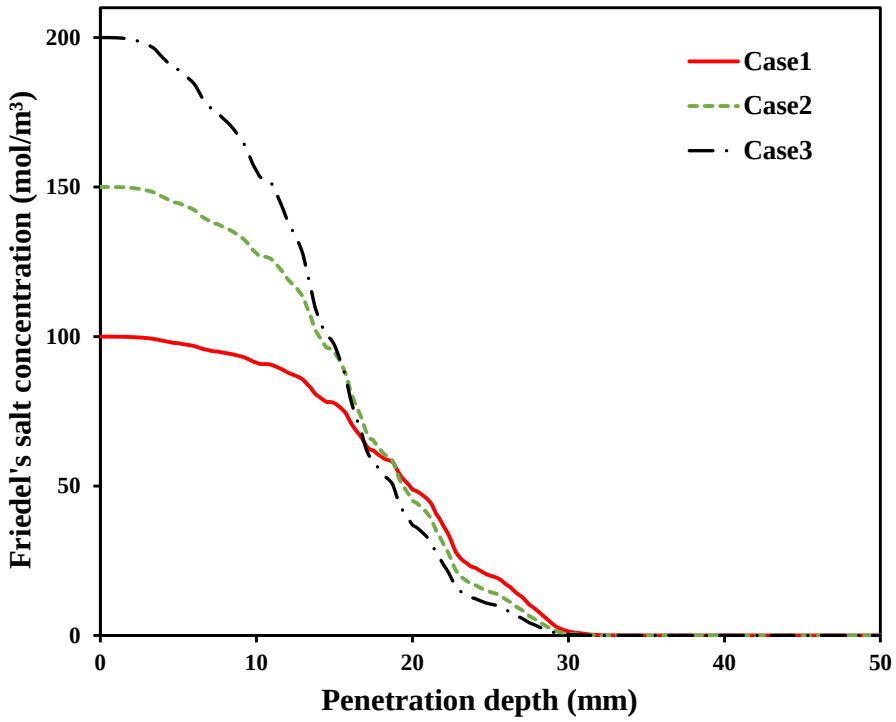

Figure 7.13 Concentration profiles of Friedel's salt in models with three different initial AFm contents in concrete after 24-hour migration test

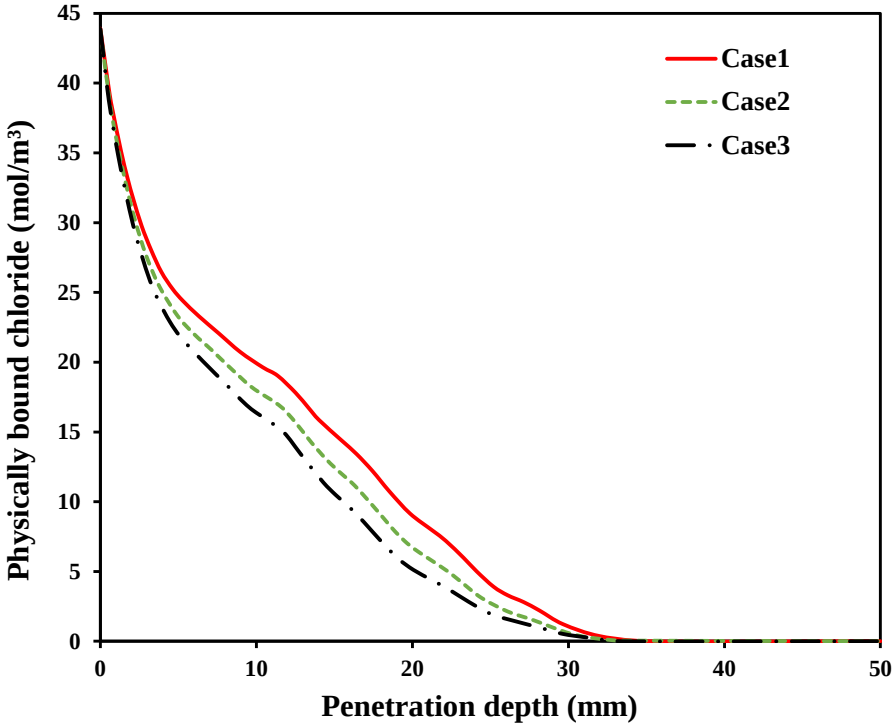

Figure 7.14 Concentration profiles of physically bound chloride in models with three different initial AFm contents after 24-hour migration test

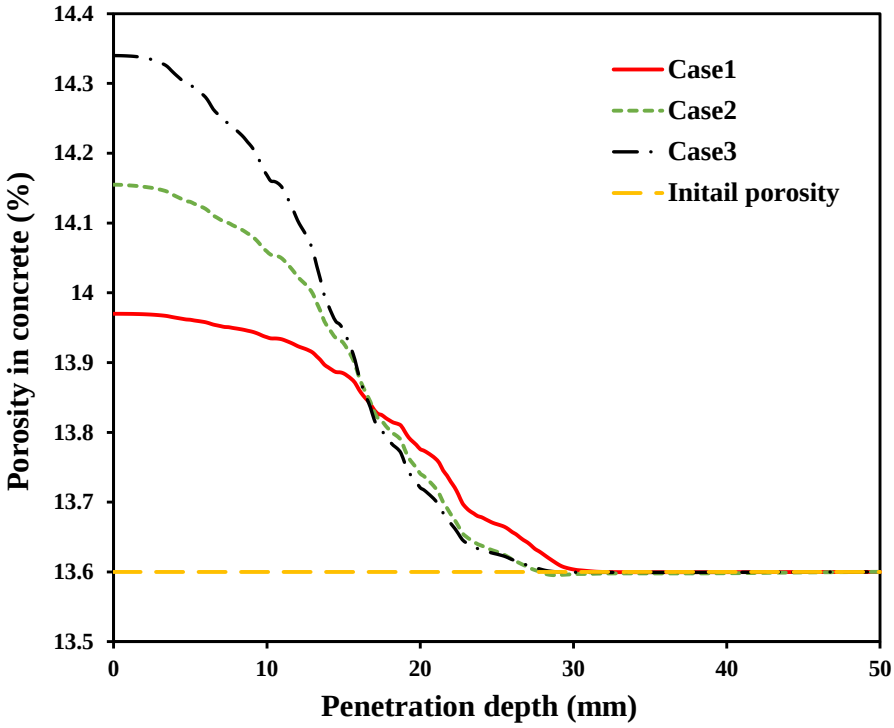

Figure 7.15 Profiles of porosity in models with three different initial AFm contents after 24-hour migration test

7.3.3. Pore constrictivity

Pore constrictivity is a dimensionless parameter used to examine the influence of pore size on the length of ionic migration path in porous concrete (Yang et al., 2017). Fig. 7.16 shows variations in the distribution profiles of free chloride ions with varying pore constrictivity factors. According to Equations (2.70) and (3.10), an increase in pore constrictivity leads to a longer ionic migration path, resulting in a decrease in ionic migration velocity. Therefore, it is evident that both the penetration depth and content of chloride ions decrease with increasing pore constrictivity. Correspondingly, the concentrations of both physically and chemically bound chlorides decrease with increasing pore constrictivity, as shown in Figs. 7.17 and 7.18. It is worth noting that the migration front of chloride profiles in cases with high ionic migration velocity appears to be more gradual than that in cases with low ionic migration velocity. This does not imply that migration is not the dominant process in concrete with low pore constrictivity, characterized by high ionic migration velocity, during chloride migration tests. The faster

ingress of chloride ions in the low pore constrictivity case leads to a higher concentration of bound chloride in concrete, which subsequently affects the wave front of ionic distribution.

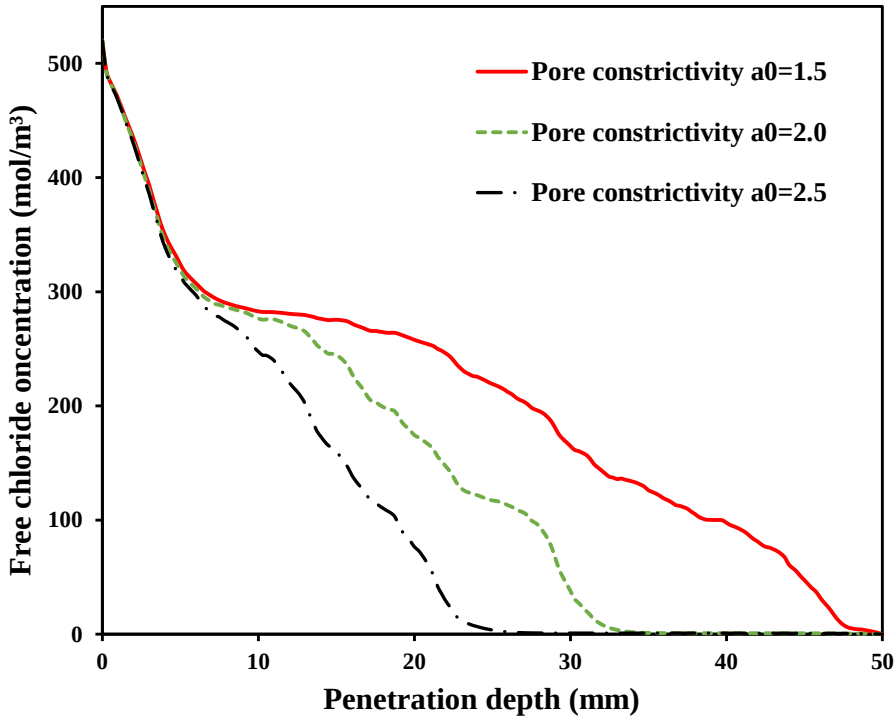

Figure 7.16 Concentration profiles of free chloride ions in models with three different pore constrictivity factors after 24-hour migration test

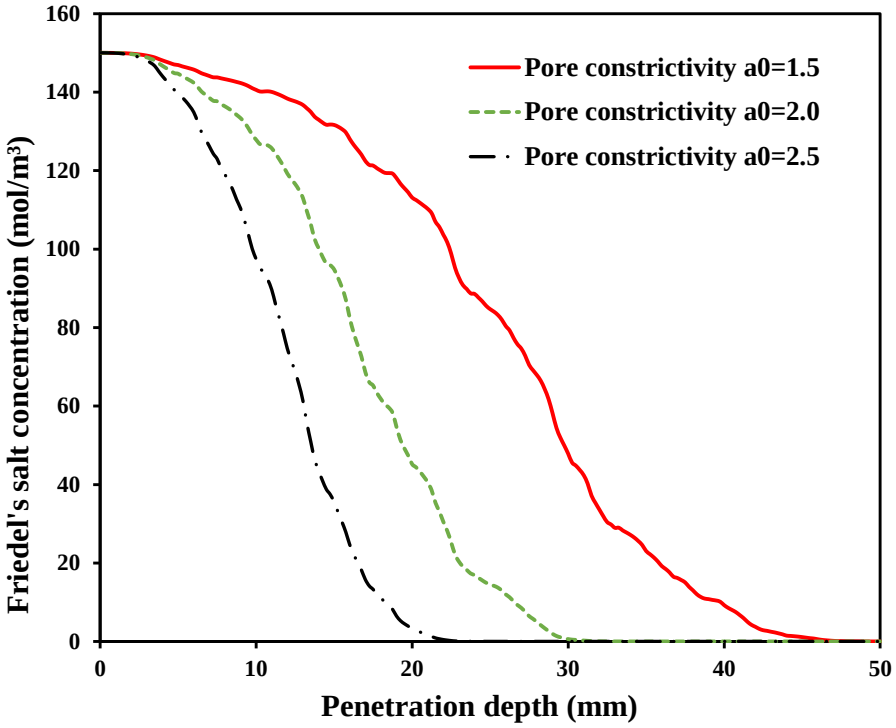

Figure 7.17 Concentration profiles of Friedel's salt in models with three different pore constrictivity factors after 24-hour migration test

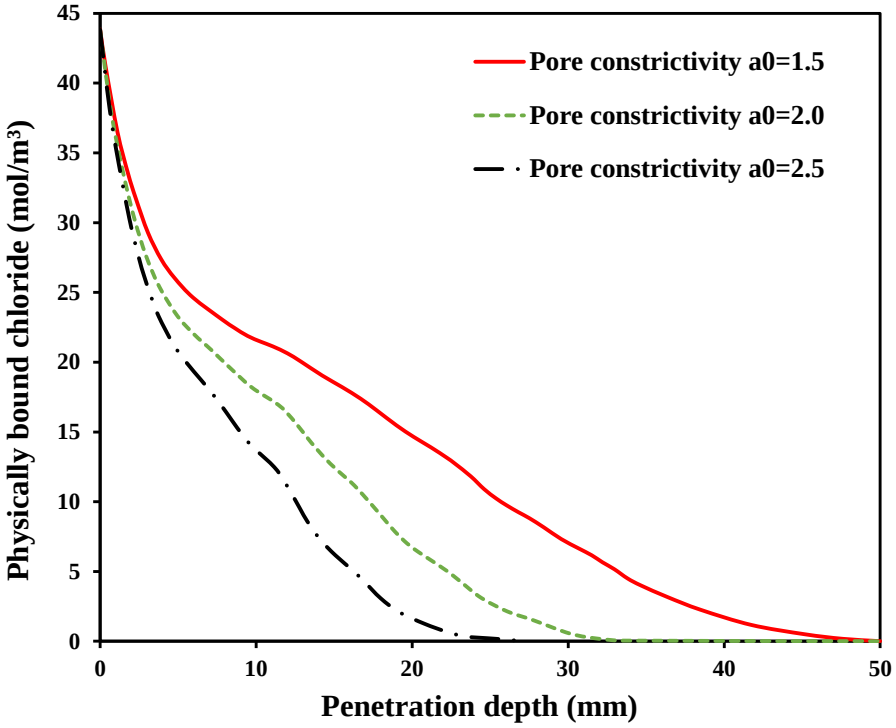

Figure 7.18 Profiles of physically bound chloride in models with three different pore constrictivity factors after 24-hour migration test

7.3.4. Recycled concrete aggregate

Fig. 7.19 demonstrates the distribution profiles of free chlorides in NAC and RAC. It is evident that RAC exhibits lower chloride resistance compared to NAC due to the existing old mortar and ITZ in RCA. However, the increase in the volume fraction of old mortar in RCA does not significantly affect the penetration depth or concentration of chlorides. Fig. 7.20 shows that the average concentrations of physically and chemically bound chlorides are almost the same in all four cases. These findings can be attributed to the fact that the old mortar in RCA has dual effects on chloride penetration in RAC: 1) The inherent porosity or microcracks in old mortar provide extra paths for ionic transport (enhancing chloride penetration). This is supported by SEM observations conducted by Meng et al. (2020) and numerical results from Chapter 5 (Figs. 5.6 and 5.12). 2) Cement hydrates in old mortar provide more reaction sites and absorb more free ions (reducing chloride penetration). This is evidenced by the significant increase in the total amount of physically and chemically bound chlorides in concrete over time, as shown in Fig. 7.21. These findings suggest that the application of high-quality RCA that has a strong chloride absorption capacity is a viable strategy for enhancing the chloride resistance of RAC.

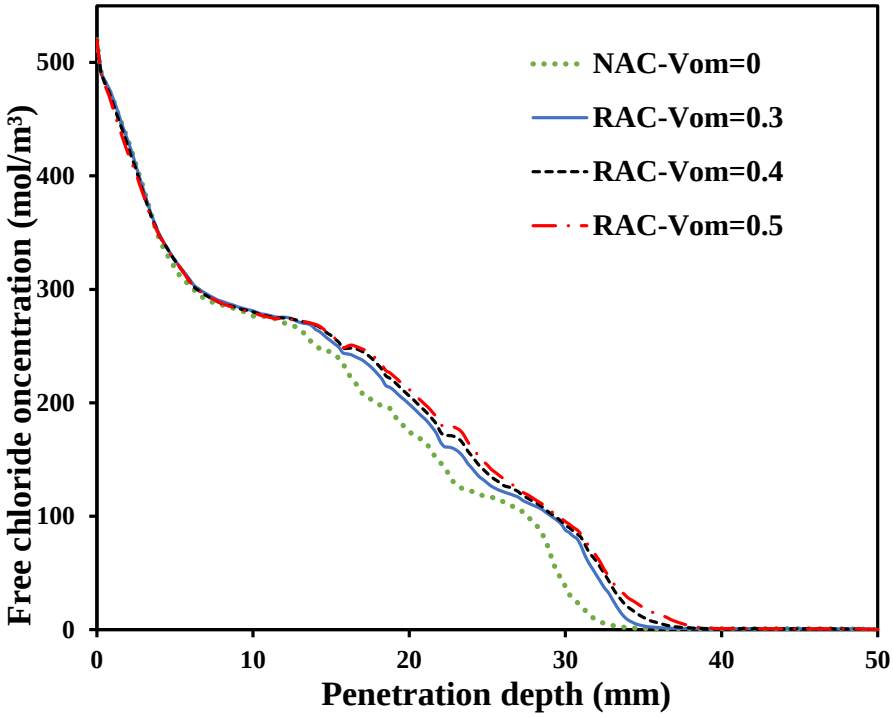

Figure 7.19 Concentration profiles of free chloride ions in NAC and RAC with three different volume fractions of old mortar after 24-hour migration test

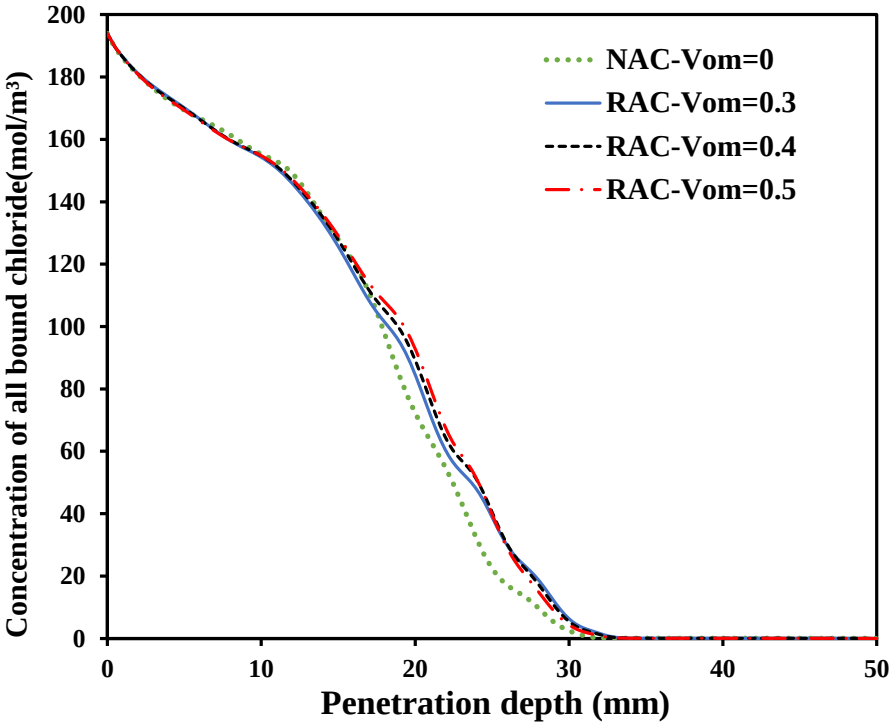

Figure 7.20 Concentration profiles of bound chloride (chemically bound chloride plus physically bound chloride) in NAC and RAC with three different volume fractions of old mortar after 24-hour migration test

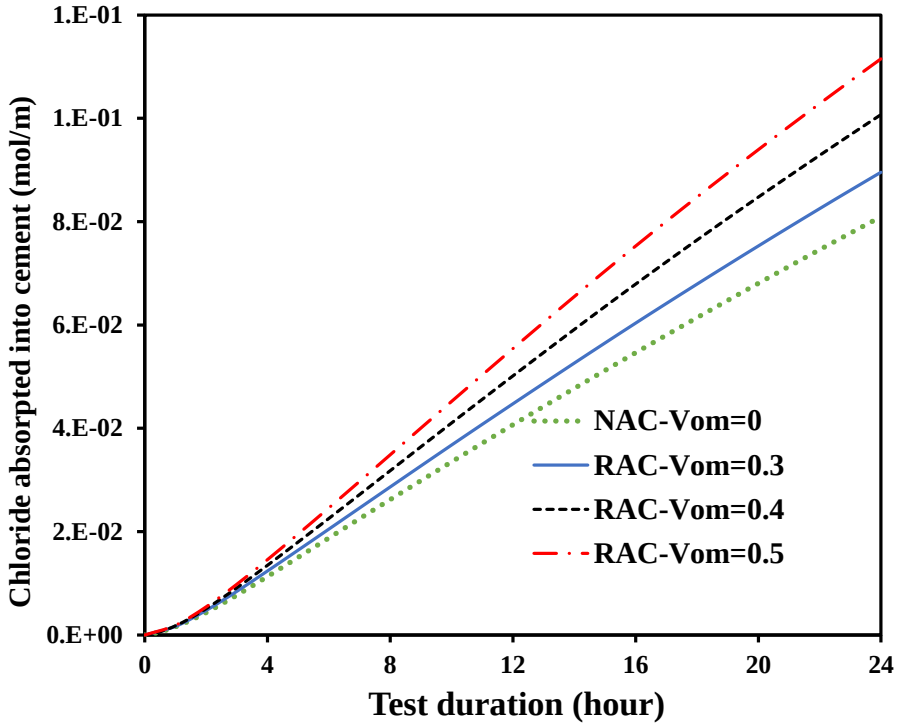

Figure 7.21 The total amount of bound chloride in NAC and RAC with three different volume fractions of old mortar after 24-hour migration test

7.4. Summary

Based on the reactive mass transport model and non-equilibrium binding model demonstrated in Section 3.4, the influence of physicochemical reactions between free ions and cement hydrates, particularly chloride binding, on ionic transport in concrete has been examined. The variations in free ionic species and the cement hydrates involved in chloride penetration are presented. Based on the numerical results obtained, the following conclusions are summarized:

1) Incorporating thermodynamic equilibrium into the reactive mass transport model enables a more precise representation of actual reaction kinetics during chloride migration tests, as opposed to the preset binding isotherm utilized in non-equilibrium model. Therefore, the chloride concentration profiles obtained from reactive mass transport model present more gradual migration fronts.

2) As chloride ions penetrate into concrete, a fraction of the AFm phase undergoes

transformation into Friedel's salt. The formation of Friedel’s salt can contribute to an increase in concrete porosity, which in turn slightly accelerates chloride transport in concrete.

3) The concentrations of physically bound potassium, sodium, calcium, and sulfate are significantly lower compared to that of physically bound chloride.

4) The effect of AFm content on Friedel's salt formation hinges on the concentration of chloride ions in the concrete. With abundant chloride ions, an increase in AFm content can enhance Friedel's salt formation. Conversely, if chloride ions are scarce, their concentration becomes crucial in controlling Friedel's salt formation.

5) Free and bound chloride concentrations in concrete during migration tests are significantly influenced by pore constrictivity. Higher pore constrictivity leads to a lower ionic migration velocity and a decrease in the concentrations of free and bound chlorides.

6) The application of RCA in concrete has two opposite effects on chloride transport. On the one hand, the porous old mortar and ITZ in RCA can accelerate the ingress of chloride. On the other hand, the cement hydrates in old mortar can adsorb more chloride ions, potentially reducing the penetration of chloride.

CHAPTER 8 CONCLUSIONS AND FUTURE PERSPECTIVES

8.1. Conclusions

The aim of this thesis is to investigate the ionic transport properties in heterogenous concrete and to develop reliable and rational prediction models to estimate the chloride penetration during diffusion and migration tests. Based on the understanding of each sub-process of ionic transport in concrete, such as diffusion, electromigration, polarization, physicochemical adsorption and desorption, several numerical and analytical models of chloride ingress in natural and recycled aggregate concrete have been proposed and verified. Firstly, ion-ion interactions between different ionic species in pore solution and their influence on ionic transport behaviors in concrete have been examined by three multi-species coupling models (Chapter 4). Secondly, each individual phase in concrete, such as natural impermeable aggregate, old ITZ, old mortar, new ITZ, and new mortar, and their influences on concrete resistance to chloride attack have been investigated by a five-phase numerical model and a two-step analytical model (Chapter 5). Thirdly, the polarization induced overpotential between electrode and concrete surface and its influence on inner ionic transport during migration tests have been assessed using overpotential models (Chapter 6). Finally, physicochemical reactions between free ions and solid cement hydrations and their influence on free- and bound-chloride distribution have been examined by a reactive mass transport model and a non-equilibrium model (Chapter 7). The main findings obtained from the present study are concluded as follows:

Multi-species coupling and its effects on ionic transport behaviors:

1) During chloride diffusion tests, multi-species coupling does not influence chloride penetration significantly. While, in the case of chloride migration tests, it has a remarkable effect, accelerating chloride ingress into concrete up to approximately 67% in the present simulation.

2) Both Poisson's and current conservation law methods can describe the impacts of

multi-species coupling on chloride transport during migration tests.

3) Current conversation law is a better choice to balance computation burden and accuracy when modelling multi-species transport in migration tests with an external voltage or current.

4) Poisson's equation is appropriate for modelling chloride migration tests with an external voltage when both multi-species coupling and physicochemical reactions are involved.

Heterogeneity of concrete and its influences on chloride resistance:

1) Incorporating RCA into concrete enhances its effective chloride diffusion, as RCA is generally not impermeable. This rate of increase depends on the volume fractions of the old mortar and ITZ, their respective chloride diffusivities, and the w/b or w/c ratio of both old and new mortars.

2) The extremely thin old and/or new ITZs in concrete significantly increase the effective chloride diffusivity of RAC.

3) The effective diffusion coefficient decreases with increasing total volume fraction of aggregate, regardless of the replacement rate of RCA used. Furthermore, concretes with a greater RCA replacement rate experience a smaller decrease in effective chloride diffusivity compared to those with a lower RCA replacement rate.

4) When the quality and replacement rate of RCA are given, the present five-phase numerical model and two-step analytical model provide reliable and precise predictions of concrete's chloride resistance.

Outside polarization and its influences on inner ionic transport during migration tests:

1) Overpotential, induced by polarization, contributes to a marked decrease in chloride penetration depth during migration tests. Overpotential experiences a steady decline over time. Nevertheless, its effect on the distribution of each ionic species increases as time progresses.

2) The effect of polarization on chloride penetration depends on both the absolute value of overpotential and its proportion in relation to the externally provided voltage. Overpotential effects on chloride transport behavior increase with decreasing external voltage.

3) Factors such as external voltage, initial ionic concentration in pore solution, and RCA replacement rate exhibit a relatively small impact on the overpotential magnitude. However, these factors considerably affect the penetration depth and/or the total amount of chloride ions in concrete.

4) Tafel parameters, which are dependent on the conditions of the electrolyte and electrode, have a notable influence on overpotential variation. The selection of electrolyte and electrode is crucial to improving the efficiency of chloride migration tests.

Physicochemical reactions and their impacts on ionic transport behaviors during migration tests:

1) Physical and chemical reactions between free ions and cement hydrations markedly decelerate the ingress of chloride ions. Neglecting chloride binding in simulation may result in underestimating the concrete's resistance to chloride.

2) Compared to the pre-designed binding isotherm used in non-equilibrium binding

model, the thermodynamic equilibrium integrated into reactive mass transport model enables a more accurate description of the real reaction kinetics during chloride migration tests.

3) Chloride penetration induces a phase transition from AFm to Friedel's salt, resulting in an increase in porosity within concrete. This increase in porosity correspondingly slightly accelerates ionic transport in concrete.

4) The concentration of AFm in concrete does not markedly influence chloride penetration depth. However, it plays an important role in the formation of bound chloride.

5) Increased pore constrictivity results in reduced migration velocity of chloride ions and a decreased quantity of physically and chemically bound chlorides.

6) The increase in old mortar in RCA has a small impact on chloride penetration. This can be attributed to its ability to adsorb free ions and its porous microstructure that offers additional pathways for ionic transport.

8.2. Future work

This section suggests several aspects of ionic transport properties in heterogenous concrete that need further to study, which are summarized as follows:

1) All concrete models employed in present thesis are saturated, and as such, convection behavior is not considered in chloride penetration processes. Hence, the multi-species transport in an unsaturated cement-based materials should be explored in future.

2) The present simulation of chloride migration tests assumes a constant ionic concentration in the external electrolyte. However, electrochemical reactions at electrodes have the potential to generate or consume hydroxyl or hydrogen ions,

which may influence chloride penetration through ion-ion interactions. Therefore, the effects of time-varying concentration of hydroxyl ions in electrolyte cells during chloride migration tests should be studied in future.

3) In present five-phase models for RAC, old aggregates are assumed to be fully enclosed by old mortar, which is not a realistic situation. Random distribution of old mortar may change the ionic transport path, ultimately affecting the effective chloride diffusivity of RAC. Further studies are recommended to investigate the effects of randomly distributed old mortar.

4) Initial porosity in present numerical models is assumed to be uniform in concrete specimens. However, pore distribution is typically nonhomogeneous in cement-based materials, particularly when NA or RCA are involved. Therefore, future investigations should consider the influence of randomly distributed porosity on ionic transport in concrete.

5) Pore solution and hydration products vary in concrete using different binders, such as fly ash, silica fume, and pozzolan, which can influence the desorption and absorption of all ionic species. Hence, future work should further explore the applicability of present multi-species, multi-phase, and multi-physical field models in different types of concrete.

REFERENCES

AASHTO-T259 1980. Standard method of test for resistance of concrete to chloride ion penetration. American Association of State Highway and Transportation Officials, Washington, DC, USA.

AASHTO-T259 2002. Standard method of test for resistance of concrete to chloride ion penetration. American Association of State Highway and Transportation Officials, Washington, DC, USA.

AASHTO-T277 1983. Standard Method of Test for Rapid Determination of the Chloride Permeability of Concrete. American Association of State Highway and Transportation Officials, Washington, DC, USA.

AASHTO-TP6403 2003. Standard Method of Test for Predicting Chloride Penetration of Hydraulic Cement Concrete by the Rapid Migration Procedure. American Association of State Highway and Transportation Officials, Washington, DC, USA.

Abyaneh, S. D., Wong, H. & Buenfeld, N. 2013. Modelling the diffusivity of mortar and concrete using a three-dimensional mesostructure with several aggregate shapes. *Computational Materials Science,* 78, 63-73.

Addassi, M. & Johannesson, B. 2020. Reactive mass transport in concrete including for gaseous constituents using a two-phase moisture transport approach. *Construction and Building Materials,* 232, 117148.

Amey, S. L., Johnson, D. A., Miltenberger, M. A. & Farzam, H. 1998. Predicting the service life of concrete marine structures: an environmental methodology. *Structural Journal,* 95, 205-214.

Andreu, G. & Miren, E. 2014. Experimental analysis of properties of high performance recycled aggregate concrete. *Construction and Building Materials,* 52, 227-235.

Arnold, J., Duddu, R., Brown, K. & Kosson, D. S. 2017. Influence of multi-species solute transport on modeling of hydrated Portland cement leaching in strong nitrate solutions. *Cement and Concrete Research,* 100, 227-244.

ASTM-C1202 2012. Standard Test Method for Electrical Indication of Concrete's Ability to Resist Chloride Ion Penetration, American Society for Testing and Materials, Philadelphia.

ASTM-C1543 2002. Standard test method for determining the penetration of chloride ion into concrete by ponding, American Society for Testing and Materials, Philadelphia.

ASTM-C1556 2003. Standard test method for determining the apparent chloride diffusion coefficient of cementitious mixtures by bulk diffusion. *Annual book ASTM standards. West Conshohocken,* American Society for Testing and Materials, Philadelphia.

Angst, U. 2011. Chloride induced reinforcement corrosion in concrete: Concept of critical chloride content–methods and mechanisms. *Norwegian University of Science and Technology, Norwegian, Doctor Thesis.*

Backe, K., Lile, O. & Lyomov, S. 2001. Characterizing curing cement slurries by electrical conductivity. *SPE Drilling & Completion*, 16, 201-207.

Balonis, M. & Glasser, F. P. 2009. The density of cement phases. *Cement and Concrete Research,* 39, 733-739.

Bao, J., Li, S., Zhang, P., Ding, X., Xue, S., Cui, Y. & Zhao, T. 2020. Influence of the incorporation of recycled coarse aggregate on water absorption and chloride penetration into concrete. Construction and Building Materials, 239, 117845.

Baquerizo, L. G., Matschei, T., Scrivener, K. L., Saeidpour, M. & Wadsö, L. 2015. Hydration states of AFm cement phases. *Cement and Concrete Research,* 73, 143-157.

Baroghel-Bouny, V., Thiéry, M. & Wang, X. 2011. Modelling of isothermal coupled moisture-ion transport in cementitious materials. *Cement and Concrete Research,* 41, 828-841.

Baur, I., Keller, P., Mavrocordatos, D., Wehrli, B. & Johnson, C. A. 2004. Dissolution-precipitation behaviour of ettringite, monosulfate, and calcium silicate hydrate. *Cement and concrete research,* 34, 341-348.

Bensted, J. 1983. Hydration of Portland cement. *Advances in cement technology*. Elsevier.

Berke, N. S. & Hicks, M. C. 1992. Estimating the life cycle of reinforced concrete decks and marine piles using laboratory diffusion and corrosion data. *Corrosion forms and control for infrastructure.* ASTM International.

Bertolini, L. 1995. Controllo della Corrosione delle Armature nel Calcestruzzo Mediante Circolazione di Corrente: Aspetti Elettrochimici. Ph.D. Thesis, Politecnico di Milano, Dipartmento di Chimica Fisica.

Bertolini, L., Carsana, M. & Pedeferri, P. 2007. Influence of stray currents on corrosion of steel in concrete.

Boddy, A., Hooton, R. & Gruber, K. 2001. Long-term testing of the chloride-penetration resistance of concrete containing high-reactivity metakaolin. *Cement and concrete research*, 31, 759-765.

Bourdette, B., Ringot, E. & Ollivier, J. 1995. Modelling of the transition zone porosity. *Cement and concrete research*, 25, 741-751.

Bruggeman, V. D. 1935. Berechnung verschiedener physikalischer Konstanten von heterogenen Substanzen. I. Dielektrizitätskonstanten und Leitfähigkeiten der Mischkörper aus isotropen Substanzen. *Annalen der physik*, 416, 636-664.

BS 1097-3 1998. Tests for mechanical and physical properties of aggregates. *Determination of loose bulk density and voids.* British Standard Institution.

BS 7361-1. 1991. Cathodic Protection, Part 1: Code of Practice for Land and Marine Applications. British Standard Institution.

BS 933-11 2012. Tests for Geometrical Properties of Aggregates—Part 2: Determination of Particle Size Distribution. *Test Sieves, Nominal Size of Apertures.* British Standard Institution.

Cao, Y., Guo, L., Chen, B. & Wu, J. 2020. Thermodynamic modelling and experimental investigation on chloride binding in cement exposed to chloride and chloride-sulfate solution. *Construction and Building Materials*, 246, 118398.

Caré, S. 2003. Influence of aggregates on chloride diffusion coefficient into mortar. *Cement and Concrete Research*, 33, 1021-1028.

Caré, S. & Hervé, E. 2004. Application of a n-phase model to the diffusion coefficient of chloride in mortar. *Transport in porous media*, 56, 119-135.

Castellote, M., Andrade, C. & Alonso, C. 1999. Chloride-binding isotherms in concrete submitted to non-steady-state migration experiments. *Cement and Concrete Research*, 29, 1799-1806.

Cheng, X., Xia, J., Wang, W., Jin, S., Huang, N. & Jin, W. 2020. Numerical modeling of the effect of concrete porosity evolution on electrochemical chloride removal from concrete structures. *Construction and Building Materials*, 120929.

Damrongwiriyanupap, N., Liang, Y. C. & Xi, Y. P. 2011. Diffusion of multi-ionic species in recycled aggregate concrete. *Key Engineering Materials*, 56-64.

De Sitter, W. Costs of service life optimization" The Law of Fives". CEB-RILEM Workshop on Durability of Concrete Structures (Copenhagen, Denmark, May 18-20, 1983), 1984. Comité Euro-International du Béton, 131-134.

Debye, P. & Hückel, E. 1923. The interionic attraction theory of deviations from ideal behavior in solution. *Z. Phys,* 24, 185.

Delagrave, A., Bigas, J. P., Ollivier, J. P., Marchand, J. & Pigeon, M. 1997. Influence of the interfacial zone on the chloride diffusivity of mortars. *Advanced Cement Based Materials,* 86-92.

Diamond, S. & Huang, J. 2001. The ITZ in concrete–a different view based on image analysis and SEM observations. *Cement and concrete composites,* 23, 179-188.

Du, F., Jin, Z., She, W., Xiong, C., Feng, G. & Fan, J. 2020. Chloride ions migration and induced reinforcement corrosion in concrete with cracks: a comparative study of current acceleration and natural marine exposure. *Construction and Building Materials,* 263, 120099.

Du, X., Jin, L. & Ma, G. 2014. A meso-scale numerical method for the simulation of chloride diffusivity in concrete. *Finite Elements in Analysis and Design,* 85, 87-100.

Duan, H., Karihaloo, B. L., Wang, J. & Yi, X. 2006. Effective conductivities of heterogeneous media containing multiple inclusions with various spatial distributions. *Physical Review B,* 73, 174203.

Duan, Z. H. & Poon, C. S. 2014. Properties of recycled aggregate concrete made with recycled aggregates with different amounts of old adhered mortars. *Materials & Design,* 58, 19-29.

El-Reedy, M. 2007. *Steel-reinforced concrete structures: assessment and repair of corrosion*, CRC press.

Elakneswaran, Y., Iwasa, A., Nawa, T., Sato, T. & Kurumisawa, K. 2010. Ion-cement hydrate interactions govern multi-ionic transport model for cementitious materials. *Cement and concrete research,* 40, 1756-1765.

Etxeberria, M., Vázquez, E. & Mari, A. 2006. Microstructure analysis of hardened recycled aggregate concrete. *Magazine of Concrete Research,* 58, 683-690.

Feldman, R., Jr, L. & Chan, G. 1999. Rapid chloride permeability test on blended cement and other concretes: correlations between charge, initial current and conductivity. *Construction & Building Materials,* 13, 149-154.

FloreaL, M. & Brouwers, H. 2012. Chloride binding related to hydration products: Part I: Ordinary Portland Cement. *Cement and Concrete Research*, 42, 282-290.

Friedmann, H., Amiri, O. & Aît-Mokhtar, A. 2008a. Shortcomings of geometrical approach in multi-species modelling of chloride migration in cement-based materials. *Magazine of Concrete Research,* 60, 119-124.

Friedmann, H., Amiri, O. & Aït-Mokhtar, A. 2008b. Physical modeling of the electrical double layer effects on multispecies ions transport in cement-based materials. *Cement & Concrete Research*.

Friedmann, H., Amiri, O., Aıt-Mokhtar, A. & Dumargue, P. 2004. A direct method for determining chloride diffusion coefficient by using migration test. *Cement and Concrete Research,* 34, 1967-1973.

Garboczi, E. & Bentz, D. 1996. Modelling of the microstructure and transport properties of concrete. *Construction and Building Materials,* 10, 293-300.

Garcia-Lodeiro, I., Palomo, A. & Fernández-Jiménez, A. 2015. An overview of the chemistry of alkali-activated cement-based binders. *Handbook of alkali-activated cements, mortars and concretes*, 19-47.

Glass, G. 1999. The 100-mV potential decay cathodic protection criterion. *Corrosion*, 55.

Glass, G. & Buenfeld, N. 2000. The influence of chloride binding on the chloride induced corrosion risk in reinforced concrete. *Corrosion Science,* 42, 329-344.

Gommes, C. J., Bons, A. J., Blacher, S., Dunsmuir, J. H. & Tsou, A. H. 2009. Practical methods for measuring the tortuosity of porous materials from binary or gray - tone tomographic reconstructions. *AIChE Journal*, 55, 2000-2012.

Guo, B., Hong, Y., Qiao, G., Ou, J. & Li, Z. 2018. Thermodynamic modeling of the essential physicochemical interactions between the pore solution and the cement hydrates in chloride-contaminated cement-based materials. *Journal of colloid and interface science,* 531, 56-63.

Guo, B., Li, Z., Fu, Q., Wang, Y., Huang, D. & Niu, D. 2021a. Reactive transport modelling of chloride ingress in saturated coral aggregate concrete. *Frontiers in Materials*, 420.

Guo, B., Qiao, G., Han, P., Li, Z. & Fu, Q. 2022. Effect of natural carbonation on chloride binding behaviours in OPC paste investigated by a thermodynamic model. *Journal of Building Engineering,* 49, 104021.

Guo, B., Qiao, G., Li, D. & Ou, J. 2021b. Multi-species reactive transport modeling of electrochemical corrosion control in saturated concrete structures including electrode reactions and thermodynamic equilibrium. *Construction and Building Materials,* 278, 122228.

Gutiérrez, A. & De Juan, M. Influence of attached mortar content on the properties of recycled concrete aggregate. International RILEM Conference on the Use of Recycled Materials in Building and Structures, 2004. RILEM Publications SARL, 536-544.

Halamickova, P., Detwiler, R. J., Bentz, D. P. & Garboczi, E. J. 1995. Water permeability and chloride ion diffusion in portland cement mortars: Relationship to sand content and critical pore diameter. *Cement & Concrete Research,* 25, 790-802.

Hansson, I. & Hansson, C. M. 1993. Electrochemical extraction of chlorides from concrete part I-A qualitative model of the process. *Cement and concrete research,* 23, 1141-1152.

Hassan, Z. 2001. Binding of external chloride by cement pastes. *Toronto: University of Toronto*.

Hassanein, A., Glass, G. & Buenfeld, N. 2002. Protection current distribution in reinforced concrete cathodic protection systems. *Cement and Concrete Composites,* 24, 159-167.

Haverkort, J. & Rajaei, H. 2020. Electro-osmotic flow and the limiting current in alkaline water electrolysis. *Journal of Power Sources Advances,* 6, 100034.

Hervé, E. & Zaoui, A. 1995. Elastic behaviour of multiply coated fibre-reinforced composites. *International Journal of Engineering Science,* 33, 1419-1433.

Hobbs, D. 1999. Aggregate influence on chloride ion diffusion into concrete. *Cement and Concrete Research,* 29, 1995-1998.

Holzer, L., Wiedenmann, D., Münch, B., Keller, L., Prestat, M., Gasser, P., Robertson, I. & Grobéty, B. 2013. The influence of constrictivity on the effective transport properties of porous layers in electrolysis and fuel cells. *Journal of materials science,* 48, 2934-2952.

Hosokawa, Y., Yamada, K., Johannesson, B. & Nilsson, L.-O. 2011a. Development of a multi-species mass transport model for concrete with account to thermodynamic phase equilibriums. *Materials and structures,* 44, 1577-1592.

Hosokawa, Y., Yamada, K., Johannesson, B. & Nilsson, L. O. 2011b. Development of a multi-species mass transport model for concrete with account to thermodynamic phase equilibriums. *Materials and structures,* 44, 1577-1592.

Hu, Z., Mao, L., Xia, J., Liu, J., Gao, J., Yang, J. & Liu, Q. 2018. Five-phase modelling for effective diffusion coefficient of chlorides in recycled concrete. *Magazine of Concrete Research,* 70, 583-594.

Huang, K. & Yang, C. 2018. Using RCPT determine the migration coefficient to assess the durability of concrete. *Construction and Building Materials,* 167, 822-830.

Huang, K. & Yang, C. 2020. Using the chloride penetration depth obtained from RCPT to acess the permeability of concrete. *Journal of Marine Science and Technology,* 28, 5.

Jensen, M. M. 2014. A Coupled Transport and Chemical Model for Durability Predictions of Cement Based Materials. *Technical University of DenmarkDanmarks Tekniske Universitet, Department of Structural Engineering and MaterialsInstitut for Bærende Konstruktioner og Materialer*.

Jensen, M. M., Johannesson, B. & Geiker, M. R. 2014. Framework for reactive mass transport: Phase change modeling of concrete by a coupled mass transport and chemical equilibrium model. *Computational materials science,* 92, 213-223.

Jiang, L., Song, Z., Yang, H., Pu, Q. & Zhu, Q. 2013. Modeling the chloride concentration profile in migration test based on general Poisson Nernst Planck equations and pore structure hypothesis. *Construction and Building Materials,* 40, 596-603.

Jie, W., Dassekpo, J. B. M., Wan, C. & Zha, X. 2017. Experimental and numerical modeling of chloride diffusivity in hardened cement concrete considering the aggregate shapes and exposure-duration effects. *Results in physics,* 7, 1427-1432.

Johannesson, B. 2010a. Comparison between the Gauss' law method and the zero current method to calculate multi-species ionic diffusion in saturated uncharged porous materials. *Computers and Geotechnics,* 37, 667-677.

Johannesson, B. 2010b. Development of a generalized version of the Poisson-Nernst-Planck equations using the hybrid mixture theory: presentation of 2D numerical examples. *Transport in Porous Media,* 85, 565-592.

Johannesson, B., Hosokawa, Y. & Yamada, K. 2009. Numerical calculations of the effect of moisture content and moisture flow on ionic multi-species diffusion in the pore solution of porous materials. *Computers & structures,* 87, 39-46.

Johannesson, B., Yamada, K., Nilsson, L.-O. & Hosokawa, Y. 2007. Multi-species ionic diffusion in concrete with account to interaction between ions in the pore solution and the cement hydrates. *Materials and structures,* 40, 651.

Júnior, N. S. A., Silva, G. A., Dias, C. M. & Ribeiro, D. V. 2019. Concrete containing recycled aggregates: Estimated lifetime using chloride migration test. *Construction and Building Materials,* 222, 108-118.

Kakali, G., Tsivilis, S., Aggeli, E. & Bati, M. 2000. Hydration products of C3A, C3S and Portland cement in the presence of CaCO3. *Cement and concrete Research,* 30, 1073-1077.

Kassir, M. K. & Ghosn, M. 2002. Chloride-induced corrosion of reinforced concrete bridge decks. *Cement and Concrete Research,* 32, 139-143.

Khitab, A., Lorente, S. & Ollivier, J. 2005. Predictive model for chloride penetration through concrete. *Magazine of Concrete Research,* 57, 511-520.

Kitowski, C. & Wheat, H. 1997. Effect of chlorides on reinforcing steel exposed to simulated concrete solutions. *Corrosion,* 53, 216-226.

Kou, S. 2006. Reusing recycled aggregates in structural concrete. *Pao Yue-kong Library, The Hong Kong Polytechnic University, Hung Hom, Kowloon, Hong Kong*.

Kou, S. & Poon, C. 2015. Effect of the quality of parent concrete on the properties of high performance recycled aggregate concrete. *Construction and Building Materials,* 77, 501-508.

Kou, S. & Poon, C. S. 2006. Compressive strength, pore size distribution and chloride-ion penetration of recycled aggregate concrete incorporating class-F fly ash. *Journal of Wuhan University of Technology-Mater. Sci. Ed.,* 21, 130-136.

Kou, S. & Poon, C. S. 2012. Enhancing the durability properties of concrete prepared with coarse recycled aggregate. *Construction and building materials,* 35, 69-76.

Koulouris, K. & Apostolopoulos, C. 2020. An experimental study on effects of corrosion and stirrups spacing on bond behavior of reinforced concrete. *Metals,* 10, 1327.

Kubo, J., Sawada, S., Page, C. & Page, M. 2007. Electrochemical injection of organic corrosion inhibitors into carbonated cementitious materials: Part 2. Mathematical modelling. *Corrosion science,* 49, 1205-1227.

Landauer, R. 1952. The electrical resistance of binary metallic mixtures. *Journal of applied physics,* 23, 779-784.

Li, L. Y. 2014. A pore size distribution-based chloride transport model in concrete. *Magazine of concrete research,* 66, 937-947.

Li, L. Y., Easterbrook, D., Xia, J. & Jin, W. 2015. Numerical simulation of chloride penetration in concrete in rapid chloride migration tests. *Cement and Concrete Composites,* 63, 113-121.

Li, L. Y. & Page, C. 1998. Modelling of electrochemical chloride extraction from concrete: Influence of ionic activity coefficients. *Computational Materials Science,* 9, 303-308.

Li, L. Y., Xia, J. & Lin, S. 2012. A multi-phase model for predicting the effective diffusion coefficient of chlorides in concrete. *Construction and Building Materials,* 26, 295-301.

Li, L. Y. & Page, C. 2000. Finite element modelling of chloride removal from concrete by an electrochemical method. *Corrosion Science,* 42, 2145-2165.

Li, Z., Zhou, X., Ma, H., & Hou, D. 2022. *Advanced concrete technology.* Hoboken, New Jersy: John Wiley & Sons.

Lin, J., Chen, H., Zhao, Q. & Li, M. 2021. Statistical analysis of the critical percolation of ITZ around polygonal aggregates in three-phase concrete materials. *Physica A: Statistical Mechanics and its Applications,* 572, 125878.

Liu, J., Wang, X., Qiu, Q., Ou, G. & Xing, F. 2017. Understanding the Effect of Curing Age on the Chloride Resistance of Fly Ash Blended Concrete by Rapid Chloride Migration Test. *Materials Chemistry and Physics,* 196, 315-323.

Liu, Q. 2014. Multi-phase modelling of multi-species ionic migration in concrete. *University of Plymouth, UK, Doctor Thesis.*

Liu, Q., Easterbrook, D., Yang, J. & Li, L. 2015a. A three-phase, multi-component ionic transport model for simulation of chloride penetration in concrete. *Engineering Structures,* 86, 122-133.

Liu, Q., Feng, G., Xia, J., Yang, J. & Li, L. 2018. Ionic transport features in concrete composites containing various shaped aggregates: a numerical study. *Composite Structures,* 183, 371-380.

Liu, Q., Li, L., Easterbrook, D. & Yang, J. 2012. Multi-phase modelling of ionic transport in concrete when subjected to an externally applied electric field. *Engineering Structures,* 42, 201-213.

Liu, Q., Xia, J., Easterbrook, D., Yang, J. & Li, L. 2014. Three-phase modelling of electrochemical chloride removal from corroded steel-reinforced concrete. *Construction and Building Materials,* 70, 410-427.

Liu, Q., Yang, J., Xia, J., Easterbrook, D., Li, L. & Lu, X. 2015b. A numerical study on chloride migration in cracked concrete using multi-component ionic transport models. *Computational Materials Science,* 99, 396-416.

Liu, Y. & Shi, X. 2012. Ionic transport in cementitious materials under an externally applied electric field: Finite element modeling. *Construction & Building Materials,* 27, 450-460.

Liu, Z., Zhang, Y., Liu, L. & Jiang, Q. 2013. An analytical model for determining the relative electrical resistivity of cement paste and C-S-H gel. *Construction and Building Materials,* 48, 647-655.

Lothenbach, B. 2010. Thermodynamic equilibrium calculations in cementitious systems. *Materials and Structures,* 43, 1413-1433.

Lothenbach, B., Kulik, D. A., Matschei, T., Balonis, M., Baquerizo, L., Dilnesa, B., Miron, G. D. & Myers, R. J. 2019. Cemdata18: A chemical thermodynamic database for hydrated Portland cements and alkali-activated materials. *Cement and Concrete Research,* 115, 472-506.

Lu, B. & Torquato, S. 1992. Nearest-surface distribution functions for polydispersed particle systems. *Physical Review A,* 45, 5530.

Tang, L. 1996. Chloride transport in concrete-measurement and prediction. *Chalmers University of Technology, Sweden, Doctor Thesis.*

Tang, L. 2008. Engineering expression of the ClinConc model for prediction of free and total chloride ingress in submerged marine concrete. *Cement and Concrete Research,* 38, 1092-1097.

Tang, L. & Nilsson, L. O. 1992. Chloride diffusivity in high strength concrete at different ages. *Nordic Concrete Research Publication*.

Tang, L. & Nilsson, L. O. 1993. Chloride binding capacity and binding isotherms of OPC pastes and mortars. *Cement and concrete research,* 23, 247-253.

Mao, L., Hu, Z., Xia, J., Feng, G., Azim, I., Yang, J. & Liu, Q. 2019. Multi-phase modelling of electrochemical rehabilitation for ASR and chloride affected concrete composites. *Composite Structures,* 207, 176-189.

Mao, L., Li, L. & Kim, B. 2022. Modelling of multi-species transport in concrete under the action of external electric field: Influence of the overpotential at electrode-electrolyte interfaces. *Journal of Electroanalytical Chemistry,* 907, 116079.

Marchand, J. 2001. Modeling the behavior of unsaturated cement systems exposed to aggressive chemical environments. *Materials and Structures,* 34, 195-200.

Marriaga, J. L. & Claisse, P. 2009. Effect of the non-linear membrane potential on the migration of ionic species in concrete. *Electrochimica Acta,* 54, 2761-2769.

Martın-Pérez, B., Zibara, H., Hooton, R. & Thomas, M. 2000. A study of the effect of chloride binding on service life predictions. *Cement and concrete research,* 30, 1215-1223.

Matschei, T., Lothenbach, B. & Glasser, F. 2007. The AFm phase in Portland cement. *Cement and concrete research,* 37, 118-130.

Mccarthy, M. J. & Dyer, T. D. 2019. Pozzolanas and pozzolanic materials. *Lea's Chemistry of Cement and Concrete,* 5, 363-467.

Mcdonald, D. B. 1994. The rapid chloride permeability test and its correlation to the 90-day chloride ponding test. *Pci Journal,* 39, 38-47.

Mcgrath, P. & Hooton, R. 1996. Influence of voltage on chloride diffusion coefficients from chloride migration tests. *Cement and concrete research,* 26, 1239-1244.

Meck, E. & Sirivivatnanon, V. 2003. Field indicator of chloride penetration depth. 33, 1113-1117.

Medina, C., Sánchez, J., Del Bosque, I. S., Frías, M. & De Rojas, M. S. 2019. Meso-structural modelling in recycled aggregate concrete. *New Trends in Eco-Efficient and Recycled Concrete.* Elsevier.

Meyer, C. 2009. The greening of the concrete industry. *Cement and concrete composites,* 31, 601-605.

Meng, T., Zhang, J., Wei, H. & Shen, J. 2020. Effect of nano-strengthening on the properties and microstructure of recycled concrete. Nanotechnology Reviews, 9, 79-92.

Muehlenkamp, E., Koretsky, M. & Westall, J. 2005. Effect of moisture on the spatial uniformity of cathodic protection of steel in reinforced concrete. *Corrosion,* 61.

Narsilio, G., Li, R., Pivonka, P. & Smith, D. 2007. Comparative study of methods used to estimate ionic diffusion coefficients using migration tests. *Cement and Concrete Research,* 37, 1152-1163.

NT BUILD-335 1997. Concrete, mortar and cement-based repair materials: chloride diffusion coefficient from migration cell experiments. Nordtest, Esbo,Finland.

NT BUILD-443 1995. Concrete, hardened: accelerated chloride penetration. Nordtest, Esbo,Finland.

NT BUILD-492 1999. Concrete, mortar and cement-based repair materials: chloride migration coefficient from non-steady-state migration experiments. Nordtest, Esbo,Finland.

Oikonomou, N. D. 2005. Recycled concrete aggregates. *Cement and concrete composites,* 27, 315-318.

Oleiwi, H. M., Wang, Y., Curioni, M., Chen, X., Yao, G., Augusthus-Nelson, L., Ragazzon-Smith, A. & Shabalin, I. 2018. An experimental study of cathodic protection for chloride contaminated reinforced concrete. *Materials and structures,* 51, 1-11.

Ozbakkaloglu, T., Gholampour, A. & Xie, T. 2018. Mechanical and durability properties of recycled aggregate concrete: effect of recycled aggregate properties and content. *Journal of Materials in Civil Engineering,* 30, 04017275.

Padmini, A., Ramamurthy, K. & Mathews, M. 2009. Influence of parent concrete on the properties of recycled aggregate concrete. *Construction and Building Materials,* 23, 829-836.

Pan, Z., Wang, D., Ma, R. & Chen, A. 2018. A study on ITZ percolation threshold in mortar with ellipsoidal aggregate particles. *Computers and Concrete,* 22, 551-561.

Pang, L. & Li, Q. 2016. Service life prediction of RC structures in marine environment using long term chloride ingress data: Comparison between exposure trials and real structure surveys. *Construction and Building Materials,* 113, 979-987.

Park, B., Jang, S. Y., Cho, J. Y. & Kim, J. Y. 2014. A novel short-term immersion test to determine the chloride ion diffusion coefficient of cementitious materials. *Construction and Building Materials,* 57, 169-178.

Pedro, D., De Brito, J. & Evangelista, L. 2014. Influence of the use of recycled concrete aggregates from different sources on structural concrete. *Construction and Building Materials,* 71, 141-151.

Pointeau, I., Reiller, P., Macé, N., Landesman, C. & Coreau, N. 2006. Measurement and modeling of the surface potential evolution of hydrated cement pastes as a function of degradation. *Journal of colloid and interface science,* 300, 33-44.

Polder, R. B. & Peelen, W. H. 2002. Characterisation of chloride transport and reinforcement corrosion in concrete under cyclic wetting and drying by electrical resistivity. *Cement and Concrete Composites,* 24, 427-435.

Poon, C. S., Shui, Z. & Lam, L. 2004. Effect of microstructure of ITZ on compressive strength of concrete prepared with recycled aggregates. *Construction and building materials,* 18, 461-468.

Qiao, C., Suraneni, P. & Weiss, J. 2018. Damage in cement pastes exposed to NaCl solutions. *Construction and Building Materials,* 171, 120-127.

Roy, D. M. 1988. Relationships between permeability, porosity, diffusion and microstructure of cement pastes, mortar, and concrete at different temperatures. *MRS Online Proceedings Library (OPL),* 137.

Saetta, A. V., Scotta, R. V. & Vitaliani, R. V. 1993. Analysis of chloride diffusion into partially saturated concrete. *Materials Journal,* 90, 441-451.

Samson, E., Lemaire, G., Marchand, J. & Beaudoin, J. J. 1999a. Modeling chemical activity effects in strong ionic solutions. *Computational Materials Science,* 15, 285-294.

Samson, E. & Marchand, J. 2007a. Modeling the effect of temperature on ionic transport in cementitious materials. *Cement and Concrete Research,* 37, 455-468.

Samson, E. & Marchand, J. 2007b. Modeling the transport of ions in unsaturated cement-based materials. *Computers & Structures,* 85, 1740-1756.

Samson, E., Marchand, J. & Beaudoin, J. 1999b. Describing ion diffusion mechanisms in cement-based materials using the homogenization technique. *Cement and Concrete Research,* 29, 1341-1345.

Šavija, B., Luković, M. & Schlangen, E. 2014. Lattice modeling of rapid chloride migration in concrete. *Cement and Concrete Research,* 61, 49-63.

Scrivener, K. 1999. Characterisation of the ITZ and its quantification by test methods. *RILEM report*, 3-18.

Scrivener, K. L. & Pratt, P. L. 1996. Characterization of interfacial microstructure. *Interfacial Transition Zone in Concrete*, 2, 3-18.

Sengul, O. 2014. Use of electrical resistivity as an indicator for durability. *Construction and Building Materials*, 73, 434-441.

Sengul , O. & Gjørv, O. E. 2008. Electrical resistivity measurements for quality control during concrete construction. *ACI Materials Journal*, 105, 541.

Sergi, G., Yu, S. & Page, C. 1992. Diffusion of chloride and hydroxyl ions in cementitious materials exposed to a saline environment. *Magazine of Concrete Research*, 44, 63-69.

Shakouri, M. & Trejo, D. 2017. A time-variant model of surface chloride build-up for improved service life predictions. *Cement and Concrete Composites*, 84, 99-110.

Shane, J. D., Aldea, C. D., Bouxsein, N. F., Mason, T. O. & Shah, S. P. 1999. Microstructural and pore solution changes induced by the rapid chloride permeability test measured by impedance spectroscopy. *Materials & Structures*, 1(2), 110-119.

Shi, C. 2004. Effect of mixing proportions of concrete on its electrical conductivity and the rapid chloride permeability test (ASTM C1202 or ASSHTO T277) results. *Cement and concrete research*, 34, 537-545.

Shi, C., Yuan, Q., He, F. & Hu, X. 2019. *Transport and Interactions of Chlorides in Cement-based Materials*, CRC Press.

Siregar, A., Rafiq, M. I. & Mulheron, M. 2017. Experimental investigation of the effects of aggregate size distribution on the fracture behaviour of high strength concrete. *Construction and Building Materials*, 150, 252-259.

Snyder, K. A. & Marchand, J. 2001. Effect of speciation on the apparent diffusion coefficient in nonreactive porous systems. *Cement and Concrete Research*, 31, 1837-1845.

Spiesz, P., Ballari, M. & Brouwers, H. 2012. RCM: a new model accounting for the non-linear chloride binding isotherm and the non-equilibrium conditions between the free-and bound-chloride concentrations. *Construction and Building Materials*, 27, 293-304.

Spiesz, P. & Brouwers, H. 2012. Influence of the applied voltage on the Rapid Chloride Migration (RCM) test. *Cement and Concrete Research*, 42, 1072-1082.

Spiesz, P. & Brouwers, H. 2013. The apparent and effective chloride migration coefficients obtained in migration tests. *Cement and concrete Research,* 48, 116-127.

Spragg, R., Qiao, C., Barrett, T. & Weiss, J. 2016. Assessing a concrete's resistance to chloride ion ingress using the formation factor. *Corrosion of steel in concrete structures.* Elsevier.

EN 206-1 2013. Concrete-Part 1: Specification, Performance, Production and Conformity. European Committee for Standarization (CEN) Brussels.

Stanish, K., Hooton, R. & Thomas, M. 2004. A novel method for describing chloride ion transport due to an electrical gradient in concrete: Part 1. Theoretical description. *Cement and Concrete Research,* 34, 43-49.

Stanish, K. & Thomas, M. 2003. The use of bulk diffusion tests to establish time-dependent concrete chloride diffusion coefficients. *Cement and Concrete Research,* 33, 55-62.

Streicher, P. & Alexander, M. 1995. A chloride conduction test for concrete. *Cement and Concrete Research,* 25, 1284-1294.

Sun, G., Zhang, Y., Sun, W., Liu, Z. & Wang, C. 2011. Multi-scale prediction of the effective chloride diffusion coefficient of concrete. *Construction and Building Materials,* 25, 3820-3831.

Tam, V. W., Gao, X. & Tam, C. 2005a. Carbonation around near aggregate regions of old hardened concrete cement paste. *Cement and Concrete Research,* 35, 1180-1186.

Tam, V. W., Gao, X. & Tam, C. M. 2005b. Microstructural analysis of recycled aggregate concrete produced from two-stage mixing approach. *Cement and concrete research,* 35, 1195-1203.

Thomas, M., Jewell, R. & Jones, R. 2017. Coal fly ash as a pozzolan. *Coal Combustion Products.* Woodhead Publishing.

Tian, Y., Tian, Z., Jin, N., Jin, X. & Yu, W. 2018. A multiphase numerical simulation of chloride ions diffusion in concrete using electron microprobe analysis for characterizing properties of ITZ. *Construction and Building Materials,* 178, 432-444.

Tran, V. Q., Soive, A. & Baroghel-Bouny, V. 2018. Modelisation of chloride reactive transport in concrete including thermodynamic equilibrium, kinetic control and surface complexation. *Cement and Concrete Research,* 110, 70-85.

Truc, O., Ollivier, J. P. & Nilsson, L. O. 2000. Numerical simulation of multi-species transport through saturated concrete during a migration test—MsDiff code. *Cement and Concrete Research,* 30, 1581-1592.

Truesdell, A. H. & Jones, B. F. 1974. WATEQ, a computer program for calculating chemical equilibria of natural waters. *Jour. Research U.S. Geol. Survey,* 2, 233-248.

Tuutti, K. 1982. Analysis of pore solution squeezed out of cement paste and mortar. *Nordic Concrete Research*.

Vázquez, E., Barra, M., Aponte, D., Jiménez, C. & Valls, S. 2014. Improvement of the durability of concrete with recycled aggregates in chloride exposed environment. Construction and Building Materials, 67, 61-67.

Violetta, B. 2002. Life-365 service life prediction model. *Concrete international,* 24, 53-57.

Wang, Y., Li, L. Y. & Page, C. L. 2001. A two-dimensional model of electrochemical chloride removal from concrete. 20, 0-212.

Wang, Y., Liu, C., Wang, Y., Li, Q. & Yan, B. 2020. Semi-empirical prediction model of chloride-induced corrosion rate in uncracked reinforced concrete exposed to a marine environment. *Electrochimica Acta,* 331, 135376.

Wang, Y., Wu, L., Wang, Y., Liu, C. & Li, Q. 2018. Effects of coarse aggregates on chloride diffusion coefficients of concrete and interfacial transition zone under experimental drying-wetting cycles. *Construction and Building Materials,* 185, 230-245.

Wee, T., Suryavanshi, A. K. & Tin, S. 2000. Evaluation of rapid chloride permeability test (RCPT) results for concrete containing mineral admixtures. *Materials Journal,* 97, 221-232.

Weyers, R. E. 1998. Service life model for concrete structures in chloride laden environments. *Materials Journal,* 95, 445-453.

Whiting, D. 1981. Rapid measurement of the chloride permeability of concrete. *Public Roads,* 45, 101-112.

Wu, K., Long, J., Xu, L. & De Schutter, G. 2019. A study on the chloride diffusion behavior of blended cement concrete in relation to aggregate and ITZ. *Construction and Building Materials,* 223, 1063-1073.

Wu, L., Ju, X., Liu, M., Guan, L., Ma, Y. & Li, M. 2020. Influences of multiple factors on the chloride diffusivity of the interfacial transition zone in concrete composites. *Composites Part B: Engineering,* 199, 108236.

Xi, Y. & Bažant, Z. P. 1999. Modeling chloride penetration in saturated concrete. *Journal of Materials in Civil Engineering,* 11, 58-65.

Xia, J. & Li, L. 2013. Numerical simulation of ionic transport in cement paste under the action of externally applied electric field. *Construction and Building Materials,* 39, 51-59.

Xia, J., Li, T., Fang, J. & Jin, W. 2019. Numerical simulation of steel corrosion in chloride contaminated concrete. *Construction and Building Materials,* 228, 116745.

Xiao, J., Li, W., Sun, Z., Lange, D. A. & Shah, S. P. 2013. Properties of interfacial transition zones in recycled aggregate concrete tested by nanoindentation. *Cement and Concrete Composites,* 37, 276-292.

Xiao, J., Ying, J. & Shen, L. 2012. FEM simulation of chloride diffusion in modeled recycled aggregate concrete. *Construction and Building Materials,* 29, 12-23.

Xiao, L., Ren, Z., Shi, W. & Wei, X. 2016. Experimental study on chloride permeability in concrete by non-contact electrical resistivity measurement and RCM. *Construction and Building Materials,* 123, 27-34.

Yang, C. C. 2005. Effect of the percolated interfacial transition zone on the chloride migration coefficient of cement-based materials. *Materials Chemistry and Physics,* 91, 538-544.

Yang, C. C. & Chiang C. T. 2013. Relation between the chloridemigration coefficients of concrete from the colorimetric method and the chloride profile method. *Journal of the Chinese Institute of Engineers,* 32(6): 801–809.

Yang, C. C. & Cho, S. 2003. An electrochemical method for accelerated chloride migration test of diffusion coefficient in cement-based materials. *Materials Chemistry and Physics,* 81, 116-125.

Yang, C. C. & Cho, S. W. 2005. Approximate migration coefficient of percolated interfacial transition zone by using the accelerated chloride migration test. *Cement and concrete research,* 35, 344-350.

Yang, C. C., Cho, S. W. & Huang, R. 2002. The relationship between charge passed and the chloride-ion concentration in concrete using steady-state chloride migration test. *Cement & Concrete Research,* 32, 217-222.

Yang, C. C. & Weng, S. H. 2013. A three-phase model for predicting the effective chloride migration coefficient of ITZ in cement-based materials. *Magazine of Concrete Research,* 65, 193-201.

Yang, L., Ma, Q. & Yu, B. 2018. Analytical solution and experimental validation for dual time-dependent chloride diffusion in concrete. *Construction and Building Materials,* 161, 676-686.

Yang, L., Pathirage, M., Su, H., Alnaggar, M., Di Luzio, G. & Cusatis, G. 2022. Computational modeling of expansion and deterioration due to alkali–silica reaction: Effects of size range, size distribution, and content of reactive aggregate. *International Journal of Solids and Structures,* 234, 111220.

Yang, P., Sant, G. & Neithalath, N. 2017. A refined, self-consistent Poisson-Nernst-Planck (PNP) model for electrically induced transport of multiple ionic species through concrete. *Cement and Concrete Composites,* 82, 80-94.

Ying, J., Xiao, J., Shen, L. & Bradford, M. A. 2013a. Five-phase composite sphere model for chloride diffusivity prediction of recycled aggregate concrete. *Magazine of Concrete Research,* 65, 573-588.

Ying, J., Xiao, J. & Tam, V. 2013b. On the variability of chloride diffusion in modelled recycled aggregate concrete. *Construction & Building Materials,* 41, 732-741.

Yoo, D. Y., Banthia, N., Fujikake, K., Borges, P. H. & Gupta, R. 2017. Electrical Resistivity of Concrete for Durability Evaluation: A Review. *Advances in Materials Science and Engineering*.

Yu, L., Liu, C., Mei, H., Xia, Y., Liu, Z., Xu, F. & Zhou, C. 2022. Effects of aggregate and interface characteristics on chloride diffusion in concrete based on 3D random aggregate model. *Construction and Building Materials,* 314, 125690.

Yu, Y., Chen, X., Gao, W., Wu, D. & Castel, A. 2019. Modelling non-isothermal chloride ingress in unsaturated cement-based materials. *Construction and Building Materials,* 217, 441-455.

Yu, Y. & Lin, L. 2020. Modeling and predicting chloride diffusion in recycled aggregate concrete. *Construction and Building Materials,* 264, 120620.

Yu, Y. & Wu, B. 2019. Discrete element mesoscale modeling of recycled lump concrete under axial compression. *Materials,* 12, 3140.

Yuan, Q., Deng, D., Shi, C. & De Schutter, G. 2013. Chloride binding isotherm from migration and diffusion tests. *Journal of Wuhan University of Technology-Mater,* 28, 548-556.

Yuan, Q., Shi, C., De Schutter, G., Audenaert, K. & Deng, D. 2009. Chloride binding of cement-based materials subjected to external chloride environment-a review. *Construction and building materials,* 23, 1-13.

Zeng, Y. 2007. Modeling of chloride diffusion in hetero-structured concretes by finite element method. *Cement and Concrete Composites,* 29, 559-565.

Zhang, J., Ying, Z., Chen, Z., Wang, H., Li, J., Yue, H. & Zheng, J. 2021. Analytical Solution for Chloride Diffusivity of Concrete with Aggregate Shape Effect. *Materials,* 14, 3957.

Zhao, J., Fan, Z., Xiong, J., Zhang, D. & Wu, Q. 2021. Experiment research on multi-factor model for chloride migration coefficient within concrete. *IOP Conference Series: Earth and Environmental Science,* 676, 012108 (6pp).

Zheng, J. & Zhou, X. 2007. Prediction of the chloride diffusion coefficient of concrete. *Materials and Structures,* 40, 693-701.

Zheng, J. & Zhou, X. 2008. Three-phase composite sphere model for the prediction of chloride diffusivity of concrete. *Journal of Materials in Civil Engineering,* 20, 205-211.

Zheng, J. & Zhou, X. 2013. Effective medium method for predicting the chloride diffusivity in concrete with ITZ percolation effect. *Construction and Building Materials,* 47, 1093-1098.

Zheng, J., Zhou, X., Huang, X. & Fu, C. 2014. Experiment and modeling of the effect of aggregate shape on the chloride diffusivity of concrete. *Journal of materials in civil engineering,* 26, 04014048.

Zheng, J., Zhou, X., Wu, Y. & Jin, X. 2012. A numerical method for the chloride diffusivity in concrete with aggregate shape effect. *Construction and Building Materials,* 31, 151-156.

PUBLICATIONS

Wei bin Yuan, Li xuan Mao, Long yuan Li. (2022): A two-step approach for calculating chloride diffusion coefficient in concrete with both natural and recycled concrete aggregates[J]. Science of The Total Environment, https://doi.org/10.1016/j.scitotenv.2022.159197

Li xuan Mao, Long yuan Li, Boksun Kim. (2022): Modelling of multi-species transport in concrete under the action of external electric field: Influence of the overpotential at electrode–electrolyte interfaces[J]. Journal of Electroanalytical Chemistry, https://doi.org/10.1016/j.jelechem.2022.116079

Li xuan Mao, Long yuan Li, Boksun Kim. (2022): Chloride removal from recycled aggregate concrete by using electrochemical method. 18-th International Conference: Structural Faults + Repair-2022, 20th-23rd June, Edinburgh, UK.

APPENDIX A: MATLAB CODE FOR MULTI-PHASE GEOMETRIC MODEL

The generation and placement of aggregates in a 2-D concrete model can be divided into four steps: 1) Initializing the geometric parameters in concrete model, including the size of concrete specimen, total volume fraction of aggregates, replacement rate of RCA, aggregate shape, 2) Determining the diameter of aggregates, which are randomly generated and follow Fuller gradation, 3) Placing aggregates generated in step 2 in a 2-D square concrete model and saving the diameter and center coordinates of aggregates, 4) Importing the geometric parameters of aggregates into COMSOL using COMSOL Multiphysics with MATLAB. MATLAB code for the above mentioned four steps is written as follows,

```
function Aggregates2D
%%  random 2D round aggregates generation
%       Dmin, Dmax, Ai, Aa, a, b, t, e
%       result.txt
%       including Aggregates NO., Diameter and Center coordinate
    clear;
% Maximum and minimum size of aggregate
    Dmax =15;
    Dmin =2;
 % Size of concrete specimen
    a = 50;
    b = 50;
 % N - aggregate shape
    N = 1;
 %  Aggregates parameters
    Aa=0.5;
    V=0.5; re=0;
    Aa1 = Aa*(1-re);
    Aa2 = Aa*re;
 % Number of concrete specimen
    I = 1;
 % ITZ thickness
    t =0.0008;
 % Minimum distance between aggregate
    e =0.2;
```

```
clc;
fprintf('Aggregate area ratio %3.3f is generating....\n',(Aa1+Aa2));
con{I}.dmin = Dmin;
con{I}.dmax = Dmax;
con{I}.smax = N;
con{I}.t = t;
con{I}.e = e;
con{I}.length = a;
con{I}.width = b;
con{I}.fillrate = Aa1+Aa2;
con{I}.n = 0;
fprintf('Aggregate N %d is generating....\n',N);

%% Generation of aggregates
if N == 1
   clear d;
   Ai = 0;
   Ai1 = 0;
   Ai2 = 0;
   n = 0;
   w = rand(4000,1);
   while(Ai < Aa*a*b)
      n = n+1;
      fprintf('Aggregate NO. %d is generating.... Now Aa = %3.3f.\n',n,Ai/a/b);
      d(n) = P2DFullerSolve(con{I},w(n));
    if (s(n)==N)
      if(Ai1+d2area(d(n),s(n)) <= Aa1*a*b)
        Ai1 = Ai1+d2area(d(n),s(n));
      elseif(Ai1+d2area(d(n),s(n)) > Aa1*a*b)
         d(n) = area2d(Aa1*a*b-Ai1,s(n));
         Ai1 = Ai1+d2area(d(n),s(n));
         if( Ai2>=Aa2*a*b)
           break;
         else
          s(n)=0;d(n)=0.1;
          Ai1 = Ai1;
         end
      end

    elseif(s(n)==N)
      if(Ai2+d2area(d(n),s(n)) <= Aa2*a*b)
         Ai2 = Ai2+d2area(d(n),s(n));
      elseif(Ai2+d2area(d(n),s(n)) > Aa2*a*b)
         d(n) = area2d(Aa2*a*b-Ai2,s(n));
```

```
        Ai2 = Ai2+d2area(d(n),s(n));

        if( Ai1>=Aa1*a*b)
          break;
        else
         s(n)=0;d(n)=0.1;
         Ai2 = Ai2;
      end
    end
    con{I}.n = n;

    [d,index] = sort(d,2,'descend');
    for i = 1:n
      con{I}.agg{i}.n = 1;
      con{I}.agg{i}.r(1) = d(i)/2;
      con{I}.agg{i}.isused = 1;
    end
    fprintf('Aggregate generation has been finished!\n');
elseif N == 2
    clear d d1;
    Ai = 0;
    n = 0;
    w = rand(4000,1);
    while(Ai < Aa*a*b)
      n = n+1;
      fprintf('Aggregate NO. %d is generating.... Now Aa = %3.3f.\n',n,Ai/a/b);
      d(n) = P2DFullerSolve(con{I},w(n));
     if (s(n)==N)
      if(Ai1+d2area(d(n),s(n)) <= Aa1*a*b)
        Ai1 = Ai1+d2area(d(n),s(n));
      elseif(Ai1+d2area(d(n),s(n)) > Aa1*a*b)
        d(n) = area2d(Aa1*a*b-Ai1,s(n));
        Ai1 = Ai1+d2area(d(n),s(n));
        if( Ai2>=Aa2*a*b)
          break;
        else
         s(n)=0;d(n)=0.1;
         Ai1 = Ai1;
        end
      end

     elseif(s(n)==N)
      if(Ai2+d2area(d(n),s(n)) <= Aa2*a*b)
        Ai2 = Ai2+d2area(d(n),s(n));
```

```
        elseif(Ai2+d2area(d(n),s(n)) > Aa2*a*b)
            d(n) = area2d(Aa2*a*b-Ai2,s(n));
            Ai2 = Ai2+d2area(d(n),s(n));

            if( Ai1>=Aa1*a*b)
              break;
            else
             s(n)=0;d(n)=0.1;
             Ai2 = Ai2;
            end
        end
    end
    con{I}.n = n;
    [d,index] = sort(d,'descend');
    for i = 1:n
        con{I}.agg{i}.n = 2;
        con{I}.agg{i}.r(1) = d(i)/2;
        con{I}.agg{i}.rot = 2*pi()*rand();
        con{I}.agg{i}.isused = 1;
    end
    fprintf('Aggregate generation has been finished!\n');
else
    clear d;
    Ai1 = 0;
    Ai2 = 0;
    n = 0;
    w = rand(4000,1);
    s = fix(2*rand(4000,1))+N;
      if (s(n)==101)

       if(Ai1+d2area(d(n),s(n)) <= Aa1*a*b)
          Ai1 = Ai1+d2area(d(n),s(n));
       elseif(Ai1+d2area(d(n),s(n)) > Aa1*a*b)
          d(n) = area2d(Aa1*a*b-Ai1,s(n));
          Ai1 = Ai1+d2area(d(n),s(n));
          if( Ai2>=Aa2*a*b)
            break;
          else
           s(n)=0;d(n)=0.1;
           Ai1 = Ai1;
          end
       end

     elseif(s(n)==102)
```

```
        if(Ai2+d2area(d(n),s(n)) <= Aa2*a*b)
            Ai2 = Ai2+d2area(d(n),s(n));
        elseif(Ai2+d2area(d(n),s(n)) > Aa2*a*b)
            d(n) = area2d(Aa2*a*b-Ai2,s(n));
            Ai2 = Ai2+d2area(d(n),s(n));

            if( Ai1>=Aa1*a*b)
              break;
            else
             s(n)=0;d(n)=0.1;
             Ai2 = Ai2;
            end
      while((Ai1+Ai2) < ((Aa1+Aa2)*a*b))
        n = n+1;
        fprintf('Aggregate NO. %d is generating.... Now Aa
= %3.3f.\n',n,(Ai1+Ai2)/a/b);
        d(n) = P2DFullerSolve(con{I},w(n));


        end
       end
      end

      con{I}.n = n;
      s = s(1:n);
      [d,index] = sort(d,'descend');
      s = s(index);
      for i = 1:n
        con{I}.agg{i}.n = s(i);
        con{I}.agg{i}.r(1) = d(i)/2;
        con{I}.agg{i}.ang = 2*pi()/N;
        con{I}.agg{i}.rot = 2*pi()*rand();
        con{I}.agg{i}.isused = 1;

       if d(i) > 0.1
         anum(i)=1;
       else
         anum(i)=0;
       end
      end
        num=sum(anum(:))

      fprintf('Aggregate generation has been finished!\n');
   end
```

```
%% Placement of aggregates
   i = 1;
   fprintf('Aggregate NO. %d is placing....\n',i);
   ntry = 0;
   while(i <= con{I}.n)

      if( ntry > n_max)
         ntry = 0;
         fprintf('max times is reached. Aggregate NO. %d is failed.\n',i);
         con{I}.agg{i}.cenx = -50;
         con{I}.agg{i}.ceny = -50;
         if i == con{I}.n
            break;
         else
            i = i+1;
            fprintf('Aggregate NO. %d is placing....\n',i);
         end
      end

      xi = con{I}.agg{i}.r(1)+t+e;
      yi = con{I}.agg{i}.r(1)+t+e;
      if(i == 1)
         con{I}.agg{i}.cenx = xi;
         con{I}.agg{i}.ceny = yi;
      else
         tag = 0;
         for j = 1:i-1
            if con{I}.agg{j}.isused == 1
               if sqrt(((xi-con{I}.agg{j}.cenx)^2+(yi-con{I}.agg{j}.ceny)^2)) <
con{I}.agg{i}.r(1)
                  tag = 1;
                  break;
               end
            end
         end
         if tag == 1
            ntry = ntry+1;
            continue;
         else
            con{I}.agg{i}.cenx = xi;
            con{I}.agg{i}.ceny = yi;
         end
      end
      i = i+1;
```

```
        ntry = ntry+1;
        fprintf('%d times OK\n',ntry);
        if i <= con{I}.n
            fprintf('Aggregate NO. %d is placing....\n',i);
        end
        ntry = 0;

    end

    fprintf('All aggregate has been placed!\n');



%% save result to file
    fprintf('Saving data to file!\n');
    paths=['C:\OneDrive\OneDrive - University of Plymouth\matlab-
aggregates\RCA\data'];
    save([paths,num2str(Aa1+Aa2),num2str(N),'.mat'],'con');
    fprintf('Finish!\n');

end
function d = P2DFullerSolve(con,w)
%% random 2D Fuller aggregates diameter generation

    x1 = con.dmin;
    x2 = con.dmax;
    F1 = P2DFuller(con,x1)-w;
    F2 = P2DFuller(con,x2)-w;
    while(1)
        x = 0.5*(x1+x2);
        F = P2DFuller(con,x)-w;
        if(sign(F) == sign(F1))
            x1 = x;
            F1 = F;
        else
            x2 = x;
            F2 = F;
        end
        if(abs(x1-x2)>1e-5 && abs(F)>1e-6)
            continue;
        else
            break;
        end
    end
```

```
    d=0.5*(x1+x2);

end
%% import geometric parameters into COMSOL
clc;clear;
import com.comsol.model.*
import com.comsol.model.util.*

model = ModelUtil.create('Model');

model.modelPath(['D:\OneDrive - University of Plymouth\
aggregate\aggregate\triangle' native2unicode(hex2dec('684c'), 'Cp1252')
native2unicode(hex2dec('9762'), 'Cp1252') ]);

model.modelNode.create('mod1');

model.geom.create('geom1', 2);

model.mesh.create('mesh1', 'geom1');

model.physics.create('chds', 'DilutedSpecies', 'geom1', {'c'});

model.study.create('std1');
model.study('std1').feature.create('time', 'Transient');

N = 1;
Aa = 0.1;
B4=4;
Bn=4;

load('C:\OneDrive\OneDrive - University of Plymouth\matlab-
aggregates\RCA\data\0.5_re20_cir_2mm_15mm.mat','con');
for i = 1:con{N}.n
    str = ['c',int2str(i)];
    str1 = ['cc',int2str(i)];
    str2 = ['ccc',int2str(i)];
    str3 = ['cccc',int2str(i)];

    if con{N}.agg{i}.n == 1
    model.geom('geom1').create(str, 'Circle');
        model.geom('geom1').feature(str).set('base', 'center');
        model.geom('geom1').feature(str).set('pos', {num2str(con{N}.agg{i}.cenx/scale)
num2str(con{N}.agg{i}.ceny/scale)});
        model.geom('geom1').feature(str).set('r', num2str(con{N}.agg{i}.r(1)/scale*rm));
```

```
        model.geom('geom1').run(str);
    model.geom('geom1').create(str1, 'Circle');
        model.geom('geom1').feature(str1).set('base', 'center');
        model.geom('geom1').feature(str1).set('pos', {num2str(con{N}.agg{i}.cenx/scale)
num2str(con{N}.agg{i}.ceny/scale)});
        model.geom('geom1').feature(str1).set('r', num2str(con{N}.agg{i}.r(1)/scale));
        model.geom('geom1').run(str1);
    model.geom('geom1').create(str2, 'Circle');
        model.geom('geom1').feature(str2).set('base', 'center');
        model.geom('geom1').feature(str2).set('pos', {num2str(con{N}.agg{i}.cenx/scale)
num2str(con{N}.agg{i}.ceny/scale)});
        model.geom('geom1').feature(str2).set('r',
num2str(con{N}.agg{i}.r(1)/scale*rm+t));
        model.geom('geom1').run(str2);
    model.geom('geom1').create(str3, 'Circle');
        model.geom('geom1').feature(str3).set('base', 'center');
        model.geom('geom1').feature(str3).set('pos', {num2str(con{N}.agg{i}.cenx/scale)
num2str(con{N}.agg{i}.ceny/scale)});
        model.geom('geom1').feature(str3).set('r', num2str(con{N}.agg{i}.r(1)/scale+t));
        model.geom('geom1').run(str3);


    elseif con{N}.agg{i}.n == 2
     model.geom('geom1').create(str, 'Ellipse');
        model.geom('geom1').feature(str).set('base', 'center');
        model.geom('geom1').feature(str).set('pos', {num2str(con{N}.agg{i}.cenx/scale)
num2str(con{N}.agg{i}.ceny/scale)});
        model.geom('geom1').feature(str).set('a', num2str(con{N}.agg{i}.r(1)/scale*rm));
        model.geom('geom1').feature(str).set('b',
num2str(con{N}.agg{i}.r(1)/scale*2/3*rm));
        model.geom('geom1').feature(str).set('rot',
num2str(con{N}.agg{i}.rot*360/2/pi+t));
        model.geom('geom1').run(str);
     model.geom('geom1').create(str1, 'Ellipse');
        model.geom('geom1').feature(str1).set('base', 'center');
        model.geom('geom1').feature(str1).set('pos', {num2str(con{N}.agg{i}.cenx/scale)
num2str(con{N}.agg{i}.ceny/scale)});
        model.geom('geom1').feature(str1).set('a', num2str(con{N}.agg{i}.r(1)/scale));
        model.geom('geom1').feature(str1).set('b', num2str(con{N}.agg{i}.r(1)/scale*2/3));
        model.geom('geom1').feature(str1).set('rot',
num2str(con{N}.agg{i}.rot*360/2/pi+t));
        model.geom('geom1').run(str1);
     model.geom('geom1').create(str2, 'Ellipse');
        model.geom('geom1').feature(str2).set('base', 'center');
```

```
        model.geom('geom1').feature(str2).set('pos', {num2str(con{N}.agg{i}.cenx/scale)
num2str(con{N}.agg{i}.ceny/scale)});
        model.geom('geom1').feature(str2).set('a',
num2str(con{N}.agg{i}.r(1)/scale*rm+t));
        model.geom('geom1').feature(str2).set('b',
num2str(con{N}.agg{i}.r(1)/scale*2/3*rm+t));
        model.geom('geom1').feature(str2).set('rot', num2str(con{N}.agg{i}.rot*360/2/pi));
        model.geom('geom1').run(str2);
     model.geom('geom1').create(str3, 'Ellipse');
        model.geom('geom1').feature(str3).set('base', 'center');
        model.geom('geom1').feature(str3).set('pos', {num2str(con{N}.agg{i}.cenx/scale)
num2str(con{N}.agg{i}.ceny/scale)});
        model.geom('geom1').feature(str3).set('a', num2str(con{N}.agg{i}.r(1)/scale+t));
        model.geom('geom1').feature(str3).set('b',
num2str(con{N}.agg{i}.r(1)/scale*2/3+t));
        model.geom('geom1').feature(str3).set('rot', num2str(con{N}.agg{i}.rot*360/2/pi));
        model.geom('geom1').run(str3);
        Bn = Bn+4;
    else
        B4 = B4+con{N}.agg{i}.n;
        Bn = Bn+con{N}.agg{i}.n;
        x1 = con{N}.agg{i}.cenx/scale+con{N}.agg{i}.r/scale*cos(con{N}.agg{i}.rot);
        y1 = con{N}.agg{i}.ceny/scale+con{N}.agg{i}.r/scale*sin(con{N}.agg{i}.rot);
        Pc{1,1} = num2str(x1);
        Pc{2,1} = num2str(y1);
            xrm1 =
con{N}.agg{i}.cenx/scale+con{N}.agg{i}.r*rm/scale*cos(con{N}.agg{i}.rot);
            yrm1 =
con{N}.agg{i}.ceny/scale+con{N}.agg{i}.r*rm/scale*sin(con{N}.agg{i}.rot);
            Pcrm{1,1} = num2str(xrm1);
            Pcrm{2,1} = num2str(yrm1);
            xt1 =
con{N}.agg{i}.cenx/scale+(con{N}.agg{i}.r/scale+t)*cos(con{N}.agg{i}.rot);
            yt1 =
con{N}.agg{i}.ceny/scale+(con{N}.agg{i}.r/scale+t)*sin(con{N}.agg{i}.rot);
            Pct{1,1} = num2str(xt1);
            Pct{2,1} = num2str(yt1);
            xrmt1 =
con{N}.agg{i}.cenx/scale+(con{N}.agg{i}.r*rm/scale+t)*cos(con{N}.agg{i}.rot);
            yrmt1 =
con{N}.agg{i}.ceny/scale+(con{N}.agg{i}.r*rm/scale+t)*sin(con{N}.agg{i}.rot);
            Pcrmt{1,1} = num2str(xrmt1);
            Pcrmt{2,1} = num2str(yrmt1);
        for j = 1:con{N}.agg{i}.n
```

```
        x1 =
con{N}.agg{i}.cenx/scale+con{N}.agg{i}.r/scale*cos(con{N}.agg{i}.rot+2*pi()*j/con
{N}.agg{i}.n);
        y1 =
con{N}.agg{i}.ceny/scale+con{N}.agg{i}.r/scale*sin(con{N}.agg{i}.rot+2*pi()*j/con{
N}.agg{i}.n);
        Pc{1,j+1} = num2str(x1);
        Pc{2,j+1} = num2str(y1);
           xrm1 =
con{N}.agg{i}.cenx/scale+con{N}.agg{i}.r*rm/scale*cos(con{N}.agg{i}.rot+2*pi()*j/
con{N}.agg{i}.n);
           yrm1 =
con{N}.agg{i}.ceny/scale+con{N}.agg{i}.r*rm/scale*sin(con{N}.agg{i}.rot+2*pi()*j/
con{N}.agg{i}.n);
           Pcrm{1,j+1} = num2str(xrm1);
           Pcrm{2,j+1} = num2str(yrm1);
           xt1 =
con{N}.agg{i}.cenx/scale+(con{N}.agg{i}.r/scale+t)*cos(con{N}.agg{i}.rot+2*pi()*j/
con{N}.agg{i}.n);
           yt1 =
con{N}.agg{i}.ceny/scale+(con{N}.agg{i}.r/scale+t)*sin(con{N}.agg{i}.rot+2*pi()*j/c
on{N}.agg{i}.n);
           Pct{1,j+1} = num2str(xt1);
           Pct{2,j+1} = num2str(yt1);
           xrmt1 =
con{N}.agg{i}.cenx/scale+(con{N}.agg{i}.r*rm/scale+t)*cos(con{N}.agg{i}.rot+2*pi(
)*j/con{N}.agg{i}.n);
           yrmt1 =
con{N}.agg{i}.ceny/scale+(con{N}.agg{i}.r*rm/scale+t)*sin(con{N}.agg{i}.rot+2*pi(
)*j/con{N}.agg{i}.n);
           Pcrmt{1,j+1} = num2str(xrmt1);
        Wc{2*j-1} = '1';
        Wc{2*j} = '1';
      end
      model.geom('geom1').create(str, 'BezierPolygon');
      model.geom('geom1').feature(str).set('p', Pcrm);
      model.geom('geom1').feature(str).set('w', Wc);
      model.geom('geom1').feature(str).set('degree', Degreec);
      model.geom('geom1').run(str);
   model.geom('geom1').create(str1, 'BezierPolygon');
      model.geom('geom1').feature(str1).set('p', Pc);
      model.geom('geom1').feature(str1).set('w', Wc);
      model.geom('geom1').feature(str1).set('degree', Degreec);
      model.geom('geom1').run(str1);
```

```
    model.geom('geom1').create(str2, 'BezierPolygon');
      model.geom('geom1').feature(str2).set('p', Pcrmt);
      model.geom('geom1').feature(str2).set('w', Wc);
      model.geom('geom1').feature(str2).set('degree', Degreec);
      model.geom('geom1').run(str2);
   model.geom('geom1').create(str3, 'BezierPolygon');
      model.geom('geom1').feature(str3).set('p', Pct);
      model.geom('geom1').feature(str3).set('w', Wc);
      model.geom('geom1').feature(str3).set('degree', Degreec);
      model.geom('geom1').run(str3);
   end
end

model.geom('geom1').create('sq1', 'Square');
model.geom('geom1').feature('sq1').set('base', 'corner');
model.geom('geom1').feature('sq1').set('pos', {'0' '0'});
model.geom('geom1').feature('sq1').set('l', '0.05');
model.geom('geom1').run('sq1');
```

APPENDIX B: MATLAB CODE FOR TWO-STEP ANALYTICAL MODEL

This MATLAB code was developed to solve the two-step analytical model proposed in Section 3.2.2. By initializing the basic parameters of aggregates as given in Table 3.3, the effective chloride diffusion coefficient of concrete can be easily obtained.

```
function Variation of effective chloride diffusivity for RCA with quality of old mortar
   Dnm=2.03e-12; Doitz=3.0*Dnm;
   Dnitz1=2*Dnm; Dnitz2=2*Dnm;
   Vnitz1=0.05;  Vnitz2=0.05;
   Vm=0.5;rRA=0.5;

for m=1: 3
   if m==1, Dom=0.2*Dnm; end;
   if m==2, Dom=1.5*Dnm; end;
   if m==3, Dom=3.0*Dnm; end;
for k = 1: length(x)
   Vom=x(k); Voitz=0.03;

   Voa=1-Voitz-x(k);
   Doaplus=2*Voitz*Doitz/(Voitz+Voa)/3;
   DRCA=((3-2*Vom)*Doaplus+2*Vom*Dom)/(Vom*Doaplus+Dom*(3-
Vom))*Dom;
   DRCAp=(3*DRCA+2*Vnitz2*Dnitz2)/(Vnitz2*DRCA+3*Dnitz2)*Dnitz2;
   DNAp=2/3*Vnitz1*Dnitz1;

     Deff0=0;
     I0=1;
     while(I0 >= 0.000001)
      Inew=(Dnm-Deff0)/(Dnm+2*Deff0)*Vm+(DNAp-Deff0)/(DNAp+2*Deff0)*(1-
Vm)*(1-rRA)+(DRCAp-Deff0)/(DRCAp+2*Deff0)*(1-Vm)*(rRA);
       I0=Inew;
       Deff0=Deff0+0.0001*6.0e-12;
     end
     Deff=Deff0;
     y(m,k)=Deff/Dnm;
end;
```

```
function Variation of effective chloride diffusivity for RCA with total volume fraction
of aggregate
   Vom=0.25; Voitz=0.05; Voa=1-Vom-Voitz;
   Dom=1.5*6.0e-12; Doitz=2.0*6.0e-12;
   Doaplus=2*Voitz*Doitz/(Voitz+Voa)/3;
   DRCA=((3-2*Vom)*Doaplus+2*Vom*Dom)/(Vom*Doaplus+Dom*(3-
Vom))*Dom;
   x=linspace(0.01, 0.99, 200);
   Dnitz1=1.6*6.0e-12; Dnitz2=1.6*6.0e-12;
for m=1: 3
   if m==1, kf=0.25; end;  if m==2, kf=0.5; end;  if m==3, kf=0.75; end;
   Vnitz1=0.05; Vnitz2=0.05; VRCA=1-Vnitz2; VNA=1-Vnitz1;
   DRCAp=(3*DRCA+2*Vnitz2*Dnitz2)/(Vnitz2*DRCA+3*Dnitz2)*Dnitz2;
   DNAp=2/3*Vnitz1*Dnitz1;
   Dm=6.0e-12; Vm=0.5;
 for k = 1: length(x)
   Deff=x(k)*Dm;
   g1=Deff/(Dm/3+2/3*Deff); g2=Deff/(DNAp/3+2/3*Deff);
g3=Deff/(DRCAp/3+2/3*Deff);
   g4=g2*kf+g3*(1-kf); g5=(1-g4)/(g1-g4);
   y(k)=1-g5;
 end;

function Variation of effective chloride diffusivity for RAC with replacement rate of
RCA
   Vom=0.1; Voitz=Vom/5; Voa=1-Vom-Voitz;
   Dom=6.0e-12; Doitz=1.5*6.0e-12;
   Doaplus=2*Voitz*Doitz/(Voitz+Voa)/3;
   DRCA=((3-2*Vom)*Doaplus+2*Vom*Dom)/(Vom*Doaplus+Dom*(3-
Vom))*Dom;
   x=linspace(0.01, 0.99, 200);
for m=1: 2
   if m==1, kf=1.2; end;  if m==2, kf=2.4; end; %
   Vnitz1=0.02*kf; Vnitz2=0.02*kf; VRCA=1-Vnitz2; VNA=1-Vnitz1;
   Dm=kf*1.8e-12; Vm=0.6; Dnitz1=1.5*Dm; Dnitz2=1.5*Dm;
   DRCAp=(3*DRCA+2*Vnitz2*Dnitz2)/(Vnitz2*DRCA+3*Dnitz2)*Dnitz2;
   DNAp=2/3*Vnitz1*Dnitz1;
   for k = 1: length(x)
   Deff=x(k)*Dm;
   g1=1/Deff-Vm/(Dm/3+2/3*Deff); g2=1/(DNAp/3+2/3*Deff);
g3=1/(DRCAp/3+2/3*Deff);
   y(m,k)=(g1-g2*(1-Vm))/(g3-g2)/(1-Vm);
   end;
end;
```